

UNCLASSIFIED

AD NUMBER

AD909223

LIMITATION CHANGES

TO:

Approved for public release; distribution is unlimited.

FROM:

Distribution authorized to U.S. Gov't. agencies only; Test and Evaluation; DEC 1971. Other requests shall be referred to Space and Missile Systems Organization, Attn: SMSDI-STINFO, Los Angeles, CA 90045.

AUTHORITY

SAMSO ltr, 29 Sep 1976

THIS PAGE IS UNCLASSIFIED

THIS REPORT HAS BEEN DELIMITED
AND CLEARED FOR PUBLIC RELEASE
UNDER DOD DIRECTIVE 5200.20 AND
NO RESTRICTIONS ARE IMPOSED UPON
ITS USE AND DISCLOSURE.

DISTRIBUTION STATEMENT A

APPROVED FOR PUBLIC RELEASE;
DISTRIBUTION UNLIMITED.

Noted

L
AD909223

**(U) Proceedings of the Boundary
Layer Transition Workshop
Held 3-5 November 1971**

Volume III

**Prepared by W. D. McCauley
Technology Division**

71 DEC 20

**Prepared for SPACE AND MISSILE SYSTEMS ORGANIZATION
AIR FORCE SYSTEMS COMMAND
Air Force Unit Post Office
Los Angeles, California 90045**

CONTRACT No. F04701-71-C-0172



**San Bernardino Operations
THE AEROSPACE CORPORATION**

ACCESSION for		<input type="checkbox"/> Write Section <input checked="" type="checkbox"/> Div. Section
NTIS		
DOC		
UNANNOUNCED		
JUSTIFICATION		
BY	DISTRIBUTION/AVAILABILITY CODES	
DCL 	REG. NO. OF SPECIAL 	68-2

(18) SAMSOTR-73-155 VOL-3

(14) Report No.
TOR-0172(S2816-16)-5 - Vol-3

Technical operating rept.

PROCEEDINGS OF THE BOUNDARY LAYER
TRANSITION WORKSHOP HELD 3-5 NOVEMBER 1971.
Volume III.

Prepared by

(10) W. D. McCauley
Technology Division

(11) 24 Dec 71
~~11 DEC 20~~

(12) 42p.

DDC
RECEIVED
APR 28 1973
E

San Bernardino Operations
THE AEROSPACE CORPORATION
San Bernardino, California

Prepared for

SPACE AND MISSILE SYSTEMS ORGANIZATION
AIR FORCE SYSTEMS COMMAND
Air Force Unit Post Office
Los Angeles, California 90045

elle
1473

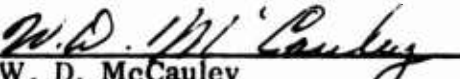
(15)
Contract No. F04701-71-C-0172

Distribution limited to U.S. Gov't. agencies only; Test and
Evaluation; 71 DEC 20. Other requests for this document
must be referred to SAMSOT/RNSE.

472 467

(U) PROCEEDINGS OF THE BOUNDARY LAYER
TRANSITION WORKSHOP HELD 3-5 NOVEMBER 1971
Volume III

Prepared


W. D. McCauley
Flight Performance Evaluation

Approved


T. A. Bergstrahl, General Manager
Technology Division

FOREWORD

(U) The Boundary Layer Transition Specialists Workshop was held on November 3-5, 1971 at Aerospace Corporation, San Bernardino, California. The objective of the meeting was to make transition specialists aware of the most recent data and techniques for transition prediction and to focus on the solution of design problems associated with boundary layer transition.

(U) The Proceedings of the meeting have been compiled by Aerospace Corporation, San Bernardino Operations, under Contract No. F04701-71-C-0172 as TOR-0172(S2816-16)-5. The Air Force program monitor is Col. C. Zimmerman, USAF (SAMSO/RNS). The Proceedings were edited by William D. McCauley and submitted for publication in December 1971.

(U) The chairman and co-chairmen of the meeting were Dr. Richard A. Hartunian, Dr. Frank L. Fernandez and William D. McCauley of the Aerospace Corporation, respectively. Principle contributors selected for their demonstrated expertise in the field of Boundary Layer Transition include those listed as authors in the Table of Contents. The session and committee chairmen are indicated in the meeting notes which follow.

(U) The proceedings consist of four volumes. Volume I contains the Keynote address on the NASA Transition Study Group and the session on Transition Design Problems and Information Needed for Their solution. Volume II contains the session on Recent Flight Test Transition Data and Correlations. Volume III contains the session on Recent Ground Test Transition Data and Correlations. Volume IV contains the session on Boundary Layer Stability Theory, Tests and Transition Modeling, and the recommendations of four committees for future efforts on boundary layer transition.

UNCLASSIFIED ABSTRACT

(U) BOUNDARY LAYER TRANSITION
SPECIALISTS WORKSHOP, Volumes I
through IV, Edited by W. D. McCauley

TOR-0172(S2816-16)-5
Volumes I-IV
December 1971

The workshop consisted of introductory remarks, a keynote address, four reporting investigation sessions and a session involving all participants on four committees. The objective of the meeting was to make transition specialists aware of the most recent data and techniques for transition prediction and to focus on the solution of design problems associated with boundary layer transition. The first session showed how transition affects reentry vehicle design in terms of nosetip thermostress and ablation, transpiration cooled nosetips, frustum ablation, reentry observables, plasma attenuation, vehicle dynamics and space shuttle design. The second session presented ABRES reentry vehicle transition data and prediction techniques obtained since the previous meeting four years ago. The third session presented recent data obtained from government laboratories. The fourth session presented recent applications of stability theory, additional confirmation of the theory and work toward transition modeling. In the last session the meeting participants worked on four committees to arrive at recommendations for future efforts on boundary layer transition.

(Secret Formerly Restricted Data Report)

MEETING NOTES

(U) About four years ago SAMSO/Aerospace held a similar meeting to make transition specialists aware of the recent flight test data, discrepancies between laboratory and flight data and correlations of flight transition data which were being used for transition prediction but were not compatible with all of the trends of the laboratory investigations. Since that meeting, a significant amount of additional flight data has been obtained by SAMSO/Aerospace and a variety of transition correlations have been developed utilizing the seemingly abundant data.* Unfortunately, none of these correlations has resulted in completely successful prediction of transition occurrence on flight vehicles and some surprises in the low altitude occurrence of transition during reentry were obtained most notably on the SAMAST and RVTO-2B vehicles which are shown in detail in the proceedings.

(U) Dr. Mark Morkovin attempted to instigate a similar type of meeting through the NASA committee on which he served over a year ago. Though this meeting did not materialize it was probably instrumental in establishing the NASA Transition Study Group. Dr. Eli Reshotko reports on the activities of this group in the proceedings as our keynote speaker. This approach of integrating theoretical and ground test efforts, understanding facility limitations and developing quiet tunnels for transition research should ultimately yield a more complete understanding of transition phenomena.

(U) The success of the meeting can really be attributed to the caliber and efforts of the chairmen, speakers, and attendees who were invited to participate. The meeting was organized around five primary sessions. Introductory remarks by Dr. Brian D. Henshall, Associate General Manager, Aerospace Corporation, San Bernardino Operations, and a keynote address by Dr. Eli Reshotko on the NASA Transition Study Group set the stage for the meeting. The first session Transition Design Problems and Information

*Though abundant data exist it is with few sensors per flight, different types of sensors, different configurations and different materials making separation of the variables which affect transition difficult.

Needed for Their Solution, chaired by E. Hertler of Aerospace, was organized to show how transition affects reentry vehicle design in terms of nosetip thermostructure and ablation, transpiration cooled nosetips, frustum ablation, reentry observables, plasma attenuation, vehicle dynamics and space shuttle design. The second session, Recent Flight Test Transition Data and Correlations chaired by Dr. N. Jaffe of Aerospace, was used to present the ABRES flight transition data and flight data correlations obtained since the meeting which occurred four years ago. Since the results of the first two sessions were for the most part classified, they are presented in the classified Volumes I and II of the proceedings. The third session, Recent Ground Test Data and Correlation chaired by Dr. W. R. Warren of the Aerospace Laboratory, presented the most recent work obtained throughout the government laboratories. Examination of these papers in the proceedings shows the significant influence of the NASA Transition Study Group already being made on quiet tunnel development and resolving discrepancies between transition results from the various government facilities.

(U) The fourth session, Boundary Layer Stability Theory, Transition Modeling, and Confirming tests, chaired by Dr. John Laufer of the University of Southern California, gave the most recent results of stability theory applications, additional confirmation of the theory by supporting tests, and an attempt to construct an analytic model of transition. In the fifth session, Workshop Committees and Recommendations, was chaired by Dr. R. Kenneth Iobb of the Naval Ordnance Laboratory; all of the attendees and speakers of the workshop were invited to participate on committees of their specialties, and considering the many problems associated with their specialties, to come up with recommendations for studies or approaches for solutions to these problems. There were four committees in this session including:

Committee A: Theoretical Approaches

Dr. Eli Reshotho, Chairman

Committee B: Transition Data Correlation Approaches

Dr. Leith Potter, Chairman

Committee C: Transition Flight Test Efforts Needed

Dr. Frank Fernandez, Chairman

Committee D: Transition Ground Test Efforts Needed

Dr. Mark Morkovin, Chairman

The results of these committee meetings were summarized by the committee chairmen to all of the workshop participants. These summaries were taped at the meeting, have been transcribed and are presented in Volume IV of the Proceedings.

(U) In the organization of the meeting, many individuals contributed to its success. Most notable was our secretary, Shirley Jelen, the Technology Division Administrator Gordon Lamb and the projectionist Bob Lemke. Publication of the proceedings occurred in a timely manner through the dedicated efforts of George Waggoner in our publications department.

VOLUME III

CONTENTS

SESSION III RECENT GROUND TEST TRANSITION DATA AND CORRELATION

1.	EFFECTS OF MASS ADDITION DISTRIBUTION AND ROUGHNESS ON BOUNDARY LAYER TRANSITION AT MACH 12 , by C. J. Stalmach, Jr. and T. C. Pope - Vought Aeronautics Co.; J. J. Bertin - Univ. of Texas at Austin; and R. L. Wright - NASA Langley Research Center	1-1
	Abstract	1-1
	Introduction	1-2
	Experimental Apparatus	1-3
	Test Results	1-6
	Conclusions	1-14
	References	1-17
	Nomenclature	1-19
2.	EFFECTS OF NOSE BLUNTNES AND FREE-STREAM UNIT REYNOLDS NUMBER ON SLENDER CONE TRANSITION AT HYPERSONIC SPEEDS , by James F. Muir and Amado A. Trujillo Sandia Laboratories	2-1
	Abstract	2-1
	Nomenclature	2-3
	Introduction	2-5
	Experimental Program	2-7
	Results	2-9
	Discussion	2-11
	Conclusions	2-27
	References	2-30
3.	FREE FLIGHT DETERMINATION OF BOUNDARY LAYER TRANSITION ON SMALL SCALE CONES IN THE PRESENCE OF SURFACE ABLATION , by Max E. Wilkins and Gary T. Chapman - Ames Research Center	3-1
	Introduction	3-1
	Facility, Models and Experimental Technique	3-2

CONTENTS (Continued)

	Results and Discussion	3-4
	Concluding Remarks	3-7
	Symbols	3-9
	References	3-12
4.	EFFECTS OF WALL COOLING AND ANGLE OF ATTACK ON BOUNDARY-LAYER TRANSITION ON SHARP CONES AT $M_{\infty} = 7.4$; by George G. Matur - Ames Research Center	4-1
	Abstract	4-1
	Nomenclature	4-2
	Introduction	4-3
	Apparatus and Tests	4-3
	Results and Discussion	4-4
	Conclusions	4-9
	References	4-10
5.	SOME SPECIAL FEATURES OF BOUNDARY LAYER TRANSITION ON AEROBALLISTIC RANGE MODELS by J. Leith Potter - ARO Inc.	5-1
	Abstract	5-1
	Nomenclature	5-1
	Introduction	5-3
	Models and Range Systems	5-4
	The Influence of Angle of Attack	5-5
	Surface Roughness	5-10
	The Influence of Model Variation	5-14
	Non-Uniform Wall Temperature	5-19
	Concluding Remarks	5-21
	References	5-21

CONTENTS (Continued)

6.	HYPERSONIC SIMULATION FOR LIFTING BODY TRANSITION STUDIES by S. R. Pate and J. C. Adams - ARO, Inc.	6-1
	Abstract	6-2
	Nomenclature	6-3
	Introduction	6-5
	Crossflow Parameters and Simulation Requirements	6-6
	Correlation of Transition with a Critical Crossflow Reynolds Number (X_{max})	6-8
	Transition and Crossflow Reynolds Numbers on a Supersonic Swept Wing	6-10
	Prediction of Upwash Angles and Entrained Vortices Leading to Transition	6-11
	Effects of Surface Roughness on Lifting Body Transition Locations	6-16
	Summary and Concluding Remarks	6-19
	References	6-21
7.	EFFECT OF TRANSITION ON THREE-DIMENSIONAL SHOCK WAVE-BOUNDARY LAYER INTERACTION by R. H. Korkegi - Wright-Patterson AFB	7-1
	Abstract	7-1
	Introduction	7-1
	Shock Interaction Due to Blunt Protuberances	7-2
	Shock Interaction Due to an Axial Compression Corner	7-3
	Concluding Remarks	7-4
	References	7-5
8.	HYPERSONIC SHOCK TUNNEL TRANSITION STUDIES by D. H. Ross, J. W. Ellinwood and R. L. Varwig - The Aerospace Corp.	8-1
	Task 1. Free Stream Turbulence Measurements	8-1
	Task 2. Stability Theory Calculations	8-3
	Task 3. Cone Surface Measurements	8-4
	Conclusion	8-4

CONTENTS (Continued)

9A.	OPEN QUESTIONS - TRANSITION TO TURBULENCE AT HIGH SPEEDS , 1971 by Mark V. Morkovin - Illinois Institute of Technology <i>and</i>	9a-1
	Abstract	9a-1
	Introduction	9a-2
	Factors in High-Speed Transition	9a-2
	Indeterminacy of High-Speed Transition, Paradoxes, and Discrepancies	9a-5
	Speculations on Possible Transition Research and Development	9a-14
	References	9a-18
	Appendices	9a-22
9B.	LESSONS FROM TRANSITION OF SHOCK-TUBE BOUNDARY LAYERS by Mark V. Morkovin - Illinois Institute of Technology	9b-1
	Abstract	9b-1
	List of Symbols	9b-2
	Introduction	9b-3
	Precritical Nature of Shock-Tube Transition	9b-3
	Transition Reversal and Re-reversals in Shock-Tubes	9b-4
	Disturbance Environment and Natural Transition	9b-6
	Finite Disturbances, Spots and Transition in Shock Tubes	9b-8
	Recapitulation and Prospects	9b-10
	References	9b-12

FIGURES

SESSION III

1-1.	Sensor Locations on the Double-Skin Model	1-23
1-2a.	Injectant Passageway in the Double-Skin Model	1-24
1-2b.	Porous Model Prior to Final Assembly	1-24
1-3a.	Measured "Similar" (Variable) Injectant Distribution	1-25
1-3b.	Measured Constant (Uniform) Injectant Distribution	1-26
1-4a.	Double-Skin Model in the Tunnel Test Section	1-27
1-4b.	Double-Skin Model with a Screen Overlay in the Tunnel Test Section	1-27
1-5.	Performance Envelope for Hypervelocity Wind Tunnel	1-28
1-6.	Comparison of the Heat-Transfer-Rate Distribution and the Shadowgraph for Condition 17	1-29
1-7.	Correlation of Transition Data for Slender Cones	1-30
1-8.	Comparison of the Experimental and the Theoretical Heat-Transfer-Rate Distribution	1-31
1-9.	The Variation of the Transition Reynolds Number with the Correlation Parameter of Ref. 11, Constant Mass-Injection Distribution	1-37
1-10.	The Variation of the Transition Reynolds Number with the Correlation Parameter of Ref. 11, "Similar" Mass-Injection Distribution	1-38
1-11.	The Effect of Screen-Type Surface Roughness on the Nonblowing Heat-Transfer-Rate Distribution	1-39
1-12.	The Effect of Mass-Injection on the Heat-Transfer-Rate Distribution for Roughened Cone	1-40
1-13.	The Effect of Mass-Injection on the Heat-Transfer-Rate Distribution for Roughened Cone	1-41

FIGURES (Continued)

2-1.	Sketch of Model Geometry	2-36
2-2.	Model Photograph	2-37
2-3.	Variation of Stanton Number with Free-Stream Reynolds Number	2-38
2-4.	Typical Temperature-Time Data for Blunt Test Model	2-39
2-5.	Variation of Stanton Number with Free-Stream Reynolds Number for Blunt Test Model	2-40
2-6.	Time History of Transition Region	2-41
2-7.	Transition Location History	2-42
2-8.	Effect of Wall Cooling on Local Transition Reynolds Number	2-43
2-9.	Variation of Free-Stream Transition Reynolds Number with Free-Stream Unit Reynolds Number and Nose Radius - NOL Data	2-44
2-10.	Variation of Free-Stream Transition Reynolds Number with Free-Stream Unit Reynolds Number and Nose Radius - Data of References 12-15	2-45
2-11.	Variation of Free-Stream Transition Reynolds Number Ratio with Bluntness Reynolds Number	2-48
2-12.	Comparison of NOL Sharp Cone Results with Pate Correlation	2-49
2-13.	Variation of Local Transition Reynolds Number with Bluntness Reynolds Number - NOL Data	2-50
2-14.	Variation of Local Transition Reynolds Number with Bluntness Reynolds Number - AVCO Data	2-51
2-15.	Variation of Momentum Thickness Transition Reynolds Number with Bluntness Reynolds Number - NOL and AVCO Data	2-52
2-16.	Variation of Swallowing Distance Parameter with Cone Angle, Mach Number, and Unit Reynolds Number	2-53

FIGURES (Continued)

2-17.	Variation of Local Transition Reynolds Number Ratio with Transition-to-Swallowing Distance Ratio - NOL Data	2-54
2-18.	Variation of Local Transition Reynolds Number Ratio with Transition-to-Swallowing Distance Ratio - AVCO Data	2-55
2-19.	Variation of Momentum Thickness Transition Reynolds Number Ratio with Transition-to-Swallowing Distance Ratio - NOL and AVCO Data	2-56
2-20.	Correlation of Local Transition Reynolds Number Ratio with Transition-to-Swallowing Distance Ratio	2-57
2-21.	Local Reynolds Number Distributions for Various Nose Radii and Altitudes Compared with Blunt Cone Transition Correlations	2-58
2-22.	Comparison of Local Reynolds Number Histories with Blunt Cone Transition Correlations at $S = 4$ ft	2-61
3-1.	Model Configuration, $\theta_c = 50^\circ$	3-13
3-2.	Typical profiles of Delrin models before launch and after recovery	3-14
	(a) $\theta_c = 30^\circ$, $V_o = 6.4$ km/sec	3-14
	(b) $\theta_c = 50^\circ$, $V_o = 4.9$ km/sec	3-14
3-3.	Total mass loss for Delrin cones	3-15
	(a) $\theta_c = 30^\circ$	3-15
	(b) $\theta_c = 50^\circ$	3-15
3-4.	Surface recession (averaged around periphery) on Delrin cones, $\theta_c = 30^\circ$, $p/p_o = 1$	3-16
	(a) $V_o = 5.03$ km/sec	3-16
	(b) $V_o = 5.37$ km/sec	3-16
	(c) $V_o = 5.95$ km/sec	3-16

FIGURES (Continued)

3-5.	Surface recession (averaged around periphery) on Delrin cones, $\theta_c = 30^\circ$	3-17
(a)	$V_o = 5.19$ km/sec, $p/p_o = 0.591$	3-17
(b)	$V_o = 5.80$ km/sec, $p/p_o = 2.72$	3-17
(c)	$V_o = 5.49$ km/sec, $p/p_o = 1.0$, $r_n/r_b = 0.07$	3-17
3-6.	Surface recession (averaged around periphery) on Delrin cones, $\theta_c = 50^\circ$	3-18
(a)	$V_o = 5.94$ km/sec (DDC-6 & DDC-9), $V_o = 6.10$ km/sec (LDC-1), $p/p_o = 3.1$	3-18
(b)	$V_o = 5.49$ km/sec (DDC-5), $V_o = 5.70$ km/sec (LDC-6), $p/p_o = 3.1$	3-18
(c)	$V_o = 4.88$ km/sec, $p/p_o = 3.1$	3-18
(d)	$V_o = 4.27$ km/sec, $p/p_o = 3.1$	3-18
(e)	$V_o = 4.27$ km/sec, $p/p_o = 4.1$	3-18
3-7.	Surface recession (averaged around periphery) on Lexan cones	3-19
(a)	$\theta_c = 30^\circ$	3-19
(b)	$\theta_c = 30^\circ$, $V_o = 6.31$ km/sec, $p/p_o = 0.399$	3-19
(c)	$\theta_c = 50^\circ$, $V_o = 4.12$ km/sec, $p/p_o = 3.14$	3-19
3-8.	Surface recession (averaged around periphery) on cones of different materials, $\theta_c = 30^\circ$	3-20
4-1.	Models	4-13
4-2.	Effect of wall cooling on boundary-layer transition	4-14
4-3.	Effect of angle of attack on transition; $\theta_c = 15^\circ$, $M_\infty = 7.4$	4-15
4-4.	Effect of angle of attack on transition; $\theta_c = 5^\circ$, $M_\infty = 7.4$	4-16

FIGURES (Continued)

4-5.	Effect of angle of attack and meridian angle on the length of the transition region; $M_{\infty} = 7.4$, $\theta_c = 15^\circ$	4-16
4-6.	Correlation of the beginning of transition; windward ray of cones	4-17
5-1.	Cones Used in Experiments	5-24
5-2.	Typical Cone Trajectory	5-25
5-3.	Some Published Data on the Influence of Angle of Attack on Transition Location	5-26
5-4a.	Effect of Angle of Attack on Transition Location, from Ward	5-27
5-4b.	Ward's (Modified) Data for 10-deg Semi-Angle Cone	5-28
5-5.	Roughened Cone	5-29
5-6.	Effect of Surface Roughness	5-30
5-7.	Laser-Front-Lighted Photograph of Cone in Flight at Mach 5	5-31
5-8.	Apparatus for Studying Vibrational Characteristics of Aluminum and Lexan Cones	5-32
5-9.	Strain Measurement Apparatus	5-33
5-10.	Vibrational Response of Aluminum and Lexan Cones	5-34
6-1.	Velocity Profiles in Three-Dimensional Boundary Layer Flow (from Ref. 9)	6-24
6-2.	Sharp Cone Geometry and Nomenclature	6-25
6-3.	Critical Crossflow Influence on the Boundary-Layer Transition Profile	6-26
6-4.	Correlation of Transition and Crossflow Reynolds Numbers	6-27
6-5.	Transition and Crossflow Reynolds Numbers on a Biconic 3-Percent Thick Supersonic Airfoil $M_{\infty} = 3$, $r = 24^\circ$ (from Ref. 9)	6-28
6-6.	Comparison of Calculated and Measured Vortex Angles at $\phi = 90^\circ$ on a Sharp Cone at Incidence	6-29

FIGURES (Continued)

6-7.	Maximum Crossflow Reynolds Number Distribution on Sharp Cones at Incidence	6-30
6-8.	Developed-Surface Plot Showing Onset to Vortex Formation Relative to Lines of Constant Maximum Crossflow Reynolds Number on Sharp Cones at Incidence	6-31
6-9.	Distribution of Upwash Angles and Maximum Crossflow Reynolds Numbers on a Sharp Cone at Incidence	6-33
6-10.	Effect of Wall Temperature on Calculated Maximum Crossflow Reynolds Number Distributions on a Sharp Cone at Incidence	6-34
6-11.	Heating Distributions and Transition Locations on MDAC STS Orbiter in VKF Tunnels B and F	6-35
6-12.	Observations of Transition on MDAC STS Orbiter Windward Surface in VKF Tunnels B and F	6-38
6-13.	Transition Reynolds Number on MDAC STS Orbiter in VKF Tunnels B and F	6-47
7-1.	Blunt Fin-Flat Plate Interaction - $d = 3/4$ in. (oil flow photographs from the study of Ref. 2)	7-6
7-2.	Blunt Fin-Flat Plate Interaction - $d = 1/8$ in. (oil flow photographs from the study of Ref. 2)	7-7
7-3.	Interaction in the Corner of Axially Intersecting Wedges (oil flow photographs from Ref. 3)	7-8
7-4.	Transitional Interaction Due to a Sharp Wedge on a Flat Plate at $M = 5$ (from Ref. 4)	7-9
8-1.	Hot-Film Probes and Cone-Cylinder Model	8-5
8-2.	Surface Temperature Traces	8-6
8-3.	Expanded Trace Showing Probe Temperature Fluctuations	8-7
8-4.	Analog Processed Heat Transfer and Fluctuations	8-8
8-5.	Power Spectrum of Free-Stream Turbulence	8-9

FIGURES (Continued)

8-6.	Stability Diagram	8-10
8-7.	Steady State Heat Transfer on Cone Model	8-11
9a-1.	Laminar Boundary Layer as a Linear and a Nonlinear Operator	9a-25
9a-2.	Transition Reynolds Number as Function of Free-Stream Disturbance Intensity. Courtesy: Spangler and Wells, Ref. 11	9a-26
9a-3.	Transition Sensitivity to Cooling in Various Wind Tunnels	9a-27
9a-4.	Transition on Cones in Flight in Terms of Local Reynolds Number and Local Cooling Ratio	9a-28
9a-5.	Transition on Cones in Flight in Terms of Local Mach Number and Local Reynolds Number	9a-29
9a-6.	Early Transition on Multipurpose Reusable Spacecraft at Mach Ten at Angles of Attack of 0°, 10°, 15°, and 20°. Courtesy: Young, Reda, and Roberge, Ref. 35	9a-30
9b-1.	Shock-generated laminar and turbulent boundary layer in laboratory coordinates	9b-14
9b-2.	Local transition Reynolds number as function of the cooling parameter	9b-15

TABLES

SESSION III

1-1	Model Summary Data	1-21
1-2	Test Condition Summary	1-22
2-1	Results for Sharp Through 16-Percent Blunt Models	2-33
2-2	Results for 32-Percent Blunt Model	2-34
2-3	Variable Temperature Results for Blunt Test Model	2-35
3-1	Mass Loss and Tip Radius Measurements	3-10
4-1	Test Conditions for Wall-Cooling Data	4-11
4-2	Test Conditions for Angle-of-Attack Data	4-12
5-1	Experiments on Effect of Angle of Attack on Transition	5-7
5-2	Frequency and Amplitude Data	5-15

(This page intentionally left blank)

SESSION III
RECENT GROUND TEST TRANSITION
DATA AND CORRELATION

SECTION 1

EFFECTS OF MASS ADDITION DISTRIBUTION AND ROUGHNESS ON BOUNDARY LAYER TRANSITION AT MACH 12* (Unclassified)

by C. J. Stalmach, Jr. and T. C. Pope
Vought Aeronautics Company
Dallas, Texas

J. J. Bertin
University of Texas at Austin
Austin, Texas

R. L. Wright
NASA Langley Research Center
Hampton, Virginia

ABSTRACT

Surface heat-transfer rates and pressures were measured at hypersonic speeds on sharp cones at zero angle of attack with and without gas injection. The non-injection results were employed as reference data for the definition of the effects of surface roughness and injectant rate, distribution and composition on transition location. For a given mass injection rate the transition location was sensitive to the injection distribution. The transition Reynolds numbers were significantly greater when the injection distribution was constant than when the distribution decreased rapidly with distance from the apex. Transition Reynolds number results obtained during this program with a variable injection distribution compared favorably with the limited amount of data available for a degrading model tested in a different facility.

*Sponsored by NASA Langley Research Center, Contract NAS1-9524

The transition measurements for a constant injection distribution were correlated with earlier wind tunnel results. Tests with screen-type roughness had a strong tripping action on the boundary layer that tended to mask any effects caused by low rates of mass addition combined with the roughness. The measured heating data and surface pressures were significantly affected by the cavity effect of this type of roughness.

INTRODUCTION

Several flow and model conditions influence boundary layer transition during hypersonic reentry. This paper will touch on the following two:

- (1) The influence of mass addition, particularly the effects of mass addition distribution, and
- (2) the influence of screen-type roughness, with and without mass addition.

This paper is based on heat-transfer-rate, surface pressure and shadowgraph data obtained on sharp cones in the Vought Aeronautics Company Hypervelocity Wind Tunnel during 1970. The analysis was performed at the University of Texas (Austin) and NASA Langley Research Center provided program support. Total

comprehensive program results are given in NASA CR 1908 (reference 1) which includes tabulations of boundary layer flow conditions and transition location for each run and the correlations of laminar and turbulent heating with mass addition parameters. Additional correlations of the heating and transition data are given in reference 2. Reference 3 served as a working report prior to the publication of reference 1 and provides added details of the analysis.

EXPERIMENTAL APPARATUS

Models: The sharp-nose conic models that were tested are summarized in Table I. No-injection measurements were made with 5 and 12-degree models to provide reference data. These models had an 0.004-inch thick nickel skin that was bonded to a solid insulating surface. The 12-degree porous models, used for mass addition tests, had an 0.008-inch thick porous outer skin of sintered nickel. Thermocouple junctions were obtained by spot welding 0.003-inch diameter chromel and constantan wires to the inner surface of the nickel skin of each model and provided the heat-transfer-rate measurements. The skins

were unsupported in the vicinity of the thermocouple junctions to minimize conduction losses. Figure 1 shows the thermocouple and static pressure orifice locations for a porous skin model and is typical of the instrumentation of the other models.

Two mass addition distributions were obtained with one basic model through the arrangement shown in Figure 2. The basic model had a single porous skin. The injectant was supplied to the nose region, where a portion of the mass rate exited the porous skin at a high velocity and the remainder entered the annular passageway between the porous skin and the supporting inner cone. The injectant then flowed through the remaining skin area at decreasing velocity with x . This simple model technique had been used in previous programs (reference 4, for instance) at VAC to provide reasonable approximations of a "similar" distribution, i. e., $\rho_w v_w = Cx^{-1/2}$. Those previous tests, however, were performed at a much lower static pressure at the cone surface. This apparently allowed supersonic expansion of the injectant within the annular passageway that resulted in a relatively smooth exponential decay of injection velocity if proper selections of skin porosity and gap configuration were made. The model static pressure in this study was twenty times higher than the earlier tests and, therefore, altered the internal expansion

process and produced a less desirable distribution as exemplified in Figure 3a. The velocity distribution was measured with a compensating hot wire system which was developed by VAC (reference 5) to provide good velocity resolution at relatively low static pressure levels. The sharp "dips" in the $\lambda = 135^\circ$ survey are caused by the presence of the pressure orifices.

A velocity distribution essentially constant with x , as shown in Figure 3b, was obtained by adding a second porous skin spaced slightly above the first skin of the basic model as illustrated in Figure 2a.

Roughness was added to the double-skin porous model by overlaying a conic skin fabricated from stainless screen. The geometries of the two screen overlays are defined in Table IB. Smooth and rough porous configurations are shown installed in the wind tunnel in Figure 4.

Test Conditions: The tunnel flow conditions of this program are shown in relation to the facility performance envelope in Figure 5. Most of the tests were conducted at Mach 12 and a Reynolds number per foot of 7×10^6 . This condition resulted in transition

on the conic models with no injection and the transition location remained within the instrumented region for essentially all injection rates tested. The injectants were nitrogen (N_2), methane (CH_4), and Freon-22 ($CHClF_2$). The rate of injection, C_i , is defined as the total flow rate through the porous skin non-dimensionalized by the freestream flow rate through an area equal to the model base area. The maximum injection rate tested was 2%. The run schedule shown in Table II summarizes the test conditions.

The facility is an arc-discharge tunnel with a variable-volume arc chamber which allows the flow properties to be maintained essentially constant during a run. Figure 5 reflects an increase in performance capability after a modification of the facility in 1971.

TEST RESULTS

Reference Data: The beginning and end of transition were measured by two rays of heat transfer sensors. The end of transition was also observed from shadowgraph photographs and agreed well with the heat transfer measurements as indicated in Figure 6.

No-injection transition results were obtained with the non-porous and the porous models at the same flow conditions as the subsequent mass injection tests (see Table II). These reference runs were compared to results available in the literature. The transition Reynolds numbers based on local flow properties at the edge of the boundary layer and the displacement thickness are given in Figure 7. The shadowgraph-determined locations compare favorably with the values obtained previously at VAC (reference 6). The data also compare favorably with the correlation from a summary of wind tunnel data which appeared in reference 7. Although Figure 7 represents a broad range of acceptable values of transition, it does show that transition data from the present program are consistent with previous results and, therefore, serves as a satisfactory reference to establish the effect of gas injection.

Heat-transfer data and theoretical laminar heating distributions are given in Figure 8 for several sample runs with a smooth outer skin. The theoretical distributions help determine the beginning of transition and were calculated using three different methods:

- (1) Eckert's reference temperature method (reference 8)
with the inviscid flow properties assumed constant

along the cone and computed using the sharp cone value of the pressure (reference 9), designated ERT, TP,

- (2) Eckert's reference temperature method with the inviscid flow properties computed assuming an isentropic expansion in accordance with the measured experimental pressure distribution, designated ERT, EP, and
- (3) a numerical routine (reference 10) developed at the University of Texas to solve the laminar boundary layer equations accounting for nonsimilar effects which are present with the inviscid flow properties computed assuming an isentropic expansion in accordance with the experimental pressure distribution, designated NONSIMBL, EP.

Figure 8a indicates that the three calculation methods and the experimental heating data agree well for the no-injection condition. The NONSIMBL, EP agreed well with the experimental data for most of the injectants, injection rates and injection distributions as indicated in Figures 8b-8e. High rates of Freon injection resulted in the poorest agreement as shown in Figure 8f.

The variable distribution promoted early transition as is indicated in Figure 8b. This figure also demonstrates the difficulty in accurately determining the beginning-of-transition location for early transition that begins near the first thermocouple.

Mass Distribution Effects: Effects of molecular weight and injection rate on heat-transfer-rate and transition location were measured and are reported in Reference 1. These effects are in agreement with other investigations. Correlations of the mass addition effect on the laminar and turbulent heat-transfer-rate are given in References 1 and 2.

An effort was made to correlate the transition Reynolds number data. The reduction in the transition Reynolds number for the tests with constant injection is presented in Figure 9 as a function of F, where

$$F = \frac{\int_{x_0}^{x_{tr}} \rho_w v_w dA}{\rho_\infty u_\infty A_{b, tr}} \quad (1)$$

a parameter suggested by Marvin and Akin (reference 11). Also included in Figure 9 is the correlation line

$$\frac{Re_{x, tr}}{Re_{x, tr, 0}} = 1 - 0.25 \left(\frac{MW_{str}}{MW_{inj}} \right)^{0.25} F \quad (2)$$

and the data of reference 11, which also were for a "constant" injection distribution but with different injection gasses and obtained from a different type of test facility. The beginning-of-transition location for the data presented from reference 11 were determined using the heat-transfer method. For the current test, the heat-transfer-rate determined transition Reynolds numbers for runs with injection were referenced to the transition Reynolds number with no injection obtained with the non-porous model. The shadowgraph value of the transition Reynolds numbers for the tests with injection were referenced to the transition Reynolds number with no injection obtained by using the shadowgraphs of the porous model with no injection. The philosophy of these choices is discussed in reference 3.

The data of Figure 9 indicate that the length of laminar flow decreases as the parameter F , modified by the usual molecular weight ratio, increases. These "constant" injection data are considered to be in relatively good agreement with the correlation of reference 11 wherein the injectants employed were air, argon and helium compared to the current test with nitrogen, methane and Freon-22.

Data for the "similar" or variable mass-injection distribution are shown in Figure 10. It is evident that this distribution causes a significantly greater reduction in the transition Reynolds number for a given amount of mass injection (integrated to the transition location). It seems logical that the relatively large local injection into the thin viscous layer near the apex would accentuate the destabilizing effect of injection.

Data from reference 12 are also presented in Figure 10. Since these data are from an ablating cone of paradichlorobenzene, the amount of gas injected into the boundary layer is dependent on the local heat transfer rate, i. e., the mass injection rate is a function of x and is greatest near the apex. Thus, the distribution of reference 12 is of a somewhat similar nature to the variable injection distribution of the present program. However, the non-degrading region near the apex represented 23% of the ablating models of reference 12, but only about 4% of the models of the present program were non-porous. The agreement between the data of reference 12 and those of the present program is considered to be relatively good (Figure 10), considering the differences between the two tests and the limited amount of data for this distribution.

Roughness Combined with Mass Addition: For a degrading ablative thermal protection system, the surface roughness poses an ill-defined, time-dependent problem. In an attempt to simultaneously simulate both the roughened surface of the degrading ablator and the gaseous injection of the ablation process, fine screens were overlayed on the porous skin of the 12° cone which had a constant injectant distribution (as shown in Figure 3b). The dimensional characteristics of the two screens which were used are given in Table I. The length-to-depth ratios were approximately constant for the elements of the K_1 and K_2 screens. The diameter of the finer screen wire was approximately equal to the computed value of the displacement thickness at the first thermocouple for the smooth model and was approximately one-fourth the computed displacement thickness for the last thermocouple of the smooth model.

Static pressure and heat-transfer-rate measurements were obtained for the test conditions of Table II on the surface of the skin, i. e., measurements on the floor of the cavities formed by the screen overlay. The pressure results are given in References 1 and 3 and agree with that expected for flow over cavities.

Heat-transfer-rate data are shown in Figures 11, 12 and 13 for the K_1 and K_2 screens, Reynolds numbers per foot of 3×10^6 and 7×10^6 and $C_i=0$ and $C_i=0.3\%$ methane injection. Laminar theory for a smooth cone is shown for reference. For clarity of discussion, experimental fairings are also indicated for the heating rates as measured on the floor of the cavities. Figure 11 indicates agreement in "laminar" heating rates for the two different roughness heights for the no-injection case, possibly because of the similar length-to-depth ratio of the screen elements. Both screens greatly reduced the transition Reynolds number, since for this lower free-stream Reynolds number the smooth model was completely laminar. The larger diameter screen, K_2 , caused earlier transition than K_1 as indicated in Figure 11.

The injection of fairly low rates of methane through both of the roughness models tended to lower the "laminar" heating but did not show any change in transition location or the "turbulent" heating level for the two Reynolds numbers tested as indicated in Figures 12 and 13.

The screen overlay form of roughness was used to explore the feasibility of this simple means of providing a controlled

roughness on a porous model. Because of the strong tripping action observed, future tests with combined roughness and mass injections should consider a graduated degree of roughness. Grooving of the porous model should also be considered such that the heat transfer measurements are obtained on the extremities of the model surface and thus avoid the difficulties in interpreting the heating rates on the floor of a shallow cavity. Grooving may also improve the simulation of reentry roughness. Controlled grooving, or graduated screens, obviously will be more difficult to achieve than the technique reported.

CONCLUSIONS

The following conclusions are made for the data presented in this paper. Additional conclusions from this test program are found in reference 1.

1. The agreement between the theoretical and the experimental heat-transfer rate in the laminar region was acceptable, with the exceptions of the heat-transfer data for the higher rates of Freon injection and for screen overlaid roughness models.

2. For a given mass injection rate in a given distribution the transition Reynolds number decreases as the molecular weight of the injectant decreases.
3. For a given injectant in a given distribution the transition Reynolds number decreases as the injection rate increases.
4. The heating rate distributions confirmed that the shadowgraphs reliably locate the end of transition and that turbulent bursts were normally located in the transition zone.
5. For a given mass injection rate (integrated over the surface of the entire cone), the transition location is sensitive to the mass injection distribution. The transition Reynolds numbers were significantly greater when the local injection rate was constant over the surface of the cone, i. e., $\rho_w v_w = C$, than when the local injection rate decreased rapidly with distance from the apex.

6. Transition Reynolds number results obtained with a constant injection distribution correlated well with previously published results for other gases in a different facility.
7. Transition Reynolds number results obtained with a variable injectant distribution were correlated with a limited amount of data available for a degrading model tested in a different facility.
8. Screen-type roughness over the model surface greatly reduces transition Reynolds number.
9. Low levels of methane injection through relatively large screen-type roughness had little effect on transition location compared to the roughness model without injection.

REFERENCES

1. C. J. Stalmach, J. J. Bertin, T. C. Pope, and M. H. McCloskey, A Study of Boundary Layer Transition on Outgassing Cones in Hypersonic Flow, NASA CR-1908 (November 1971).
2. J. J. Bertin, M. H. McCloskey, C. J. Stalmach, and R. L. Wright, Effect of Mass-Addition Distribution and Injectant on Heat Transfer and Transition Criteria, to be presented at AIAA 10th Aerospace Sciences Meeting (January 1972).
3. J. J. Bertin, et al., A Study of Boundary Layer Transition on Outgassing Cones in Hypersonic Flow, Parts I, II and III. Aerospace Engineering Reports 71001, 71002 and 71004, University of Texas at Austin (February 1971).
4. C. J. Stalmach, J. L. Lindsey, and T. C. Pope, Hypersonic Aerodynamic Measurements on a 10° Cone with Oscillatory Mass Addition. AIAA Paper 70-217 (January 1970).
5. D. R. Moore, C. J. Stalmach, T. C. Pope and J. E. Jenkins, Dynamic Stability Wind-Tunnel Tests of a 10° Cone with Simulated Ablation at $M=17$. AIAA Journal, pp 1372-1385 (August 1967).
6. C. J. Stalmach, and J. J. Bertin, A Proposed Study of Boundary Layer Transition of Outgassing Cones in Hypersonic Flow. LTV Aerospace Report 2-59740/8R-2514 (July 1968).
7. E. M. Sullivan, W. D. Ericson, G. L. Smith, and J. T. Suttles, Some Aspects of Interplanetary Earth Simulation. Presented at the 15th Institute of Environmental Sciences, Anaheim, California (April 1969).
8. E. R. G. Eckert, Engineering Relations for Friction and Heat Transfer to Surfaces in High Velocity Flow. Journal of the Aeronautical Sciences, Vol. 22, No. 8, pp 585-587 (August 1955).

9. Ames Research Staff, Equations, Tables, and Charts for Compressible Flow. NACA Report 1135 (1953).
10. J. J. Bertin and O. E. Byrd, Jr., The Analysis of a Nonsimilar Boundary Layer - A Computer Code (NONSIMBL). University of Texas at Austin, Aerospace Engineering Report 70002 (August 1970).
11. J. G. Marvin, and C. M. Akin, Combined Effects of Mass Addition and Noise Bluntness on Boundary-Layer Transition. AIAA Journal, Vol. 8, No. 5 (May 1970).
12. M. C. Fischer, An Experimental Investigation of Boundary Layer Transition on a 10° Half-Angle Cone at Mach 6.9. NASA TN-5766 (April 1970).

NOMENCLATURE

A	area
$A_{b, tr}$	circular area of cone at point of transition
C	constant
C_i	dimensionless, total flow rate through the porous skin $\int \rho_w v_w dA / \rho_\infty u_\infty \pi r_b^2$
F	injection correlation parameter $\int_{x_0}^{x_{tr}} \rho_w v_w dA / \rho_\infty u_\infty (A_{b, tr})$
M	Mach number
MW	molecular weight
\dot{q}	local heat transfer rate
r	radius
$Re_{x, tr}$	Reynolds number integrated over the wetted distance to the transition location
$Re_{x, tr, 0}$	no-injection value of Reynolds number integrated over the wetted distance from the apex to the transition location
$Re_{\delta^*, tr}$	transition Reynolds number based on inviscid flow properties and displacement at the transition location
$Re_{\infty/ft}$	free-stream unit Reynolds number
u	velocity parallel to cone surface
v	velocity normal to cone surface
x	distance from apex measured along conical surface
x_0	length of non-porous tip

x_L	total length along the cone surface
x_{tr}	distance from apex to transition location
z	distance from apex measured along cone centerline
θ_c	semi-vertex angle of cone
λ	instrumentation ray
ρ	density

Subscripts

b	base
e	value at edge of boundary layer
w	wall value
∞	free-stream value
inj	injectant gas
str	stream gas

Superscripts

—— average value

TABLE I. - MODEL SUMMARY DATA

A. Basic Models

Skin Material	Skin Thick- ness In.	θ_c deg.	Base Diameter In.	No. of Sensors on Primary Heat Transfer Ray	Injectant Dist.
Solid Nickel	0.004	5.0	2.615	15	-
Solid Nickel	0.004	12.0	3.950	15	-
Sintered Nickel (Porous, Single Skin)	0.008	12.0	3.950	20	Variable
Sintered Nickel (Double, Porous Skin)	0.008	12.0	4.028	20	Constant

Primary heat transfer ray was $\lambda = 0^\circ$ for all models
 Primary pressure ray (secondary heat transfer ray)
 was $\lambda = 135^\circ$ for all models except the last which was
 $\lambda = 225^\circ$

B. Screen Overlays

Overlay	Wires/inch	Wire Diameter in.	Cavity length/ depth
K ₁	28	0.005	6.1
K ₂	14	0.009	6.9

TABLE II. - TEST CONDITION SUMMARY

Condition No.	Run No.	M_{∞}	$Re_{\infty}/ft. \times 10^{-6}$	T_{t_e} °K.	C_i %	Injectant	θ_c Deg.	Distribution	Skin
1	22, 23	11.6	6.70	1870	-	-	5	-	Solid
2	21	11.6	3.17	1970	-	-		-	
3	19, 20	13.8	3.51	1520	-	-	12	-	
4	10, 11	11.5	5.30	1920	-	-		-	
5	12, 13	11.7	2.76	1990	-	-		-	
6	14, 15, 18	14.0	3.64	1480	-	-		-	
7	4	11.9	6.13	1790	0.00	-		Variable	Single, Porous
8	6, 3	11.9	5.34	1847	0.35	N ₂			
9	2, 7	12.0	5.69	1872	0.70				
10	5	12.0	6.34	1740	2.10	CH ₄		Constant	Double, Porous
11	41	11.7	6.19	1902	0.33				
12	42	11.8	6.24	1863	0.67	-		-	
13	29, 35	11.8	6.35	1851	0.00	CHClF ₂		Constant	
14	40	12.2	7.91	1602	0.32	-			
15	38	11.9	6.33	1857	0.66				
16	39	11.9	6.63	1811	2.03	N ₂			
17	31	11.9	6.77	1803	0.32				
18	34	11.8	6.72	1832	0.63				
18a	30	11.7	6.36	1881	0.80				
19	36, 37	11.8	6.52	1832	1.95	-		-	
20	50	11.9	7.50	1709	0.00	CH ₄		Constant	Double, porous +K ₁
21	49	11.9	7.30	1729	0.31	CHClF ₂		Constant	Double, porous +K ₁
22	52, 53	11.7	6.33	1873	0.33				Double, porous
23	54, 55	11.8	6.67	1836	0.17	CH ₄			
24	56	11.7	6.11	1898	1.32			-	
25	58	11.8	3.21	1921	0.00	-		Constant	Double, porous +K ₂
26	59	11.8	3.35	1876	0.25	CH ₄			
27	45	11.8	3.40	1813	0.52			Constant	Double, Porous
28	57	11.8	3.26	1872	1.04				
29	48	11.9	3.58	1784	0.00	-		-	Double, porous +K ₁
30	43	12.0	3.34	1831		-		-	Double, Porous
31	44	12.0	3.56	1768	0.26	CH ₄		Constant	Double, porous +K ₁
32	46, 47	11.8	3.40	1848					

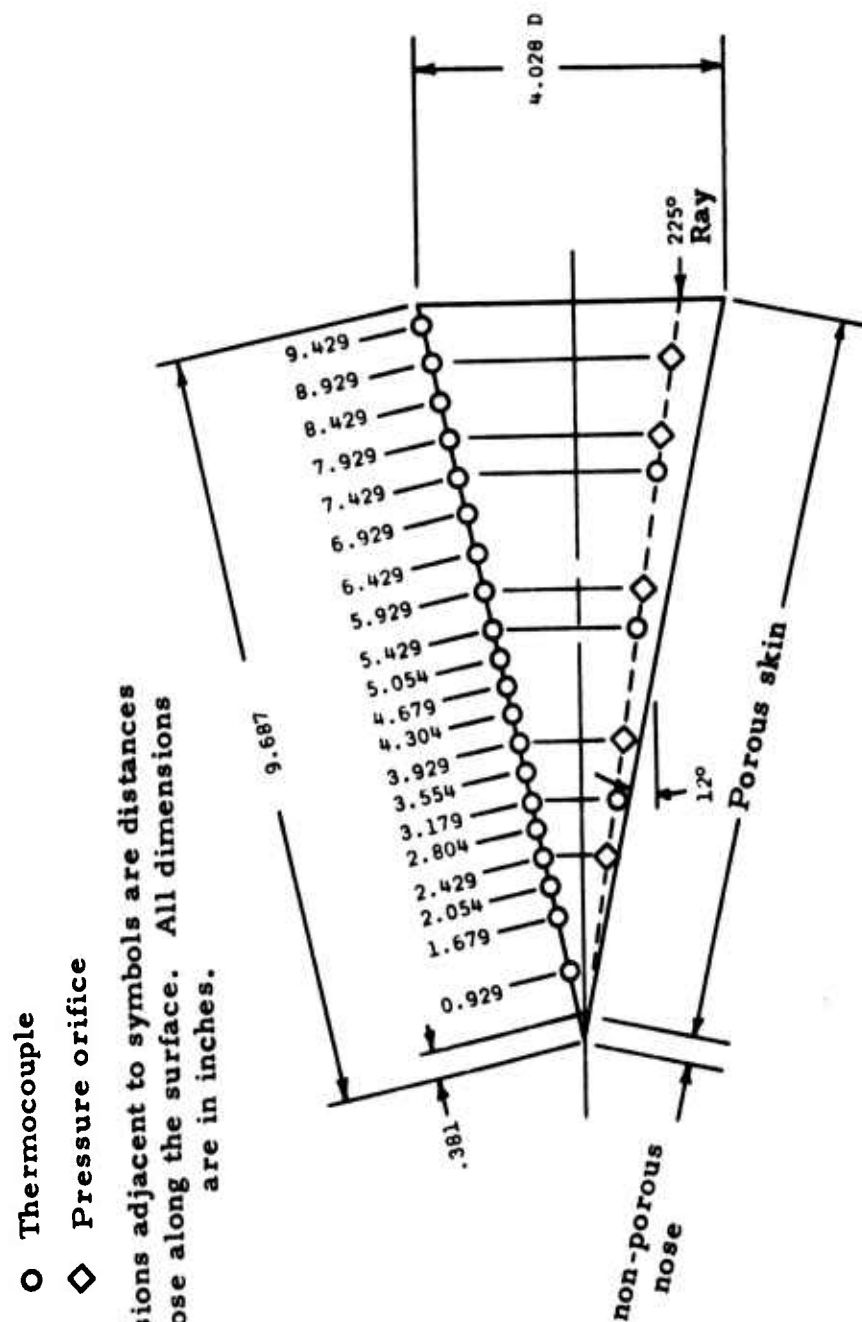


FIGURE 1 SENSOR LOCATIONS ON THE DOUBLE-SKIN MODEL

All Dimensions in Inches

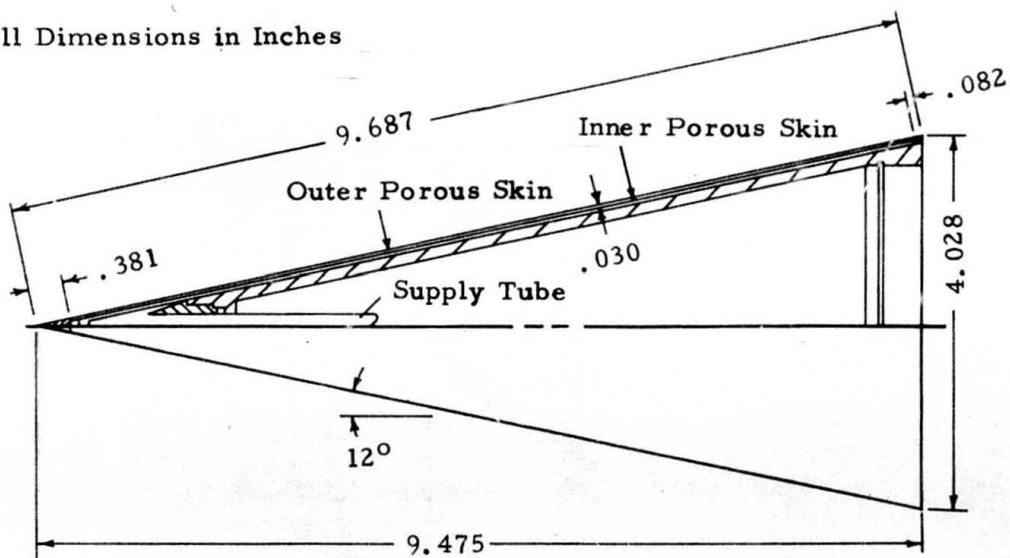


FIGURE 2a INJECTANT PASSAGEWAY IN THE DOUBLE-SKIN MODEL

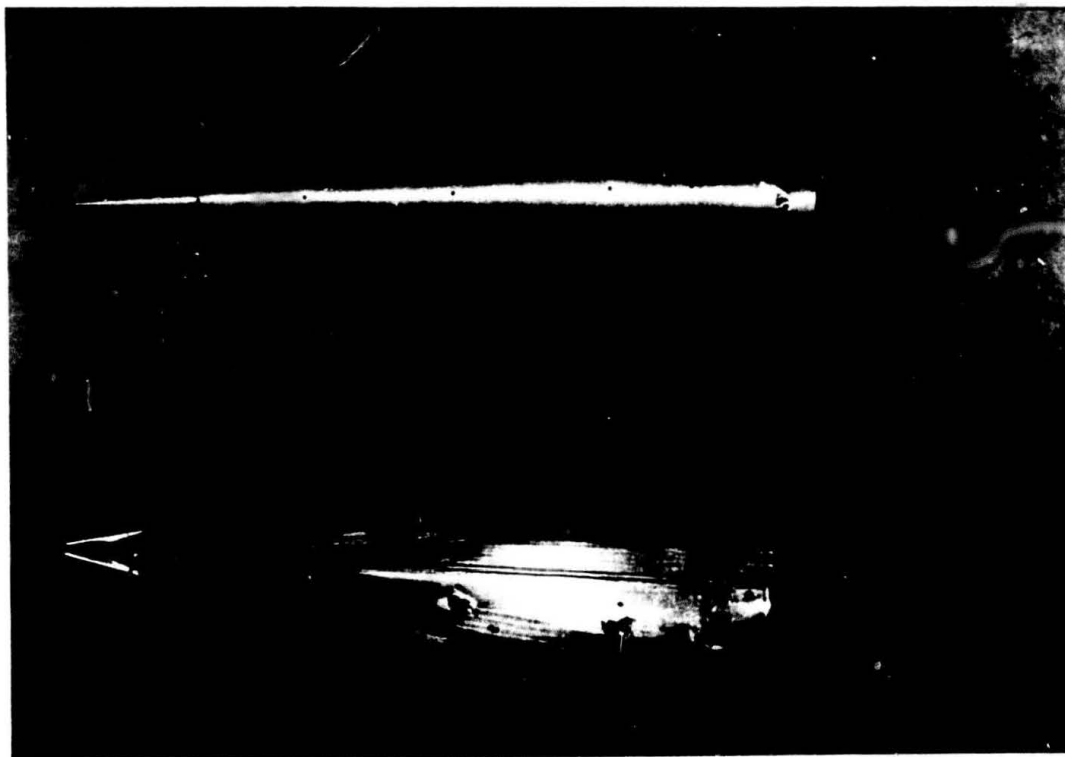


FIGURE 2b POROUS MODEL PRIOR TO FINAL ASSEMBLY

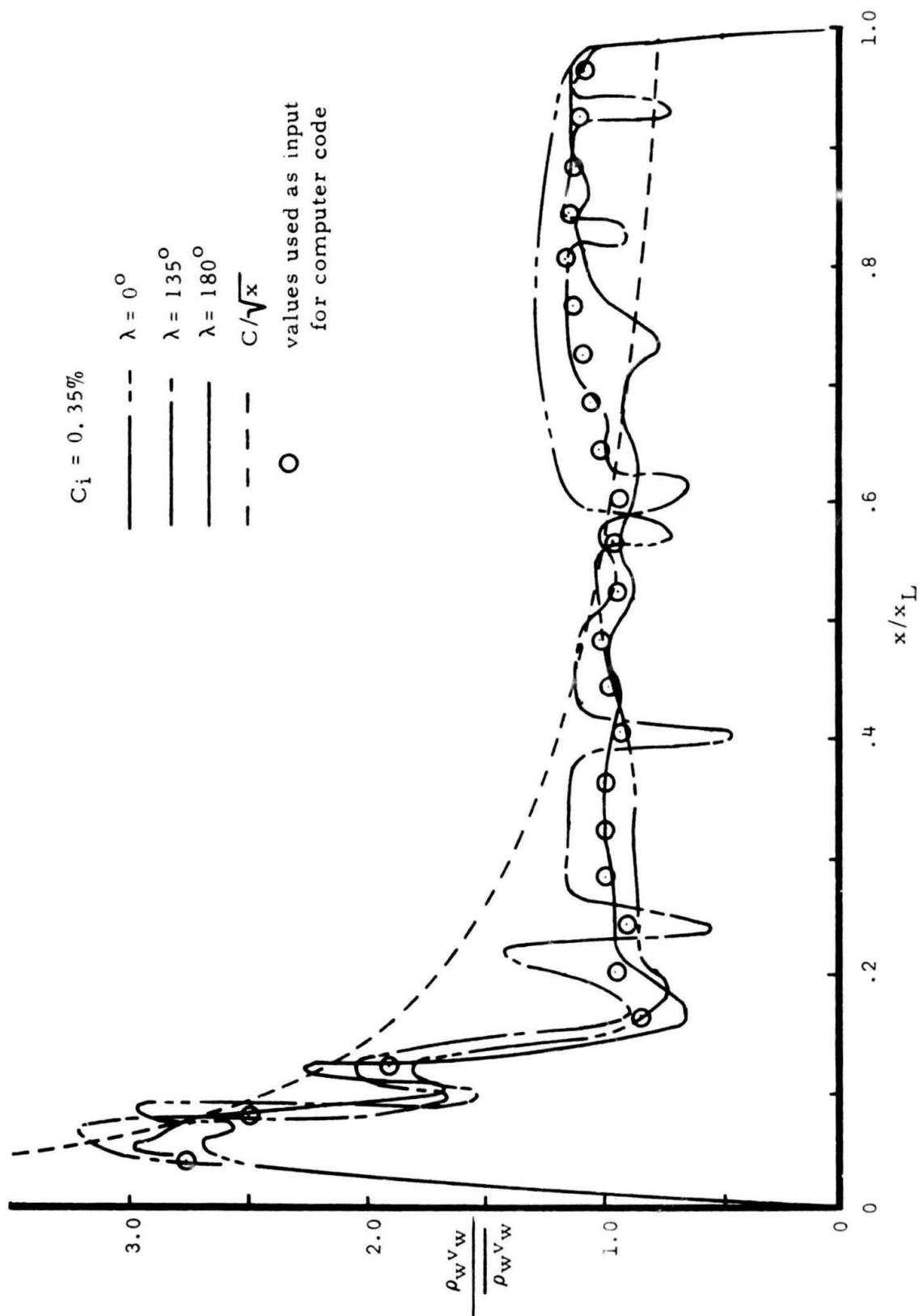


FIGURE 3a MEASURED "SIMILAR" (VARIABLE) INJECTANT DISTRIBUTION

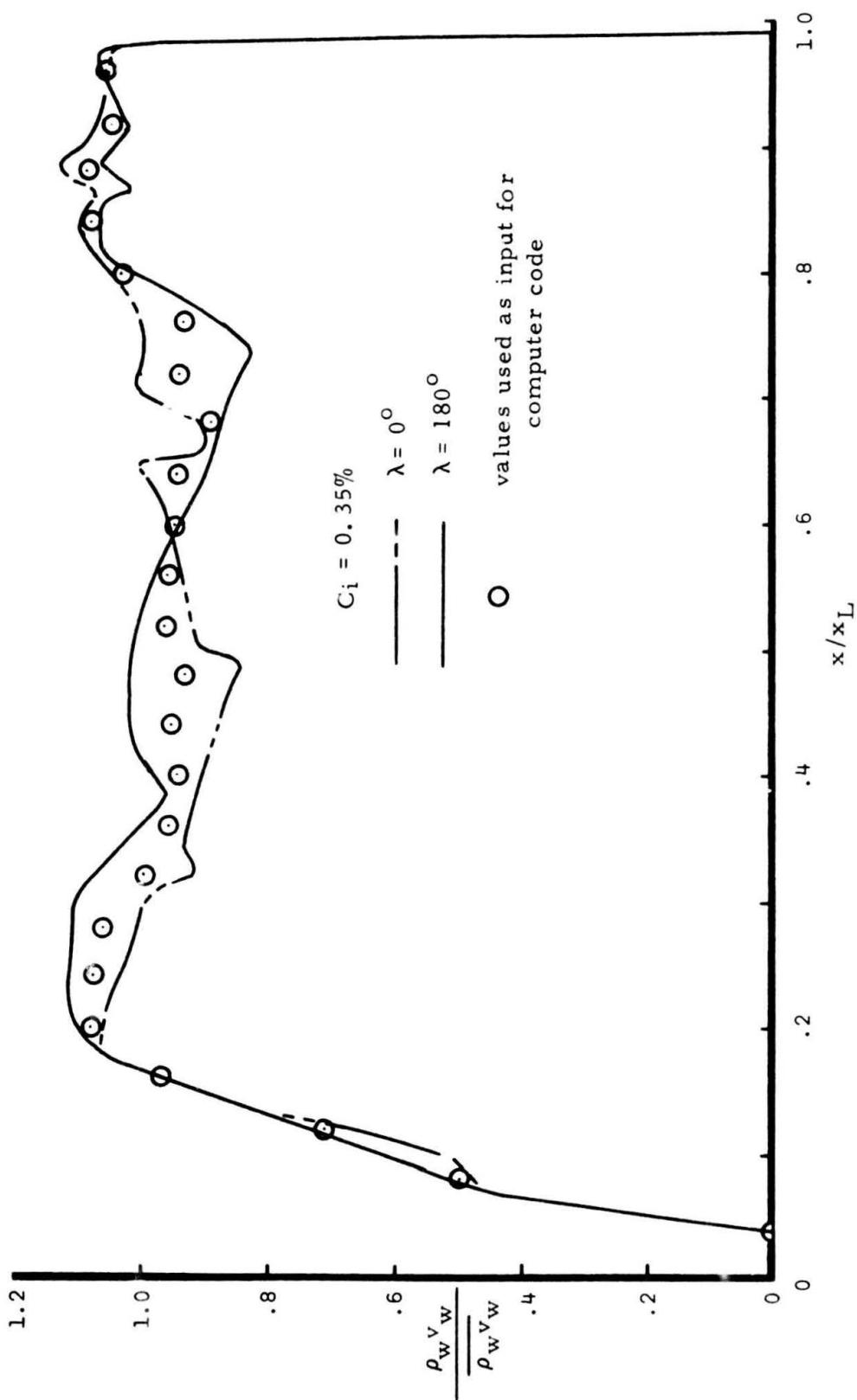


FIGURE 3b MEASURED CONSTANT (UNIFORM) INJECTANT DISTRIBUTION

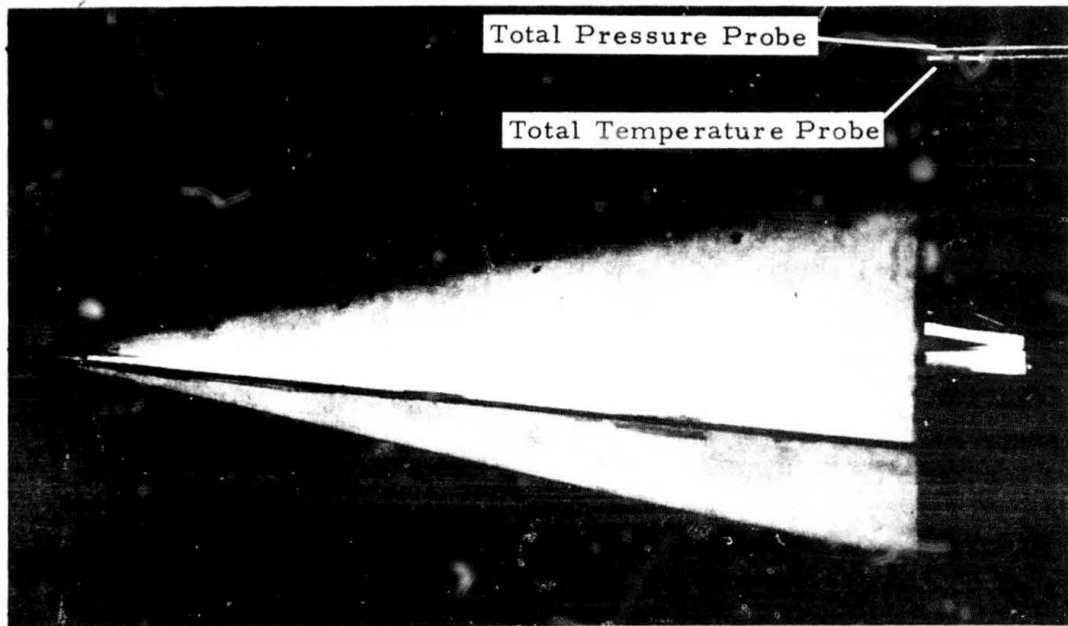


FIGURE 4a DOUBLE-SKIN MODEL IN THE TUNNEL TEST SECTION

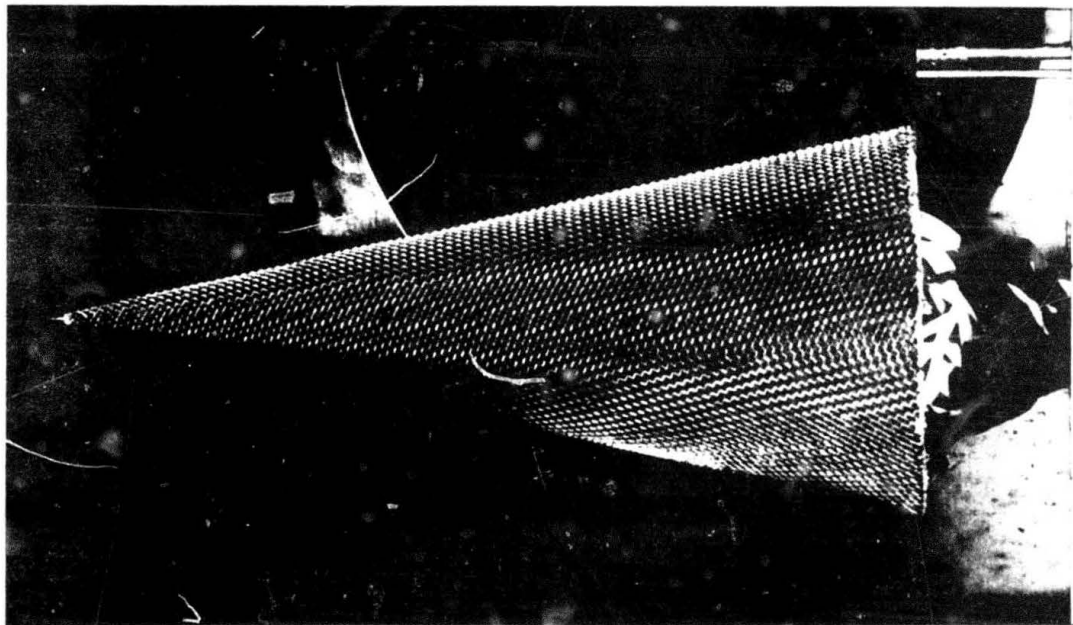


FIGURE 4b DOUBLE-SKIN MODEL WITH A SCREEN OVERLAY IN THE TUNNEL TEST SECTION

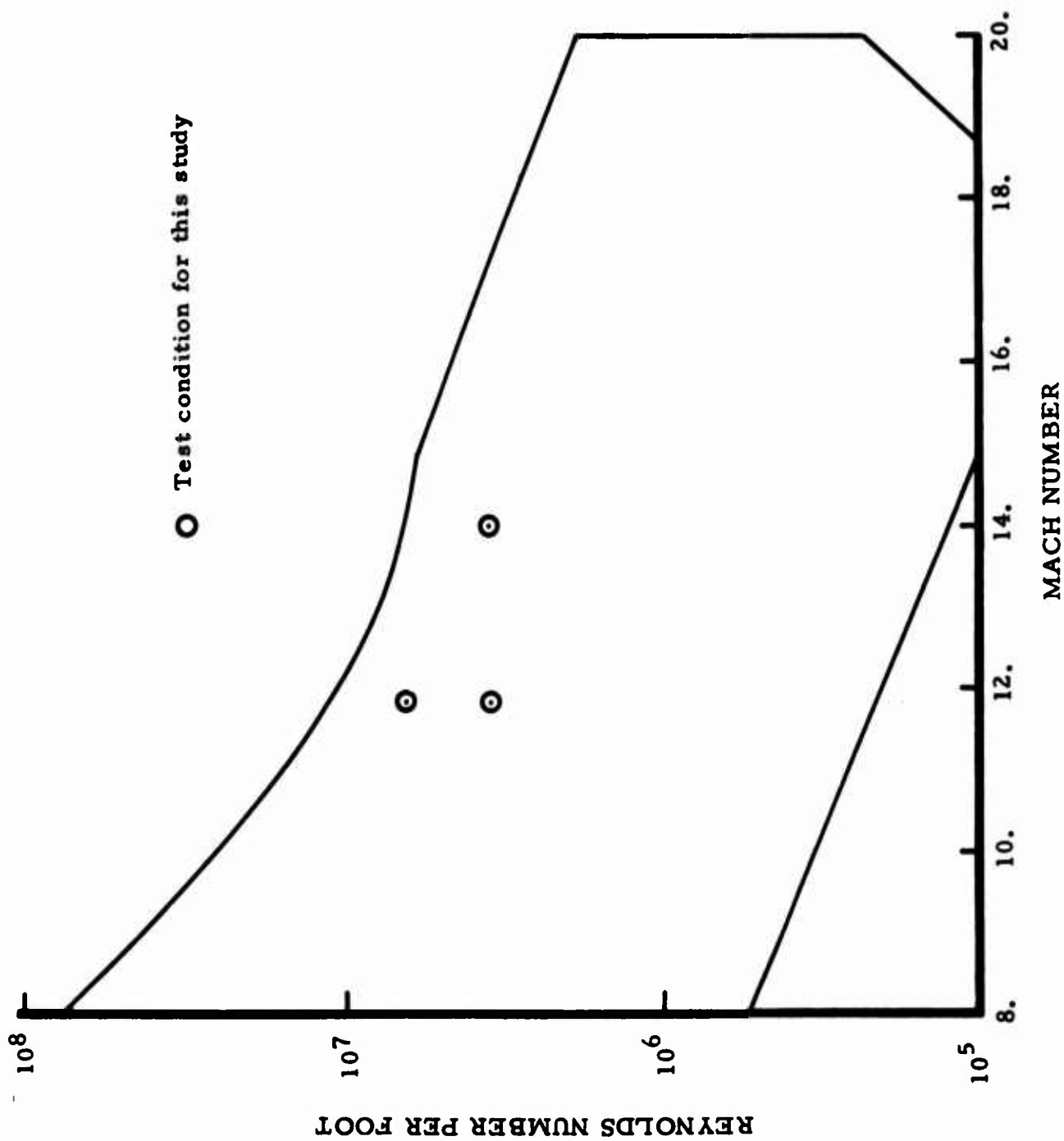


FIGURE 5 PERFORMANCE ENVELOPE FOR HYPERVELOCITY WIND TUNNEL

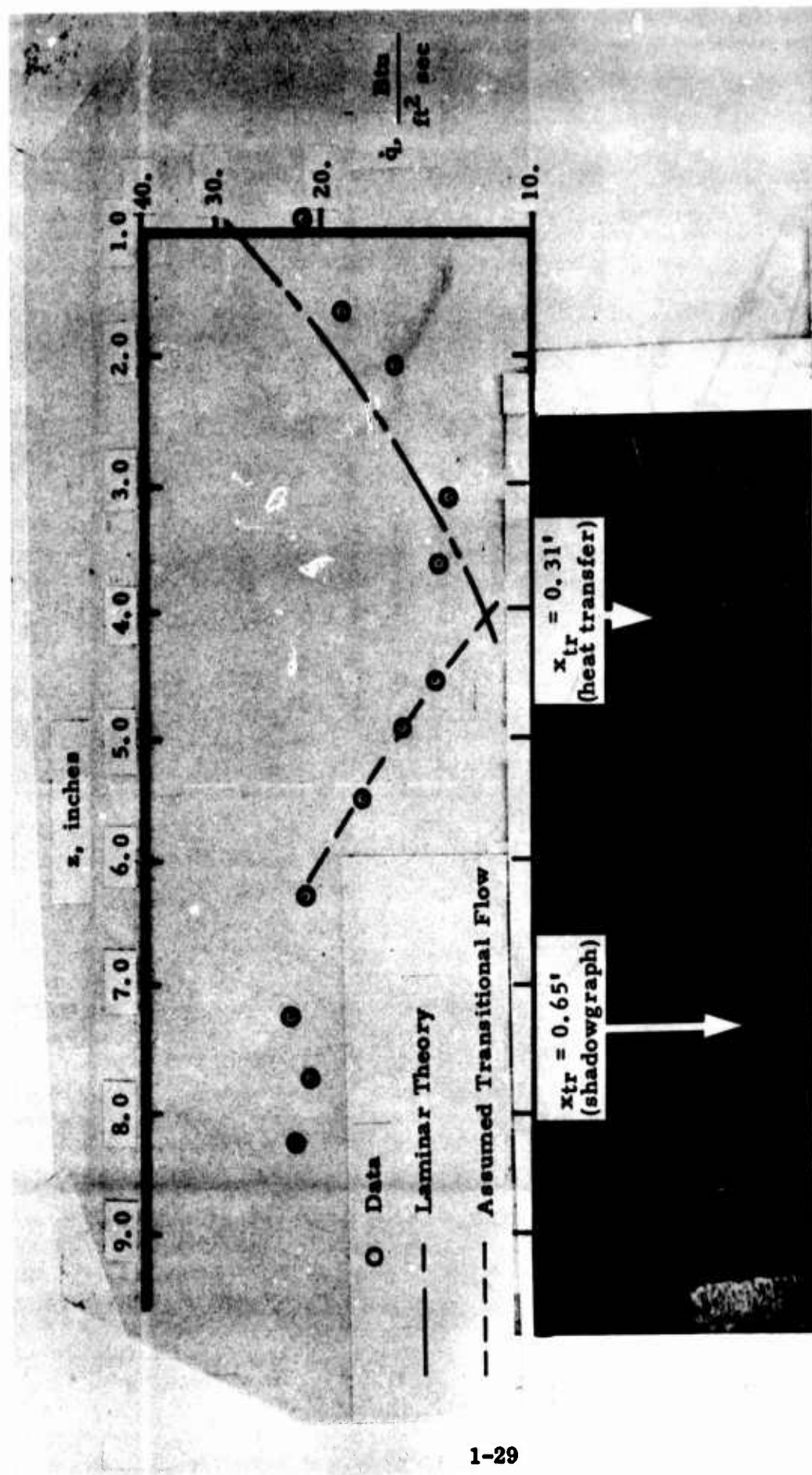


FIGURE 6 COMPARISON OF THE HEAT-TRANSFER-RATE DISTRIBUTION AND THE SHADOWGRAPH FOR CONDITION 17, $M_\infty = 11.9$, $Re_\infty / \text{ft} = 6.77 \times 10^6$, $C_i = 0.32\%$, UNIFORM NITROGEN INJECTION

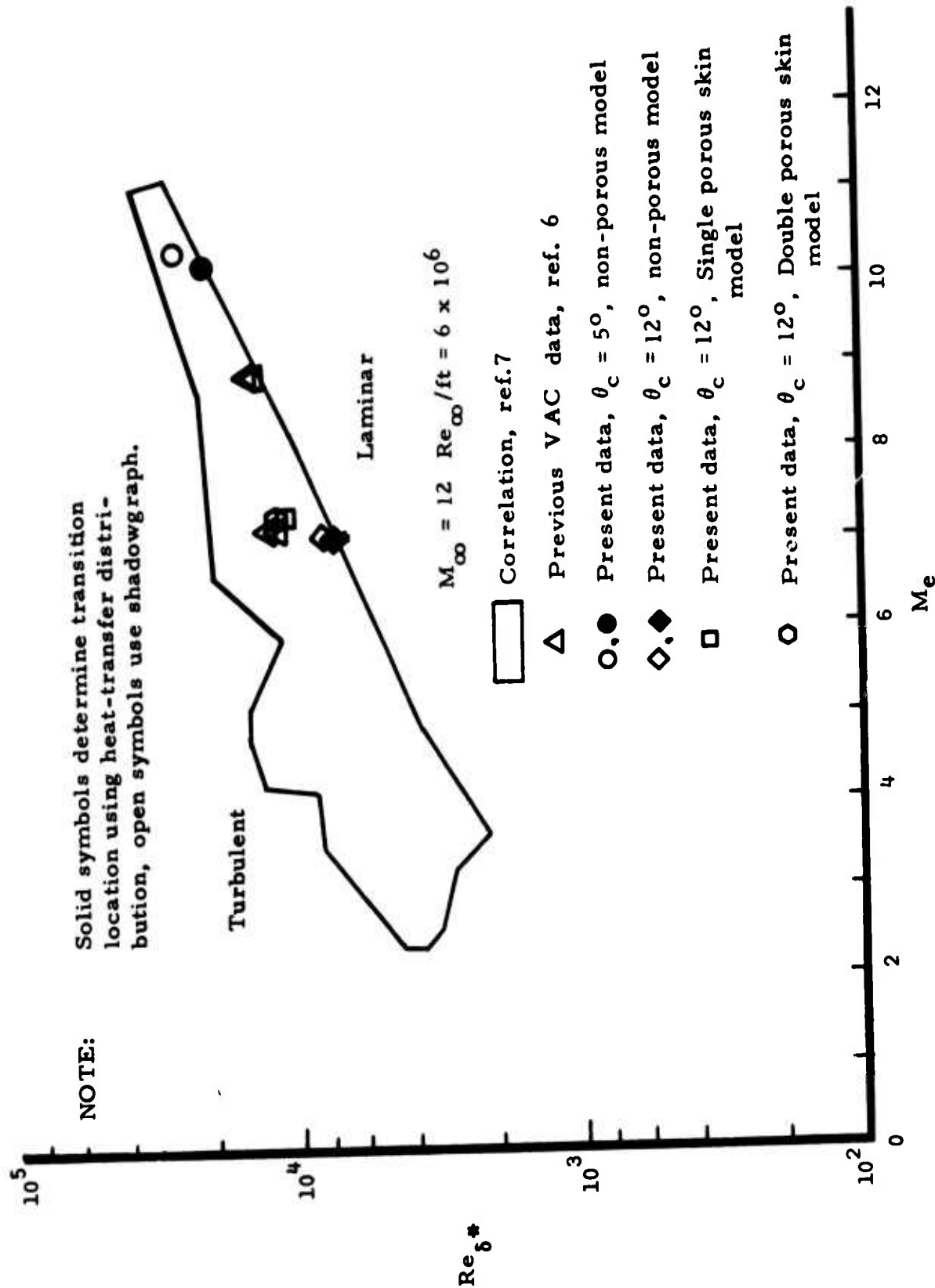
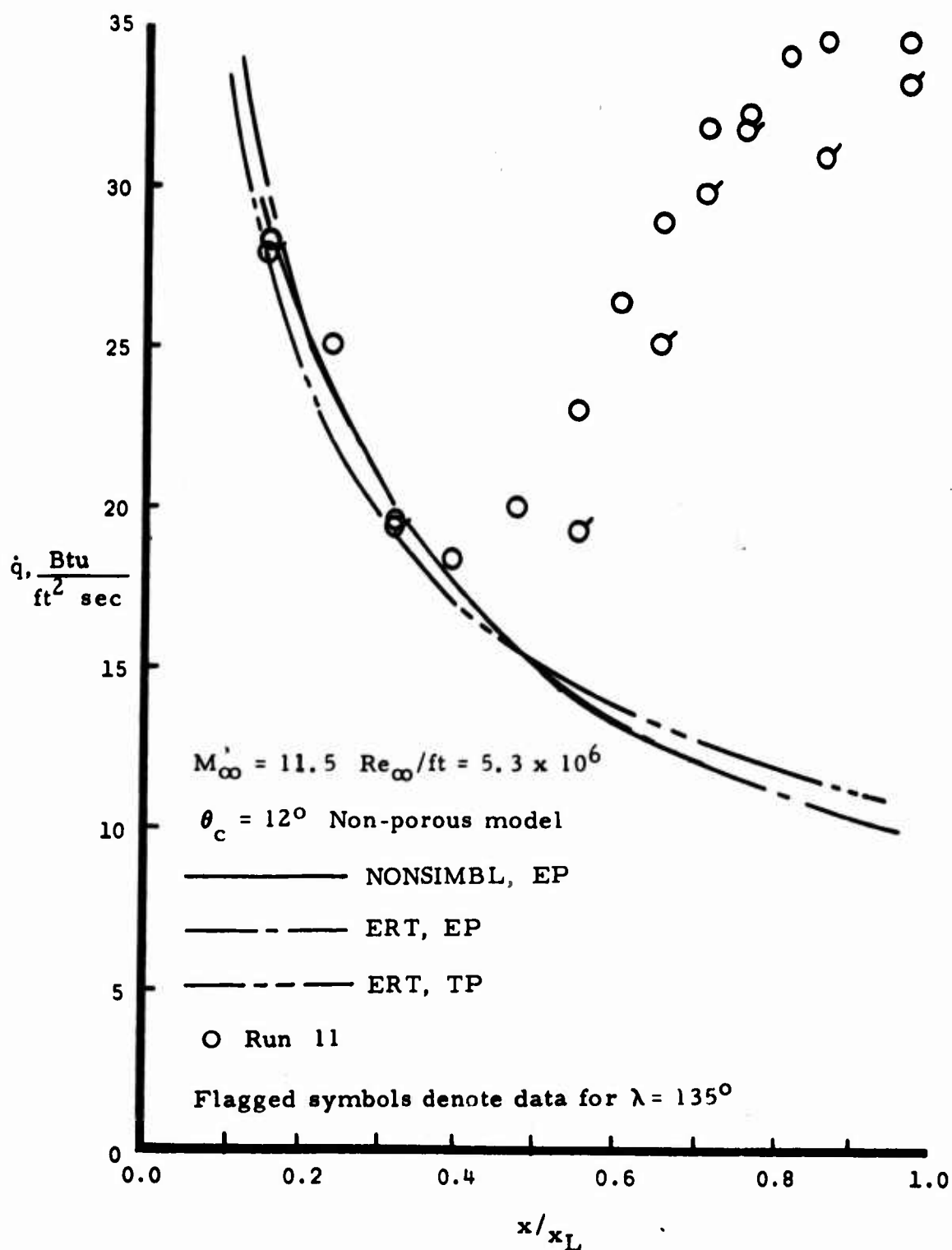
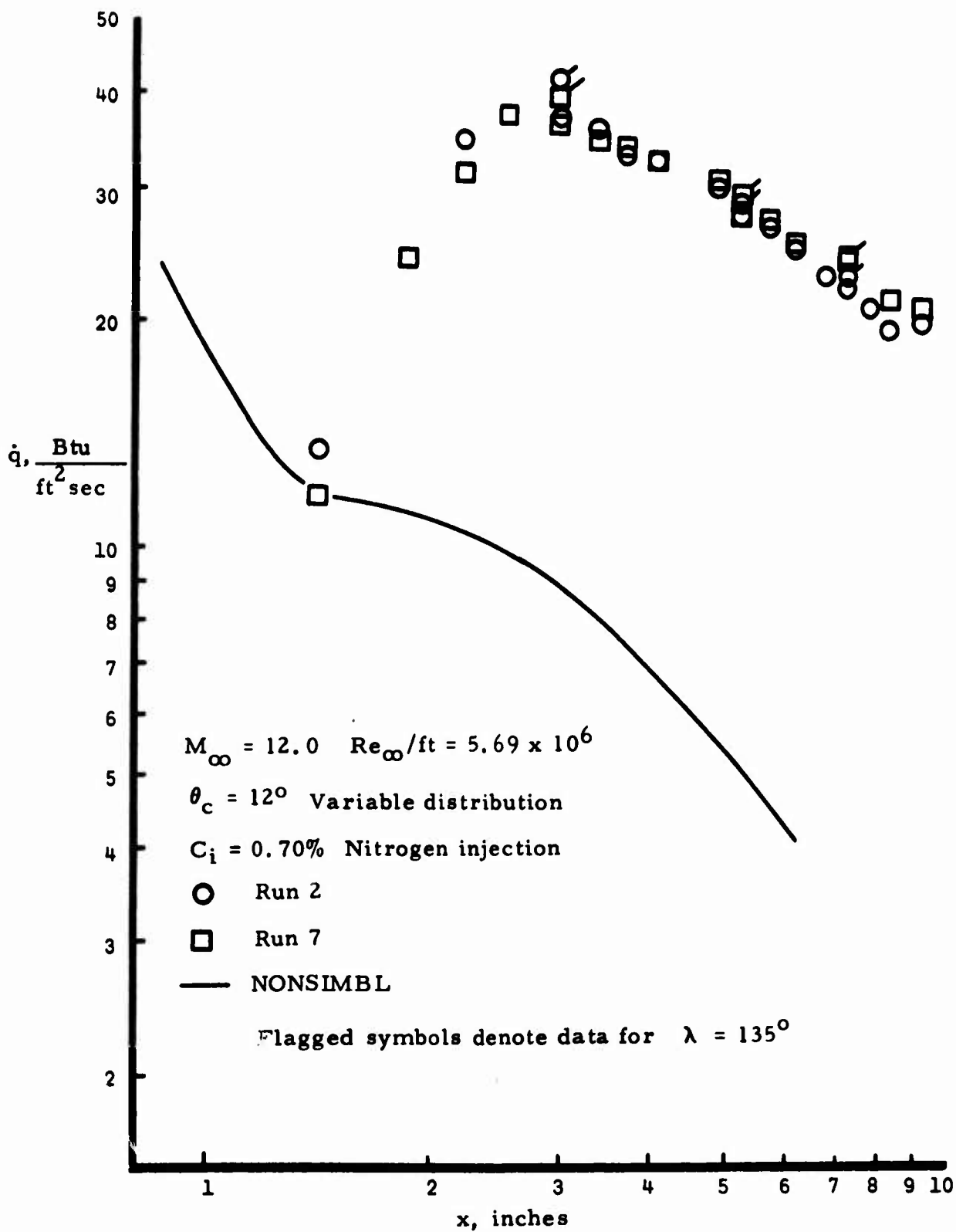


FIGURE 7 CORRELATION OF TRANSITION DATA FOR SLENDER CONES



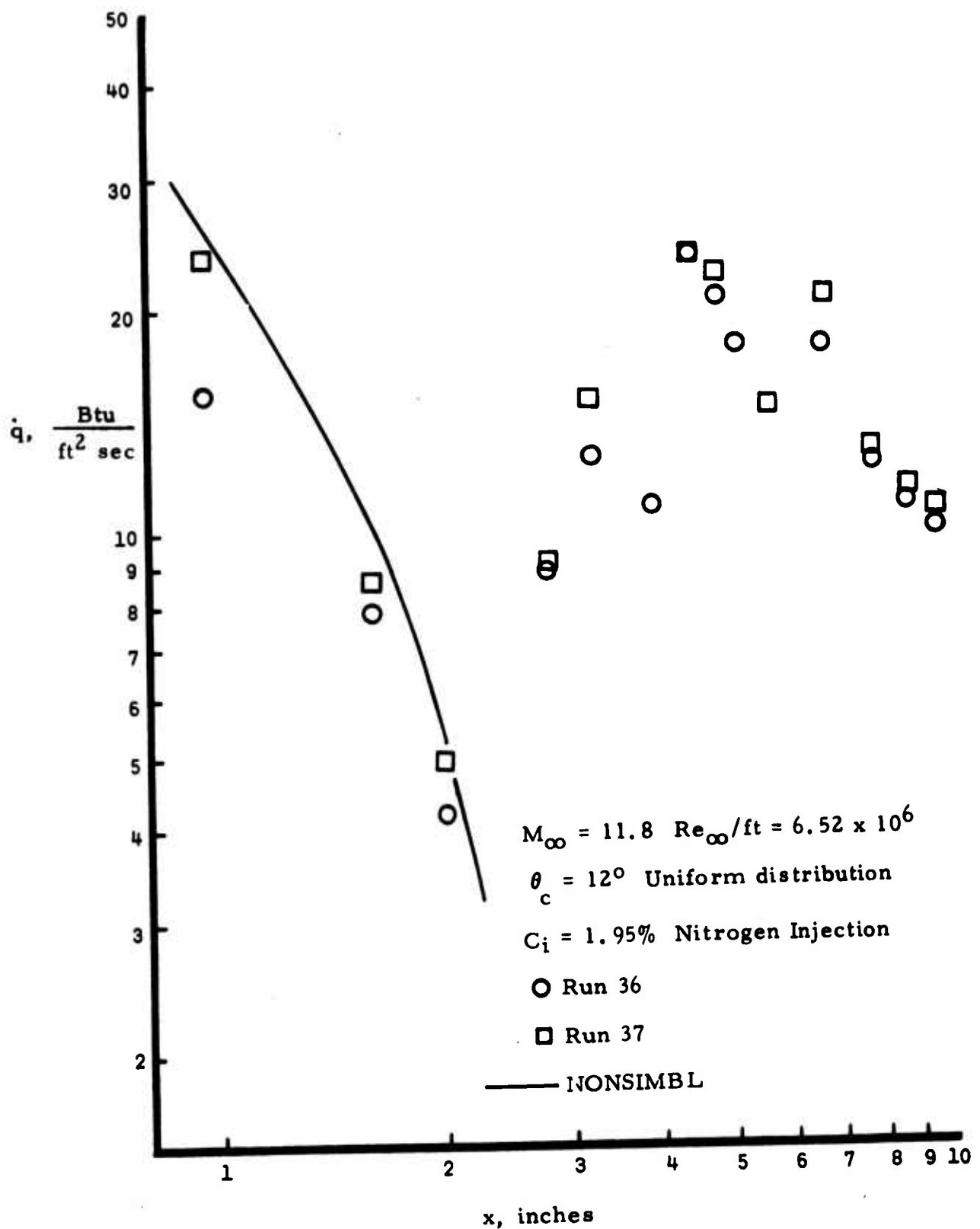
(a) Condition 4

FIGURE 8 COMPARISON OF THE EXPERIMENTAL AND THE THEORETICAL HEAT-TRANSFER-RATE DISTRIBUTION

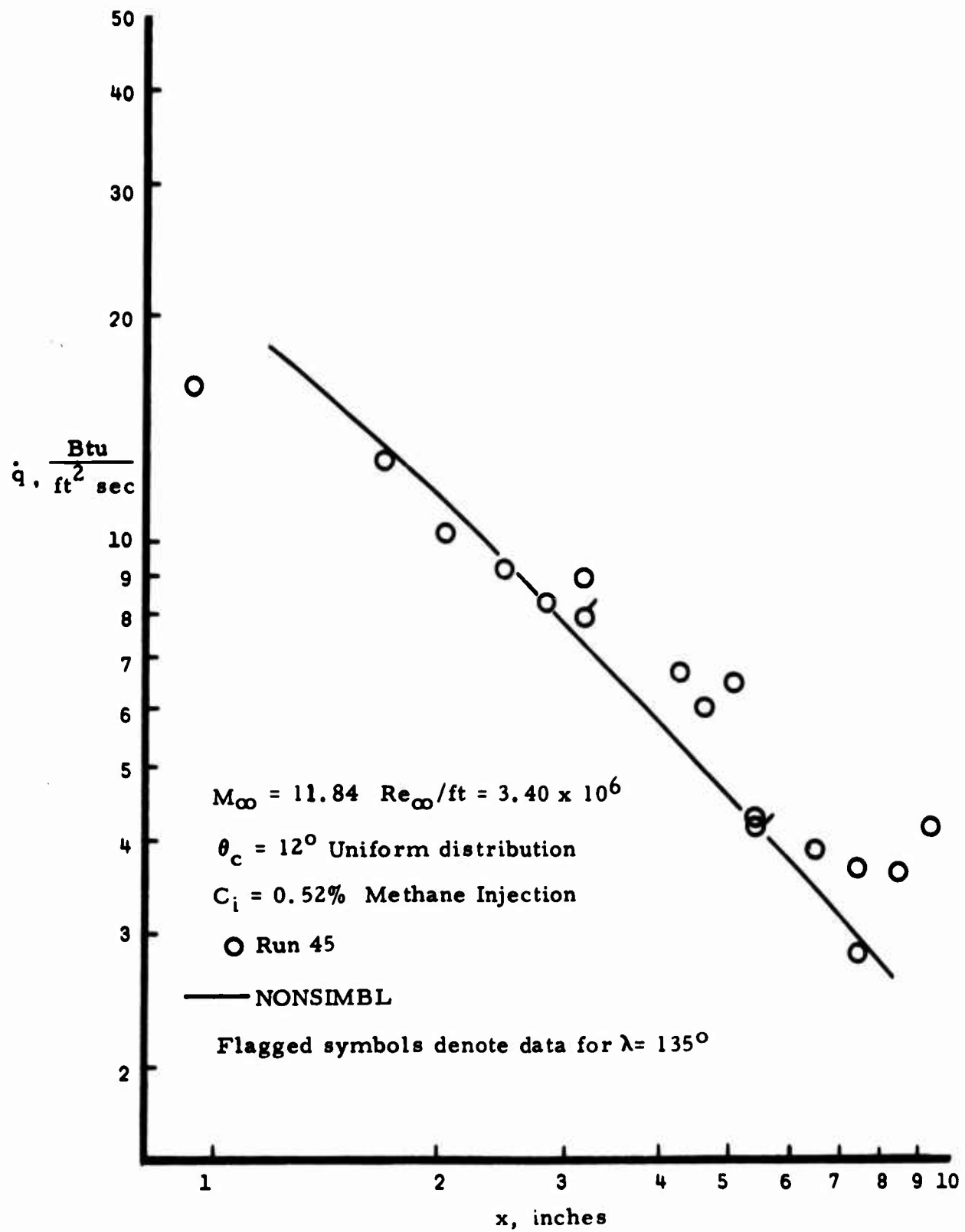


(b) Condition 9

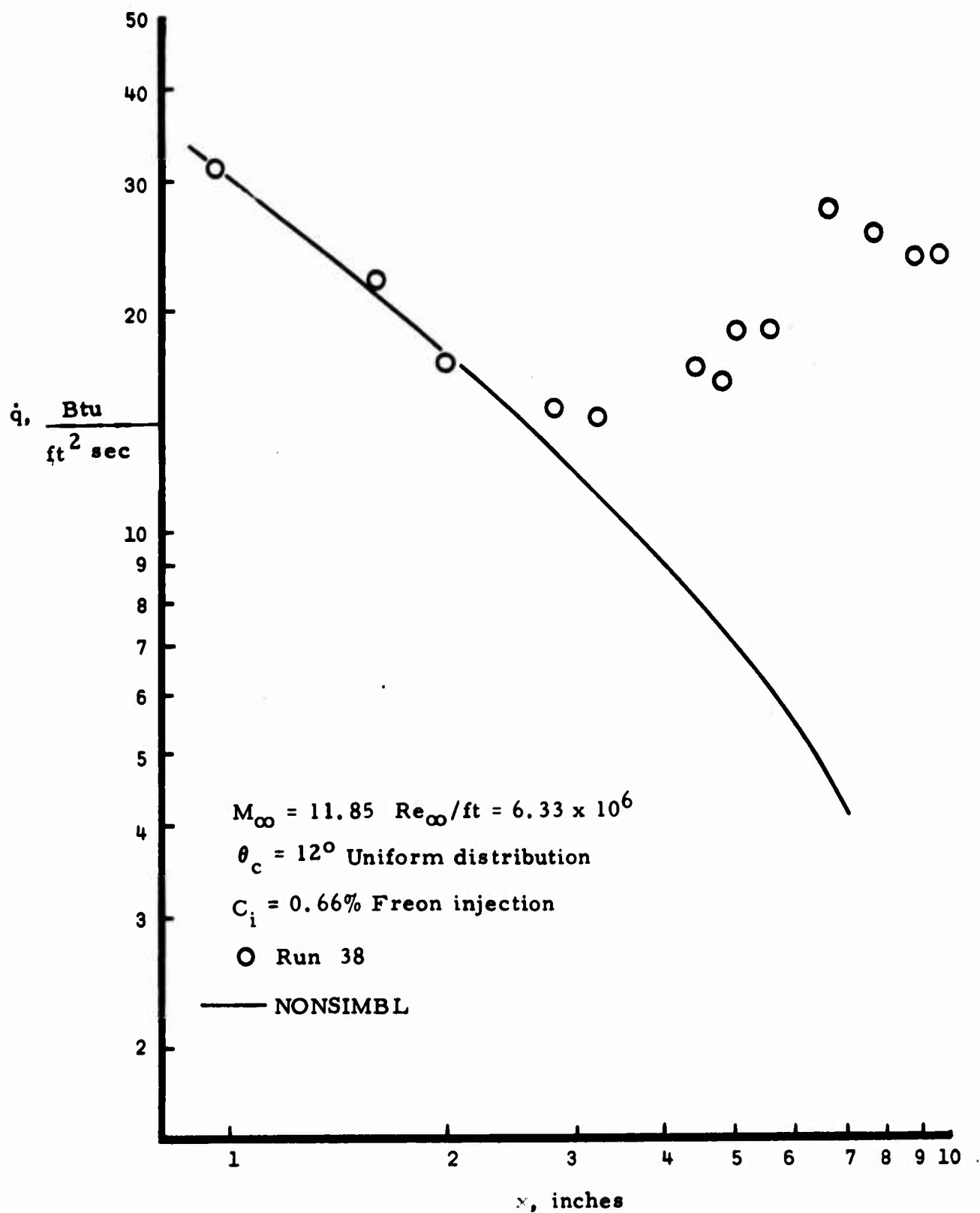
FIGURE 8 CONTINUED



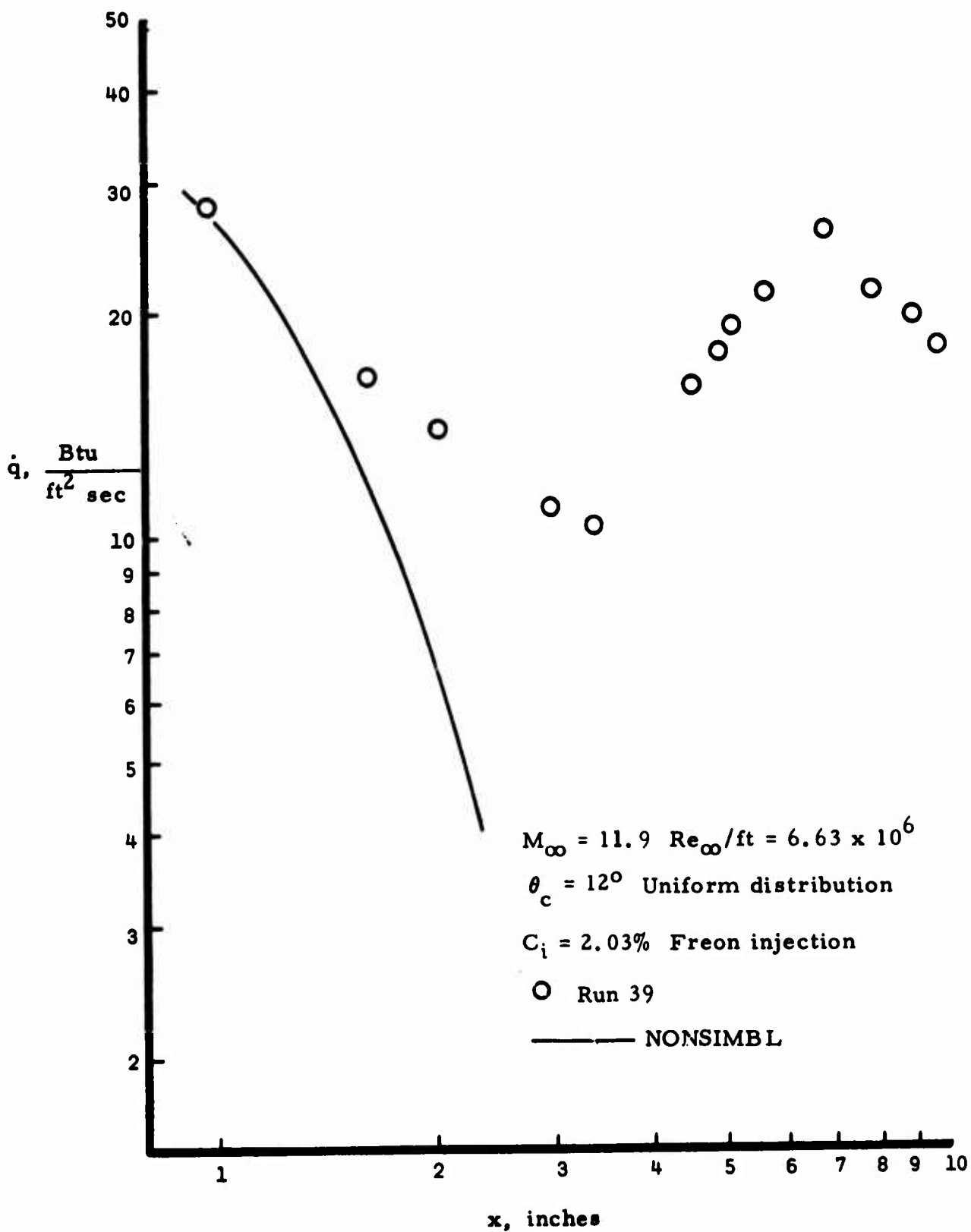
(c) Condition 19
 FIGURE 8 CONTINUED



(d) Condition 27
 FIGURE 8 CONTINUED



(e) Condition 15
 FIGURE 8 CONTINUED



(f) Condition 16
 FIGURE 8 CONCLUDED

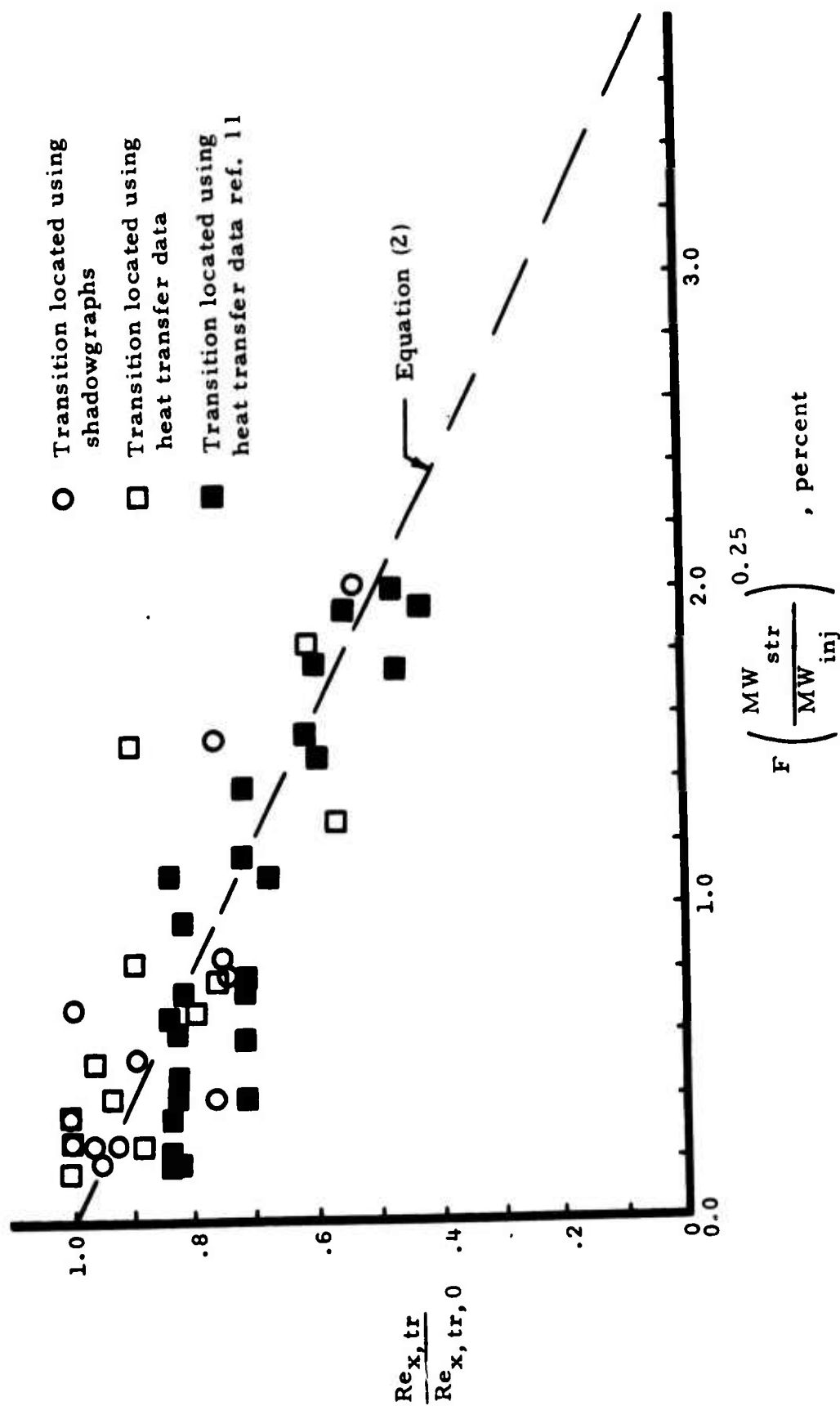


FIGURE 9 THE VARIATION OF TRANSITION REYNOLDS NUMBER WITH THE CORRELATION PARAMETER OF REF. 11, CONSTANT MASS-INJECTION DISTRIBUTION

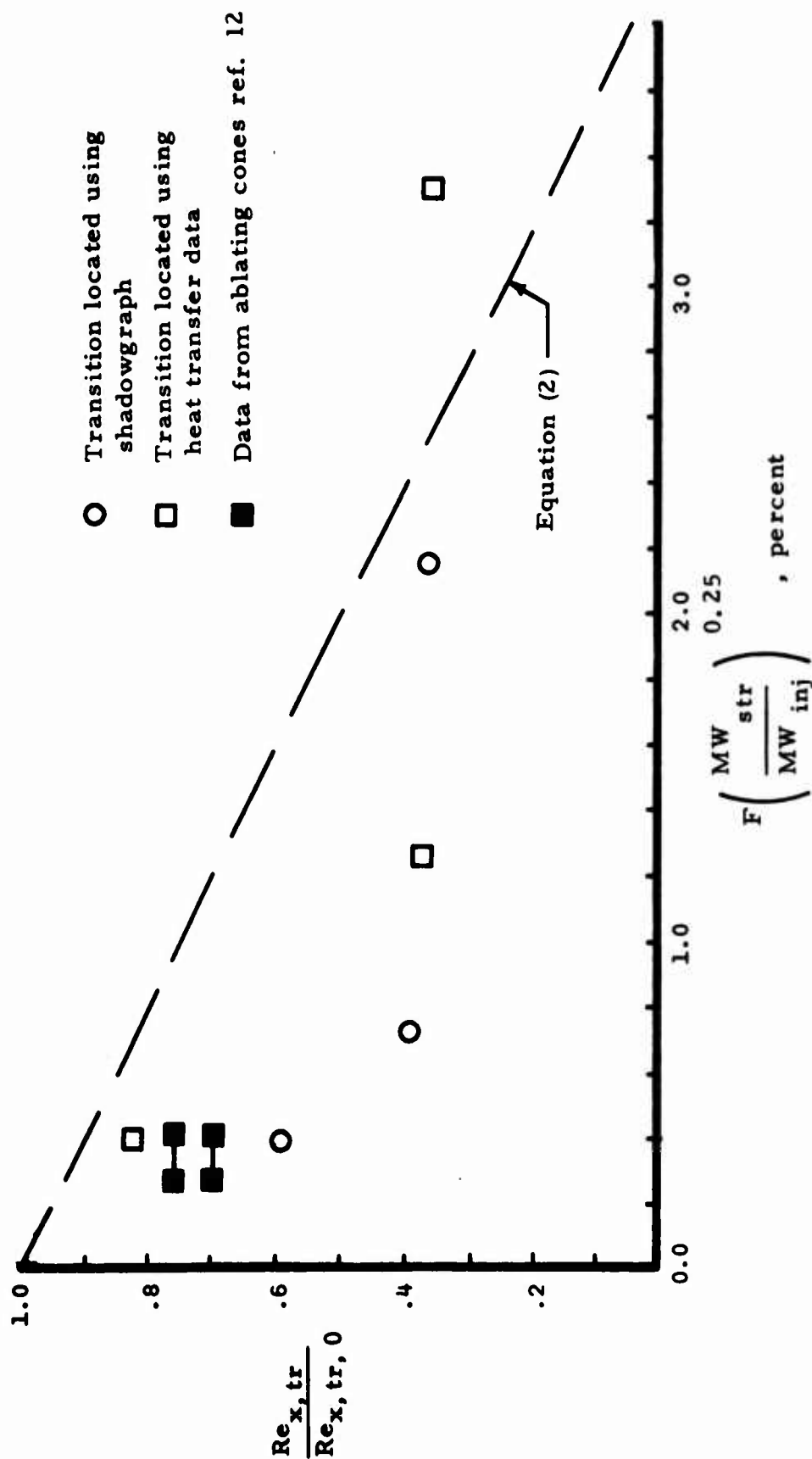


FIGURE 10 THE VARIATION OF TRANSITION REYNOLDS NUMBER WITH THE CORRELATION PARAMETER OF REF. 11, "SIMILAR" MASS-INJECTION DISTRIBUTION

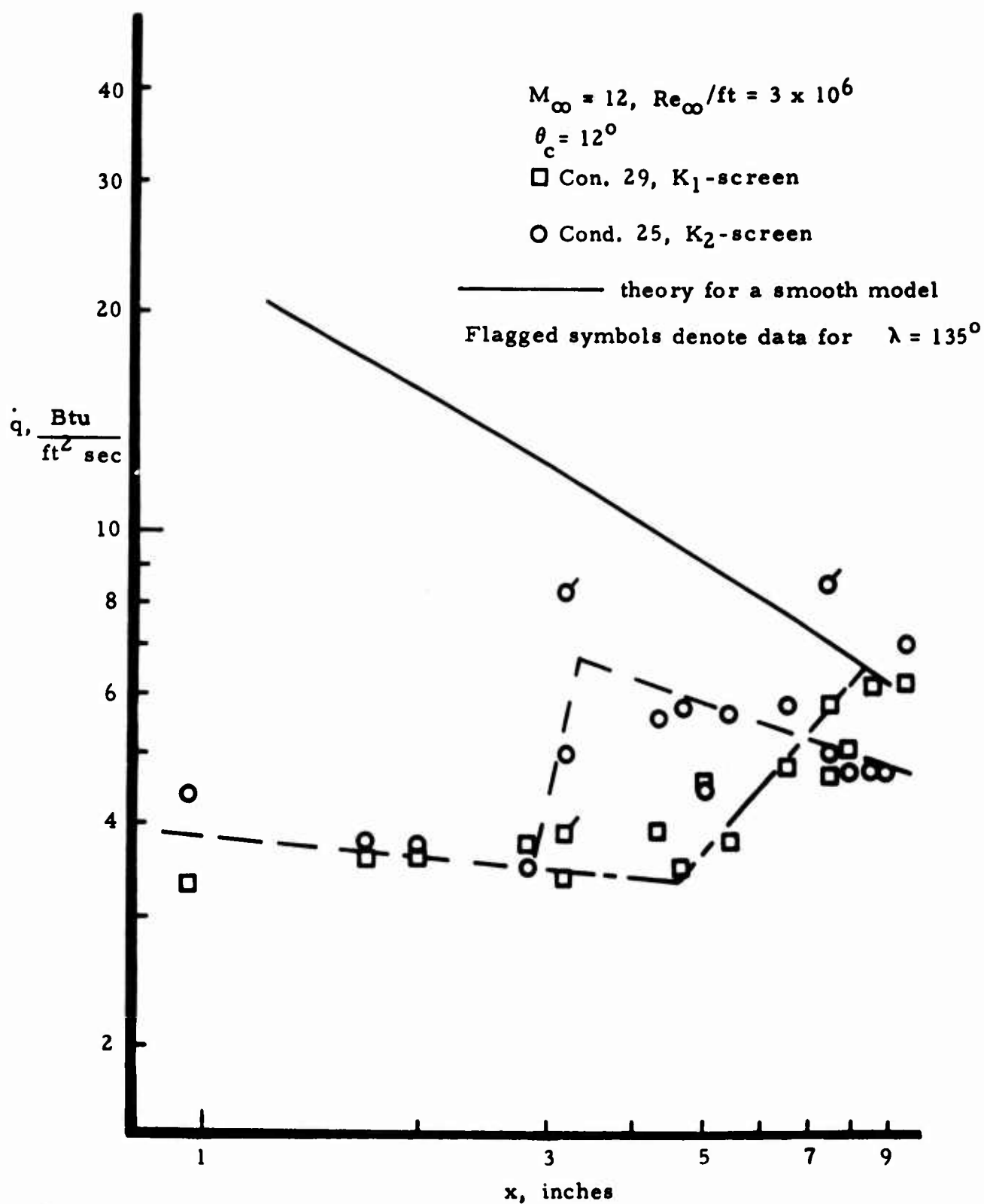


FIGURE 11 THE EFFECT OF SCREEN-TYPE SURFACE ROUGHNESS ON THE NONBLOWING HEAT-TRANSFER-RATE DISTRIBUTION.

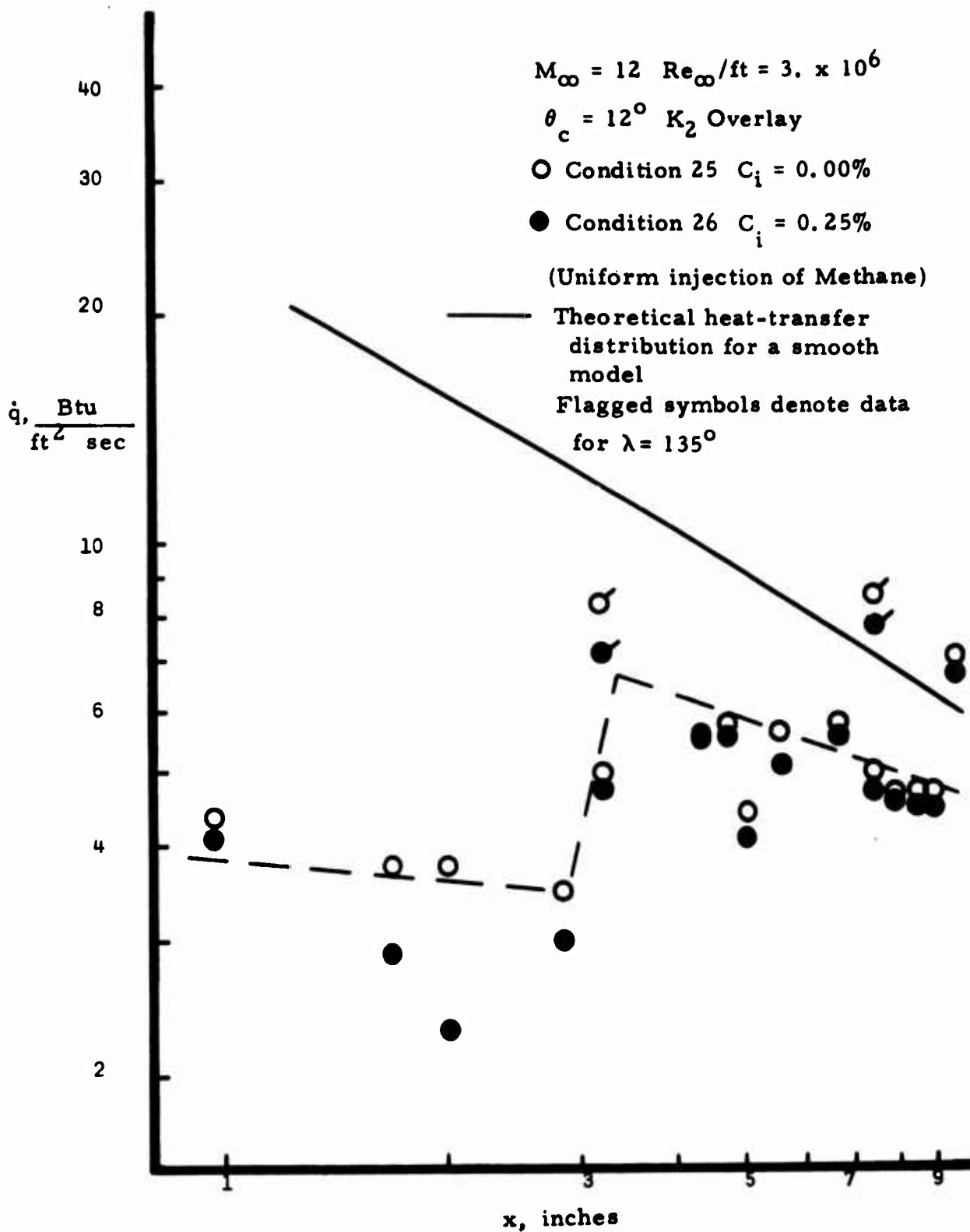


FIGURE 12 THE EFFECT OF MASS-INJECTION ON THE HEAT-TRANSFER-RATE DISTRIBUTION FOR ROUGHENED CONE

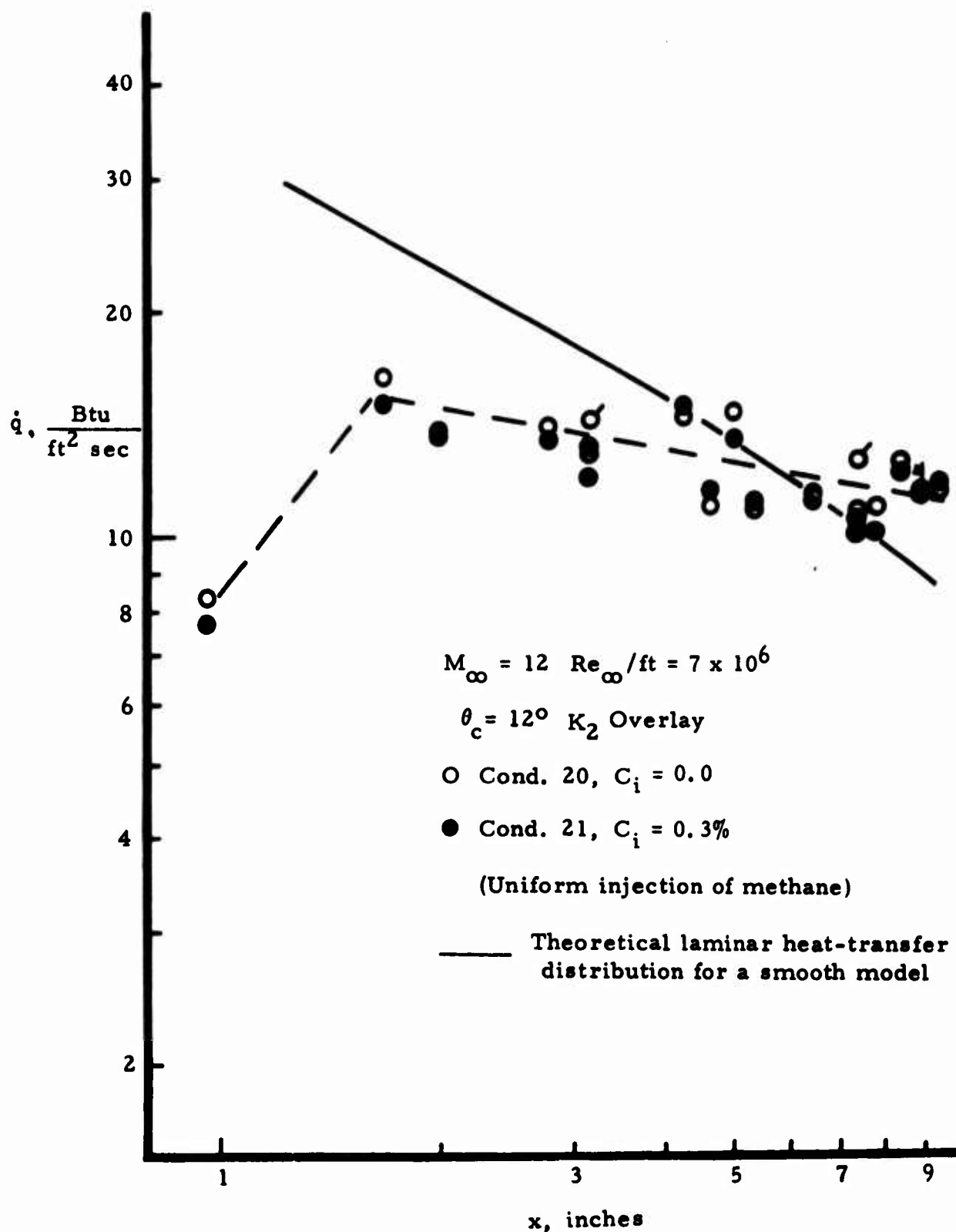


FIGURE 13 THE EFFECT OF MASS-INJECTION ON THE HEAT-TRANSFER-RATE DISTRIBUTION FOR A ROUGHENED CONE.

SECTION 2

EFFECTS OF NOSE BLUNTNESS AND FREE-STREAM UNIT REYNOLDS NUMBER ON SLENDER CONE TRANSITION AT HYPERSONIC SPEEDS*

by James F. Muir and Amado A. Trujillo
Sandia Laboratories, Albuquerque, New Mexico

ABSTRACT

Experiments have been performed to study boundary-layer transition on an 8-degree half-angle cone. The tests were conducted in the U. S. Naval Ordnance Laboratory's Hypersonic Wind Tunnel Number 8 at a Mach number of 6 and free-stream unit Reynolds numbers of 3.0, 9.7, 17.0, and $26.3 \times 10^6/\text{ft}$. The nominal wall-to-recovery temperature ratio and angle of attack were 0.6 and zero degrees, respectively. Six nosetips, having radii ranging from 0.0025 to 0.800 inch, were used in the tests. The location of boundary-layer transition was steady on all but the bluntest model where at the two highest Reynolds numbers transition moved steadily aft along the model during each run. The behavior of this transient phenomenon and its relationship to wall temperature are discussed. The present results are compared with those of other investigators, and the merits of two popular parameters for correlating blunt-cone transition data are discussed. The present transition Reynolds number variations with nose radius and free-stream unit Reynolds number are generally similar to those reported by other investigators. Because of the transient transition behavior on the bluntest model, the agreement for large bluntness is strongly dependent upon when the data are evaluated

* This work was supported by the U.S. Atomic Energy Commission.

during each run. The agreement is best, and the results exhibit the so-called blunt-body reversal, when the data are evaluated early in each run. The resulting correlations of blunt-cone transition data are compared with the local property histories during reentry of typical slender-cone vehicles having nose radii ranging from 0.1 to 2.0 inches. It is shown that, in the absence of surface roughness and mass transfer effects, a judicious choice of nose radius can result in a significant reduction in transition altitude.

NOMENCLATURE

c	Material specific heat
h	Enthalpy
M	Mach number
p	Pressure
q	Heat transfer rate
R_B	Model base radius
R_N	Model nose radius
$Re_{\infty, S}$	$\frac{u_{\infty} S}{\nu_{\infty}}$ Free-stream Reynolds number
Re_{∞, S_T}	$\frac{u_{\infty} S_T}{\nu_{\infty}}$ Free-stream transition Reynolds number
Re_{∞, R_N}	$\frac{u_{\infty} R_N}{\nu_{\infty}}$ Bluntness Reynolds number
Re_{e, S_T}	$\frac{u_e S_T}{\nu_e}$ Local transition Reynolds number
Re_{e, θ_T}	$\frac{u_e \theta_T}{\nu_e}$ Momentum thickness transition Reynolds number
S	Distance along cone surface measured from model stagnation point (wetted length)
\bar{S}	S/R_N
St	Stanton number
T	Temperature

t	Time
t_{ev}	Time during run at which data was evaluated
u	Velocity
δ	Model wall thickness
μ	Dynamic viscosity
ν	Kinematic viscosity
ρ	Density
θ	Momentum thickness
θ_c	Cone half-angle

Subscripts

E	End of transition
e	Boundary-layer edge
o	Stagnation conditions
R	Recovery value
SW	Location where boundary layer swallows nose-induced entropy layer
T	Transition location
w	Wall or surface value
∞	Free-stream conditions
$()_B$	Blunt-cone values
$()_S$	Sharp-cone values

INTRODUCTION

Increased interest in slender, high-performance reentry vehicles and high-speed cruise aircraft in recent years has stimulated a number of investigations into the nature of boundary-layer transition at supersonic and hypersonic speeds.¹⁻¹⁸ Many of the experimental studies have been oriented toward the problem of predicting the onset of transition in such flows. Generally speaking, the objective of these studies has been to determine the extent to which boundary-layer transition is affected by various flow and geometry characteristics. These include free-stream disturbances, unit Reynolds number, Mach number, angle of attack, nose radius, surface roughness, wall cooling, and surface mass transfer. This paper examines the separate and combined effects of two of these characteristics, nose bluntness and free-stream unit Reynolds number, on boundary-layer transition on slender cones at hypersonic speeds.

The controversial unit-Reynolds-number effect on transition, which has been observed and studied for many years,¹⁻⁴ is still a poorly understood phenomenon. Recent investigations by Pate et al.^{5,6} reveal that wind-tunnel transition data for sharp two-dimensional bodies⁵ and cones⁶ can be correlated in terms of parameters associated with the aerodynamic noise generated by the turbulent boundary layers on the tunnel walls. Their results suggest that the behavior of transition on models tested in supersonic and hypersonic wind tunnels is determined primarily by the aerodynamic noise irrespective of the free-stream unit Reynolds number (or Mach number). Unfortunately, however, this analysis does not explain the sharp-cone transition data of Potter⁷ and Sheetz⁸ which demonstrate that a similar unit-Reynolds-number effect can also occur in ballistic range experiments.

The effect of nose bluntness on boundary-layer transition has been investigated for both planar and axisymmetric bodies.^{1,2,4,9-16} One of the earliest and most comprehensive studies of the behavior of transition on

slender sphere-cones is the experimental investigation of Stetson and Rushton.¹² They tested an 8-degree cone with one sharp and ten spherically blunted nosetips, ranging from 1/32 to 1/2 inch in radius, in the AVCO shock tunnel at a Mach number of 5.5. Similar experiments have subsequently been performed at higher Mach numbers by Stainback,¹³ Softley,¹⁴ and Sheetz.¹⁵ In general, the trends exhibited by the results of these investigations are much the same (i.e., a favorable, followed by an adverse, effect of bluntness on transition as the nose radius or free-stream unit Reynolds number is increased), irrespective of cone angle, Mach number, and wall cooling. Nevertheless, there are discrepancies, particularly with regard to the adverse or large-bluntness effect, that emphasize the need for a better understanding of the blunt-body transition phenomenon.

Three years ago, an experimental program was initiated at Sandia Laboratories to study the effects of nose bluntness, free-stream unit Reynolds number, angle of attack, and wall-to-recovery temperature ratio (i.e., wall cooling) on slender-cone transition at hypersonic speeds. The tests were conducted in Tunnel No. 8 of the U. S. Naval Ordnance Laboratory at Mach 6 using an 8-degree half-angle blunted cone. The objective of the investigation was to obtain additional information about blunt-body transition that would help to clarify the individual effects of these parameters on transition. In addition, the program was designed to provide an independent verification of the results reported earlier by Stetson and Rushton.¹²

This paper presents only those results obtained on the effects of nose bluntness and free-stream unit Reynolds number on slender-cone boundary-layer transition.* The data are compared with the results of other investigators in terms of both free-stream and local properties. The resulting

* The angle-of-attack data, in addition to the bluntness and unit-Reynolds-number results reported herein, will be presented at the AIAA 10th Aerospace Sciences Meeting, San Diego, California, January 17-19, 1972. The data from the variable wall cooling experiments are presently being reduced. These results will be published separately.

correlations are then used to evaluate the effect of nose radius on the altitude at which a typical slender-cone vehicle experiences transition during reentry.

EXPERIMENTAL PROGRAM

Facility

The experiments were conducted in Hypersonic Tunnel Number 8 of the U. S. Naval Ordnance Laboratory, White Oak, Maryland (Reference 31). Tunnel 8 is an intermittent blowdown facility that is equipped with a pebble-bed heater, interchangeable contoured nozzles, and a model injection system that permits the model to be inserted into, or retracted from, the test stream in approximately 0.2 second. The tunnel has an open-jet test section, and the working medium is air. A two-dimensional nozzle producing a nominal free-stream Mach number of 6 was selected for the present experiments. The upper operating limits on the stagnation temperature and pressure for the nozzle are 700°F and 150 atm, respectively.

Test Conditions

The tests were conducted at a Mach number of 6, a nominal stagnation temperature of 600°F, and stagnation pressures of 15, 55, 100, and 140 atm. The corresponding free-stream unit Reynolds numbers were 3.0, 9.7, 17.0, and 23.6×10^6 per foot. For the tests reported herein, the nominal wall-to-recovery temperature ratio and model angle of attack were 0.6 and 0 degrees, respectively.

Model and Instrumentation

The basic test configuration was an 8-degree half-angle cone with a base diameter of 5 inches and six spherically blunted, interchangeable noses having radii of 0.0025, 0.025, 0.100, 0.200, 0.400, and 0.800 inch. The corresponding bluntness ratios, R_N/R_B , ranged from 0.001 to 0.32. The results of Stetson and Rushton, which were obtained for similar flow conditions,

were used as the basis for selecting the number and size of the nosetips. The model geometry is sketched in Figure 1, and a photograph of the model (disassembled) is presented in Figure 2.

The model was fabricated of Armco 17-4PH stainless steel. It had a nominal skin thickness of 0.025 inch, and a surface finish of better than 16 microinches rms. The step heights at all joints, caused by the use of interchangeable nosetips, varied from less than 0.1 mil to a maximum of 1.2 mils (out of 28 measurements, one at each of four circumferential locations at each joint, only four had step heights ≥ 1 mil). No significant out-of-roundness or waviness in the model surface was detected.

The model was instrumented with a maximum of 29 chromel-alumel thermocouples (the 16- and 32-percent blunt models had 28 and 24 thermocouples, respectively). The thermocouples were welded to the inner wall of the model along the 0- and 180-degree meridians at the locations indicated in Figure 1. Prior to thermocouple installation, wall-thickness measurements were made at each thermocouple location. In addition, four pressure taps were located 90 degrees apart around the model (beginning at 0 degrees), approximately 1/8 inch forward of the model base. When mounted in the tunnel, the model was oriented so that the 0- and 180-degree meridians were in the pitch plane. Thus, the diametrically opposed pressure ports lay in the pitch and yaw planes and permitted a very accurate alignment of the model with respect to the tunnel flow. The pitch and yaw angles were typically only a few tenths of a degree. In the plane of the thermocouples (the pitch plane) α was less than 0.1 degree for the bulk of the tests and exceeded 0.2 degree in only three runs.

Procedure

Prior to each run, the model was cooled until its surface was close to room temperature and was isothermal within $\pm 20^\circ\text{F}$. After the tunnel test conditions were established, the model was injected into the tunnel flow and

the wall temperatures, T_w , were recorded as functions of time. Aerodynamic heat-transfer rates were then computed from the thin-skin heat-transfer relation,

$$q_w = c \rho \delta \frac{dT_w}{dt}.$$

Unless otherwise noted, the data presented in this paper were evaluated approximately 1.25 seconds after the model reached the tunnel centerline.

RESULTS

Heat-transfer distributions for three of the models, $R_N/R_B = 0.001$, 0.04, and 0.16, in the form of a free-stream Stanton number,

$$St_\infty = - \frac{q_w}{\rho_\infty u_\infty (h_w - h_R)},$$

where $T_R = 0.9 T_o$, are presented in Figure 3 versus free-stream Reynolds number based on wetted length, $Re_{\infty, S}$. Also presented in Figure 3 are theoretical predictions for the laminar and turbulent Stanton numbers for the sharp cone computed by the methods of Van Driest.^{19,20} The agreement between experiment and theory is very good.

Generally speaking, the Stanton-number variations through the laminar, transitional, and turbulent regimes follow conventional patterns. The beginning of boundary-layer transition is defined herein as the intersection of a straight line through the transitional data with a line faired through the laminar portion of the data, as indicated in Figure 3 for $R_N/R_B = 0.001$. The end of transition is considered to be the point where the heat transfer reaches a maximum. These variations are representative of the heat-transfer

distributions obtained on all but the bluntest model. The location of transition on these models remained essentially constant during each run.

On the 32-percent blunt model, however, a transient transition behavior was observed at the two highest free-stream unit Reynolds numbers (at the lower unit Reynolds numbers, the flow was laminar over the entire model). When the model was first injected into the flow, boundary-layer transition occurred close to the nose: the so-called blunt-body transition behavior reported in the literature. However, in contrast to the stable transition observed on the sharper models, the transition region on the bluntest model moved steadily downstream from the time of injection and, for $(u/\nu)_{\infty} \approx 17 \times 10^6$ per foot, passed off of the model about 5 seconds after the start of each run. At the highest Reynolds-number condition, $(u/\nu)_{\infty} \approx 23.6 \times 10^6$ per foot, the transition region was still moving off the model at the end of each run; the run times varied from 10 to 15 seconds.

This transient behavior of transition is evident in the temperature-time data obtained during the runs. Typical wall-temperature histories for three locations on the model (forward, mid, and aft stations) are presented in Figure 4 for run 2-28 $[(u/\nu)_{\infty} \approx 17 \times 10^6 \text{ per foot}]$. The change from turbulent to laminar heating at each location is demonstrated by the significant and rapid decrease in the slope of the curves with increasing time.

Typical Stanton-number distributions for the 32-percent blunt model are presented in Figure 5. Consistent with the results for the sharper models, the curves in the top half of the figure represent the heat-transfer variations 1.25 seconds after the model reached the tunnel centerline. Note that, for the two flows with the highest free-stream unit Reynolds numbers, these are the instantaneous distributions at that time. However, because of the transient behavior of transition on this model, the temperature-time data for the two highest unit-Reynolds-number flows were also evaluated at several other times during each run. The resulting Stanton-number variations at four times during run 2-28 are presented in the bottom half of Figure 5. These

variations in the heat-transfer distribution provide a clear illustration of the downstream movement of transition.

The test conditions, nose radius, transition location, and local properties and transition Reynolds numbers for each run are listed in Tables I through III. Both the free-stream and local boundary-layer edge properties were calculated on the basis of perfect gas assumptions. The latter, however, as well as the local transition Reynolds numbers, were computed with the BLUNTY aerodynamic heating program.^{21,22} This program uses shock shapes and pressure distributions computed by the NASA-Ames Inviscid flow-field code,²⁸ assumes local similarity of the boundary layer, and employs a stream-tube mass-balancing technique. The momentum thickness Reynolds number is computed from the relation

$$Re_{e,\theta} = \frac{0.664}{\mu_e r} \left[\int_0^s \rho_e \mu_e u_e r^2 ds \right]^{1/2}$$

where r and s are the local body radius and surface distance, respectively.

The results for all but the bluntest model are presented in Table I. Table II contains the results for the 32-percent blunt model evaluated at 1.25 seconds and for a condition of all laminar flow over the model. (The latter corresponds to times greater than approximately 5 and 10 seconds at the 100- and 140-atm flow conditions, respectively.) The results from four additional runs at higher initial model temperatures, together with the results from two of the room-temperature runs, 2-27 and 2-28, all evaluated at 1.25 seconds, are presented in Table III.

DISCUSSION

Transient Transition Phenomenon

To the authors' knowledge, there is only one other series of experiments reported in the literature that exhibited a transient transition behavior

like that observed on the bluntest model ($R_N = 0.800$ inch) in the present tests. Diaconis, Jack, and Wisniewski⁹⁻¹¹ observed such a phenomenon during tests of sharp and blunt cone-cylinders ($\theta_c = 9.5^\circ$, $R_N = 0.000, 0.09375$, and 0.700 inch) at a Mach number of 3.12 in the 1- by 1-foot supersonic tunnel at the NACA Lewis Flight Propulsion Laboratory. The authors reported that, at the beginning of those runs for which transition was initially located somewhere on the models, the transition region moved downstream "very swiftly" until it passed completely off the models. Later on in the tests of the sharp and slightly blunt models, transition reappeared at the rear of the bodies and moved forward. This was not true of the bluntest model, however, which maintained completely laminar flow through the remainder of each run. In that the only experimental parameter which varied during each run was the model temperature, the movement of transition was associated with the wall temperature and was believed to be a wall cooling effect.

The transition behavior observed in the present tests was similar to that just described for the bluntest cone-cylinder model. The transition region moved downstream from its initial location, but its rate of movement varied considerably with the free-stream conditions. During runs at $(u/\nu)_\infty \approx 17 \times 10^6/\text{ft}$, the transition region moved completely off the model in approximately 5 seconds, while at the highest unit-Reynolds-number flow it was still partially on the model after more than 10 seconds.

To gain a better insight into this phenomenon, the motion history of the transition region during run 2-28 $\left[(u/\nu)_\infty \approx 17 \times 10^6/\text{ft} \right]$ was determined from the temperature-time variations, examples of which have been presented in Figure 4. The times at which the beginning and end of transition passed over each thermocouple were estimated by determining the points at which the laminar and turbulent portions of the T_w - t curve departed from a linear variation. The results of these measurements are presented in Figure 6. It is seen that the end of transition traveled downstream much faster than the beginning; as a result, the transition region grew rapidly as it moved (from

about 2 to 10 inches in roughly 1 second). This lengthening of the transition region can also be seen in Figure 5 by examining the manner in which the heat-transfer distributions change with increasing time. In contrast to this, the temporal variations in the heat-transfer distributions during run 2-27, at $(u/\nu)_{\infty} \approx 23.6 \times 10^6/\text{ft}$ (not shown), indicate that the length of the transition region first increased and then decreased as it moved along the body.

Unfortunately, the gradual change in the slopes of the temperature-time curves for tests at the highest unit Reynolds number made a similar determination of the transition-region history impossible. Nevertheless, the histories of the transition locations defined in Figure 3, representing the approximate beginning of transition, were determined for one run at each flow condition (runs 2-27 and 2-28); the results are compared in Figure 7. Here, the much slower movement of transition at the $(u/\nu)_{\infty} \approx 23.6 \times 10^6/\text{ft}$ condition is very evident. It is also interesting to note the different character of the two curves and the fact that the initial location of transition on the model appears to have been about the same at both flow conditions. Whether there is any significance to this is a matter of speculation at this point.

In view of the fact that the model temperature is the only experimental parameter known to be varying during the runs, it is natural to assume that this is the cause of the transient transition behavior. To ascertain whether this is indeed the case, four additional runs were made in which the model was heated to higher initial wall temperatures prior to its injection into the flow. The data from these runs were evaluated at a time of 1.25 seconds; the results are presented in Table III together with the wall-to-recovery temperature ratios (based on an average value of T_w just upstream of the transition region) and the corresponding results for runs 2-27 and 2-28. For comparison purposes, the temporal variations in Re_{e,S_T} and T_w/T_R during runs 2-27 and 2-28 were determined by evaluating the data at several times during the runs. The resulting transient and variable-temperature-constant-time results are compared in Figure 8, which also includes the transient

results reported by Diaconis, Jack, and Wisniewski⁹⁻¹¹ for both blunt- and sharp-cone cylinders.

An examination of this figure reveals:

1. With the exception of an anomalous point (run 2-58) at the lower Reynolds-number condition, the two methods for evaluating the effect of increasing wall temperature on the local transition Reynolds number (i.e., constant initial temperature and varying time versus increasing initial temperature and constant time) yielded almost identical variations of Re_{e, S_T} with T_w/T_R at each flow condition. This suggests that the transient behavior of transition on the 32-percent blunt model is closely related to the variation in the model wall temperature during the runs. This is not the complete picture, however, because the location of transition on the sharper models, which were subjected to the same environment and experienced similar increases in wall temperature, remained essentially constant during each run. Thus, it appears that the transient behavior is also a function of nose radius, possibly through its effects on the longitudinal pressure and wall-temperature variations. In addition, the two highest initial temperature runs with the bluntest model ($T_w/T_R \approx 0.77$) did not exhibit the transient transition phenomenon observed on the same model at lower initial temperatures. Although the general location of transition (S_T) remained about the same during these two runs, there was considerable scatter in the temperature-time data which suggests a quasi-steady or fluctuating behavior of the transition region. This lack of a transient behavior at the higher, but more uniform, wall temperatures may also be an indication that the wall temperature distribution is a contributing factor.

2. The slopes of the curves indicate a high sensitivity of the local transition Reynolds number to changes in wall temperature, with the sensitivity decreasing with increasing free-stream unit Reynolds number.
3. There is good agreement between the magnitudes and trends of the present data and those of Diaconis, Jack, and Wisniewski;⁹⁻¹¹ both sets indicate that increasing T_w/T_R tends to delay transition.

The last phase of the Sandia boundary-layer transition studies consisted of an extensive investigation of the effects on transition of varying the initial model wall temperature. Tests were conducted in which the models were either heated ($T_w/T_R \approx 0.85$) or cooled ($T_w/T_R \approx 0.15$ and 0.40) prior to injection. Although the data have not been completely reduced, preliminary results indicate that at the lower initial wall temperatures the transient transition behavior occurred on the next two sharper models ($R_N = 0.4$ and 0.2 inch), as well as on the bluntest model, and increasing T_w/T_R again served to delay transition. This provides further evidence that the transient transition phenomenon is caused by a complex combination of several factors, including wall temperature and the axial variations in wall temperature and pressure, which are determined primarily by the nose radius.

Finally, it is interesting to note that the two sets of transient transition data discussed above were both obtained in wind tunnels during runs of fairly long duration: 10 to 15 seconds for the present experiments and up to 100 seconds for the NACA tests.⁹⁻¹¹ On the other hand, all the ground test data which exhibit a forward movement of transition on slender cones^{12,14,15}, i.e., the large-bluntness effect, were obtained in relatively short-duration facilities, two shock tunnels and a ballistics range, where test times were of the order of a few milliseconds. This contrast in test conditions raises the following two questions.

1. In view of the rather large characteristic times associated with the transient transition phenomenon, is it possible that the same phenomenon was present in the shock tunnel and ballistics range tests, but was not detected because of the short test times?
2. Or, is this transient behavior strictly a function of the particular flow environments (including the model wall temperature variations) found in these two wind tunnels, or in wind tunnels in general?

Unfortunately, the exact cause of the transient behavior of transition is a matter of conjecture at this point, and the answers to these and many other questions must await a better understanding of the detailed mechanics of the phenomenon.

Present Results and Comparisons with Other Data

The results of this and other investigations are presented in terms of both free-stream and local parameters. Although the latter provide more meaningful correlations of transition data, the former are more suitable for transition prediction purposes (but involve a greater degree of uncertainty).

The free-stream transition Reynolds numbers, Re_{∞, S_T} , obtained from the present data are plotted in Figure 9 in terms of the two independent parameters varied during the tests: $(u/\nu)_{\infty}$ and R_N^* . The transition data reported in References 12 through 15 are presented in the same fashion in Figure 10. It is recognized that a direct comparison of these data is open to question because they were obtained in quite different facilities (hence, in different facility disturbance environments) with models having different cone

* When transition occurred downstream of the last thermocouple, the location of the thermocouple was treated as a "minimum" transition location. The corresponding "minimum" transition Reynolds numbers are plotted with an arrow indicating the direction in which their true values lie.

angles, and because of the different definitions employed for the location of transition. Nevertheless, the following observations can be made regarding the general trends exhibited by the data: As the nose radius is increased from zero, all the data except Sheetz's¹⁵ exhibit an increase in transition Reynolds number with increasing unit Reynolds number and bluntness, and an increase in the unit-Reynolds-number dependence with increasing bluntness. These variations are caused to a great extent by the decreases in local boundary-layer edge properties [e.g., M_e and $(u/\nu)_e$] that accompany the increases in R_N and/or $(u/\nu)_\infty$.

Above a certain value of nose radius, that ranges from 0.005 inch in the ballistic-range tests¹⁵ to 0.800 inch in the present experiments, the data show a rapid decrease in transition Reynolds number with increasing unit Reynolds number and bluntness. Note, however, that because of the transient behavior of transition on the bluntest model, the slope of lines faired through the $R_N = 0.800$ inch data at various times during the runs increases with increasing time. Thus, the rapid decrease in transition Reynolds number indicated by the dashed line in Figure 9 (which agrees so well with the variation reported by Stetson and Rushton,¹² Figure 10) represents the instantaneous locus of transition locations only near the beginning of the runs (at $t = 1.25$ sec). The transition locations corresponding to the time at which the flow along the model became completely laminar [$t \gtrsim 5$ and 10 seconds for $(u/\nu)_\infty \approx 17$ and $23.6 \times 10^6/\text{ft}$, respectively] are represented by the solid symbols labeled " $t \gtrsim 5$ sec." The estimated variation in Re_{∞, S_T} for the all-laminar-flow condition is indicated by the uppermost dashed line. In order to differentiate the transient and steady-state results, the trends in the $R_N = 0.800$ inch data for these two limiting conditions are indicated by dashed lines in all of the figures; whereas, the trends in the steady transition results obtained for the sharper models are indicated by solid lines.

The forward movement of transition (transition reversal) described above is the so-called "blunt-body paradox"⁴ that has yet to be satisfactorily explained. The fact that it occurs at such widely different nose radii may be

due primarily to the different free-stream unit Reynolds numbers and wall-to-recovery temperature ratios of the various experiments (T_w/T_R ranges from $\lesssim 0.07$ in the ballistic range experiments to ~ 0.6 in the present tests). Additional factors that may influence this behavior include tunnel flow gradients, facility disturbance environments, and model surface roughness.

In an effort to correlate these results and reduce the effects of free-stream unit Reynolds number and Mach number, the ratio of the transition Reynolds numbers for the blunt and corresponding sharp cones exposed to the same free-stream environment $\left[(Re_{\infty, S_T})_B / (Re_{\infty, S_T})_S = (S_T)_B / (S_T)_S \right]$ is presented in Figure 11 as a function of the product of the two independent variables, i.e., the bluntness Reynolds number, Re_{∞, R_N}^* . Generally speaking, the results exhibit a trend of increasing blunt-cone transition Reynolds number (over the corresponding sharp-cone value) with increasing R_N and/or $(u/\nu)_{\infty}$ up to the point where the transition reversal occurs in each case. However, this point occurs at widely different values of Re_{∞, R_N} for the various tests, and there is considerable scatter in the data. The effects of the different test environments, i.e., the free-stream unit Reynolds numbers, Mach numbers, wall-to-recovery temperature ratios, etc., are still evident, particularly at the higher bluntness Reynolds numbers. It is clear, therefore, that the various results do not correlate well in terms of free-stream transition and bluntness Reynolds numbers.

Nevertheless, there is one important reason for presenting transition data in this fashion: it provides a fairly direct indication of the effects of nose bluntness on the behavior of transition on a slender vehicle entering the

* In order to present the ballistics-range data of Sheetz¹⁵ in this manner, it was necessary to estimate values of the sharp-cone transition Reynolds number for the free-stream conditions of the blunt-cone shots. In view of the possible errors introduced in making such estimates, the Reynolds-number ratios for the Sheetz data involve a greater degree of uncertainty than the rest of the results.

earth's atmosphere. For example, the data in Figure 11 indicate that, by a judicious choice of nose radius, it is possible to obtain a free-stream transition Reynolds number almost an order of magnitude greater than that for a corresponding sharp cone. In terms of transition behavior during reentry, this corresponds to a reduction in transition altitude of approximately 50 kft for a typical ballistic trajectory.

Experience has shown that better and more meaningful correlations of blunt-cone boundary-layer transition data are obtained when the data are expressed in terms of local (boundary-layer edge) properties. Unfortunately, however, this introduces additional uncertainties into the results, namely those associated with the determination of the local properties, which in most instances must be computed. The problem of calculating laminar boundary-layer edge properties on blunt cones in supersonic and hypersonic flows (where variable pressure and entropy effects, induced by curvature of the bow shock, are important) has been considered by a number of investigators, and several computational schemes involving various degrees of approximation have been developed.²¹⁻²⁷ For the present analysis, boundary-layer edge properties were computed with the BLUNTY aerodynamic heating program.^{21,22}

Before evaluating the blunt-cone data, it is of interest to compare the present sharp-cone results with data obtained in other wind tunnels. Pate⁵ has successfully correlated wind-tunnel transition data for sharp, slender cones obtained in 11 different facilities over a wide range of free-stream Mach numbers and unit Reynolds numbers. The local transition Reynolds number for the end of transition, Re_{e,S_E} , is correlated in terms of test-section size and parameters associated with the aerodynamic noise radiated by the turbulent boundary layers on the tunnel walls. The sharp-cone data for the end of transition from the present experiments are compared with the Pate correlation in Figure 12. The agreement is excellent.

The local transition Reynolds numbers, Re_{e,S_T} (for the beginning of transition) for all the models tested (sharp and blunt) are presented in Figure 13 as a function of bluntness Reynolds number with lines of constant free-stream unit Reynolds number. The latter represent the variations in Re_{e,S_T} caused by changes in nose radius alone. Thus, as R_N increases from zero [and $(u/\nu)_\infty$ remains constant], the transition Reynolds number increases above its sharp-cone value, reaches a maximum, and then decreases somewhat more rapidly. At this point (depending upon the instantaneous location of transition on the bluntest model), the curves either increase slightly, to values of the order of the sharp-cone transition Reynolds numbers (when transition has moved off the model), or continue to decrease to much smaller values of Re_{e,S_T} (corresponding to the location of transition at a time of 1.25 seconds). The maximum in each of the constant $(u/\nu)_\infty$ curves appears to be greater than the corresponding sharp-cone value by a factor of roughly 1-2/3, which is slightly less than the factor of 2 reported by Softley.¹⁴ The reversal in the behavior of transition represented by these peaks in the curves separates the data into two regions, to the left and right of the peaks, which are commonly referred to as the "small bluntness" and "large bluntness" regions, respectively.

On the other hand, the trends indicated by the sets of data having the same symbol represent the variations in local transition Reynolds number associated with changes in free-stream unit Reynolds number at constant nose radius. It is clear that these variations are different from those described above for constant $(u/\nu)_\infty$, particularly for the blunter models. The significant point here is that the bluntness Reynolds number, Re_{∞,R_N} , does not properly represent the changes in local transition Reynolds number caused by changes in either $(u/\nu)_\infty$ or R_N . Thus, the practice of fairing a single line through a set of transition data [obtained for various $(u/\nu)_\infty$ and R_N] on an $Re_{e,S_T} - Re_{\infty,R_N}$ plot, which implies that the curve reflects changes in either $(u/\nu)_\infty$ or R_N , can be misleading.

Similar trends are exhibited by the data of Stetson and Rushton,^{12,14} which are presented in Figure 14, and by the momentum thickness transition Reynolds numbers, Re_{e,θ_T} , for both investigations which are presented in Figure 15.* The comments and conclusions stated above apply to the trends exhibited by the Stetson and Rushton data as well.

A comparison of the two sets of data reveals that the results of Stetson and Rushton are consistently lower than those of the present investigation. This is a result, in part, of their definition of the beginning of transition as the point where the local heat-transfer rate departs from the laminar value. As is evident from Figure 3, this occurs upstream of the transition location employed in the present study.

A better parameter for correlating local transition Reynolds numbers is the transition-to-swallowing distance ratio, S_T/S_{SW} , suggested by Stetson and Rushton.¹² The swallowing distance is the location on a blunt cone where the variable entropy layer created by the curved portion of the bow shock is "swallowed" by the boundary layer; downstream of this point, the flow is conical. Since the condition of conical flow is approached asymptotically, the authors¹² arbitrarily defined S_{SW} as the point where the local edge Mach number, M_e , becomes 0.95 of the sharp-cone value. It has been shown^{23,29} that \bar{S}_{SW} ($= S_{SW}/R_N$) is proportional to $(Re_{\infty,R_N})^{1/3}$. An advantage of \bar{S}_{SW} over Re_{e,R_N} as a correlating parameter is the fact that it is also a function of free-stream Mach number and cone angle. This has been demonstrated by Rotta,²⁹ whose results are presented in Figure 16 as $\bar{S}_{SW}/(Re_{\infty,R_N})^{1/3}$ versus θ_c with lines of constant M_∞ . For slender cones, \bar{S}_{SW} is a strong function of cone angle and only a weak function of Mach number for $M_\infty \gtrsim 8$.

* The local transition Reynolds numbers presented in Figures 14, 18, and 20 for the results of Stetson and Rushton are the values computed by Softley¹⁴ with the GE-VIZAAD program.²⁵ The corresponding momentum thickness Reynolds numbers appearing in Figures 15 and 19, however, are the values reported by Stetson and Rushton.¹²

Since there are as many methods for calculating S_{SW} as there are for computing boundary-layer edge properties, there are bound to be differences in the published results. In the present analysis, swallowing distances were determined with the BLUNTY aerodynamic heating program^{21,22} (sharp-cone Mach numbers were obtained from Reference 30). These results, along with values computed by Softley,¹⁴ with the VIZAAD program²⁵ (for his own and Stetson and Rushton's data), and Sheetz,¹⁵ using a momentum-integral method developed by Wilson,²⁶ are included for comparison in Figure 16. Also shown are curves for $M_\infty = 6$ and 10 computed with the BLUNTY code. The scatter in the results is very large; the values of Sheetz, in particular, are a factor of roughly five higher than the other results at Mach 10. Because it can be shown that such large differences do not result from variations in free-stream unit Reynolds number, Mach number, or cone angle, it appears that they are the result of differences in the calculation schemes. The swallowing distances computed by Softley for his Mach 10 and 12 flows also reflect the effects of the tunnel flow gradients that existed at those conditions.¹⁴

The present results, in the form of a local transition Reynolds-number ratio, $\left(Re_{e,S_T}\right)_B / \left(Re_{e,S_T}\right)_S$, are replotted in Figure 17 versus the transition-to-swallowing distance ratio, S_T/S_{SW} , with lines of constant free-stream unit Reynolds number. The values of $\left(Re_{e,S_T}\right)_B$ and $\left(Re_{e,S_T}\right)_S$ at each data point are for the same free-stream unit Reynolds number and Mach number. The results are presented in ratio form to minimize the effects of these two parameters.

In moving forward from the conical flow region ($S_T/S_{SW} > 1$), the variations in the constant $(u/\nu)_\infty$ curves are similar to those exhibited in Figure 13 (and described above) for increasing nose radius. The effect of free-stream unit Reynolds number (i.e., the spread between the curves), however, is much less than in Figure 13. It is virtually negligible for the small nose radii but increases with R_N to a measurable degree for the blunter models.

Once again, the same general comments apply to the Stetson and Rushton data, which are presented in the same manner in Figure 18,^{*} and to the momentum thickness transition Reynolds number results (Figure 19) for both investigations.

Attention is called to the fact that the variations exhibited in Figures 17 and 18 attain their maximum values ($\sim 1-2/3$ for the present results and ~ 2 for the data of Stetson and Rushton) in the vicinity of $S_\tau/S_{SW} = 1/2$. Furthermore, the maximum slopes in the local edge property variations, with the exception of pressure, also occur in this same general location. This raises the question of whether these two phenomena are in any way related. The fact that streamwise velocity gradients (in the presence of pressure gradients) influence the stability of flat-plate boundary layers is well known from both stability analyses and experiments. Furthermore, linear stability theory also admits the possibility that gradients in the flow variables in the absence of pressure gradients may influence the stability of a laminar boundary layer through their effects on the velocity, density, and temperature profiles within the layer. This aspect of the blunt-body transition problem bears further investigation.

Finally, the transition results from the present study and References 12, 14, and 15 are summarized in terms of the same local parameters in Figure 20.^{**} For the purposes of the following discussion, the effect of free-stream unit Reynolds number, illustrated in preceding figures, is

^{*} The swallowing distances for the data of Stetson and Rushton¹² are the values computed by Softley¹⁴ using the VIZAAD program.²⁵

^{**} The local blunt-cone parameters reported by Softley¹⁴ and Sheetz¹⁵ were computed with the VIZAAD program²⁵ and the method of Wilson,²⁶ respectively. Once again, the Reynolds-number ratios for the Sheetz data reflect an additional uncertainty introduced as a result of having to estimate the appropriate local sharp-cone transition Reynolds numbers.

ignored, and a single curve is faired through each set of data. The resulting variations exhibit the same general trends with decreasing S_T/S_{SW} . In the "small bluntness" region, the curves increase from a transition Reynolds-number ratio of unity in the conical flow regime ($S_T/S_{SW} \gtrsim 5$) to a maximum of roughly 2 at S_T/S_{SW} between 0.5 and 0.8, after which they decrease (but at different rates) to values considerably less than unity in the "large bluntness" region.

Despite the fact that the experimental variations are similar in a qualitative sense, little significance can be attached to the quantitative agreement, or disagreement, between the various sets of data. The principal reason for this is the fact that the methods employed by the various investigators for computing local Reynolds numbers and swallowing distances for blunt cones yield different results. The differences in the latter in particular, as demonstrated in Figure 16, are obviously significant. The extent to which these differences in S_{SW} influence the results presented in Figure 20 can be illustrated by using just one calculation technique for all the data; in this case, the BLUNTY Aerodynamic Heating Program.^{21,22} This was accomplished, in effect, by adjusting the values of $\bar{S}_{SW}/(Re_\infty, R_N)^{1/3}$ computed by Softley and Sheetz by the differences between their results and the curves computed with program BLUNTY.

With these adjusted swallowing distances, the results in Figure 20 are altered as follows: the Mach 10 and 12 data of Softley are shifted to the left by a factor of about 0.6. This considerably improves their agreement with the present results and the data of Stetson and Rushton, particularly for transition Reynolds-number ratios greater than unity (the $M_\infty = 10-12$ and 5.5-6 curves become essentially coincident in the "small bluntness" and part of the "large bluntness" regions). The Mach 10 and 15 data of Sheetz, on the other hand, are shifted to the right by factors of approximately 4 and 7, respectively, which now places the Mach 15 data slightly to the right of the Mach 10 points. This eliminates the close agreement between the Mach 10 results of Softley

and Sheetz exhibited in Figure 20. It is clear, therefore, that a quantitative analysis of these results is impossible under the present circumstances.

Nevertheless, the following qualitative observations can be made regarding the apparent effects of free-stream Mach number and wall cooling on transition on blunt cones. In the "small bluntness" region ($S_T/S_{SW} \gtrsim 1/2$), the data suggest that the behavior of transition will be similar to that on a sharp cone exposed to the same environment. Therefore, the effects of Mach number and wall cooling will be essentially canceled by plotting the data in ratio form, and the shapes of the curves in the "small bluntness" region should not be appreciably altered by these parameters. However, in view of the diverse variations for $S_T/S_{SW} \lesssim 1/2$, this does not appear to be the case in the "large bluntness" region. The differences between these results suggest that an increase in free-stream Mach number will effect a counterclockwise rotation and/or a shift to the right of the curves in this region. Considering the data in Figure 8 as well, it appears that an increase in wall cooling will produce the same general effect. Thus, an increase in T_w/T_R (i.e., a decrease in wall cooling) will cause the "large bluntness" portion of the curves to rotate clockwise and/or shift to the left.

Significance to Reentry-Vehicle Design

If the general trends illustrated in Figure 20 are assumed to be qualitatively correct, it is of interest to consider their significance to reentry-vehicle design. To this end, an analysis was made of the ballistic reentry of a spherically blunted, slender-cone vehicle for which five different nose radii were assumed: 0.1, 0.25, 0.5, 1.0, and 2.0 inches. Local Reynolds-number distributions along the vehicle for each nosetip were computed with the BLUNTY program at a number of altitudes below 120 kft. The variations at 100, 70, and 50 kft are presented in Figure 21 against a background of the correlation curves from Figure 20. The local Reynolds numbers are normalized by the local sharp-cone transition Reynolds number at each altitude. The latter

values were estimated from ground test data under the following assumptions:

(1) smooth wall, (2) no surface mass transfer, (3) constant wall temperature, (4) zero angle of attack, (5) the local Mach-number variation given by Softley¹⁴ (in his Figure 10), and (6) a unit-Reynolds-number dependence of $(u/\nu)^{0.4}$. Surface distances of 2, 4, and 6 feet are indicated on each of the curves.

When the blunt-cone correlation curves are used as transition criteria, the variations at 100 kft show that the vehicle with the smallest nose has already experienced transition ahead of the 2-foot location. With increasing nose radius, the location of transition moves aft and is downstream of the 6-foot station for the two bluntest noses. On the basis of the high Mach number/low T_w/T_R correlation curve (the $M_\infty = 10-12$ curve), the optimum nose radius for delaying transition at 100 kft is of the order of 1 inch.

With decreasing altitude, the local Reynolds-number distributions shift to the left, relative to the transition correlations; and the 2-, 4-, and 6-foot locations move generally up the curves. As a result, the location of transition moves forward for all nosetips, but it moves farther for the blunter noses. This is caused by the fact that the local Reynolds-number distributions and the "large bluntness" portions of the correlation curves are almost parallel. Hence, as the former shift past the latter with decreasing altitude, the forward movement of transition is very rapid. This may be one of the reasons for the almost instantaneous transition which occurs over an entire vehicle during some flights.

Referring again to the high-Mach-number/low-wall-temperature criteria for transition (including the $M_\infty = 15$ curve), the optimum nose radius for delaying transition at 70 and 50 kft appears to be closer to 1/2 inch. It should be noted, however, that if the stabilizing effect of increasing T_w/T_R is taken into account and the "large bluntness" portion of the transition correlation curves shifted up and to the left, as described in the previous section (e.g., closer to the $M_\infty = 5.5-6$ curve), the performance of the blunter noses will improve and the optimum radius may increase.

Finally, the local Reynolds-number histories at the 4-foot location for all five nose radii are compared in Figure 22 against the same blunt-cone transition curves. The disadvantage of relatively sharp nose radii, $R_N \leq 1/4$ inch, becomes obvious in this representation, in that transition occurred forward of the 4-foot location for the two sharpest noses above 120 kft. In addition, the differences between the constant altitude lines and the transition correlation curves provide a clear illustration of (1) the desirability of nose radii of the order of $1/2$ inch for delaying transition at high Mach numbers and low wall temperatures, and (2) the fact that the stabilizing influence of increasing T_w/T_R during reentry serves to reduce the transition altitude for nose radii $\geq 1/2$ inch.

CONCLUSIONS

An experimental investigation has been conducted to determine the effects of free-stream unit Reynolds number and nose bluntness on the behavior of boundary-layer transition on an 8-degree cone at a Mach number of 6. Based on an analysis of the results and comparisons with data available in the literature, the following conclusions were made:

1. For an initial wall-to-recovery temperature ratio of roughly 0.6, the location of transition was essentially constant throughout each run on all but the bluntest model. The transient behavior of transition on the 32-percent blunt model was found to depend upon nose radius (probably through its effect on the longitudinal variations in pressure and wall temperature), the free-stream unit Reynolds number, and the wall-to-recovery temperature ratio. With respect to the latter, the aft movement of transition with rising wall temperature suggests that an increase in T_w/T_R tends to delay transition in the "large bluntness" regime.

2. As nose radius is increased at constant free-stream conditions, the location of transition initially moves aft of its sharp-cone value, then reverses direction and moves forward again. This reversal of transition divides its behavior into two separate regimes commonly referred to as the "small bluntness" and "large bluntness" regions.
3. Changes in the free-stream unit Reynolds number and nose radius cause significant but different variations in the transition Reynolds numbers, Re_{∞, S_T} , Re_{e, S_T} and Re_{e, θ_T} . In the "small bluntness" region ($S_T/S_{SW} \gtrsim 1/2$), the variations are small and can be minimized by dividing by the corresponding sharp-cone transition Reynolds numbers. In the "large bluntness" region ($S_T/S_{SW} \lesssim 1/2$), however, an increase in R_N produces drastic reductions in the transition Reynolds numbers, while an increase in $(u/\nu)_{\infty}$ may cause either an increase or decrease in these parameters.
4. The transition-to-swallowing distance ratio, S_T/S_{SW} , is a better parameter for correlating local transition Reynolds numbers than the bluntness Reynolds number, Re_{∞, R_N} . The latter does not properly account for the different effects of R_N and $(u/\nu)_{\infty}$, and its use as a correlating parameter can be misleading.
5. The successful correlation of blunt-body transition data depends a great deal upon the proper calculation of local boundary-layer edge properties and swallowing distances. The various calculation schemes currently in use require further refinement to yield more consistent results.

6. When compared with other data in terms of free-stream properties, the combined results indicate that, by a judicious selection of nose radius for a given free-stream environment $[M_\infty \text{ and } (u/\nu)_\infty]$, it is possible to increase Re_{∞, S_T} over the corresponding sharp-cone value by almost an order of magnitude. In terms of transition behavior during reentry, this represents a reduction in transition altitude of roughly 50 kft for a typical ballistic trajectory.
7. An analysis of the ballistic reentry of a typical spherically blunted, slender-cone vehicle, using currently available blunt-cone transition results, suggests that it is possible to determine an optimum nose radius for delaying transition to a minimum altitude. However, before this can be accomplished with any degree of certainty, the effects of surface roughness, mass transfer, wall cooling, etc., on the blunt-cone transition variations must be evaluated. The study also indicates that the almost instantaneous transition behavior observed during some flights may be due in part to the similar variations in the local Reynolds-number distributions and the blunt-cone transition curves in the "large bluntness" region.

REFERENCES

1. Potter, J. L., and Whitfield, J. D., "Effects of Slight Nose Bluntness and Roughness on Boundary-Layer Transition in Supersonic Flows," Journal of Fluid Mech., Vol. 12, No. 4, April 1962, pp. 501-535.
2. Potter, J. L., and Whitfield, J. D., "Boundary-Layer Transition Under Hypersonic Conditions," AEDC-TR-65-99, May 1965, Arnold Engineering Development Center, Arnold Air Force Station, Tenn.
3. Whitfield, J. D., "Hypersonic Wind-Tunnel Experiments on Boundary-Layer Transition at Mach 14," Boundary Layer Transition Study Group Meeting, BSD-TR-67-213, Vol. III, August 1967, Aerospace Corporation, San Bernardino, Calif., pp. 19-1 - 19-26.
4. Morkovin, M. V., "Critical Evaluation of Transition from Laminar to Turbulent Shear Layers with Emphasis on Hypersonically Traveling Bodies," AFFDL-TR-68-149, March 1969, Air Force Flight Dynamics Laboratory, Wright-Patterson Air Force Base, Ohio.
5. Pate, S. R., and Schueler, C. J., "An Investigation of Radiated Aerodynamic Noise Effects on Boundary-Layer Transition in Supersonic and Hypersonic Wind Tunnels," AIAA Paper No. 68-375, presented at the AIAA Third Aerodynamic Testing Conference, San Francisco, Calif., April 8-10, 1968.
6. Pate, S. R., "Measurements and Correlations of Transition Reynolds Numbers on Sharp Slender Cones at High Speeds," AIAA Journal, Vol. 9, No. 6, June 1971, pp. 1082-1090; also AEDC-TR-69-172, Dec. 1969, Arnold Engineering Development Center, Arnold Air Force Station, Tenn.
7. Potter, J. L., "Observations on the Influence of Ambient Pressure on Boundary-Layer Transition," AIAA Journal, Vol. 6, No. 10, Oct. 1968, pp. 1907-1911.
8. Sheetz, N. W., Jr., "Ballistics Range Experiments on the Effect of Unit Reynolds Number on Boundary-Layer Transition," Proceedings of the 8th Navy Symposium on Aeroballistics, Naval Weapons Center, Corona, Calif., Paper No. 7, Vol. 2, June 1969, pp. 201-215.
9. Diaconis, N. S., Jack, J. R., and Wisniewski, R. J., "Boundary-Layer Transition at Mach 3.12 as Affected by Cooling and Nose Blunting," NACA TN 3928, Jan. 1957, Lewis Flight Propulsion Laboratory, Cleveland, Ohio.

10. Jack, J. R., Wisniewski, R. J., and Diaconis, N. S., "Effects of Extreme Surface Cooling on Boundary-Layer Transition," NACA TN 4094, Oct. 1957, Lewis Flight Propulsion Laboratory, Cleveland, Ohio.
11. Diaconis, N. S., Wisniewski, R. J., and Jack, J. R., "Heat Transfer and Boundary-Layer Transition on Two Blunt Bodies at Mach Number 3.12," NACA TN 4099, Oct. 1957, Lewis Flight Propulsion Laboratory, Cleveland, Ohio.
12. Stetson, K. F., and Rushton, G. H., "Shock Tunnel Investigation of Boundary Layer Transition at $M = 5.5$," AIAA Journal, Vol. 5, No. 5, May 1967, pp. 899-906.
13. Stainback, P. C., "Effect of Unit Reynolds Number, Nose Bluntness, Angle of Attack, and Roughness on Transition on a 5° Half-Angle Cone at Mach 8," NASA TN D-4961, Jan. 1969, Langley Research Center, Langley Station, Va.
14. Softley, E. J., "Boundary Layer Transition on Hypersonic Blunt, Slender Cones," AIAA Paper No. 69-705, presented at the AIAA Fluid and Plasma Dynamics Conference, San Francisco, Calif., June 16-18, 1969.
15. Sheetz, N. W., Jr., "Ballistic Range Boundary-Layer Transition Measurements on Cones at Hypersonic Speeds," Proceedings of the Navy-NASA-LTV Symposium on Viscous Drag Reduction, Spangler, J. R., and Wells, C. S., Jr., Editors, Plenum Press, Feb. 1969, pp. 53-83.
16. Martellucci, A. and Neff, R. S., "Influence of Asymmetric Transition on Reentry Vehicle Characteristics," Journal of Spacecraft, Vol. 8, No. 5, May 1971, pp. 476-482.
17. DiCristina, V., "Three-Dimensional Laminar Boundary Layer Transition on a Sharp 8° Cone at Mach 10," AIAA Journal, Vol. 8, No. 5, May 1970, pp. 852-856.
18. McCauley, W. D., Editor, Boundary Layer Transition Study Group Meeting, Report No. TR-0158 (S3816-63)-1 (Air Force Report No. BSD-TR-67-213), Volumes I-IV, Aug. 1967, Aerospace Corporation, San Bernardino, Calif.
19. Van Driest, E. R., "Investigation of Laminar Boundary Layer in Compressible Fluids using the Crocco Method," NACA TN-2597, Jan. 1952.

20. Van Driest, E. R., "The Problem of Aerodynamic Heating," Aeronautical Engineering Review, Vol. 15, No. 10, October 1956, pp. 26-41.
21. Hochrein, G. J., "A Procedure for Computing Aerodynamic Heating on Sphere Cones - Program BLUNTY, Vol. I: Concept and Results," SC-DR-69-243, June 1969, Sandia Laboratories, Albuquerque, New Mexico.
22. Hochrein, G. J., "A Procedure for Computing Aerodynamic Heating on Sphere Cones - Program BLUNTY, Vol. II: Equations, Operating Procedure, and Program Details," SC-DR-69-449, Nov. 1969, Sandia Laboratories, Albuquerque, New Mexico.
23. Zakkay, V., and Krause, E., "Boundary Conditions at the Outer Edge of the Boundary Layer on Blunted Conical Bodies," AIAA Journal, Vol. 1, No. 7, July 1963, pp. 1671-1672.
24. Rubin, I., "Shock Curvature Effect on the Outer Edge Conditions of a Laminar Boundary Layer," AIAA Journal, Vol. 1, No. 12, Dec. 1963, pp. 2850-2852.
25. Studerus, C. J., and Dienna, E. A., "Viscous Interaction Zero Angle of Attack Drag (VIZAAD) Program," TIS 64SD292, Nov. 1964, General Electric Co., Philadelphia, Pa.
26. Wilson, R. E., "Laminar Boundary Layer Growth on Slightly Blunted Cones at Hypersonic Speeds," Journal of Spacecraft and Rockets, Vol. 2, No. 4, April 1965, pp. 490-496.
27. Jacobs, H. R., "Engineering Approximation of the Effects of Blunting on Cones in Laminar and Turbulent Flow," TR-0158 (S3816-41)-1 (Air Force Report No. SAMSO-TR-68-258), Oct. 1967, Aerospace Corporation, San Bernardino, Calif.
28. Hirst, E., "A Description of the NASA-Ames Cone, Blunt Body and Method of Characteristics Flow Field Programs," SCL-TM-65-119, Feb. 1966, Sandia Laboratories, Livermore, Calif.
29. Rotta, N. R., "Effects of Nose Bluntness on the Boundary Layer Characteristics of Conical Bodies at Hypersonic Speeds," NYU-AA-66-66, Nov. 1966, New York University, School of Engineering and Science, New York, N. Y.
30. Jones, D. J., "Tables of Inviscid Supersonic Flow about Circular Cones at Incidence, $\gamma = 1.4$," AGARDograph 137, Part I, Nov. 1969.
31. Baltakis, F. P., "Performance Capability of the NOL Hypersonic Tunnel," NOLTR 68-187, Oct. 1968, U.S. Naval Ordnance Laboratory, White Oak, Md.

TABLE I

Results for Sharp through 16-Percent Blunt Models

Run No.	P _O (atm)	T _O (°R)	M _∞	R _N (in.)	$\left(\frac{u}{v}\right)_{\infty} \times 10^{-6}$ (ft ⁻¹)	S _{SW} (in.)	S _T (in.)	M _{eT}	Re _{e,S_T} × 10 ⁻⁶	Re _{e,θ_T}
1-1	137.3	1162	6.00	0.0025	23.20	0.19	2.17	5.24	5.72	917
2-30	140.5	1169	6.00	0.0025	23.53	0.19	2.09	5.24	5.58	906
2-34	140.2	1179	6.00	0.0025	23.18	0.19	2.34	5.24	6.13	949
2-35	140.1	1157	6.00	0.0025	23.83	0.19	2.32	5.24	6.27	960
1-2	99.15	1146	6.00	0.0025	17.11	0.17	2.78	5.24	5.45	895
2-31	100.9	1155	6.00	0.0025	17.21	0.17	2.90	5.24	5.72	917
2-32	100.9	1162	6.00	0.0025	17.05	0.17	3.08	5.24	5.99	938
2-36	101.1	1148	6.00	0.0025	17.40	0.17	3.15	5.24	6.27	960
1-3	54.65	1127	6.00	0.0025	9.669	0.14	4.07	5.24	4.49	812
1-14	54.51	1121	6.00	0.0025	9.722	0.14	4.29	5.24	4.77	837
2-33	53.91	1151	6.00	0.0025	9.241	0.14	4.14	5.24	4.36	800
2-37	54.21	1134	6.00	0.0025	9.502	0.14	4.27	5.24	4.63	825
1-4	15.28	1092	5.90	0.0025	2.956	0.09	10.68	5.16	3.54	721
1-15	15.58	1094	5.90	0.0025	3.006	0.09	11.67	5.16	3.95	762
2-41	15.02	1114	5.90	0.0025	2.820	0.09	10.80	5.16	3.40	707
1-5	138.2	1177	6.00	0.025	22.93	4.10	4.08	4.96	8.79	1145
1-6	99.64	1163	6.00	0.025	16.82	3.70	4.57	5.07	7.81	1080
1-7	54.46	1143	6.00	0.025	9.434	3.03	6.08	5.19	6.29	970
2-52	54.87	1147	6.00	0.025	9.455	3.03	5.81	5.18	5.99	947
1-8	15.37	1105	5.90	0.025	2.921	2.02	12.02	5.17	3.98	770
1-11	140.3	1157	6.00	0.100	23.86	26.9	6.95	3.49	4.94	859
1-12	98.93	1141	6.00	0.100	17.18	24.0	9.57	4.02	7.61	1058
1-13	54.70	1123	6.00	0.100	9.730	19.7	11.53	4.49	7.52	1055
1-9	15.37	1101	5.90	0.100	2.937	13.0	> 16.83	> 5.02	> 5.03	> 869
1-17	137.5	1136	6.00	0.200	24.04	68.4	9.70	3.03	4.56	841
1-18	99.25	1132	6.00	0.200	17.44	61.2	11.16	3.18	4.39	820
1-19	55.14	1113	6.00	0.200	9.940	50.4	13.19	3.48	3.93	770
2-45	55.21	1130	6.00	0.200	9.729	50.0	12.87	3.45	3.69	747
1-20	137.9	1156	6.00	0.400	23.49	172	10.99	2.81	3.95	821
1-21	99.57	1137	6.00	0.400	17.38	155	12.25	2.85	3.39	753
1-22	55.46	1117	6.00	0.400	9.944	128	> 15.12	> 2.96	> 2.71	> 663

TABLE II

Results for 32-Percent Blunt Model

Run No.	P _o (atm)	T _o (°R)	M _∞	R _N (in.)	$\left(\frac{u}{v}\right)_{\infty} \times 10^{-6}$ (ft ⁻¹)	S _{SW} (in.)	S _T (in.)	M _{eT}	Re _{e, S_T} × 10 ⁻⁶	Re _{e, θ_T}	t _{ev} (sec)
2-1	139.3	1190	6.00	0.800	22.71	433	2.33	2.53	0.817	573	1.25
2-2	139.8	1200	6.00	0.800	22.51	432	2.19	2.51	0.768	561	1.25
2-13	139.7	1123	6.00	0.800	24.85	446	2.60	2.56	0.962	619	1.25
2-27	139.8	1129	6.00	0.800	24.67	446	1.99	2.48	0.767	565	1.25
2-5	100.2	1168	6.00	0.800	16.80	390	4.79	2.73	1.11	600	1.25
2-6	100.0	1161	6.00	0.800	16.92	391	5.39	2.75	1.24	614	1.25
2-14	99.82	1103	6.00	0.800	18.24	402	5.53	2.76	1.36	646	1.25
2-28	100.0	1158	6.00	0.800	16.99	391	4.70	2.73	1.10	604	1.25
2-9	53.86	1130	6.00	0.800	9.491	320	> 12.85	2.82	> 1.72	> 589	1.25
2-15	54.89	1081	6.00	0.800	10.34	330	> 12.85	2.82	> 1.85	> 611	1.25
2-26	54.68	1097	6.00	0.800	10.07	327	> 12.85	2.82	> 1.81	> 604	1.25
1-25	54.43	1133	6.00	0.800	9.554	321	> 12.85	2.82	> 1.73	> 591	1.25
2-1	139.3	1190	6.00	0.800	22.71	433	> 12.85	2.79	> 4.06	> 906	≥ 5
2-2	139.8	1200	6.00	0.800	22.51	432	> 12.85	2.79	> 4.03	> 903	≥ 5
2-13	139.7	1123	6.00	0.800	24.85	446	> 12.85	2.79	> 4.37	> 941	≥ 5
2-27	139.8	1129	6.00	0.800	24.67	446	> 12.85	2.79	> 4.35	> 938	≥ 5
2-5	100.2	1168	6.00	0.800	16.80	390	> 12.85	2.80	> 3.01	> 781	≥ 10
2-6	100.0	1161	6.00	0.800	16.92	391	> 12.85	2.80	> 3.03	> 783	≥ 10
2-14	99.82	1103	6.00	0.800	18.24	402	> 12.85	2.80	> 3.22	> 808	≥ 10
2-28	100.0	1158	6.00	0.800	16.99	391	> 12.85	2.80	> 3.04	> 784	≥ 10

TABLE III
Variable Temperature Results for Bluntest Model

Run No.	P_o (atm)	T_o (°R)	M_∞	R_N (in.)	$\left(\frac{u}{v}\right)_\infty \times 10^{-6}$ (ft ⁻¹)	S_{SW} (in.)	S_T (in.)	M_{eT}	$Re_{e, S_T} \times 10^{-6}$	Re_{e, θ_T}	T_w/T_R
2-27	139.8	1129	6.00	0.800	24.67	446	1.99	2.48	0.767	565	0.63
2-56	139.7	1149	6.00	0.800	24.01	441	3.53	2.64	1.21	662	0.66
2-57	130.9	1149	6.00	0.800	22.50	431	8.75	2.80	2.64	799	0.77
2-28	100.0	1158	6.00	0.800	16.99	391	4.70	2.73	1.10	604	0.57
2-29	99.86	1181	6.00	0.800	16.47	387	8.89	2.80	2.00	695	0.61
2-58	100.3	1151	6.00	0.800	17.19	393	11.34	2.80	2.68	759	0.76

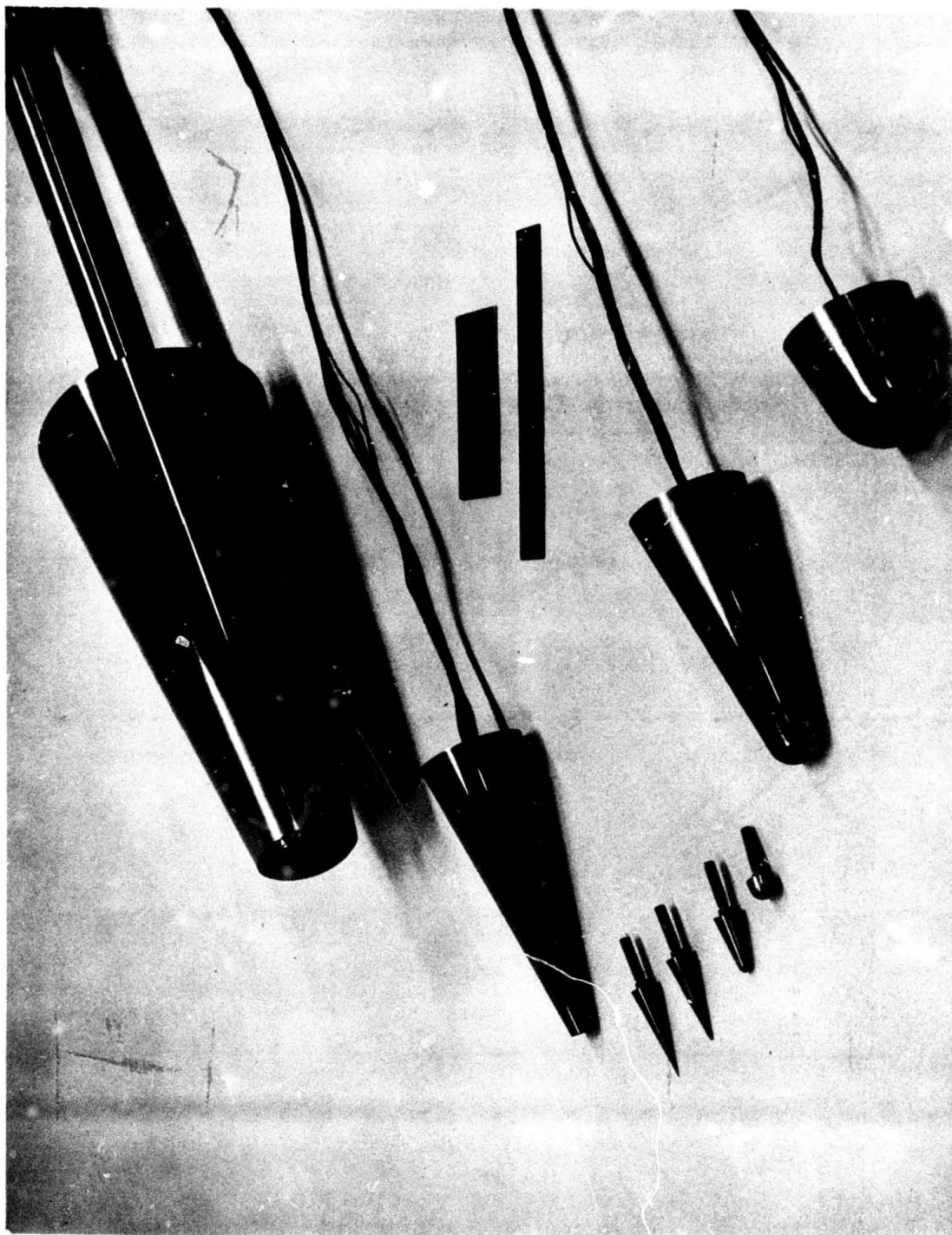


Figure 2. Model Photograph

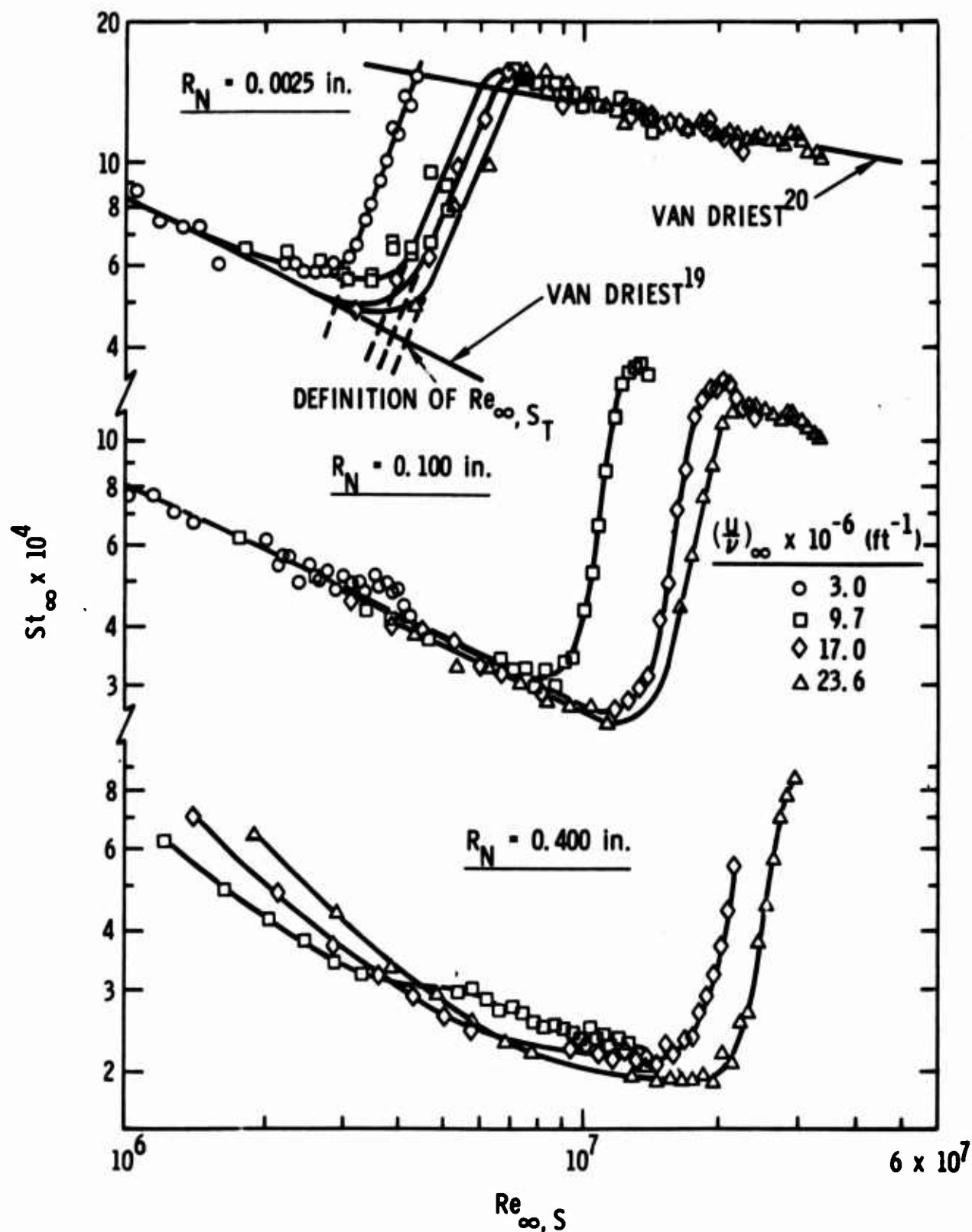


Figure 3. Variation of Stanton Number with Free-Stream Reynolds Number

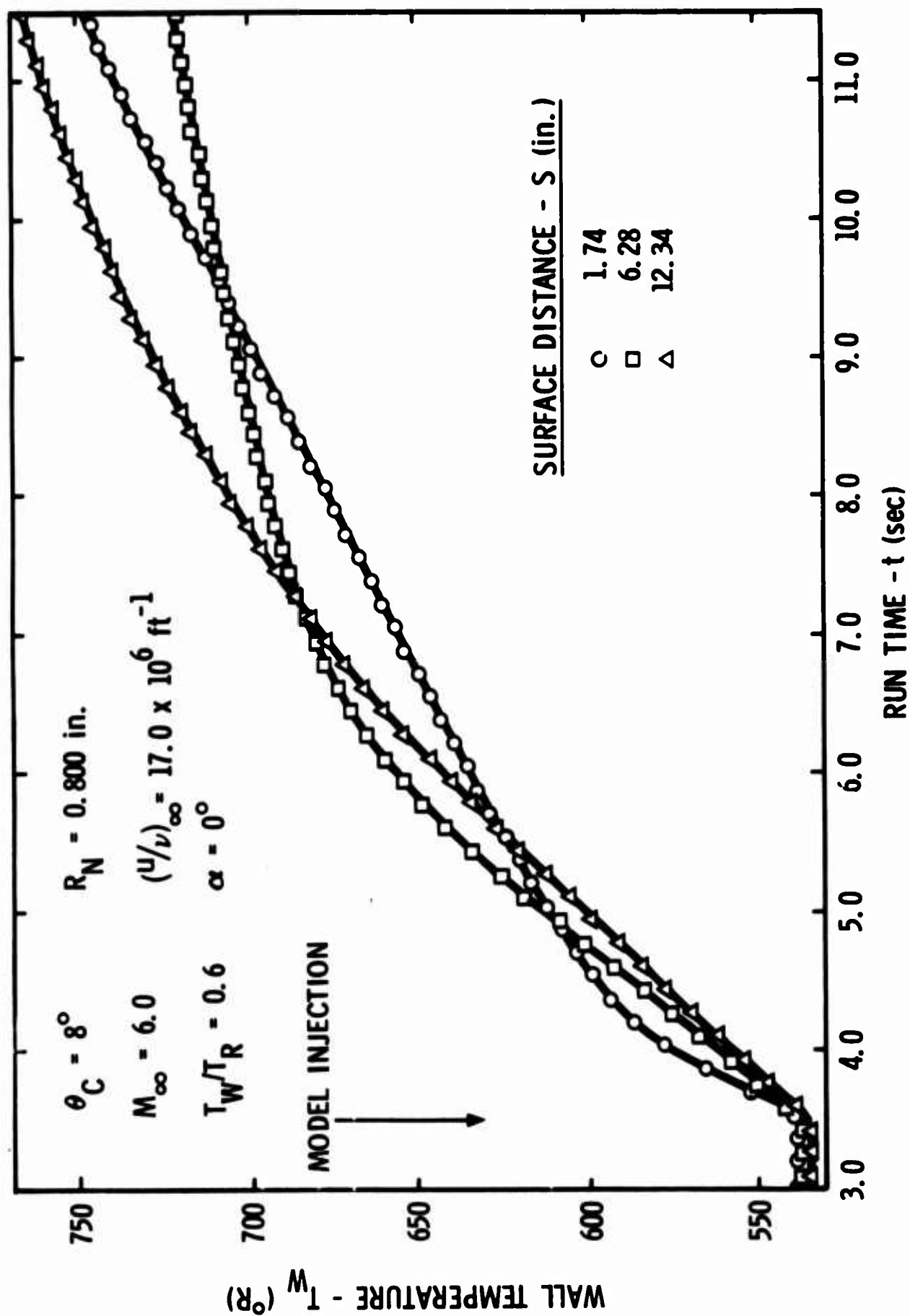


Figure 4. Typical Temperature-Time Data for Blunttest Model

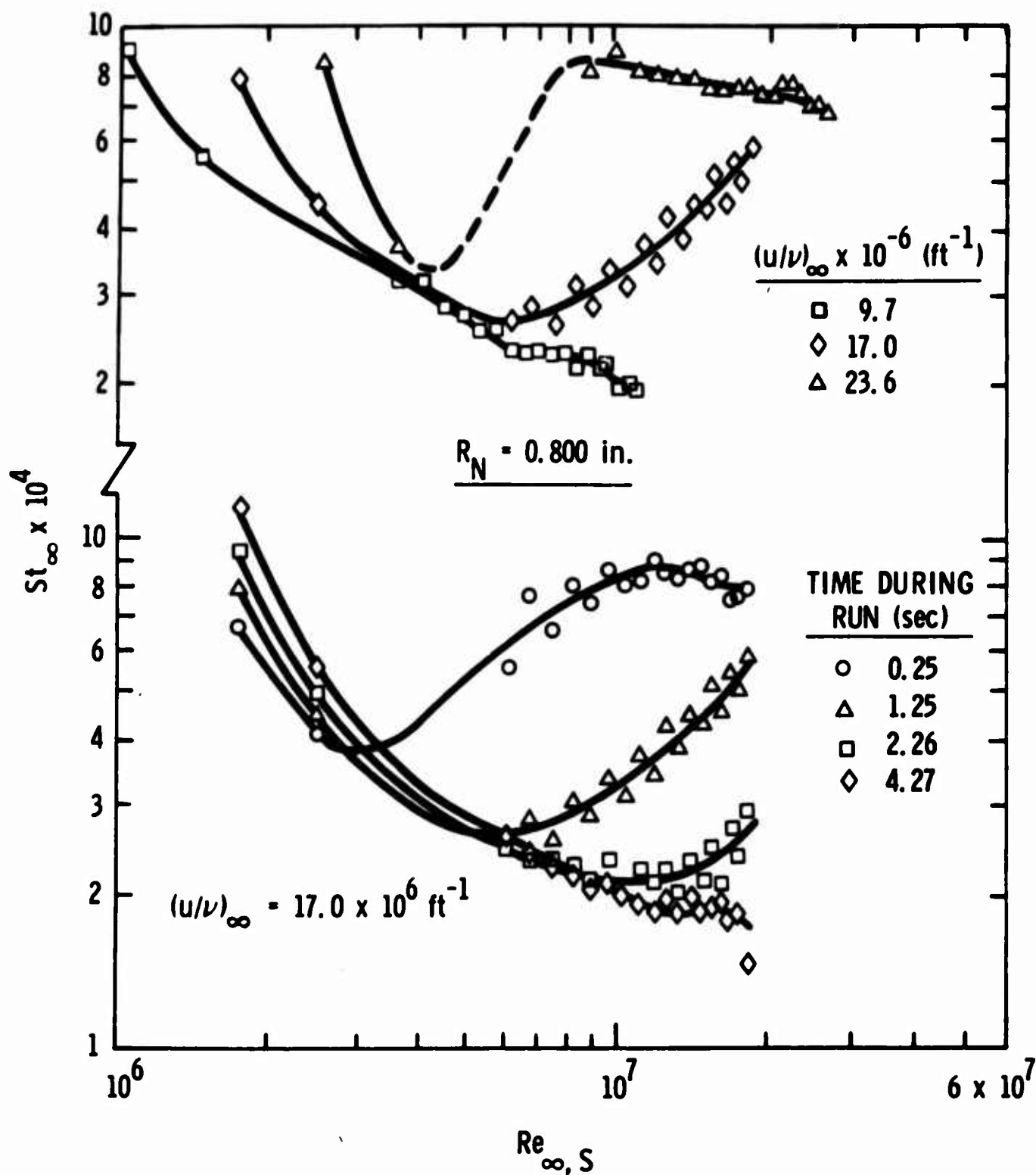


Figure 5. Variation of Stanton Number with Free-Stream Reynolds Number for Bluntest Model

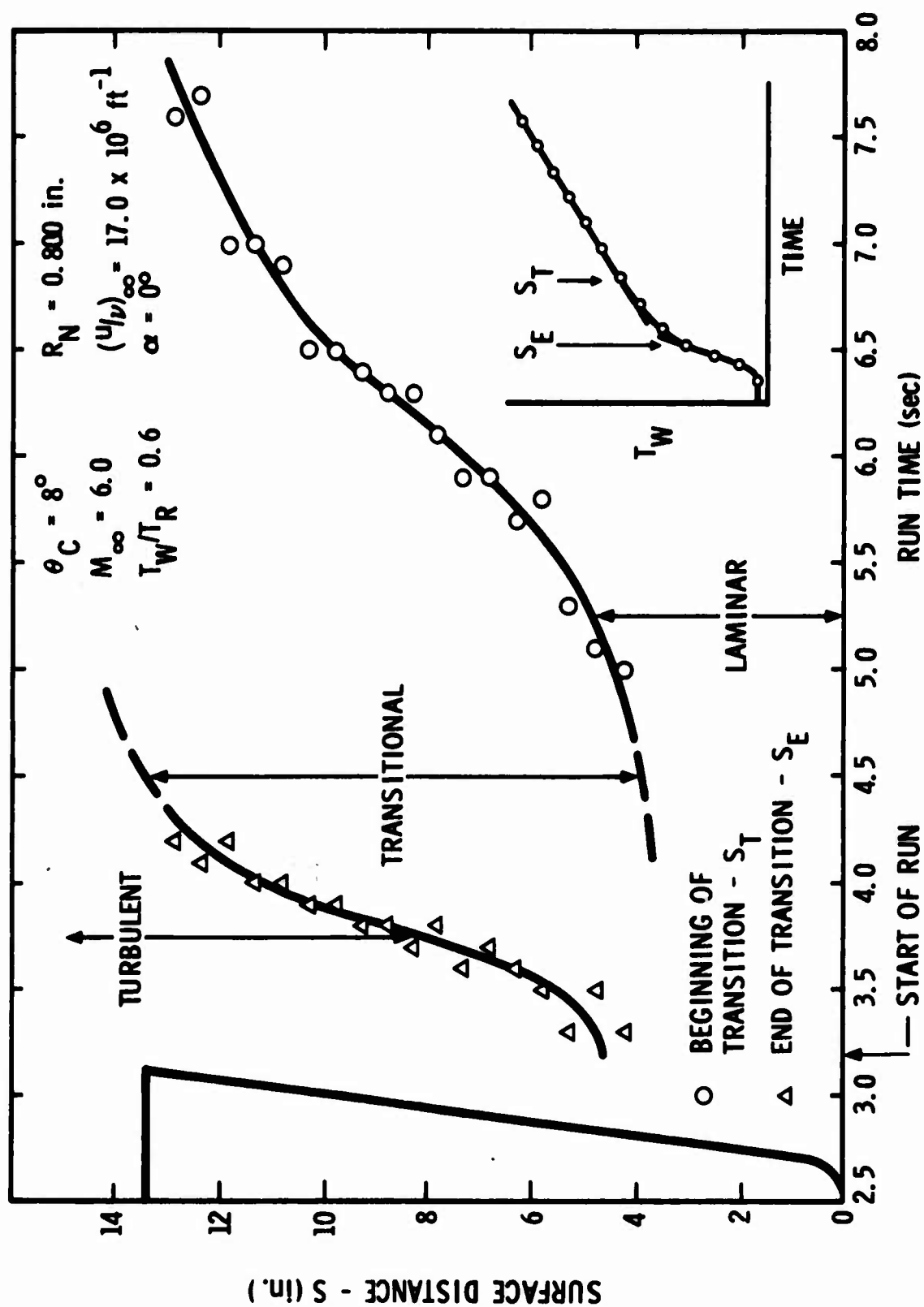


Figure 6. Time History of Transition Region

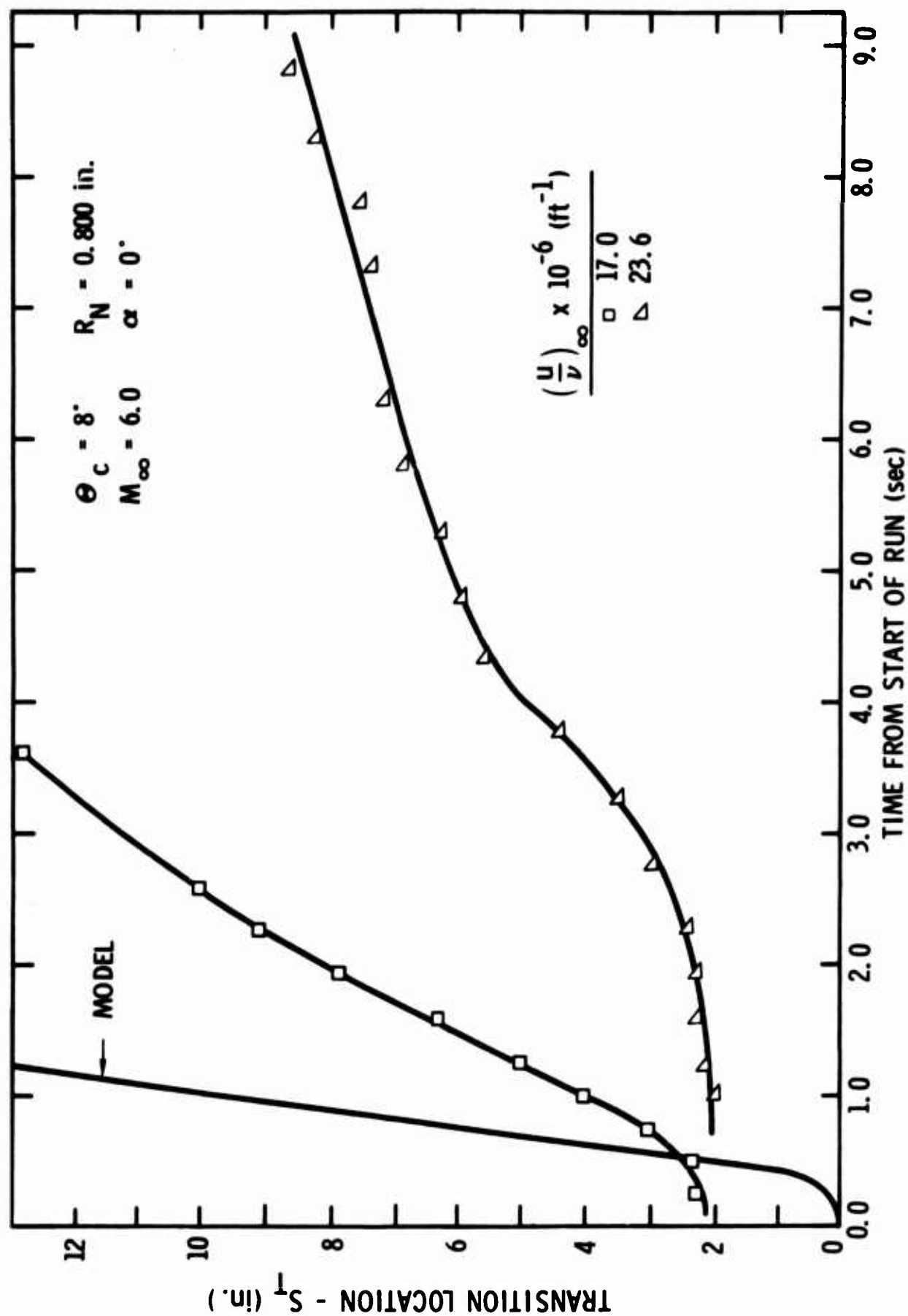


Figure 7. Transition Location History

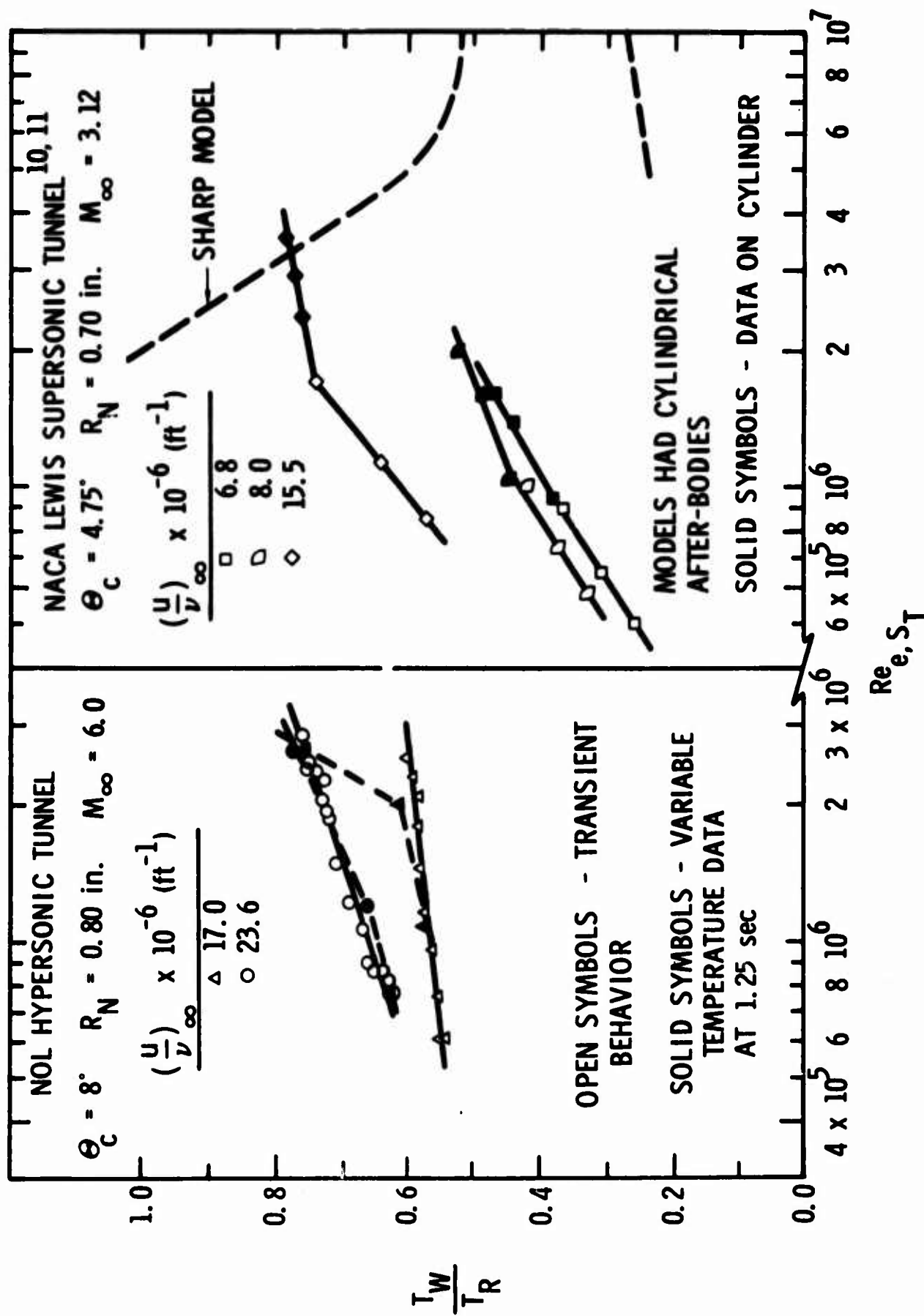


Figure 8. Effect of Wall Cooling on Local Transition Reynolds Number

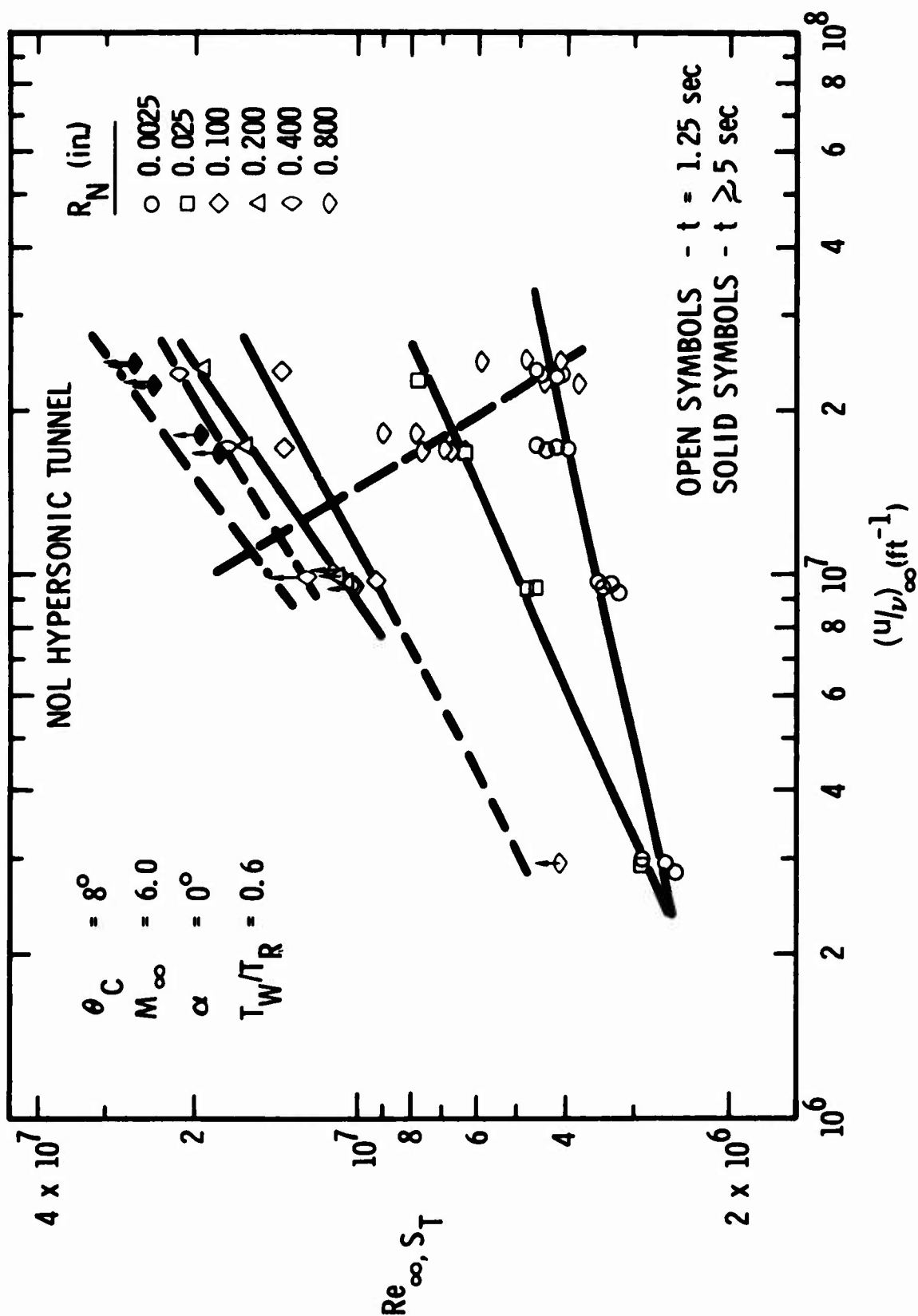


Figure 9. Variation of Free Stream Transition Reynolds Number with Free-Stream Unit Reynolds Number and Nose Radius - NOL Data

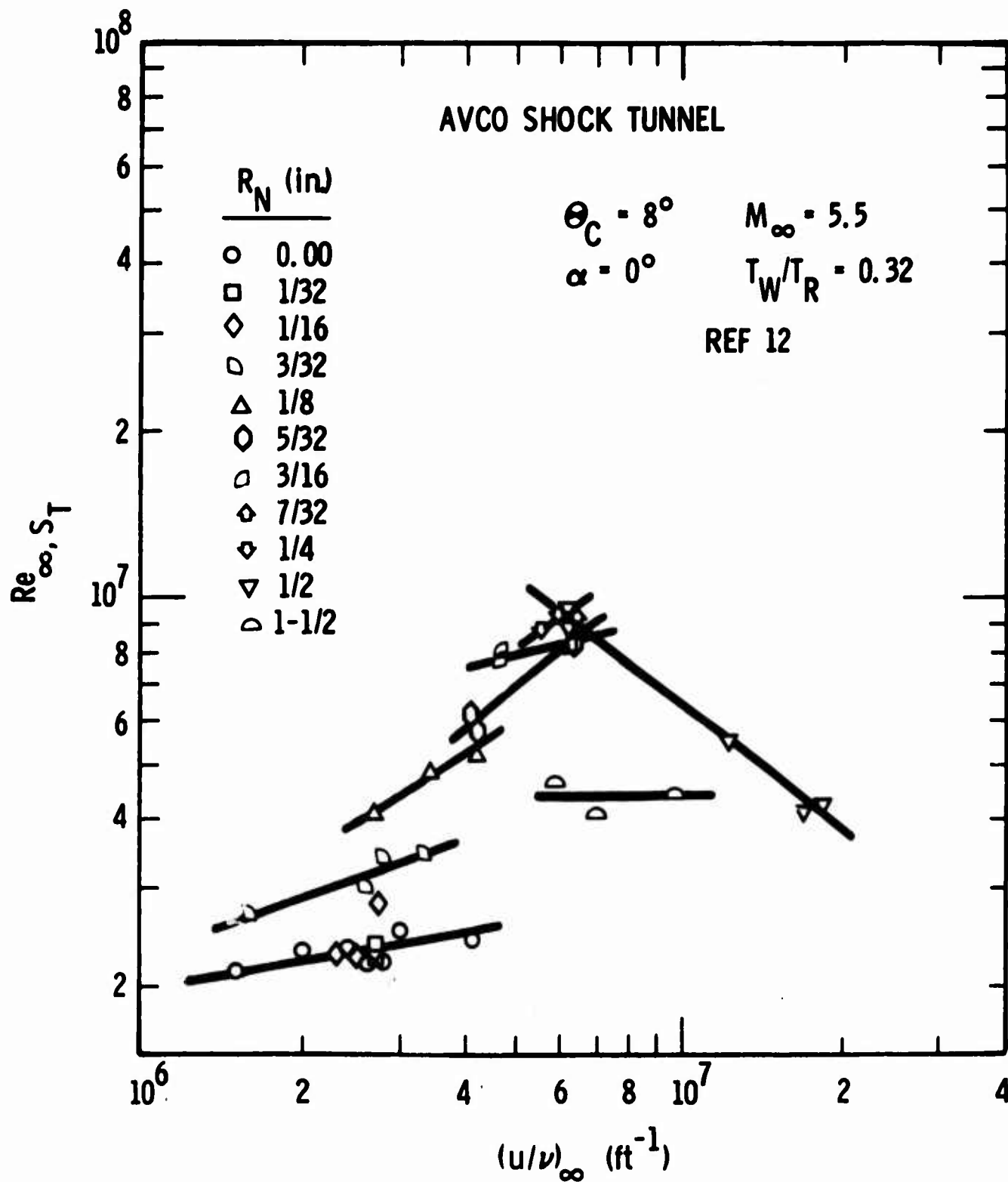


Figure 10. Variation of Free-Stream Transition Reynolds Number with Free-Stream Unit Reynolds Number and Nose Radius - Data of References 12-15

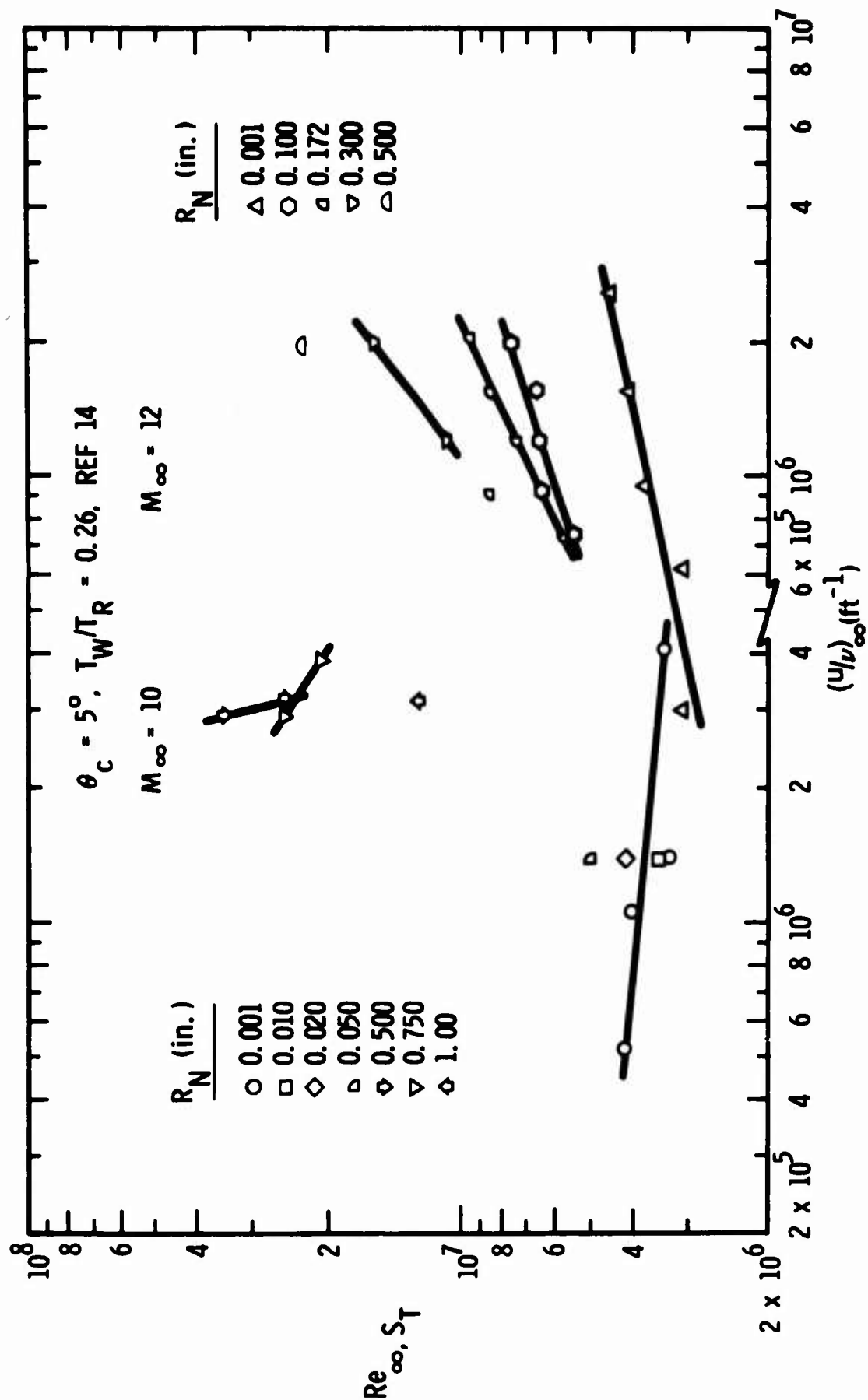


Figure 10 (cont)

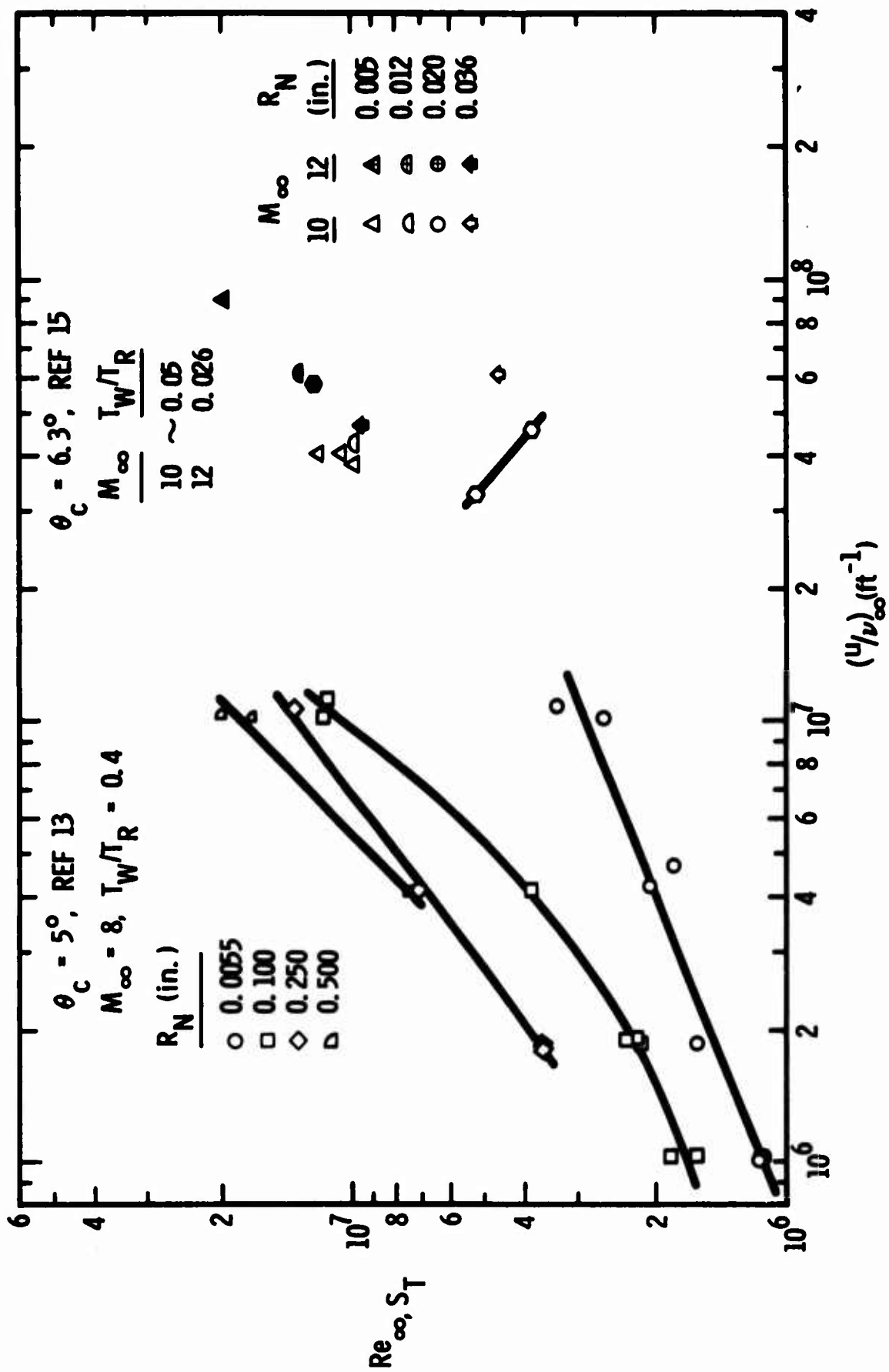


Figure 10 (cont)

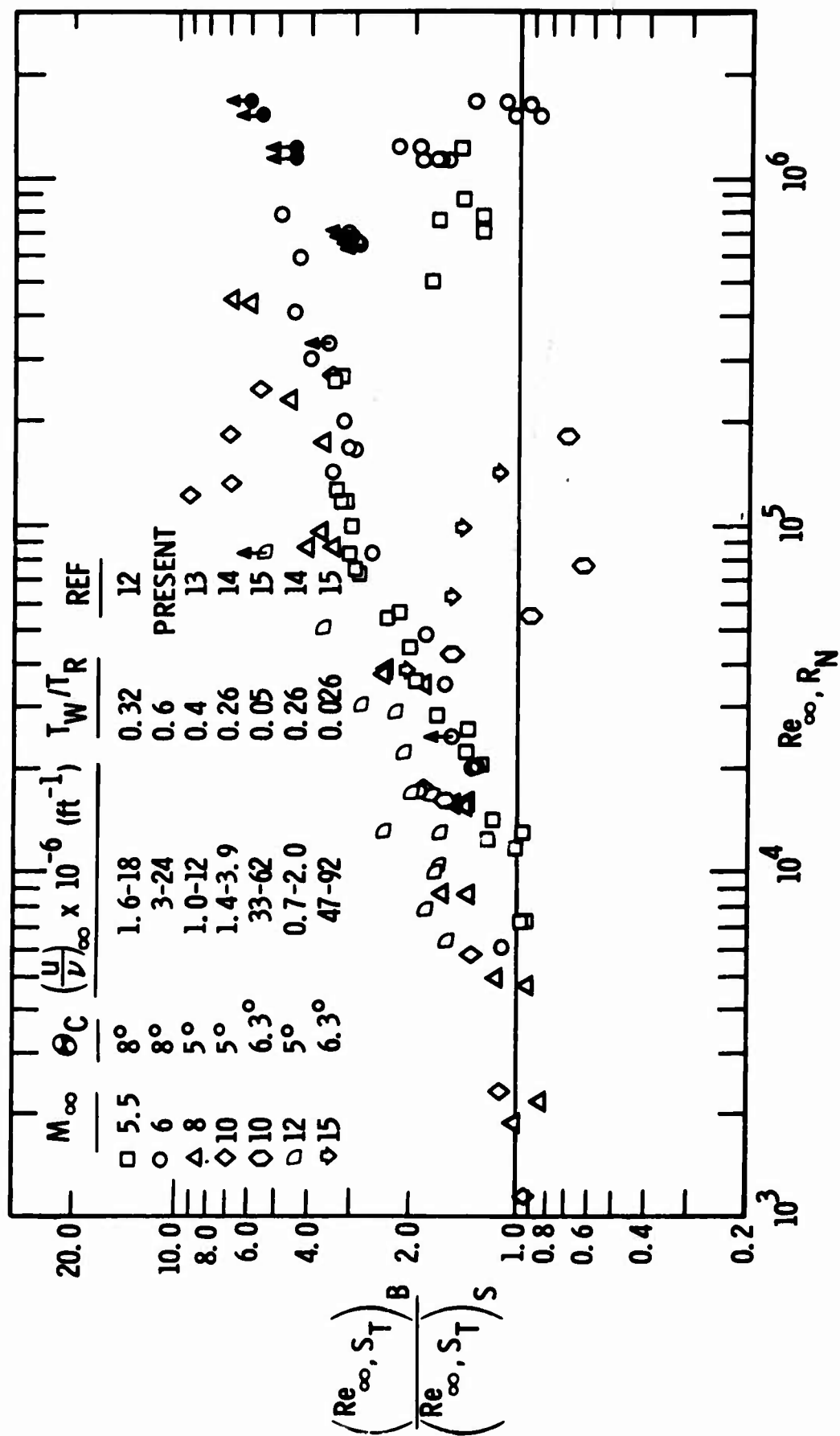


Figure 11. Variation of Free-Stream Transition Reynolds Number Ratio with Bluntness Reynolds Number

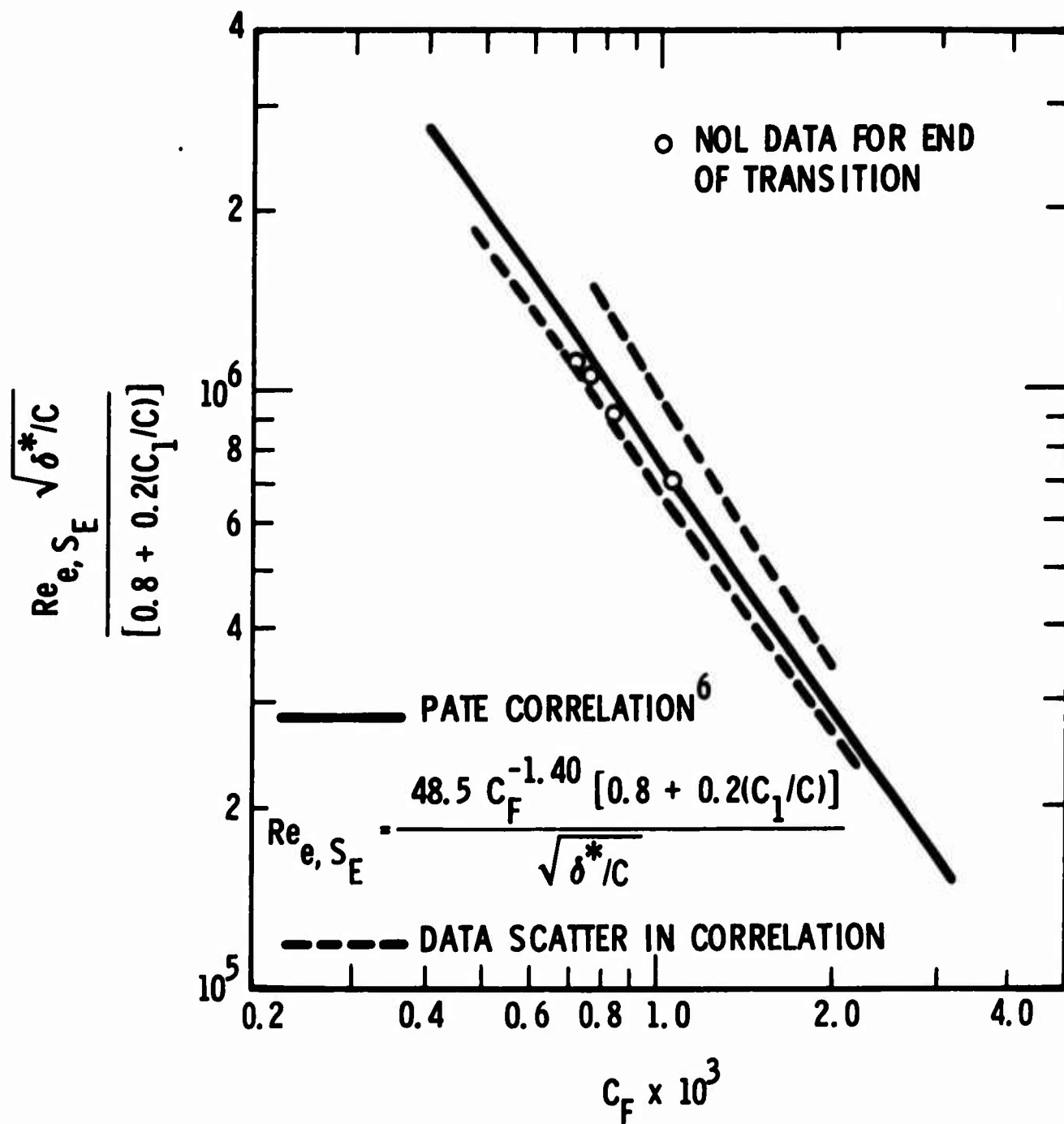


Figure 12. Comparison of NOL Sharp Cone Results with Pate Correlation

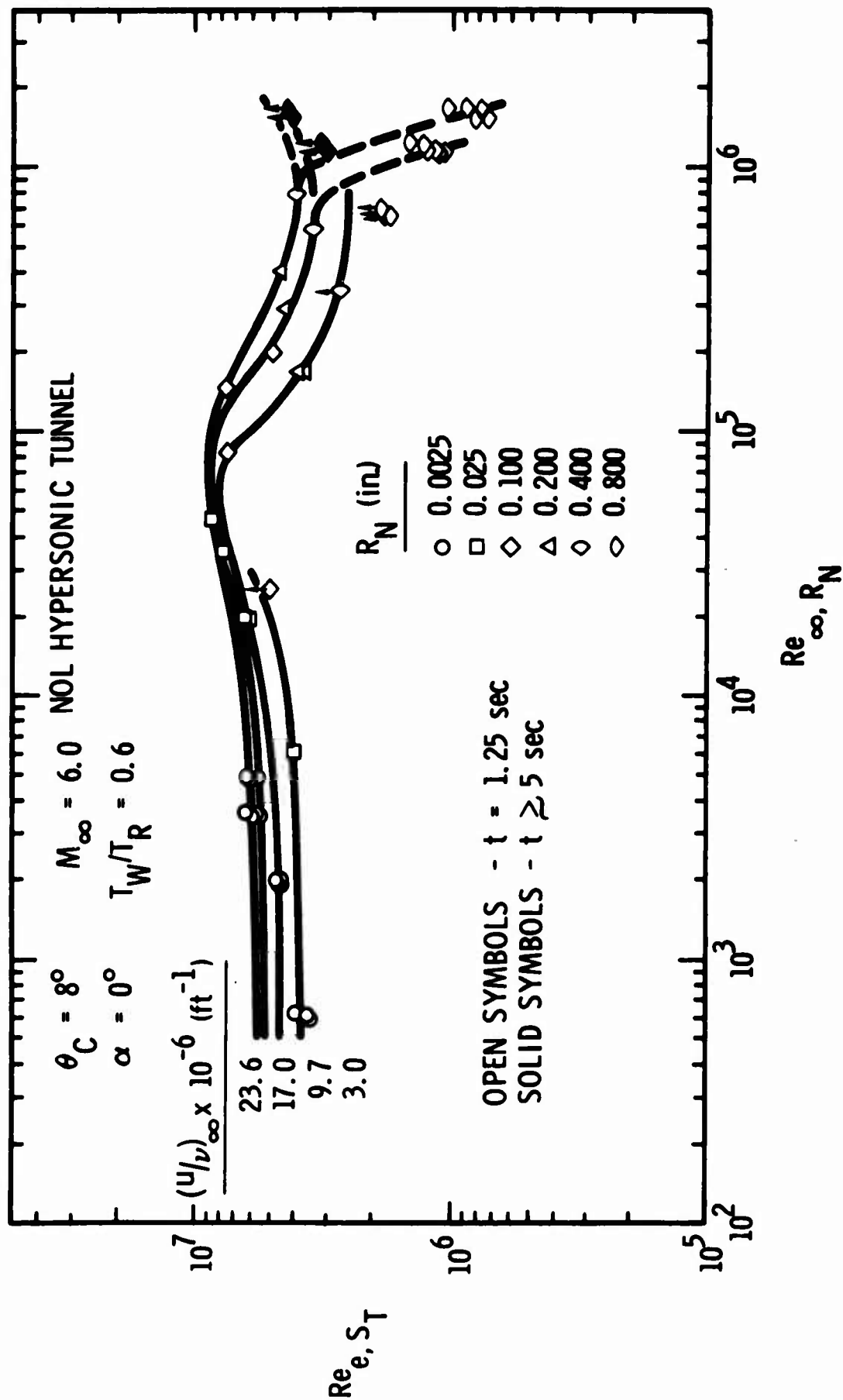


Figure 13. Variation of Local Transition Reynolds Number with Bluntness Reynolds Number - NOL Data

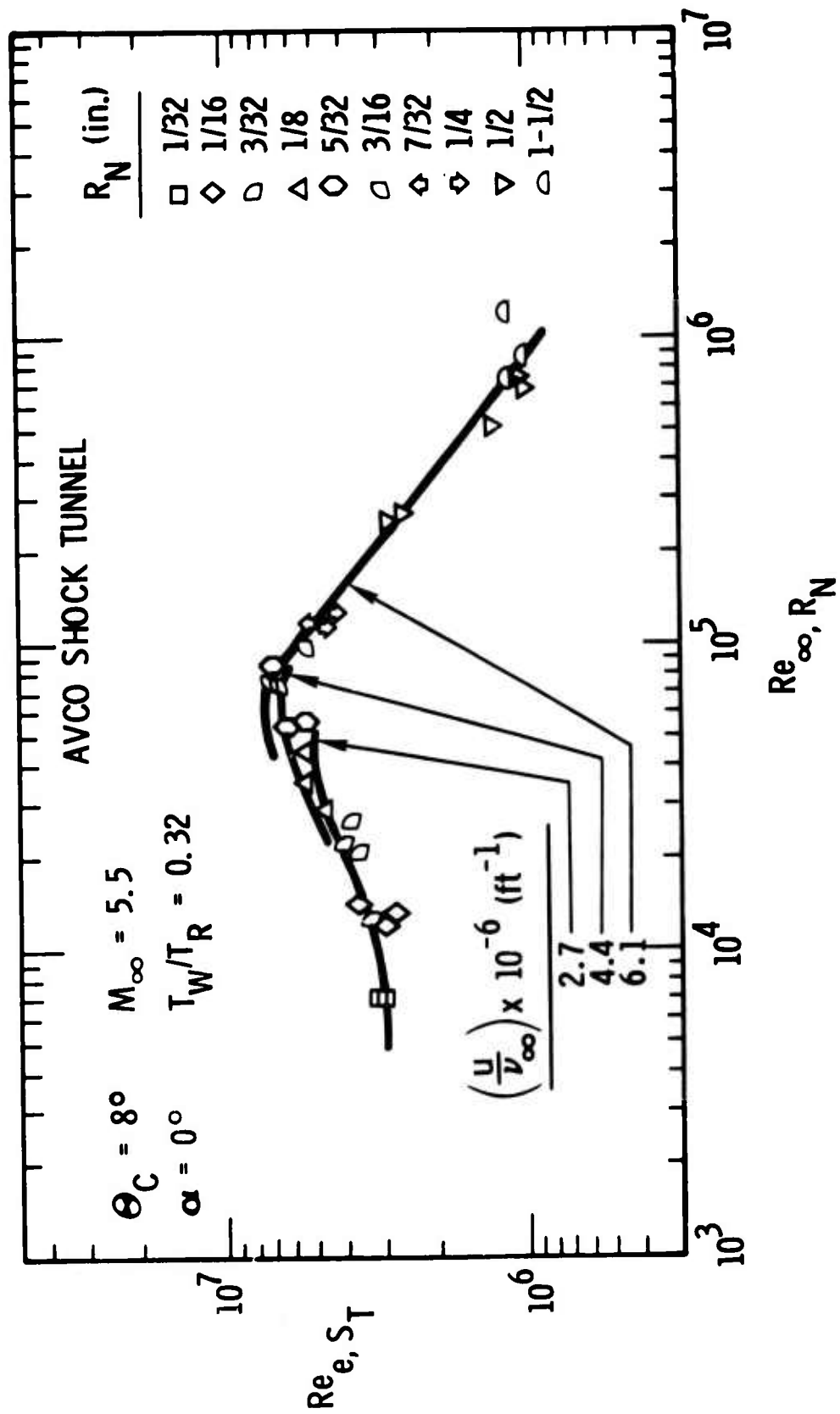


Figure 14. Variation of Local Transition Reynolds Number with Bluntness
Reynolds Number - AVCO Data

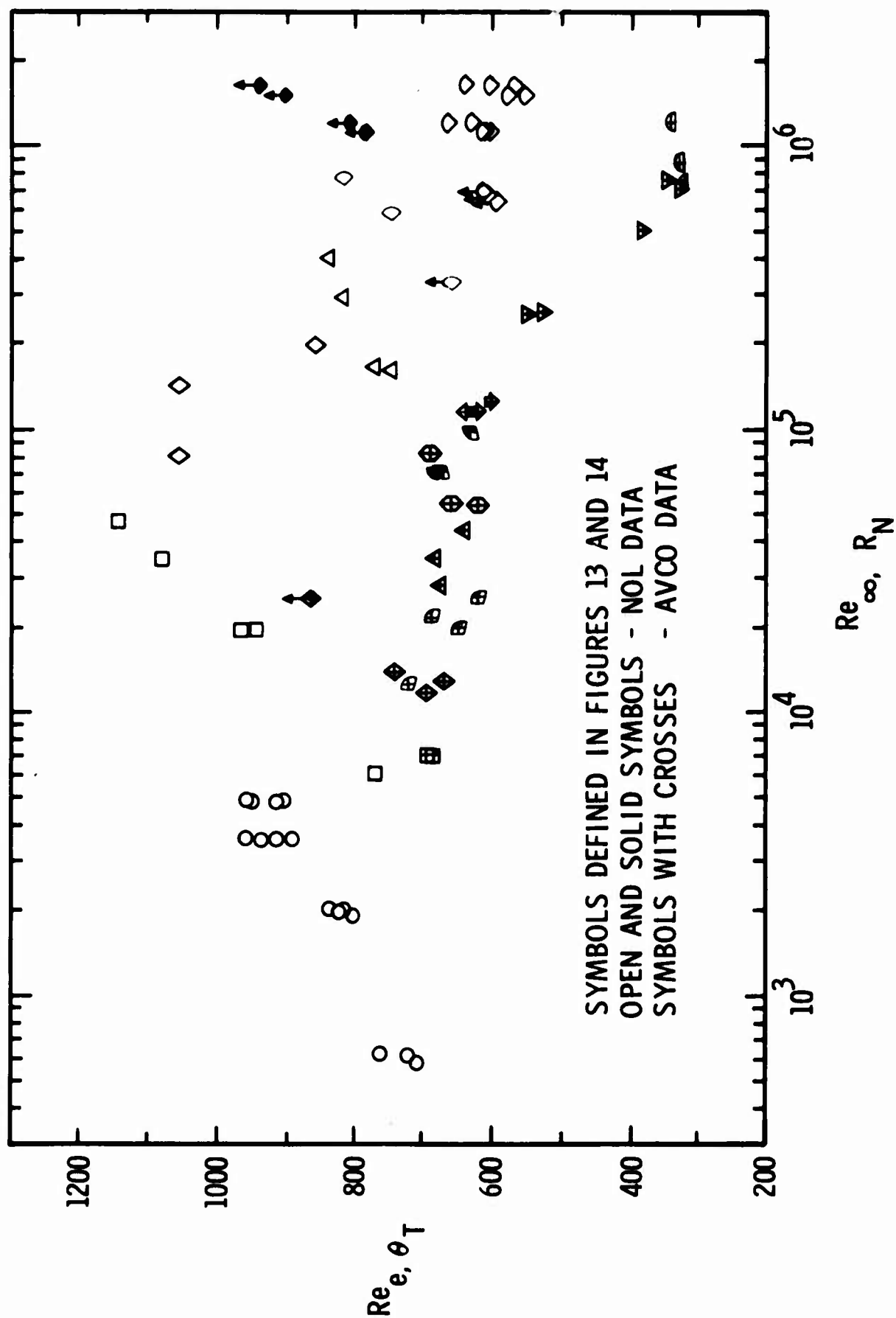


Figure 15. Variation of Momentum Thickness Transition Reynolds Number with Bluntness Reynolds Number - NOL and AVCO Data

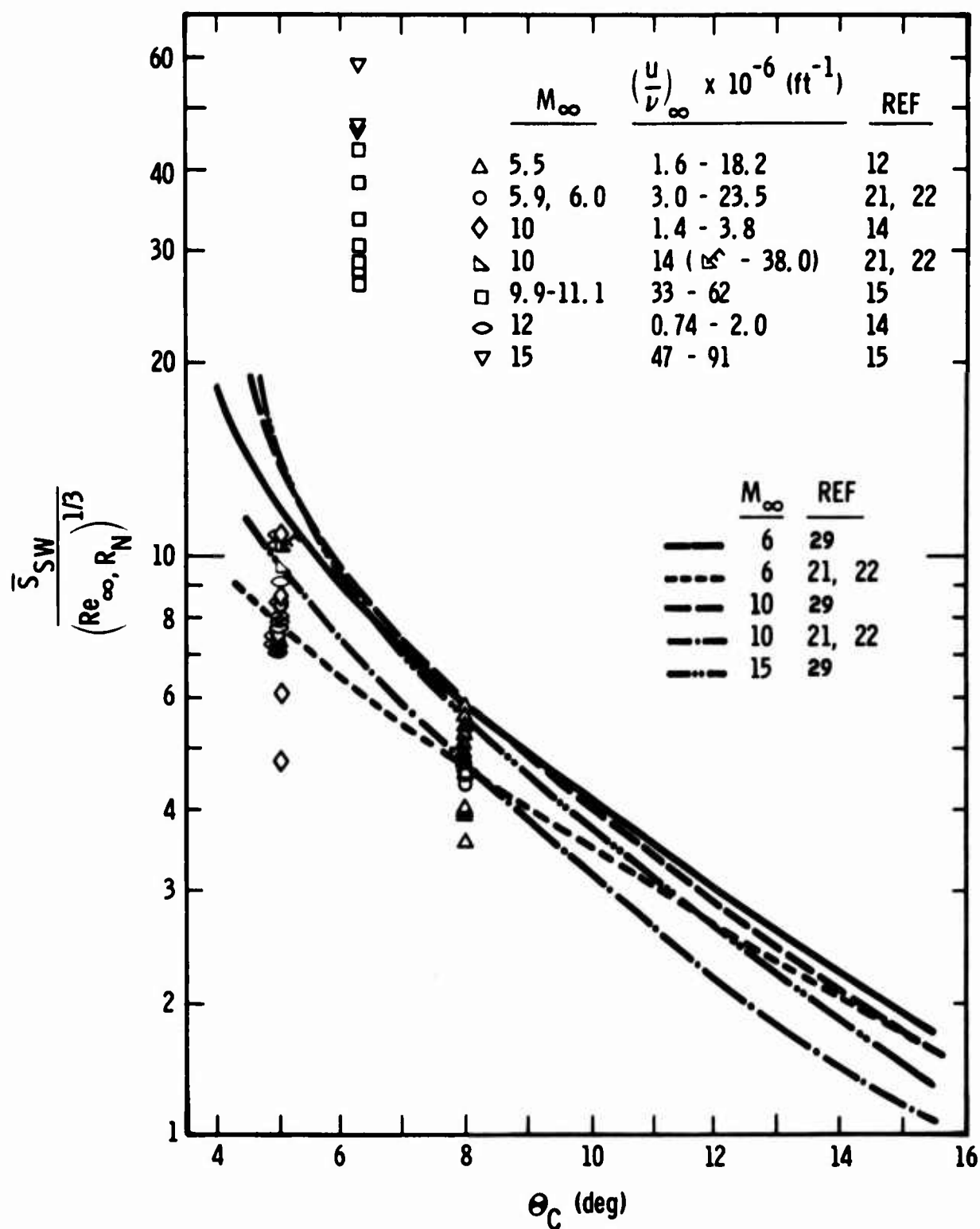


Figure 16. Variation of Swallowing Distance Parameter with Cone Angle, Mach Number, and Unit Reynolds Number

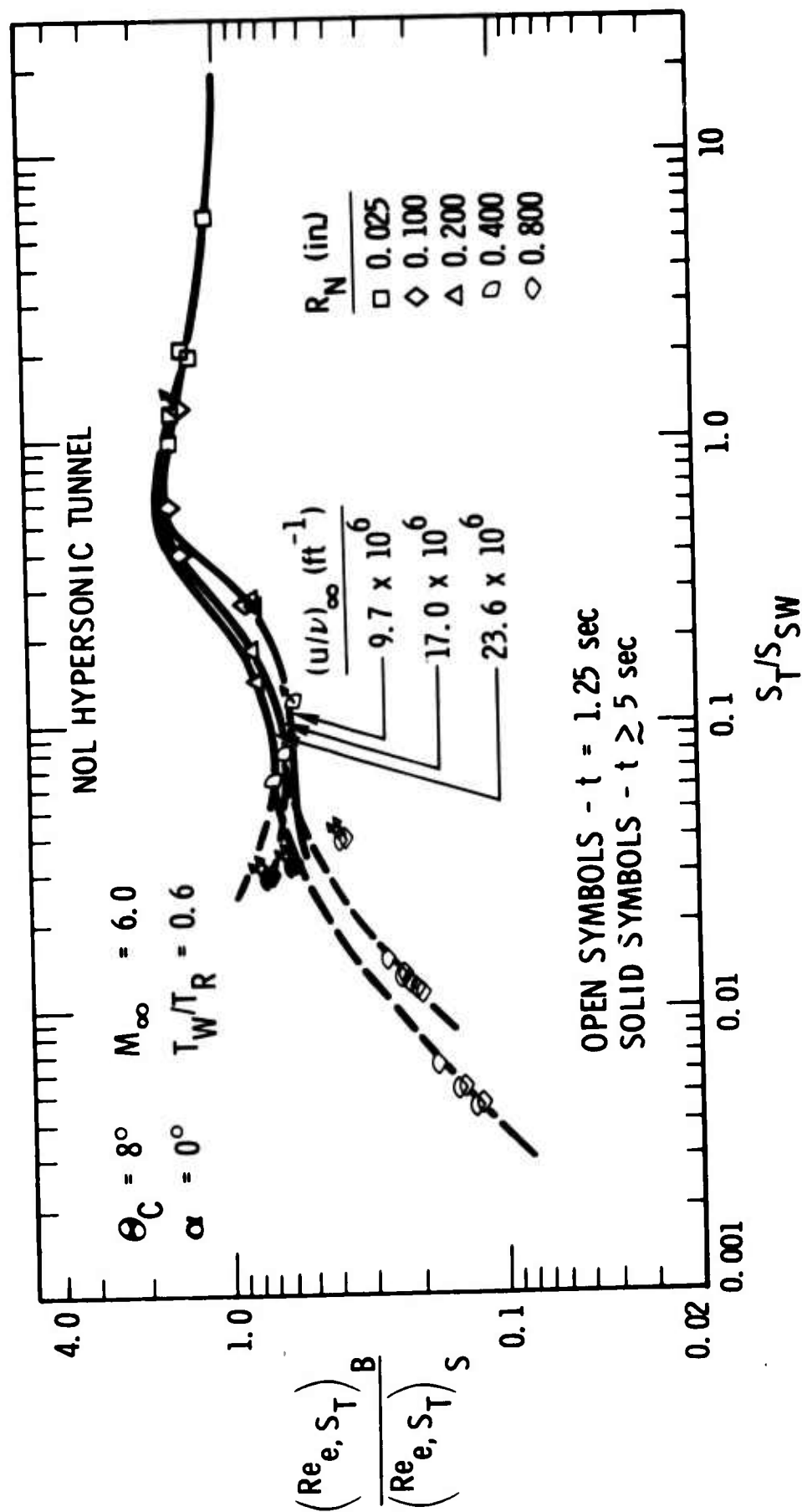


Figure 17. Variation of Local Transition Reynolds Number Ratio with Transition-to-Swallowing Distance Ratio - NOL Data

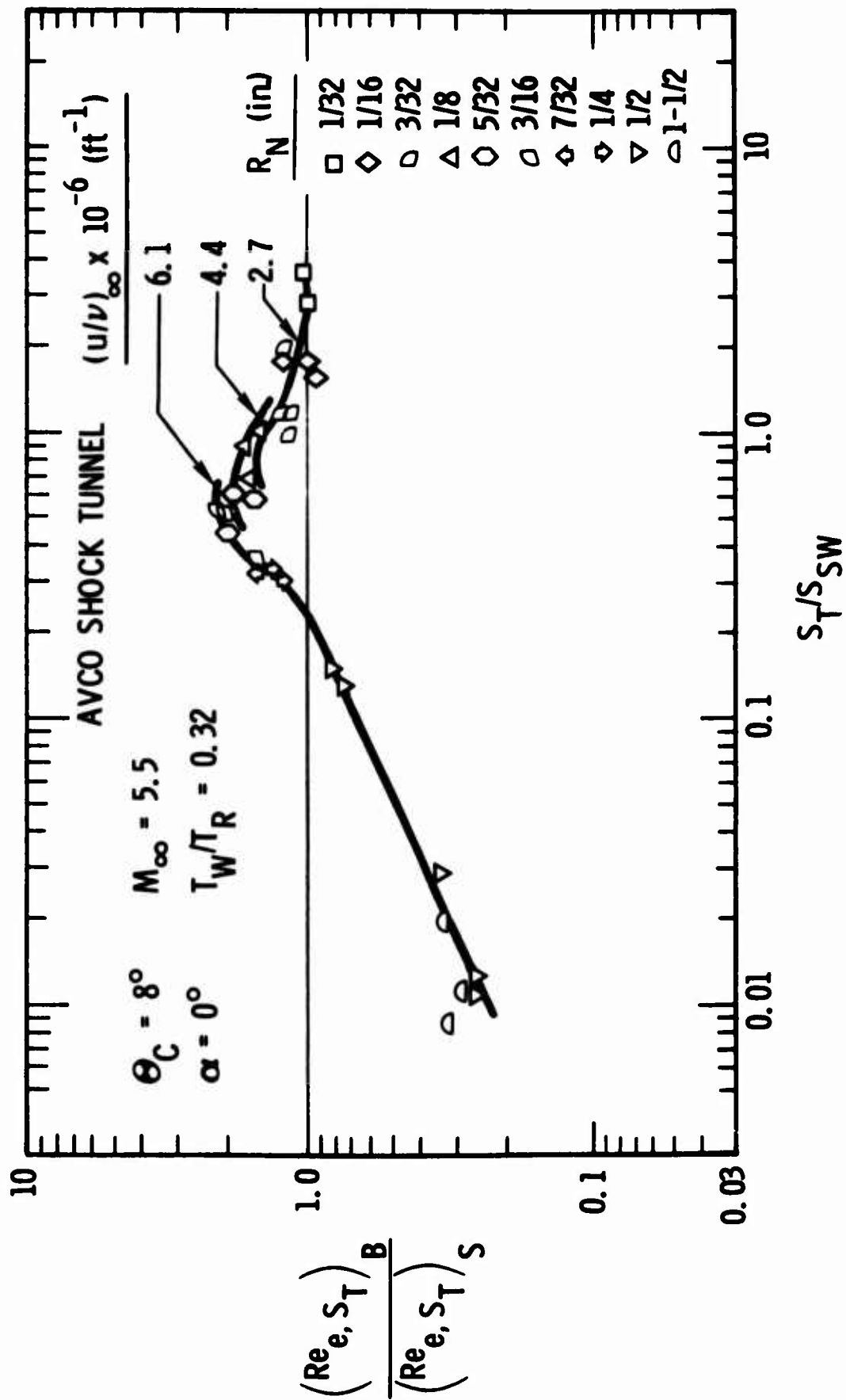


Figure 18. Variation of Local Transition Reynolds Number Ratio with Transition-to-Swallowing Distance Ratio - AVCO Data

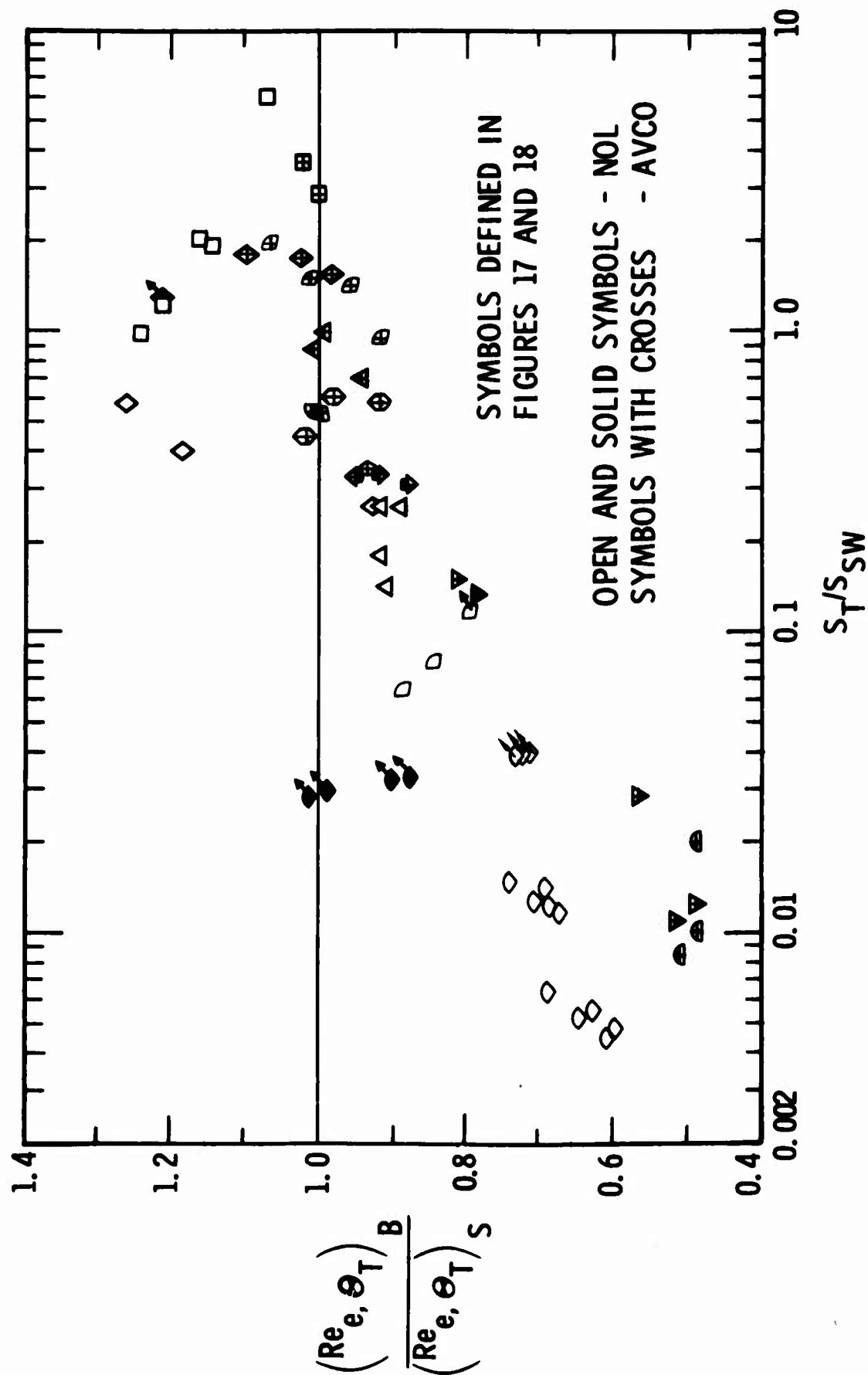


Figure 19. Variation of Momentum Thickness Transition Reynolds Number Ratio with Transition-to-Swallowing Distance Ratio - NOL and AVCO Data

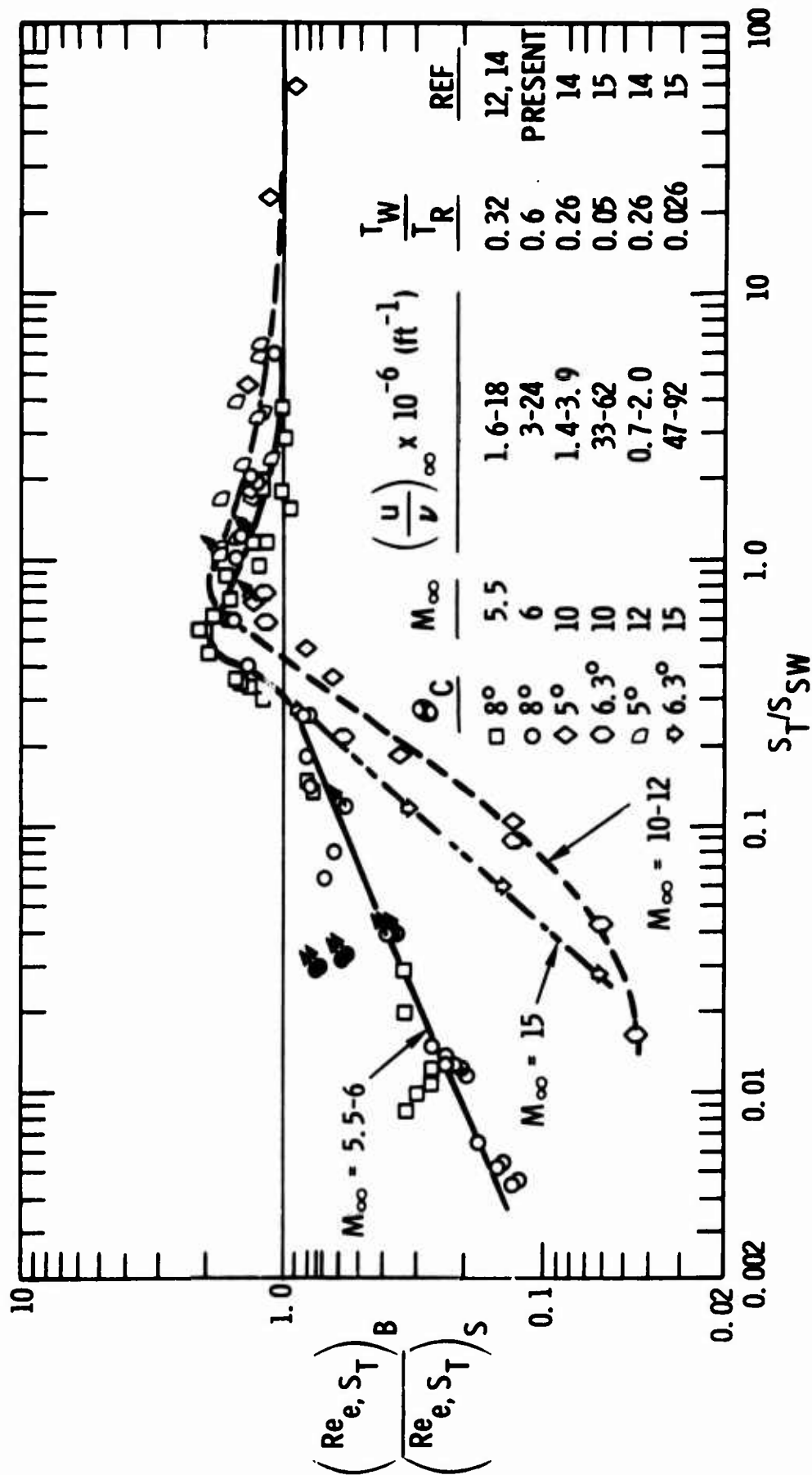


Figure 20. Correlation of Local Transition Reynolds Number Ratio with Transition-to-Swallowing Distance Ratio

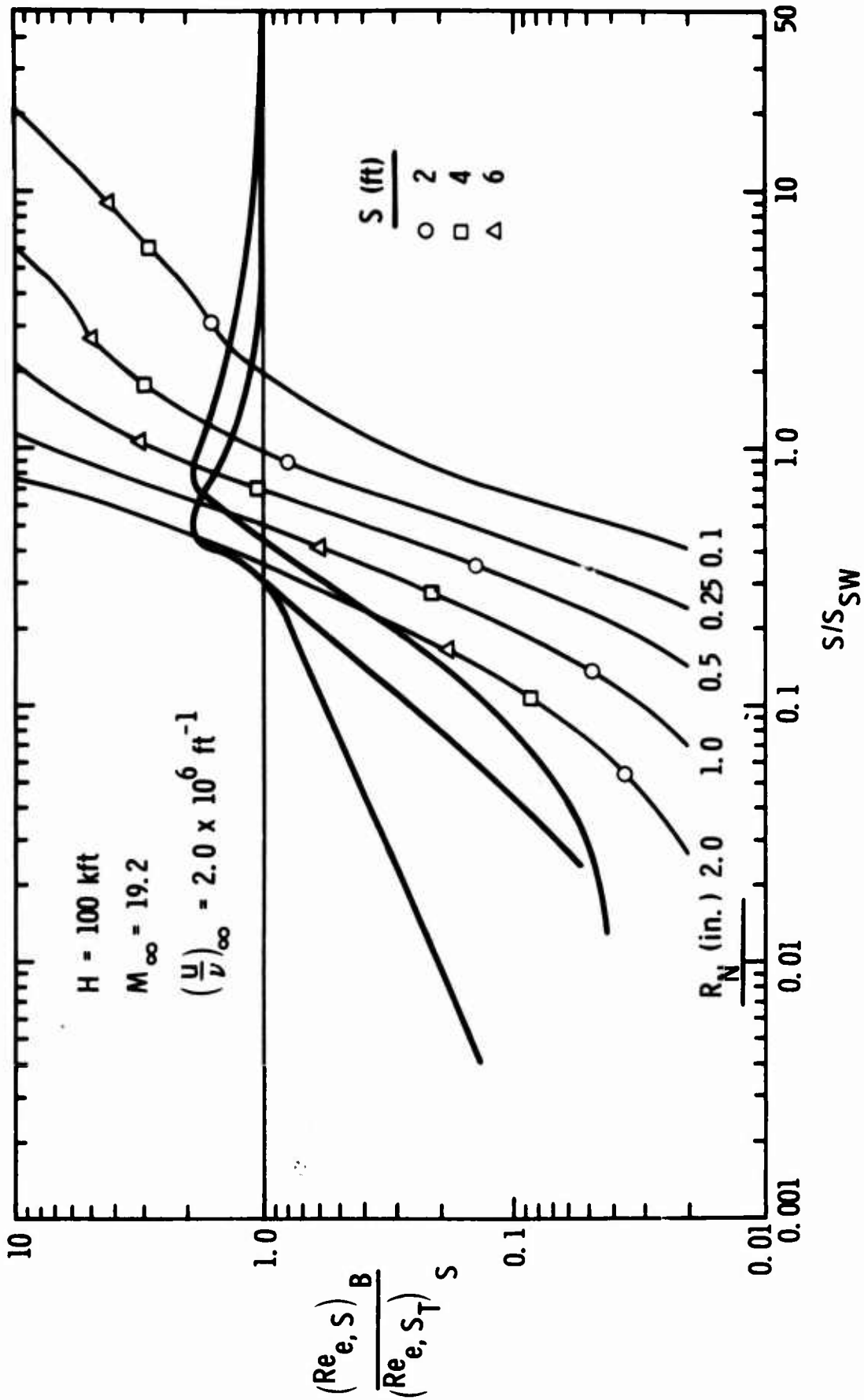


Figure 21. Local Reynolds Number Distributions for Various Nose Radii and Altitudes Compared with Blunt Cone Transition Correlations

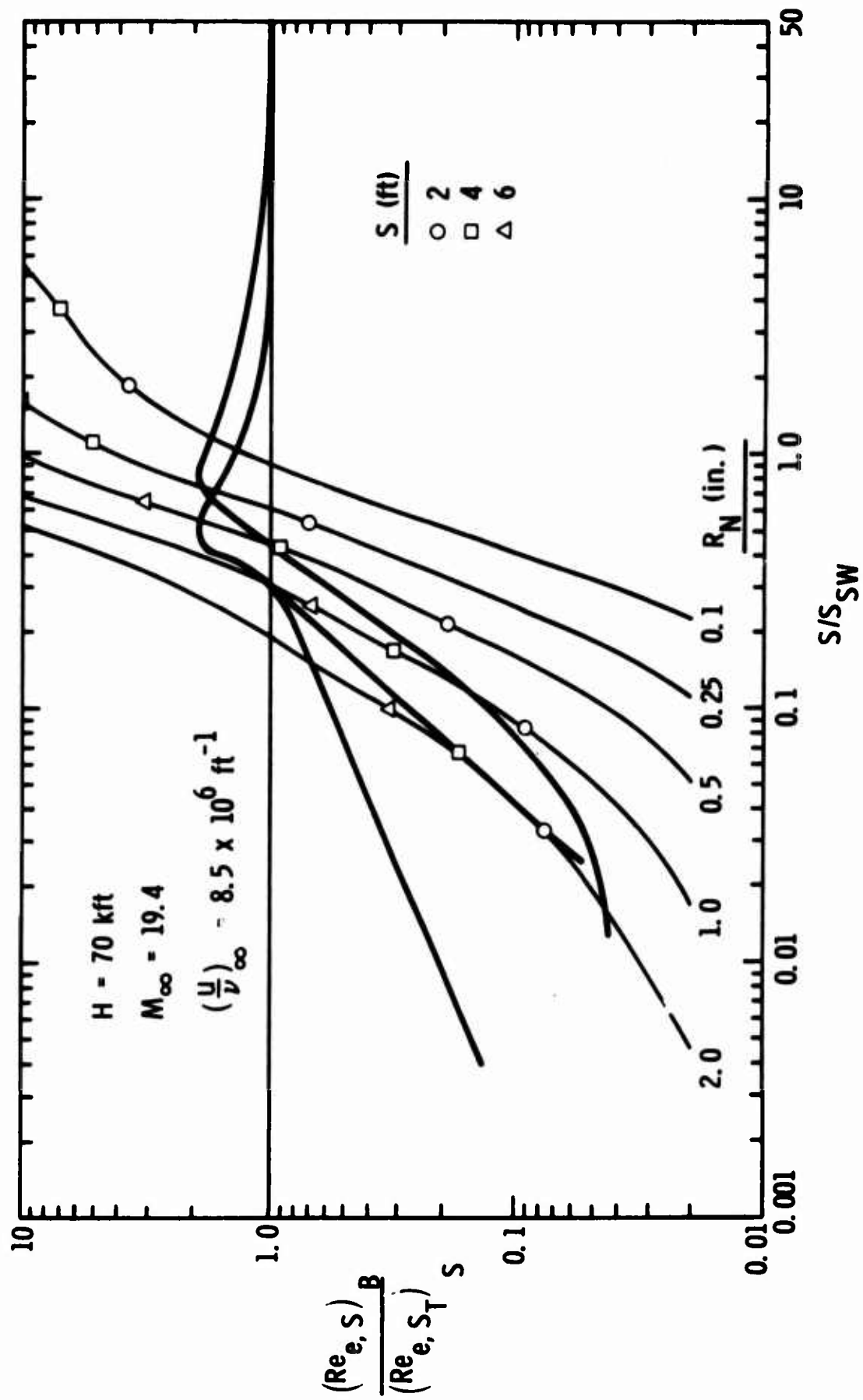


Figure 21 (cont)

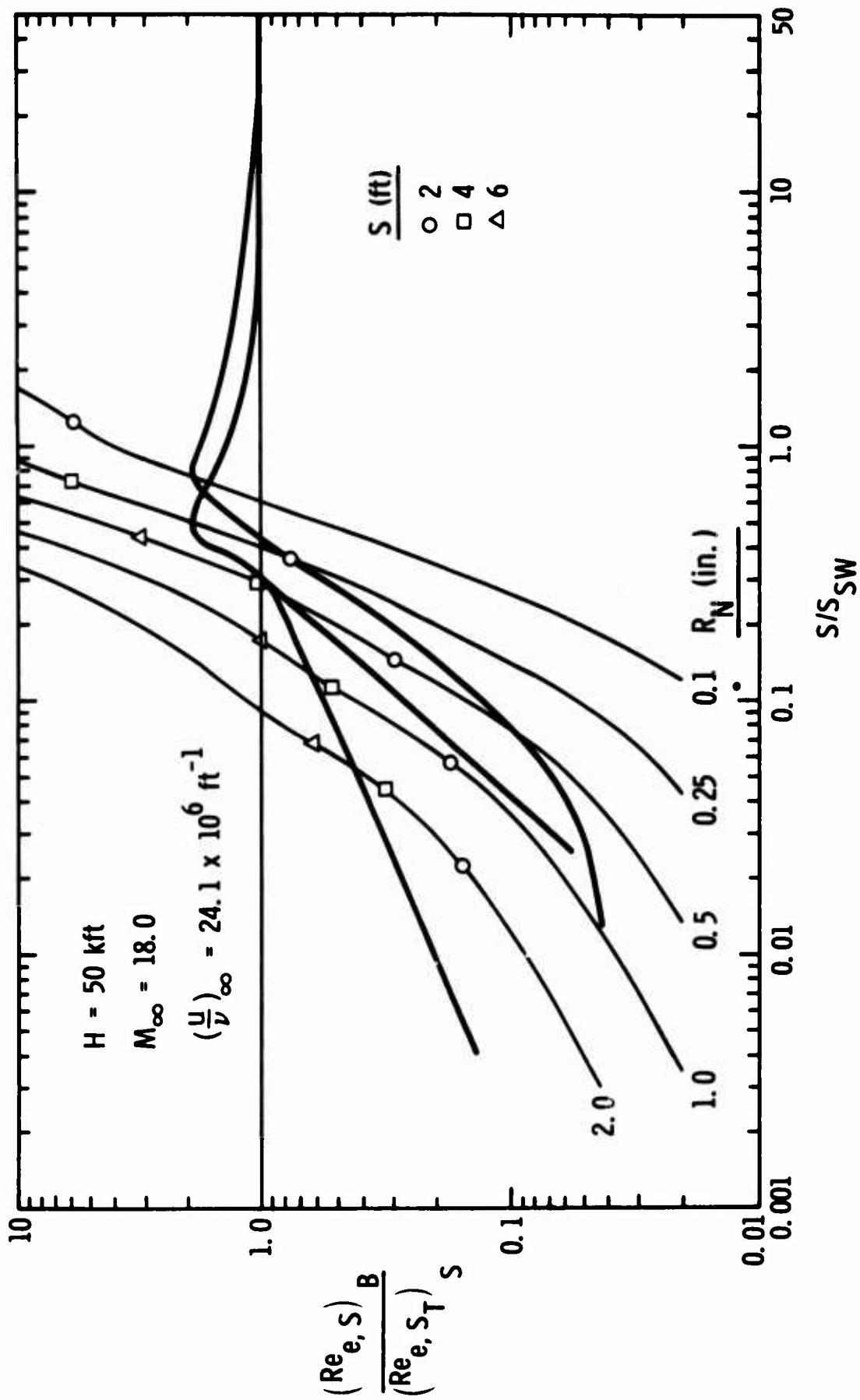


Figure 21 (cont)

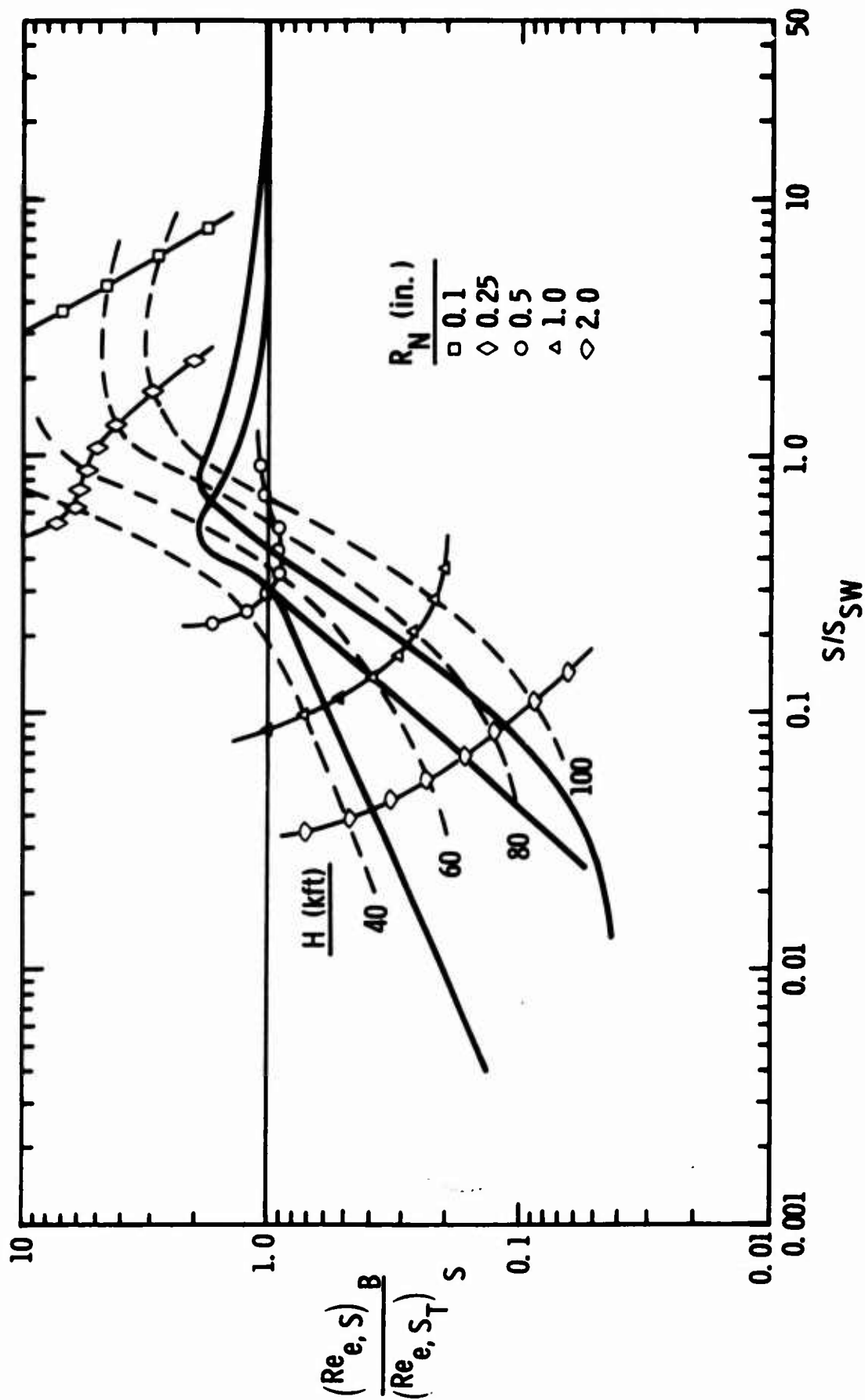


Figure 22. Comparison of Local Reynolds Number Histories with Blunt Cone Transition Correlations at $S = 4$ Ft

(This page intentionally left blank)

SECTION 3

FREE FLIGHT DETERMINATION OF BOUNDARY LAYER TRANSITION ON SMALL SCALE CONES IN THE PRESENCE OF SURFACE ABLATION (Unclassified)

by Max E. Wilkins and Gary T. Chapman

Ames Research Center, NASA, Moffett Field, Calif. 94035

INTRODUCTION

To assess the possibility of achieving extensive laminar flow on conical vehicles during hyperbolic entry, the Ames Research Center has had an ongoing program to study boundary-layer transition on ablating cones. Boundary layer transition results are presented here from ballistic range experiments with models that ablated at dimensionless mass transfer rates comparable to those expected for full scale flight at speeds up to 17 km/sec. Previous results of this study have been published in references 1-4. These early data consisted mainly of measurements of the total ablated mass and detailed studies of surface features. The measurements of mass loss were compared with the mass that should have been removed by either fully laminar or fully turbulent flow. The data all fell between these extremes and showed a reasonable progression toward the turbulent theory as the area of the model covered with clearly discernible, roughly triangular regions of increased mass removal (turbulence wedges) increased. While this correlation seemed to give a reasonable indication of the nature of the boundary-layer flow during ablation, several recovered Delrin models (which were launched at more than 5 km/sec) exhibited no perceptible turbulence wedges, but inexplicably lost more mass than predicted by laminar theory (refs. 2 and 4).

Subsequent to the publication of reference 4, it was found possible to measure the surface recession and hence more accurately identify regions of laminar, transitional, and turbulent flow along generators of the recovered cones. Some preliminary results using this technique are described in reference 1. Since then this method of interpreting data has been improved and is used extensively in the present paper.

FACILITY, MODELS, AND EXPERIMENTAL TECHNIQUE

The models were launched in free flight in air at static pressures from 0.5 to 4 atm in the Ames Pressurized Ballistic Range. Launch velocities ranged from 2 to 6 km/sec. Model cone half-angles were 30° and 50° with base diameters of 1 and 1.2 cm, respectively. The 30° cones were launched enclosed in a sabot, whereas the 50° cones were launched as cone cylinders as will be discussed later. At these velocities and free-stream pressures the models initially experience high convective heating rates and hence high ablation rates; however, because of low model density and high drag, they decelerate rapidly to low subsonic speeds after about 30 m of flight. An open cylindrical "catcher" tunnel made of aluminum and aligned with the flight path is used to capture the models essentially undamaged. (The purpose of the tunnel is to prevent the models from veering off course and damaging themselves by striking equipment within the range.)

The models were homogeneous and made of plastics strong enough to withstand the extreme launch accelerations in the light-gas-gun launch tube. The plastic, Delrin, was chiefly used although some data for Lexan and cellulose nitrate were obtained. Efforts to launch and recover Teflon models were not successful.

The surface finish on most of the 30° conical surfaces was controlled by polishing with 3/0 metallographic polishing paper. This produced a finish in the 0 to 1 micron range that proved to be much finer than required, since ablation removes material to a much greater depth. A good machine finish was found to be adequate. Some 30° conical models that had good machine finishes were launched. These gave results similar to the polished models so all of the 50° conical models were machine finished.

Most of the models launched were prepared with pointed tips. However, for a few of the 30° half-angle Delrin cones the nose was rounded prior to launch with nose radius to base radius ratios up to 9%. The nose rounding was done to determine if it had any effect on transition Reynolds number.

Analysis of Recovered Bodies

The mass loss data for the 30° cones were obtained simply by weighing the model before launch and after recovery. However, the 50° cones were flown as a cone cylinder (see fig. 1) where the model consisted of a cone with a cylindrical afterbody. This

afterbody was press fitted to the cylinder that accompanied the cone throughout the flight. After recovery, the outer cylinder was removed from the cone so that the mass loss of the conical surface could be measured. The initial mass, m_0 , used to normalize the mass loss data for the 50° cones was computed for the cone itself. It does not include the weight of the cylindrical afterbody.

In addition to weighing the models to determine mass loss, enlarged profile pictures (cf. fig. 2) were utilized to determine the local surface recession. The figure shows example profiles obtained for both the 30° and 50° cones. The outer profile was taken before launch, the inner one after recovery. Between one and six profile pictures were taken before launch and as many as required after recovery. The recession, Δr , is determined from the superimposed profiles and is measured normal to the cone axis. Small errors in aligning the profile pictures can significantly affect the accuracy of the Δr measurements; rotation of one image with respect to the other and failure to align the profiles either laterally or axially. With the aid of a pedestal providing an axis reference at the model base, the errors have been greatly reduced. Lateral errors are further reduced by averaging several values of Δr around the cone at the same axial position. Since some rays may represent surface areas that experienced laminar flow and others turbulent flow, this averaging process tends to make interpretation more difficult but the increase in absolute accuracy of $\Delta r/r_b$ is worth it. (See, for example, fig. 6, ref. 1, which shows the surface recession profiles within and without a turbulence wedge.) Displacement error along the axis is minimized by positioning the images so that the computed mass loss from the average surface recession values matches the actual mass loss measured by weighing. This is done with the relation:

$$\frac{\Delta m}{m_0} = 6\pi \left(\frac{x}{x_b} - \frac{\Delta r}{2r_b} \right) \frac{\Delta r}{r_b} \frac{\Delta x}{x_b}$$

An earlier procedure, (ref. 1) that of matching the images along the model base plane, gave incorrect total mass losses. This is thought due to optical distortion resulting from diffraction of collimated light along the planar surface of the model base.

In addition to the quantitative data from the profiles, considerable information has been gained from microscopic examination of the ablated surfaces. This material was discussed quite extensively in references 1-4 so the discussion will not be repeated here.

RESULTS AND DISCUSSION

Total Mass Loss

The flight conditions and mass loss data for the Delrin 30° and 50° cones are listed in table I. A comparison of the observed mass losses with theory is shown in figure 3. Plotted as a function of the launch velocity is the measured mass loss normalized by the predicted turbulent mass loss. Both the laminar and turbulent theoretical mass loss, as well as local recession curves to be shown later, were calculated for sharp cones in the manner described in reference 2. These calculations take into account the deceleration of the model as well as the blockage of heat transfer by the ablation process.

A comparison of figures 3(a) and (b) indicates that the 30° cone data show predominately laminar flow, in contrast to the extensive turbulent flow experienced by the 50° cones. Mass loss data previously reported in reference 2, was interpreted as showing that similar 30° Delrin cones experienced extensive turbulent flow in the same velocity range. Those models, however, invariably had a damaged tip at launch. This damage is now thought to be responsible for the large extent of turbulent flow. Models that had obvious tip damage are not included here.

The numbers adjacent to some symbols give the percentage of nose radius to base radius for the model prior to launch. The results indicate that tip rounding prior to launch did not affect the results in any significant manner. However, some tip rounding naturally occurs during the flight, so that all the models perhaps should be considered as having rounded tips. The tip rounding incurred during flight due to ablation appears to make the prelaunch rounding, to the extent done, rather ineffective. Listed in table I are measurements showing the degree of tip radius increase during flight.

Although, as noted above, the 50° cone data show predominately turbulent boundary layer flow and the 30° cone data show predominately laminar boundary layer flow, it should not be inferred that the boundary layers were totally turbulent or

laminar. It is difficult, however, to estimate the Reynolds number of transition from these total mass loss data. More direct measurement of transition Reynolds numbers can be made from the surface recession results, as will be shown next.

Surface Recession

Surface recession measurement for the Delrin 30° cones are shown in figures 4 and 5. Surface recession is plotted against the boundary layer edge Reynolds number (based on edge conditions at launch and slant length of the cone). The local recession near the nose is in close agreement with that predicted by laminar theory. Although departure from the laminar mass loss curve occurs at Reynolds numbers as low as 1 to 2 million there still appears to be significant laminar flow even at Reynolds numbers to 14 million (see fig. 5(b)). This raises the question as to just how to interpret these data that, of course, represent ablation with variation of Reynolds number during the model's decelerating flight. If transition were fixed at some body position we would expect the recession curve to be similar to the well known laminar to turbulent (i.e., transition) heating curve. The length of this change from fully laminar to fully turbulent is approximately equal to the length of the preceding laminar flow. Even if transition occurs at a constant Reynolds number of transition, for example 1 million, and the transition region is of the same length as the laminar run the rear portions of these models would exhibit fully turbulent recession because most of the mass loss occurs at high speeds before the Reynolds number changes. As an example, predicted recession curves for these two alternatives are shown in figure 4(c). Neither case is close to the measured results.

One possible interpretation is that transition is occurring at different transition Reynolds numbers on different rays. The results, then, can be interpreted in terms of the percentage of the circumference that is laminar at the launch Reynolds number. This is not the only possible interpretation of the results but it is the only one that does not require a rather complicated dependence of transition on flight conditions.

This simple view and very likely correct interpretation of the data suggests that at Reynolds numbers less than 1 million the flow is 100% laminar. At a Reynolds number of 5 million the flow is 20-30% turbulent; the exact amount depends on speed and pressure. Even at Reynolds numbers as high as 14 million only 60% of the boundary layer flow is

turbulent. These numbers, when compared with other free flight results on nonablating bodies (refs. 5 and 6), would suggest that for this ablator the effect of ablation on transition is not pronounced and if anything may even promote longer laminar flows. The low value of transition Reynolds number of 1 million for the first appearance of some turbulent flow is probably associated with local roughness effects. The evidence of considerable laminar flow at a Reynolds number of 14 million, although not impossible to obtain on a nonablating model with these local flow conditions, (e.g., refs. 5 and 6), is difficult to obtain because of roughness effects. Delrin ablates in such a manner as to yield a very smooth surface, provided there are no material imperfections. This then may be the reason for the apparent good performance during the present tests.

One final point to make is that, as noted in the preceding section, "Total Mass Loss," an initial nose radius of a few percent does not appear to alter the present results, (cf. figs. 4(b) and 5(c)).

The recession measurements for Delrin 50° cones are shown in figure 6, plotted in the same manner as the 30° cone data. Note the striking difference. The data supports an interpretation of body fixed transition to turbulent flow near the nose of the body, (evident also in fig. 3). With the exception of the high speed tests shown in figure 6(a), very good agreement with turbulent boundary layer theory is apparent. Only in figure 6(d) is there an appearance of the behavior noted for the 30° cone data. Even here we see that at Reynolds numbers greater than 3 million fully turbulent flow is experienced. The lower value of transition Reynolds number on the 50° cones is probably due in part to the lower local boundary layer edge Mach number (ref. 7) (for a 30° cone $M_c \approx 4.5$ and for a 50° cone $M_c \approx 1.8$). This large difference in transition Reynolds number does not appear to be due to ablation effects as the ablation rates for the two cone angles is similar, (typically within 10-20%).

From figure 6 we note that the lowest value of the transition Reynolds number is less than 1/2 million. In fact, for the higher speed data, values considerably less than 1/2 million are indicated—the initial recession curves are always substantially above the laminar flow theory. The reason for this is not clearly understood at present. The erratic behaviour (one high and two low) exhibited for the three tests at about 6 km/sec (fig. 6(a)) is not fully understood at this time, particularly for the two models with the

lower recession. However, these two models had relatively low mass losses as shown by the two lowest points in figure 3(b). Surface inspections of the model with the larger recession indicate possible spalling that may be caused by launch damage or by thermal stresses.

Figures 7 and 8 present some additional data for models made of Lexan and cellulose nitrate. The data for 30° and 50° Lexan cones, (fig. 7) are very similar to the data obtained for the Delrin models. This general agreement between these results and those for Delrin (i.e., similar recession curves for 30° and 50° cone angles) is not surprising since they both have similar ablation characteristics (ref. 2). The theoretical recession curves for Lexan appear to be low, particularly when compared to the turbulent results in figure 7(c). This makes the determination of the first appearance of transitional flow from the data in figures 7(a) and 7(b) questionable. However, if one shifts the theoretical laminar curves upward until the data and theory curve agree near the nose we find that the departure of the data from the theory occurs between a Reynolds number of 1/2 and 1 million on the 30° Lexan cones. This apparently lower value of Reynolds number at the beginning of transition for Lexan when compared to Delrin may be due to a slightly rougher surface.

Figure 8 shows a comparison of recession curves at nominally the same test conditions, cone angle, velocity, and pressure, for models made of Delrin, Lexan, and cellulose nitrate. Note the large change exhibited by cellulose nitrate compared to the other two materials. Although a recession theory for cellulose nitrate is not available due to lack of ablation parameters, the recession curve suggests that the flow at the cone base is fully turbulent at a Reynolds number of about 2 million. This adverse effect of cellulose nitrate on transition may be due to the much higher laminar mass loss rate evident in figure 8. It may also be associated with combustion in the boundary layer since cellulose nitrate is known to be flammable.

CONCLUDING REMARKS

From the foregoing material, it is believed that four conclusions can be drawn:

- (1) Significant amounts of laminar flow are possible on cones of moderately large half angle (30°) under some ablation conditions at Reynolds numbers (based on boundary-layer edge conditions) to 14 million.

- (2) These large laminar runs are comparable to the longest laminar runs observed on nonablating surfaces at similar conditions.
- (3) Larger angle cones (50°) experience considerable reduction in the transition Reynolds number. This is thought to be associated with the reduced edge Mach number.
- (4) Cellulose nitrate exhibits much lower transition Reynolds number than Delrin and Lexan. Whether this is due to changes in ablation rate or to combustion in the boundary layer is not known at the present time.

SYMBOLS

m	mass of cone
m_o	mass of cone at launch
p/p_o	ballistic-range static pressure, atm
r	cone radius
r_b	cone base radius
r_n	tip radius
Re	maximum local Reynolds number based on boundary-layer edge properties at launch
$(Re_x)_o$	local Reynolds number at launch along the slant length of the model
V_o	launch velocity
x	cone slant length measured from original apex
x_b	total cone slant length
θ_c	cone half angle

subscripts

m	measured
L	laminar, theoretical
T	turbulent, theoretical

TABLE I. MASS LOSS AND TIP RADIUS MEASUREMENTS

Model no.	Model material	θ_c , deg	V_o , km/sec	p/p_o , atm	m/m_o , measured	r_n/r_b , %, prelaunch	r_n/r_b , %, recovered
CN-1	cellulose nitrate	30	5.43	0.50	0.133	0.4	7.8
CN-2	cellulose nitrate	30	5.34	0.45	0.122	0.5	7.3
D-28	Delrin	30	4.88	1.0	0.0280	0.8	—
D-35	Delrin	30	5.42	1.0	0.0333	0.4	4.3
D-38	Delrin	30	4.27	1.0	0.0222	0.1	4.7
D-39	Delrin	30	2.99	1.0	0.0100	0.1	2.3
D-41	Delrin	30	6.25	1.0	0.0796	—	—
D-57	Delrin	30	3.05	1.0	0.0150	0.1	2.5
D-62	Delrin	30	3.05	1.0	0.0124	0.4	—
D-68	Delrin	30	3.81	1.0	0.0280	0.1	2.9
D-69	Delrin	30	3.66	1.0	0.0126	0.3	2.9
D-74	Delrin	30	3.89	1.0	0.0240	0.1	3.3
D-79	Delrin	30	2.20	1.0	0.0031	0.8	2.1
D-94	Delrin	30	5.73	1.0	0.0342	0.5	4.7
D-112	Delrin	30	5.43	1.0	0.0376	0.8	—
D-113	Delrin	30	5.18	1.0	0.0422	—	—
D-114	Delrin	30	5.37	1.0	0.0348	0.1	5.1
D-116	Delrin	30	5.11	1.0	0.0469	3.7	6.3
D-118	Delrin	30	5.03	1.0	0.0243	0.8	3.7
D-122	Delrin	30	6.10	1.0	0.0421	0.8	4.7
D-124	Delrin	30	5.95	1.0	0.0469	0.8	4.7
D-127	Delrin	30	5.49	1.0	0.0399	6.6	7.8
D-129	Delrin	30	5.73	1.0	0.0581	8.6	9.4
D-132	Delrin	30	6.10	1.0	0.0537	7.0	9.0
D-135	Delrin	30	5.03	1.0	0.0428	6.3	8.2
D-136	Delrin	30	5.19	0.59	0.0302	0.5	5.9
D-137	Delrin	30	5.95	0.50	0.0469	0.8	7.0
D-139	Delrin	30	5.49	0.47	0.0345	0.4	5.9

TABLE I. MASS LOSS AND TIP RADIUS MEASUREMENTS (Continued)

Model no.	Model material	θ_c , deg	V_o , km/sec	p/p_o , atm	m/m_o , measured	r_n/r_b , %, prelaunch	r_n/r_b , %, recovered
D-142	Delrin	30	5.49	0.52	0.0462	0.6	5.9
D-143	Delrin	30	5.12	0.56	0.0365	0.1	4.9
D-144	Delrin	30	5.03	0.60	0.0413	0.8	—
D-145	Delrin	30	5.34	0.51	0.0362	0.6	5.8
D-147	Delrin	30	5.49	0.45	0.0367	0.4	7.4
D-149	Delrin	30	5.18	0.43	0.0311	1.2	—
D-162	Delrin	30	5.80	2.72	0.0386	0.4	2.9
L-117	Lexan	30	6.31	0.40	0.0394	1.4	5.8
L-119	Lexan	30	5.49	0.50	0.0386	1.0	4.7
L-120	Lexan	30	5.34	0.55	0.0433	1.0	7.2
L-121	Lexan	30	5.40	0.45	0.0368	0.8	6.6
*DDC-3	Delrin	50	4.27	4.06	0.0921	0.9	4.7
DDC-5	Delrin	50	5.49	3.03	0.1743	1.7	6.3
DDC-6	Delrin	50	5.95	3.09	0.1300	0.8	5.7
DDC-7	Delrin	50	4.88	3.09	0.1288	1.2	5.3
DDC-9	Delrin	50	5.95	3.13	0.2133	1.0	5.6
DDC-10	Delrin	50	4.27	3.12	0.0834	1.3	5.0
LDC-1	Delrin	50	6.10	3.12	0.1304	1.6	6.6
LLC-4	Delrin	50	4.27	3.10	0.0961	4.7	6.3
LDC-6	Delrin	50	5.70	3.09	0.1568	0.8	5.2
LDC-7	Delrin	50	5.12	3.10	0.1190	0.7	3.3
LLC-2	Lexan	50	4.12	3.14	0.0945	1.2	4.5

* First letter denotes the model material, second letter the cylinder material,
D = Delrin, L = Lexan (see fig. 1).

REFERENCES

1. Thomas N. Canning, Michael E. Tauber, and Max E. Wilkins, Review of Recent Ballistic Range Boundary-Layer Transition Work on Ablating Bodies at Ames. Boundary Layer Transition Study Group Meeting, Vol. III, W. D. McCauley, ed., Aerospace Rep. No. TR-0158 (S3816-63) - 1, III, Aerospace Corp., San Bernardino, Calif. (August 1967). (Also available as Air Force Report No. BSD-TR-67-213, Vol. III.)
2. Max E. Wilkins and Michael E. Tauber, Boundary-Layer Transition on Ablating Cones at Speeds Up to 7 Km/Sec, AIAA J., pp. 1344-1348 (August 1966).
3. Max E. Wilkins, Evidence of Surface Waves and Spreading of Turbulence on Ablating Models, AIAA J., Vol. 3, pp. 1963-1966 (1965).
4. Thomas N. Canning, Max E. Wilkins, and Michael E. Tauber, Boundary-Layer Phenomena Observed on the Ablated Surfaces of Cones Recovered After Flights at Speeds Up to 7 Km/Sec. AGARD Specialists' Meeting on Fluid Physics of Hypersonic Wakes, Fort Collins, Colorado. May 10-12, 1967. AGARD Conference Proceedings No. 19.
5. James R. Jedlicka, Max E. Wilkins, and Alvin Seiff, Experimental Determination of Boundary-Layer Transition on a Body of Revolution at $M = 3.5$. NACA TN 3342, 1954.
6. Carlton S. James, Boundary-Layer Transition on Hollow Cylinders in Supersonic Free Flight as Affected by Mach Number and a Screwthread Type of Surface Roughness. NASA Memo 1-20-59A, 1959.
7. A. L. Nagel, Compressible Boundary Layer Stability by Time-Integration of the Navier-Stokes Equations, and an Extension of Emmons' Transition Theory to Hypersonic Flow. (Same as ref. 1 above except Vol. II, instead of III.)

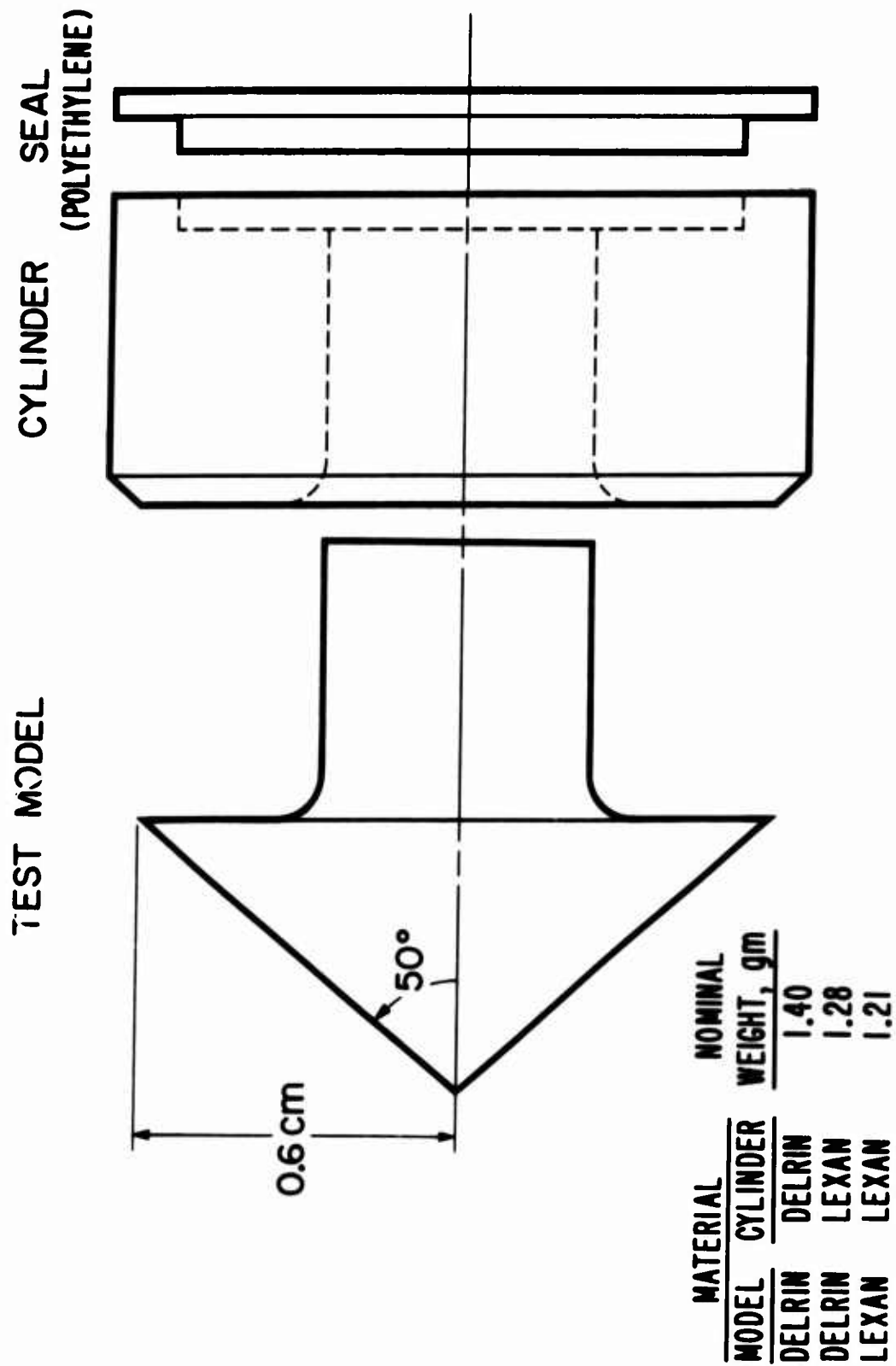


Figure 1. Model configuration, $\theta_c = 50^\circ$

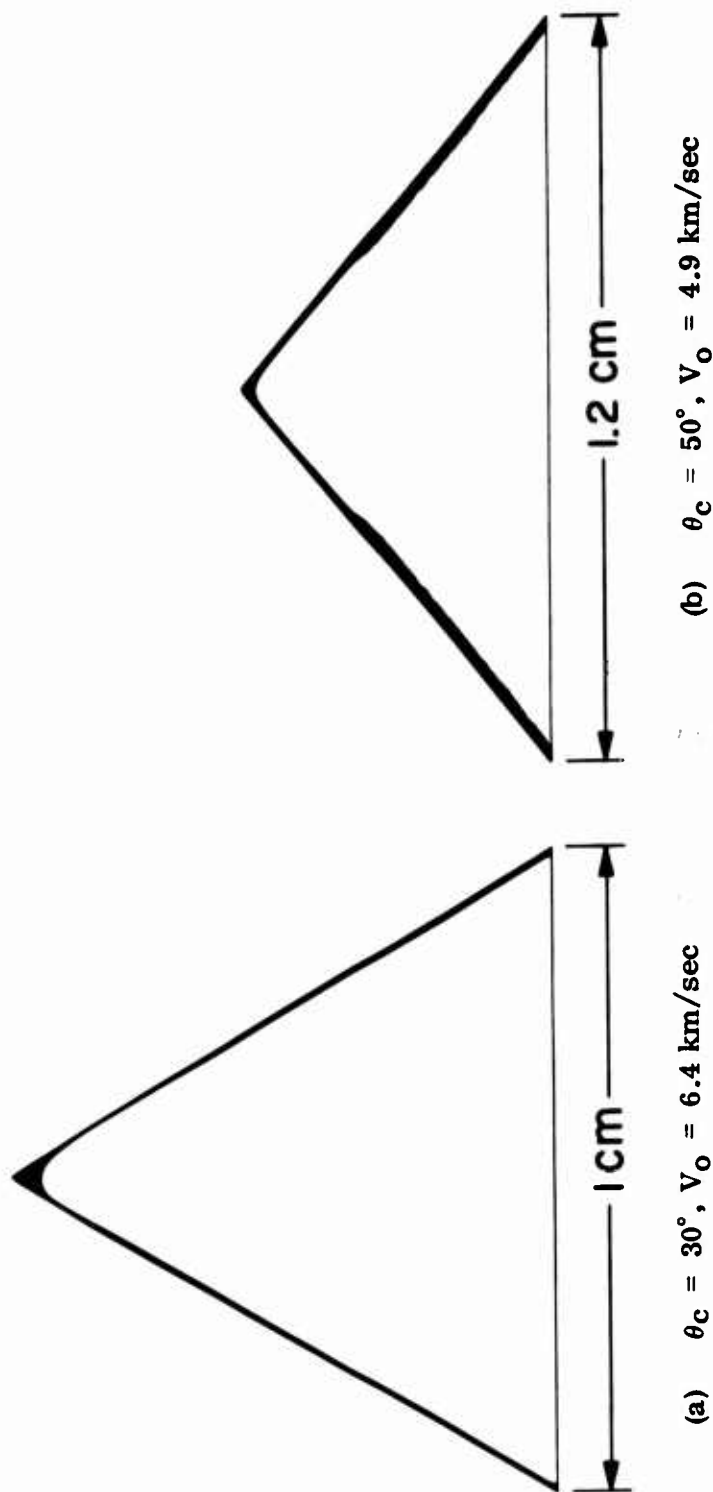


Figure 2. Typical profiles of Delrin models before launch and after recovery

NUMBERS INDICATE NOSE RADIUS PERCENTAGES

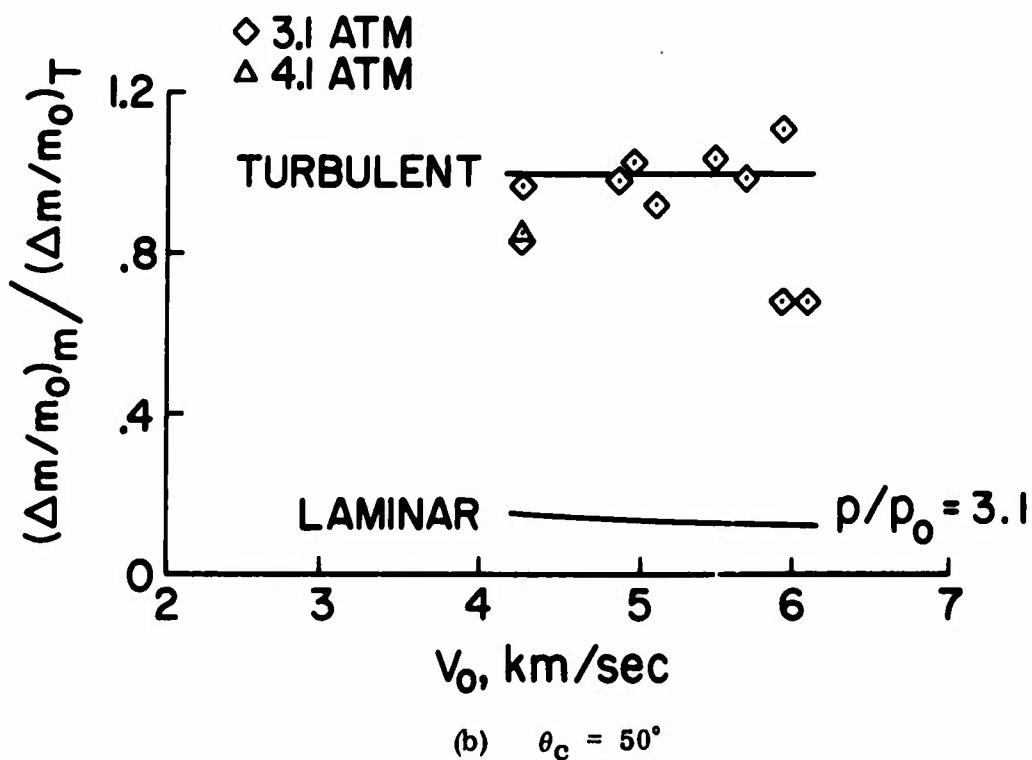
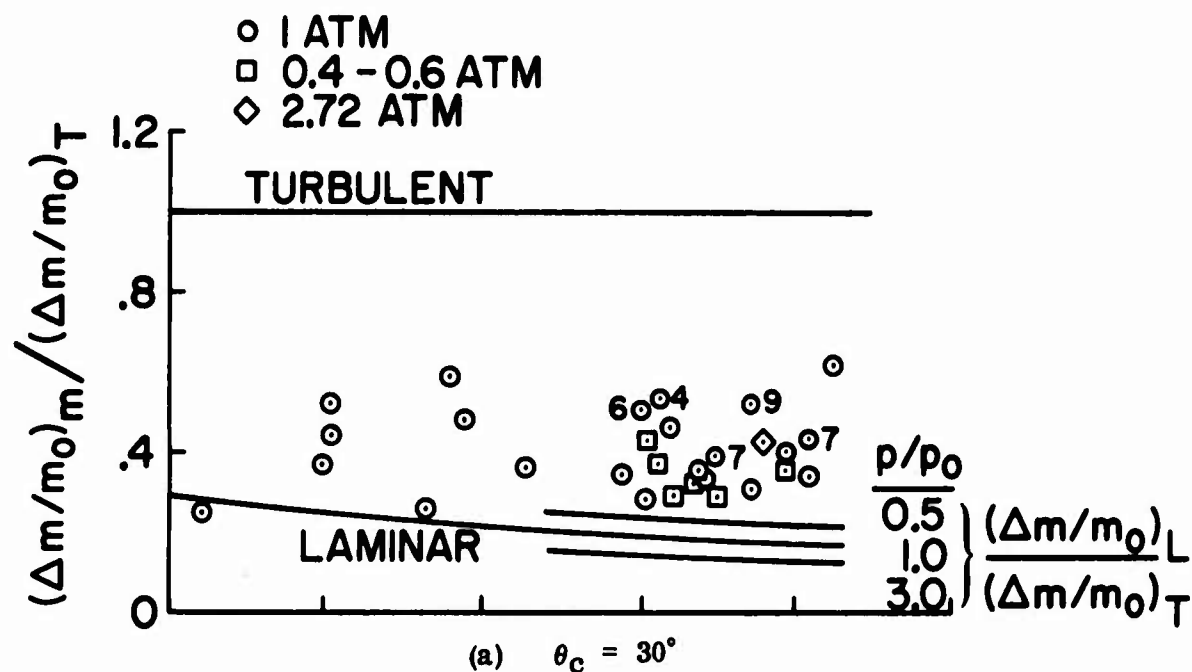


Figure 3. Total mass loss for Delrin cones

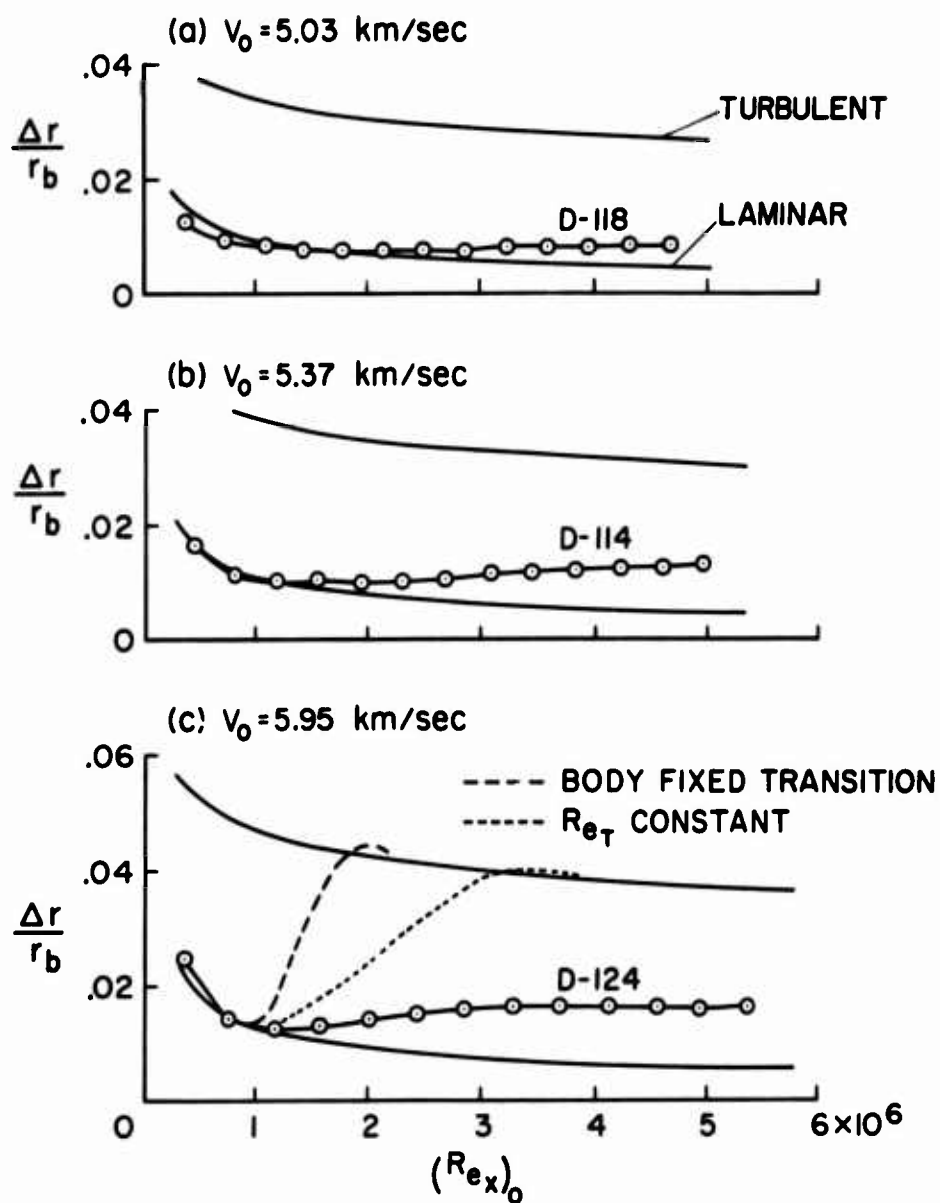


Figure 4. Surface recession (averaged around periphery) on Delrin cones, $\theta_c = 30^\circ$, $p/p_0 = 1$

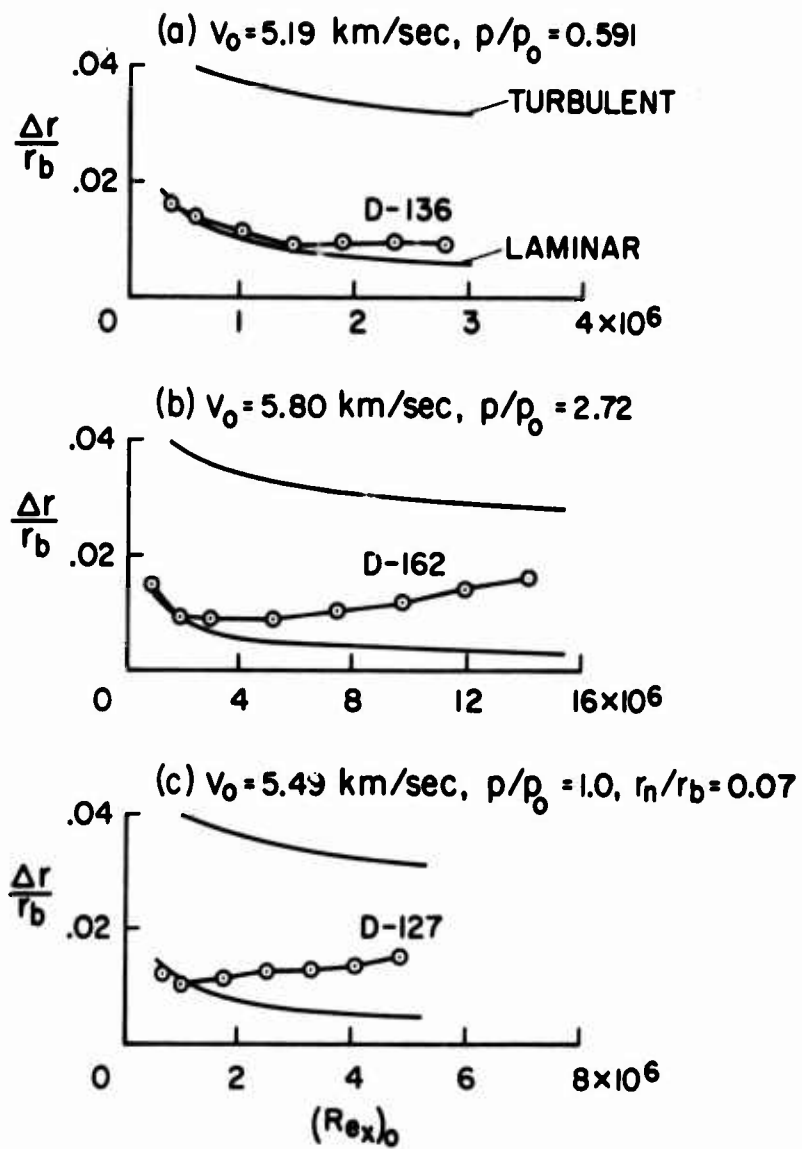
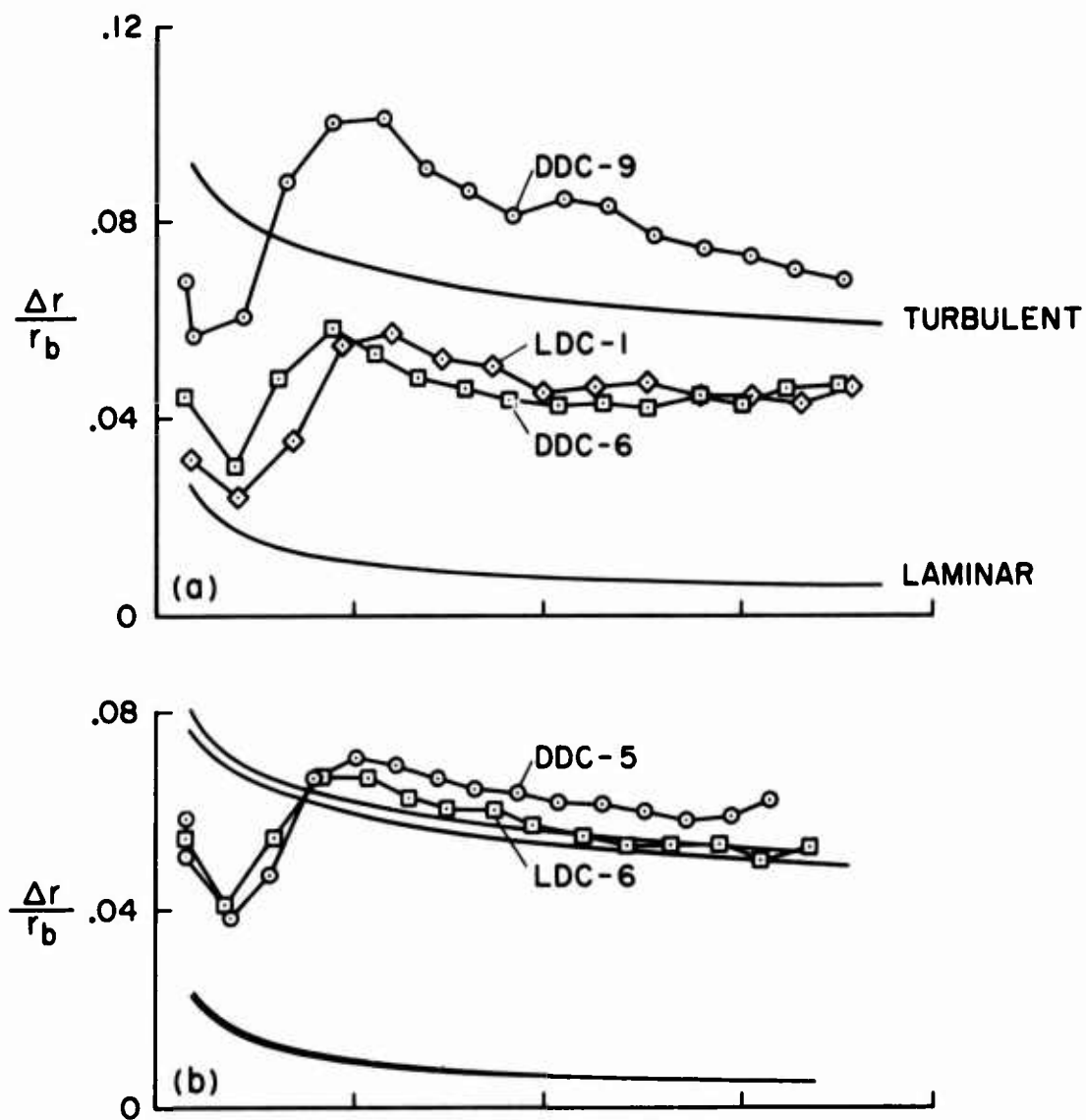
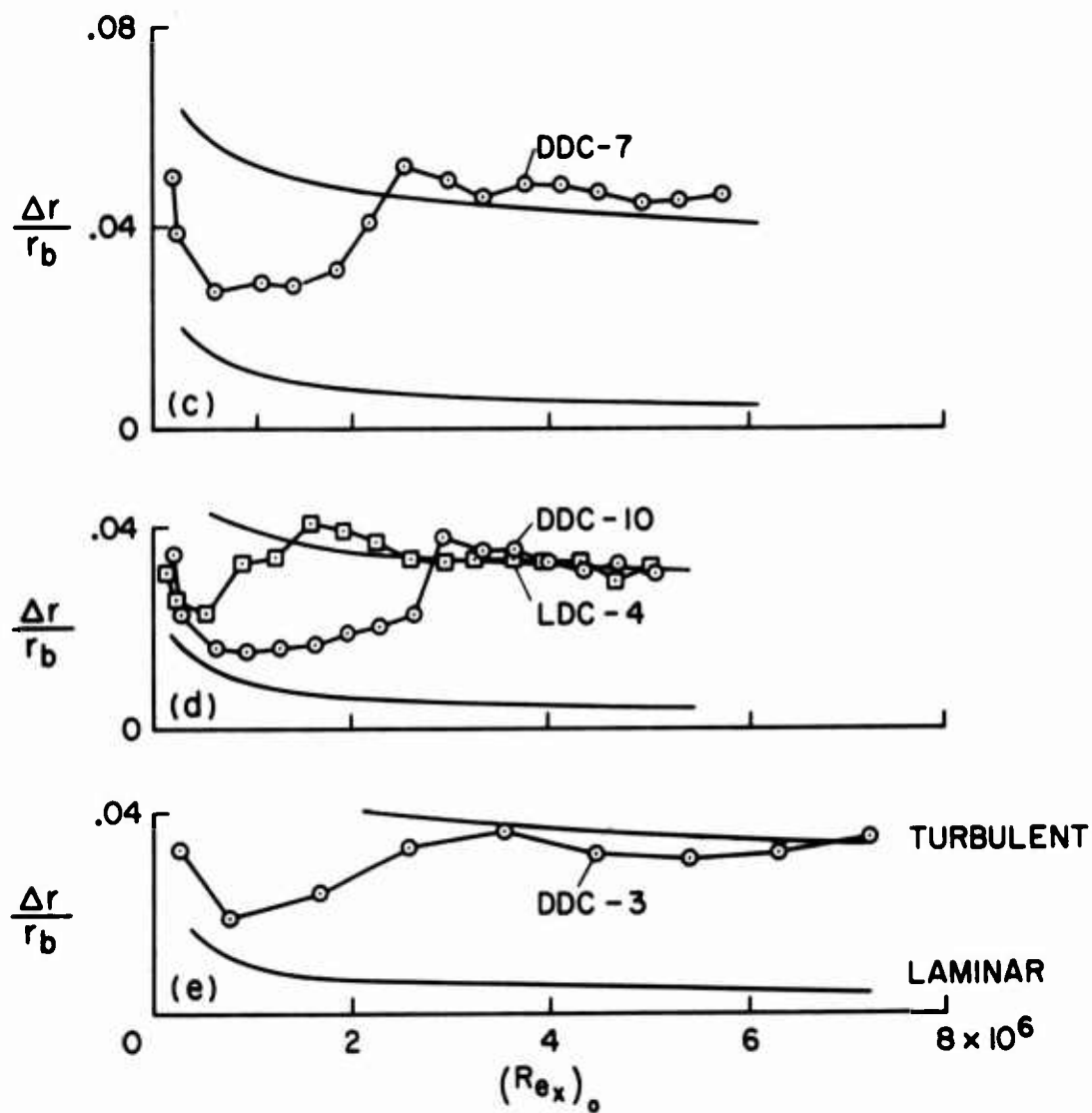


Figure 5. Surface recession (averaged around periphery) on Delrin cones, $\theta_c = 30^\circ$



- (a) $V_o = 5.94$ km/sec (DDC-6 & DDC-9), $V_o = 6.10$ km/sec (LDC-1), $p/p_o = 3.1$
- (b) $V_o = 5.49$ km/sec (DDC-5), $V_o = 5.70$ km/sec (LDC-6), $p/p_o = 3.1$

Figure 6. Surface recession (averaged around periphery) on Delrin cones, $\theta_c = 50^\circ$



(c) $V_o = 4.88 \text{ km/sec}$, $p/p_o = 3.1$

(d) $V_o = 4.27 \text{ km/sec}$, $p/p_o = 3.1$

(e) $V_o = 4.27 \text{ km/sec}$, $p/p_o = 4.1$

Figure 6 Concluded.

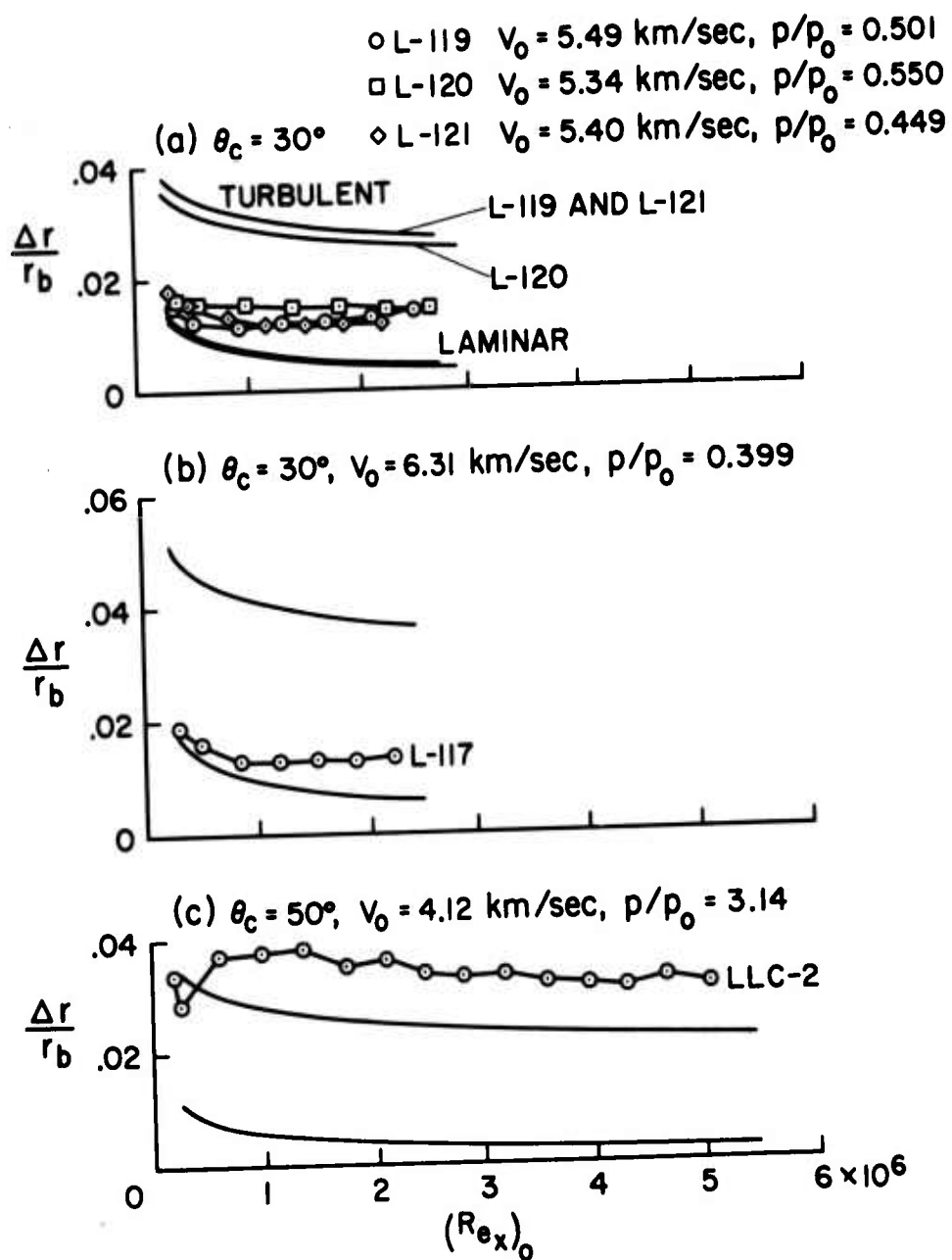


Figure 7. Surface recession (averaged around periphery) on Lexan cones

$V_0 \approx 5.4 \text{ km/sec}, p/p_0 \approx 0.5$

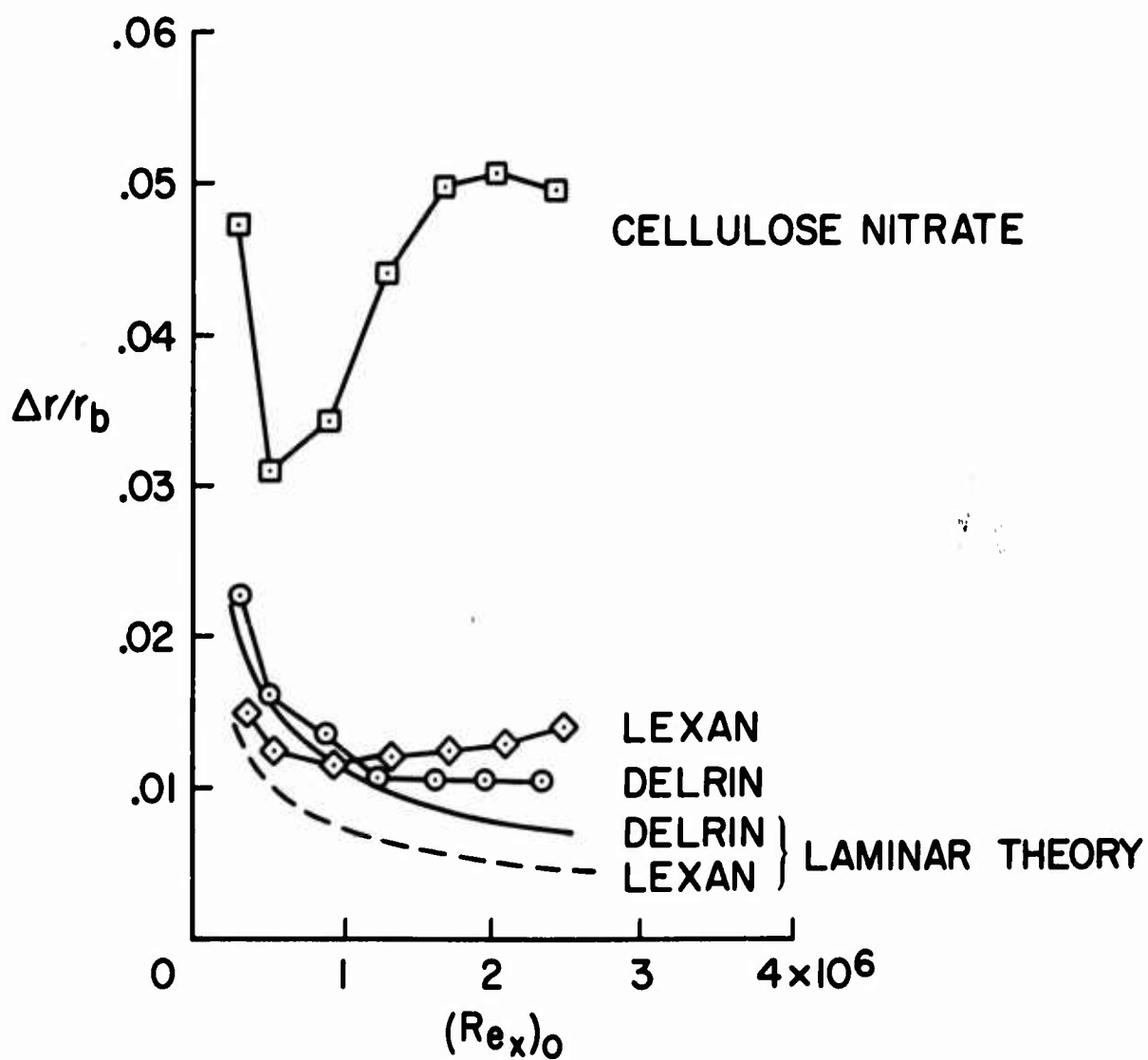


Figure 8. Surface recession (averaged around periphery) on cones of different materials, $\theta_c = 30^\circ$

(This page intentionally left blank)

SECTION 4

EFFECTS OF WALL COOLING AND ANGLE OF ATTACK ON BOUNDARY-LAYER

TRANSITION ON SHARP CONES AT $M_\infty = 7.4$ (Unclassified)

by George G. Mateer

Ames Research Center, NASA
Moffett Field, California 94035

ABSTRACT

The effects of wall cooling and angle of attack on boundary-layer transition have been investigated on 5° and 15° half-angle, sharp cones. An experimental investigation was conducted at a free-stream Mach number of 7.4, wall-to-total-temperature ratios of 0.08 to 0.4, and angles of attack from 0° to 20°. The results indicate that (1) transition Reynolds numbers decrease with decreasing temperature ratio, (2) local transition Reynolds numbers decrease in going from the windward to leeward sides of the model, (3) the length of the transition region relative to the length of laminar flow increases on the leeward side and decreases slightly on the windward side as the angle of attack increases and (4) transition data on the windward ray of cones can be correlated in terms of the crossflow velocity gradient, momentum thickness Reynolds number, local Mach number, and cone half-angle.

NOMENCLATURE

k parameter related to circumferential gradient of circumferential velocity on the windward ray of a cone;

$$k = \frac{2}{3 \sin \Theta_c} \left(\frac{1}{V_e} \frac{\partial \omega}{\partial \Phi} \right)_{\Phi = 0^\circ}$$

M Mach number

p pressure

Re/l Reynolds number per unit length

Re_θ Reynolds number based on momentum thickness

s_t length to transition along a cone generator

T temperature

V velocity along a streamline

w circumferential component of velocity

α angle of attack

θ_c cone half-angle

μ viscosity

ρ density

Φ angular coordinate around the cone (Φ = 0°; windward ray)

Subscripts

B beginning of transition

E end of transition

e boundary-layer edge condition

t total condition

w wall condition

∞ free-stream condition

INTRODUCTION

The effect of wall cooling on transition has been a subject of considerable interest largely because of the observations of transition "reversals"¹ and "rereversals"^{2, 3} and their relationships to stability theory.⁴ Although there are numerous investigations on the effects of cooling, there is a great deal of inconsistency between the observations (e.g., ref. 2 and 5). In contrast, the effect of angle of attack on transition has received relatively little attention until the recent, renewed interest in lifting reentry. The angle of attack experiments that have been performed on cones show a fairly consistent behavior, i.e., transition moves aft on the windward ray and forward on the leeward ray.^{5, 6} However, the majority of the wind-tunnel, angle-of-attack data are limited to the windward and leeward rays and to angles of attack less than the cone half-angle.

The present investigation was undertaken with two objectives in mind, 1) provide additional data to assess the effects of wall cooling on transition and 2) provide a detailed map of the transition zone on a cone at angle of attack and investigate transition at angles of attack greater than the cone half-angle. The first objective was related to an attempt to find some consistent observations among results obtained under similar test conditions. The second objective satisfied the need for more transition data on cones.

Tests were conducted on 5° and 15° half-angle cones at wall-to-total-temperature ratios of 0.08 to 0.4 and angles of attack from 0° to 20°. The free-stream Mach number was 7.4. Total temperatures ranged from 768° to 1552°K (1380°R-2800°R) and total pressures from 2.160×10^6 to 1.253×10^7 N/m² (314.0 to 1817 psia). Wall cooling data were compared with results from different investigations, and the transition zone on the 15° cone at angle of attack was mapped for meridians from 0° to 180° in 30° increments. A correlation of the transition data on the windward ray of cones is developed.

APPARATUS AND TESTS

Models

The models used in this investigation were 5° and 15° half-angle cones with surface lengths of 0.711 and 0.508 m (28 and 20 in.), respectively (a sketch is included

in fig. 1). They were of thin-walled, 0.838 mm (0.033 in.) thick electroformed nickel construction, instrumented with thermocouples spotwelded to the interior surface. The 5° cone had a single row of 22 thermocouples spaced at 2.54 cm (1 in.) intervals along one conical ray. One quadrant of the 15° cone was instrumented along conical rays having meridian angles of 0°, 30°, 60°, and 90° with 12 thermocouples on each ray. Data on other rays were obtained by rotating the models about their axis of revolution.

Facility

The tests were conducted in the NASA-Ames 3.5-Foot Hypersonic Wind Tunnel.⁷ This tunnel is a pebble-bed heated, blowdown facility equipped with interchangeable, contoured nozzles and a mechanism for quickly inserting or retracting the model from the test stream at any time during the test. A single nozzle was selected that produced a nominal free stream Mach number of 7.4. The time required to insert or retract the model was nominally 0.5 sec, and the models remained in the tunnel from a minimum of 1 sec to a maximum of 6 sec.

In the wall-cooling experiments, several tests were conducted by cooling the model with liquid nitrogen. In these instances, a plastic shroud was placed over the model and filled with coolant. When the model was inserted into the tunnel, the shroud blew off and exposed the cooled surface to the flow.

Test Conditions

A detailed listing of the test conditions are given in Tables I and II. For the wall cooling data (Table I), total temperatures ranged from 768° to 1552°K (1380°-2800°R) and total pressures from 4.178×10^6 to 1.253×10^7 N/m² (606 to 1817 psia). Wall-to-total-temperature ratios varied from 0.08 to 0.4. For the angle of attack data (Table II) the wall and total temperatures were nominally constant at 295° and 834°K (530° and 1500°R), respectively, and total pressures ranged from 2.160×10^6 to 1.210×10^7 N/m² (314.0 to 1753 psia). The angle of attack for both models was varied from 0° to 20°. The free-stream Mach number was 7.4.

RESULTS AND DISCUSSION

Examples of the heat transfer data obtained from these models are given in

reference 8 where it is shown that the heating data agreed well with laminar and turbulent heat transfer theories and were a well defined means of detecting boundary layer transition. The definition of the beginning of transition is the same as reference 8; namely, as the intersection of straight lines faired through the laminar and transitional portions of the heat transfer data, plotted logarithmically. The end of transition is defined as the intersection of straight lines faired through the transitional and turbulent portions of the heat transfer data. Although no detailed investigation of unit Reynolds number effect was made for the present study, a few check runs were made and these substantiated the conclusion of reference 8, that transition Reynolds numbers are essentially independent of free-stream unit Reynolds number. However, this observation may be related to the method used to determine transition or the definition of the beginning of transition or both. For example, in the same facility some effect of unit Reynolds number was detected by Owen and Horstman (published in these proceedings) when transition was determined from the root mean square voltage fluctuations of a thin-film gauge.

Wall-Cooling Result

The effect of wall cooling on boundary layer transition is shown on figure 2. The cooling effect is characterized by presenting transition Reynolds number, based on conditions at the edge of the boundary layer and surface length to transition, as a function of the wall-to-total-temperature ratio. Considering first the 15° cone data of figure 2a ($M_e = 5.0$), it can be seen that transition Reynolds numbers decrease as the temperature ratio decreases. The same result was observed by Stetson and Rushton⁵ at the same edge Mach number and the present results agree very well with their measurements. A similar effect was noted by Sheetz³ in testing slender cones in a ballistic range at the same edge Mach number. (Sheetz's data were not included on this figure because transition was determined in a different manner, i.e., from drag measurements.) Transition Reynolds numbers based on the end of transition also show a similar trend although not as pronounced. Finally, the length of the transition region relative to the length of laminar flow appears to be a weak function of temperature ratio.

In references 3 and 5 it was suggested that at $M_e \doteq 5$ the effect of cooling

(for $T_w/T_t < 0.4$) was initially destabilizing but that below $T_w/T_t \doteq 0.2$ this trend reversed and continued cooling stabilized the boundary layer (an effect denoted as "rereversal" in ref. 3). A similar conclusion might be made using the present data, although there are no data points in the region $0.1 < T_w/T_t < 0.2$. However, it is possible to get an indication of how transition behaves for $0.1 < T_w/T_t < 0.2$ by observing the movement of transition as the model wall temperature increases during a given test. (This technique is somewhat undesirable because temperature gradients along the model surface are introduced, and it is not known how these gradients would affect transition.) The movement of transition, as the wall temperature increases for a given test is indicated on the figure by points connected by an arrow. In this situation the beginning of transition moves forward for T_w/T_t increasing from 0.1 to 0.2, whereas, the end of transition remains essentially fixed. This result combined with the initially isothermal wall data suggest that the trend of the beginning of transition with cooling may be changing at $T_w/T_t \doteq 0.2$ although it is not clear that this is a "rereversal".

For the 5° cone data of figure 2b ($M_e = 6.6$) the effect of cooling is not as pronounced nor is there any strong indication of any change in the effect of cooling. This last observation may also be made for the data of reference 3 at $M_e \doteq 6.5$.

Angle-of-Attack Result

The angle-of-attack transition data are presented in terms of a Reynolds numbers based on boundary-layer edge conditions calculated by the method of characteristics program described in reference 9. To obtain edge conditions for angles of attack greater than the cone half-angle the following procedures were employed. 1) The 15° cone edge conditions for $\alpha \leq 15^\circ$ were extrapolated to $\alpha = 20^\circ$. 2) Windward-ray edge conditions on the 5° cone for $\alpha > 5^\circ$ were calculated by replacing the leeward side of the cone with an ellipse whose leeward-ray was aligned with the free-stream velocity vector. 3) Leeward-ray edge conditions on the 5° cone for $\alpha = 6^\circ$ were extrapolated from the calculations for $\alpha \leq 5^\circ$. In formulating the transition Reynolds number the velocity along the streamline was used in conjunction with the distance along conical rays.

The effect of angle of attack on local transition Reynolds number is illustrated in figure 3 for the 15° cone. For transition Reynolds numbers based on either the beginning (fig. 3a) or the end (fig. 3b) of transition, the influence of angle of attack depends on meridian angle, ϕ . For example, on the windward ray, local transition Reynolds numbers show an initial, slight increase with α and then a decrease; whereas, on the leeward ray, transition Reynolds numbers decrease rapidly with α .

On the 5° cone (fig. 4) the effect of α on the beginning and end of transition on the leeward ray is similar to the 15° cone; that is, leeward-ray transition Reynolds numbers decrease with increasing angle of attack. In contrast, on the windward ray the effect of α is not similar. For the 5° cone, windward-ray transition Reynolds numbers increase monotonically with angle of attack so at $\alpha = 20^\circ$ the local transition Reynolds number is at least four times the $\alpha = 0^\circ$ value. On the 15° cone the $\alpha = 20^\circ$ value is only 60% of the $\alpha = 0^\circ$ value. It will be shown in a subsequent section that the differences between the 5° and 15° cone on the windward ray are related to differences in local conditions, cone angle, and crossflow velocity gradient.

The previous figures illustrate that the length of the transition region relative to the length of laminar flow is changing with angle of attack. This is particularly evident in the 5° cone data of fig. 4. For this model the relative length of the transition region decreased on the windward ray and increases on the leeward ray as the angle of attack increases. On the 15° cone, these variations are not as obvious, and so fig. 5 was prepared to illustrate that the length of the transition region is a function of both angle of attack and meridian angle. However, the effect of angle of attack is not as strong as on the 5° cone. The length of the transition region appears to be a minimum at meridian angles from 60° to 90°, although this could be related to the manner in which transition length is defined. For example, had the length of transition been measured along streamlines instead of along conical rays the influence of meridian angle might be different.

Angle-of-Attack Correlation

Transition on cones at angle of attack can, potentially, be affected by several parameters, such as crossflow velocity, crossflow velocity gradient, pressure gradient

along streamlines, and changes in local Mach number. With so many variables to consider, it is desirable to look for situations where some effects can be eliminated so that the influence of one or two parameters can be isolated. The windward centerline affords such a situation. Here, there is no crossflow velocity or pressure gradient along the streamline, and the crossflow velocity gradient (derivative of the circumferential velocity in the circumferential direction) and local conditions can be adequately predicted.⁹ Consequently, a correlation based on changes in local conditions and crossflow velocity gradient was attempted for transition data on the windward ray, using the following procedure.

Previous investigations (e.g., ref. 3) have shown that the effects of variation in local conditions on transition on cones at $\alpha = 0^\circ$ can be accounted for by an approximately linear relationship between local momentum thickness Reynolds number (at transition) and local Mach number. In the present correlation it was assumed that a similar relationship holds at angle of attack. The local conditions were calculated using the previously described characteristics solution, and the momentum thicknesses at transition were calculated by integrating the streamwise momentum equation, using calculated laminar skin-friction coefficients from reference 10. The crossflow velocity gradient parameter, k , of reference 10 was chosen as the independent variable. A satisfactory correlation of windward-ray transition data on cones can be achieved as shown in figure 6. In addition to the present data, those of references 5, 6, and 11 were also correlated. Selection of data from other investigations was contingent upon the beginning of transition being defined in the same manner, i.e., from heat transfer measurements. The results indicate that the linear relationship between local-momentum-thickness Reynolds number and edge Mach number still exists at angle-of-attack, except, that the constant of proportionality is a function of k .

The extension of this correlation to the case of an arbitrary streamline is certainly an attractive possibility. In the general case, however, the velocity gradient may not be the correlating parameter. In this instance a parameter related to streamline spreading may be more appropriate. For example, for the specific case of the windward ray of a cone, Vaglio-Laurin¹² has shown that the variable, k , is related to streamline spreading.

CONCLUSIONS

The effects of wall cooling and angle of attack on boundary layer transition have been investigated on 5° and 15° half-angle cones. Wall-to-total-temperature ratios varied from 0.08 to 0.4 and angles of attack ranged from 0° to 20°. The tests were conducted at a free-stream Mach number of 7.4, total temperatures from 768° to 1552° K (1380° to 2800° R) and total pressures of 2.160×10^6 to 1.210×10^7 N/m² (314.0 to 1817 psia). The following is concluded from this investigation.

1. In general, transition Reynolds numbers decrease with decreasing T_w/T_t . Although, on the 15° cone, there are indications that this trend does not continue for $T_w/T_t < 0.2$, an observation consistent with that in ref. 3 and 5.
2. Local transition Reynolds numbers are a function of both angle of attack and cone half-angle. On the lee side of both models transition Reynolds numbers decreased with increasing α ; whereas, on the windward side an increase was observed on the 5° cone, and a slight increase followed by a decrease for the 15° cone.
3. The length of the transition region relative to the length of laminar flow increased on the leeward side and decreased slightly on the windward side as the angle-of-attack increased.
4. Transition data on the windward ray of cones can be correlated by accounting for variations in crossflow velocity gradient, momentum thickness Reynolds number, local Mach number, and cone half-angle.

REFERENCES

1. J. R. Jack, R. J. Wisniewski and N. S. Dianconis, Effects of Extreme Surface Cooling on Boundary-Layer Transition. NACA TN 4094 (1957).
2. R. J. Wisniewski and J. R. Jack, Recent Studies on the Effect of Cooling on Boundary-Layer Transition at Mach 4. Journal of the Aerospace Sciences, Vol. 28, No. 3, pp 250-251 (March 1961).
3. N. W. Sheetz, Jr., Ballistics Range Boundary-Layer Transition Measurements on Cones at Hypersonic Speeds. Proceedings of the Symposium on Viscous Drag Reduction, C. S. Wells, Editor, pp 53-83 (February 1969).
4. E. Reshotko, Stability Theory as a Guide to the Evaluation of Transition Data. AIAA Journal, Vol. 7, No. 6, pp 1086-1091 (June 1969).
5. K. F. Stetson and G. H. Rushton, Shock Tunnel Investigation of Boundary-Layer Transition at $M = 5.5$. AIAA Journal, Vol. 5, No. 5, pp 899-906 (May 1967).
6. V. DiCristina, Three-Dimensional Laminar Boundary-Layer Transition on a Sharp 8° Cone at Mach 10. AIAA Journal, Vol. 8, No. 5, pp 852-856 (May 1970).
7. T. E. Polek, G. H. Holdaway and J. H. Kemp, Flow Field and Surface Pressures on a Blunt Half-Cone Entry Configuration at Mach Numbers of 7.4 and 10.4. NASA TM X-1014 (1964).
8. G. G. Mateer and H. K. Larson, Unusual Boundary-Layer Transition Results on Cones in Hypersonic Flow. AIAA Journal, Vol. 7, No. 4, pp 660-664 (April 1969).
9. J. V. Rakich, A Method of Characteristics for Steady Three-Dimensional Supersonic Flow with Application to Inclined Bodies of Revolution. NASA TN D-5341 (1969).
10. E. Reshotko, Laminar Boundary Layer with Heat Transfer on a Cone at Angle-of-Attack in a Supersonic Stream. NACA TN 4152 (1957).
11. J. D. Julius, Measurements of Pressure and Local Heat Transfer on a 20° for a Mach Number of 4.95. NASA TN D-179 (1959).
12. R. Vaglio-Laurin, Laminar Heat Transfer on Three-Dimensional Blunt Nosed Bodies in Hypersonic Flow. ARS Journal, Vol. 29, No. 2, pp 123-129 (February 1959).

TABLE I. TEST CONDITIONS FOR WALL-COOLING DATA

θ_c , deg	P_t , N/m ²	P_t , psia	T_t , °K	P_t , °R	T_w , °K	T_w , °R	$(\frac{R}{l})_w$, m ⁻¹	$(\frac{R}{l})_w$, ft ⁻¹	$(s_t)_w$, m	$(s_t)_w$, ft	$(s_t)_E$, m	$(s_t)_E$, ft
15	1.346 ⁷	1810	1519	2735	119.4	215	8.035 ⁶	2.445 ⁶	0.2210	0.7250	0.3758	1.233
	7.584 ⁶	1100	1161	2089	101.1	182	8.219 ⁶	2.505	0.2514	0.8250	0.3982	1.300
	1.346 ⁷	1807	1181	2126	106.3	195	1.307 ⁷	3.983	0.1829	0.6000	0.2642	.8667
	4.178 ⁶	606	876.7	1578	87.22	157	7.490 ⁶	2.283	0.3099	1.017	O.M.	O.M.
	1.340 ⁷	1798	903.9	1627	142.8	257	2.108 ⁷	6.424	A.T.	A.T.	0.1880	.6167
	1.253 ⁷	1817	1498	2697	320.6	577	8.294 ⁶	2.528	0.2006	0.6583	0.3785	1.242
	7.667 ⁶	1112	1143	2057	305.6	550	8.554 ⁶	2.607	0.2514	0.8250	0.4139	1.356
	1.230 ⁷	1784	1042	1876	314.4	566	1.624 ⁷	4.951	0.1956	0.6417	0.2819	.9250
	1.211 ⁷	1787	1028	1850	327.8	590	1.640 ⁷	5.000	0.1854	0.6083	0.2819	.9250
	5.898 ⁶	826.4	963.3	1734	314.4	566	8.662 ⁶	2.640	0.2794	0.9167	O.M.	O.M.
	4.178 ⁶	606.0	861.7	1551	303.9	547	7.117 ⁶	2.352	0.3022	0.9917	O.M.	O.M.
	6.164 ⁶	894.0	815.6	1468	305.6	550	1.250 ⁷	3.811	0.2387	0.7833	0.3758	1.233
	1.091 ⁷	1582	837.3	1507	313.9	565	2.116 ⁷	6.450	0.1600	0.5250	0.2499	.8167
	7.380 ⁶	1066	790.0	1422	307.8	554	1.574 ⁷	4.796	0.2108	0.6917	0.2794	.9167
	6.191 ⁶	898.0	790.6	1423	316.7	570	1.324 ⁷	4.035	0.2311	0.7583	0.3682	1.206
	5.840 ⁶	847.0	781.1	1406	781.1	570	1.274 ⁷	3.884	0.2260	0.7417	0.3709	1.217
5	1.247 ⁷	1809	1552	2794	110.6	199	7.694 ⁶	2.345	0.3557	1.167	0.5891	1.933
	6.064 ⁶	878	833.3	1500	77.78	140	1.184 ⁷	3.608	0.2997	0.9833	0.4901	1.606
	1.211 ⁷	1757	828.9	1492	107.8	194	2.391 ⁷	7.287	A.T.	A.T.	0.2349	.7708
	1.251 ⁷	1815	1832	2758	325.6	586	7.924 ⁶	2.415	0.3453	1.133	0.5843	1.917
	9.398 ⁶	1343	1313	2364	320.6	577	8.058 ⁶	2.456	0.3758	1.233	0.6120	2.006
	8.143 ⁶	1181	1195	2152	323.9	583	8.347 ⁶	2.544	0.3557	1.167	0.6248	2.050
	1.139 ⁷	1652	1106	1994	306.7	552	1.346 ⁷	4.102	0.2644	0.9333	0.4672	1.500
	8.281 ⁶	1201	1010	1819	306.6	550	1.166 ⁷	3.523	0.3046	1.000	0.4953	1.625
	6.019 ⁶	873	862.2	1534	300.0	540	1.133 ⁷	3.453	0.3072	1.008	0.5004	1.642
	1.177 ⁷	1707	875.0	1575	311.1	560	2.117 ⁷	6.452	A.T.	A.T.	0.2730	.8958
	6.064 ⁶	875	850.0	1530	305.6	550	1.140 ⁷	6.064	0.3328	1.092	0.5309	1.742
	5.950 ⁶	863	851.7	1533	307.8	554	1.121 ⁷	3.417	0.3046	1.000	0.4625	1.583
	4.344 ⁶	630	807.2	1453	306.6	550	8.867 ⁶	2.733	0.4114	1.350	O.M.	O.M.
	8.039 ⁶	1166	796.7	1434	304.4	548	1.697 ⁷	5.172	0.2110	0.7250	0.3022	.9917
	5.874 ⁶	852	762.3	1383	302.2	544	1.318 ⁷	4.016	0.2921	0.9583	0.4496	1.475

O.M. - OFF MODEL A.T. - AHEAD OF THERMOCOUPLES

TABLE II. TEST CONDITIONS FOR ANGLE-OF-ATTACK DATA

Q_∞ , deg	α , deg	P_{t1} , N/m ²	P_{t1} , psia	T_{t1} , °K	T_{t1} , °R	$\left(\frac{R_e}{l}\right)_\infty$, m ⁻¹	$\left(\frac{R_e}{l}\right)_\infty$, ft ⁻¹	Φ , deg	$(st)_{H1}$, m	$(st)_{H1}$, ft	$(st)_E$, m	$(st)_E$, ft
15	2	1.209 ⁴	1753	820.0	1476	2.43 ⁷	7.41×10 ⁶	0	0.123	0.403	0.203	0.666
								30	0.179	0.587	0.282	0.926
								60	0.183	0.602	0.267	0.875
								90	0.155	0.510	0.213	0.698
		1.126 ⁴	1633	803.9	1447	2.34 ⁷	7.13×10 ⁶	120	0.159	0.522	0.244	0.799
								150	0.156	0.513	0.239	0.785
								180	0.127	0.418	0.245	0.803
	4	6.943 ³	1007	827.2	1489	1.38 ⁷	4.19×10 ⁶	0	0.303	0.993	0.522	1.713
								30	0.282	0.925	0.520	1.705
								60	0.237	0.778	0.364	1.193
								90	0.199	0.653	0.314	1.03
		5.523 ³	801.0	851.7	1533	1.04 ⁷	3.17×10 ⁶	120	0.200	0.655	0.326	1.07
								150	0.205	0.674	0.375	1.23
								180	0.216	0.708	0.373	1.225
	8	1.093 ⁴	1585	827.8	1490	2.16 ⁷	6.59×10 ⁶	0	0.208	0.682	0.405	1.33
								30	0.221	0.725	0.430	1.41
								60	0.141	0.463	0.227	0.746
								90	0.095	0.311	0.136	0.448
		4.309 ³	625.0	838.9	1510	8.33 ⁶	2.54×10 ⁶	120	0.207	0.680	0.320	1.05
								150	0.190	0.625	0.323	1.06
								180	0.102	0.335	0.219	0.720
	12	9.660 ³	1401	830.6	1495	1.90 ⁷	5.79×10 ⁶	0	0.190	0.622	0.338	1.11
								30	0.263	0.864	0.472	1.55
								60	0.168	0.553	0.242	0.794
								90	0.113	0.370	0.188	0.617
		2.751 ³	399.0	832.8	1499	5.38 ⁶	1.64×10 ⁶	120	0.277	0.910	0.616	*2.02
								150	0.229	0.752	0.460	1.51
								180	0.190	0.623	0.369	1.21
	16	1.091 ⁴	1582	812.2	1462	2.23 ⁷	6.79×10 ⁶	0	0.132	0.433	0.285	0.934
								30	0.192	0.631	0.354	1.16
								60	0.148	0.485	0.222	0.728
								90	0.107	0.350	0.176	0.579
		1.087 ⁴	1576	822.8	1481	2.17 ⁷	6.62×10 ⁶	120	0.083	0.273	0.164	0.540
								150	0.016	0.199	0.130	0.427
								180	—	—	0.090	0.297
								150	0.016	0.199	0.130	0.427
	20	1.083 ⁴	1572	868.9	1564	1.97 ⁷	6.01×10 ⁶	0	0.175	0.574	0.295	0.968
								30	0.203	0.666	0.350	1.15
								60	0.167	0.549	0.305	1.00
								90	0.112	0.368	0.224	0.736
		1.096 ⁴	1589	840.0	1512	2.11 ⁷	6.44×10 ⁶	120	0.076	0.249	0.198	0.651
								150	0.079	0.260	0.181	0.594
5	2	1.095 ⁴	1588	820.6	1477	2.20 ⁷	6.70×10 ⁶	0	0.234	0.768	0.357	1.17
		2.165 ³	314.0	783.9	1411	4.69 ⁶	1.43×10 ⁶	180	0.287	0.941	0.567	1.86
	4	1.099 ⁴	1594	830.0	1494	2.16 ⁷	6.60×10 ⁶	0	0.234	0.768	0.332	1.09
		2.220 ³	122.0	792.2	1426	4.72 ⁶	1.44×10 ⁶	180	0.288	0.946	0.622	2.04
	6	1.097 ⁴	1591	872.2	1570	1.98 ⁷	6.05×10 ⁶	0	0.280	0.917	0.369	1.21
		1.100 ⁴	1595	862.8	1553	2.03 ⁷	6.18×10 ⁶	180	0.357	1.171	0.163	0.534
	10	1.097 ⁴	1591	842.8	1517	2.10 ⁷	6.41×10 ⁶	0	0.321	1.053	0.424	1.391
	14	1.093 ⁴	1585	808.9	1456	2.25 ⁷	6.85×10 ⁶	0	0.393	1.29	0.497	1.63
	20	1.100 ⁴	1596	833.9	1501	2.15 ⁷	6.55×10 ⁶	0	0.710	2.33	—	—

*ESTIMATED

θ_c , deg	L, m (in)
5	0.711 (28)
15	0.508 (20)

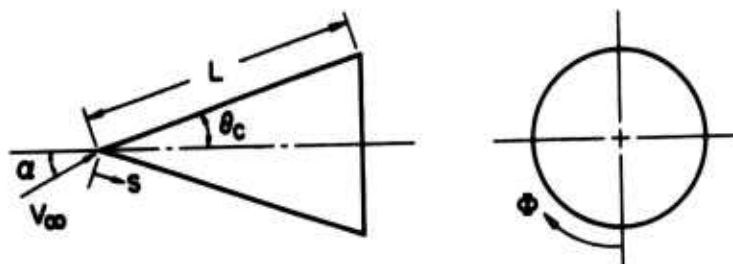
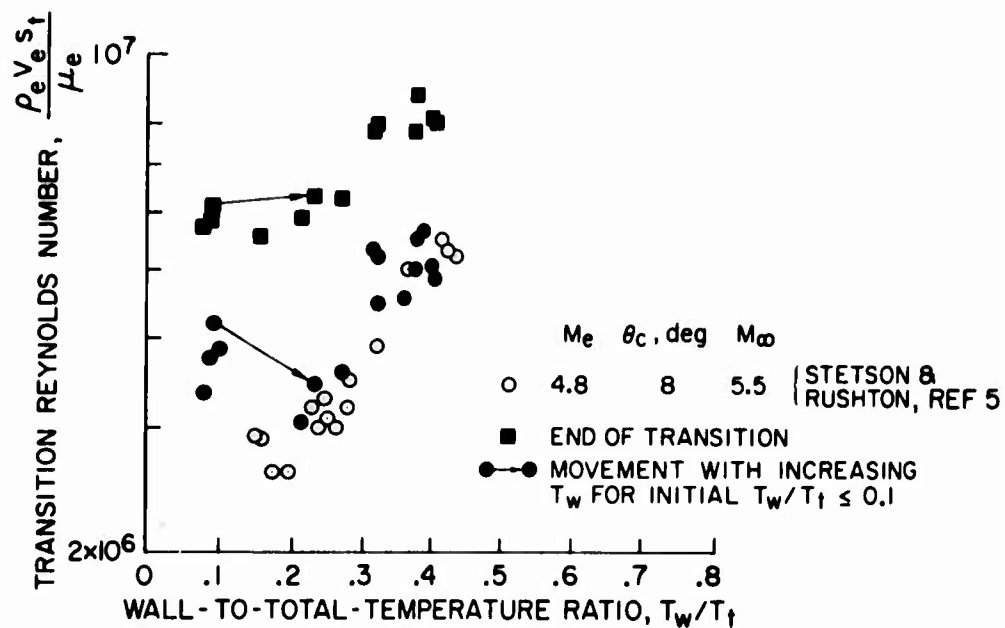
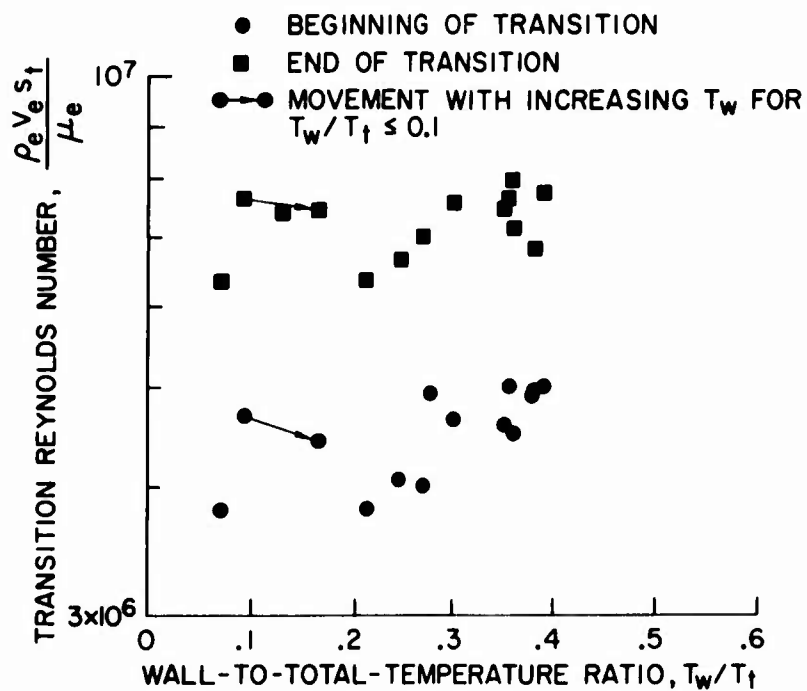


Figure 1. Models



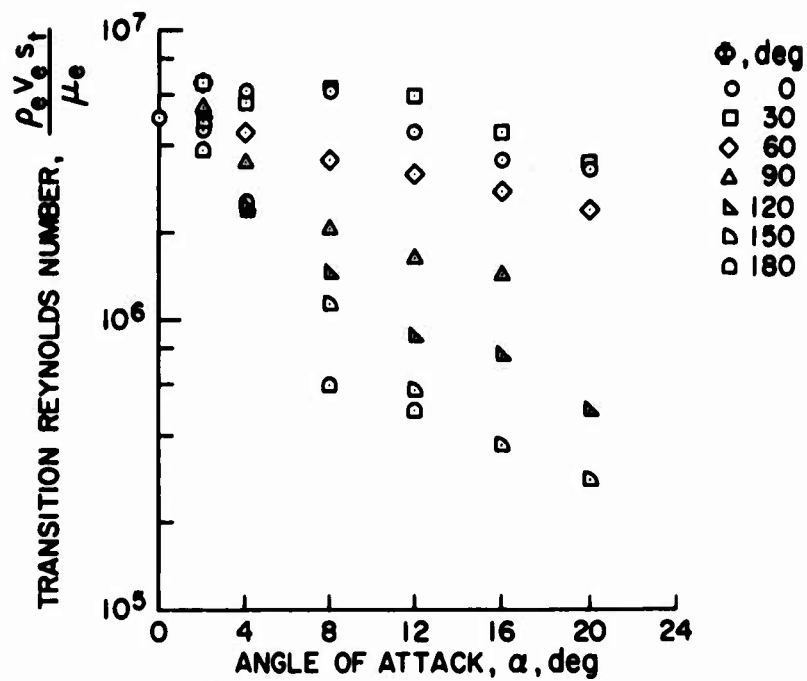
(a) $\theta_c = 15^\circ$, $M_e = 5.0$

Figure 2. Effect of wall cooling on boundary-layer transition



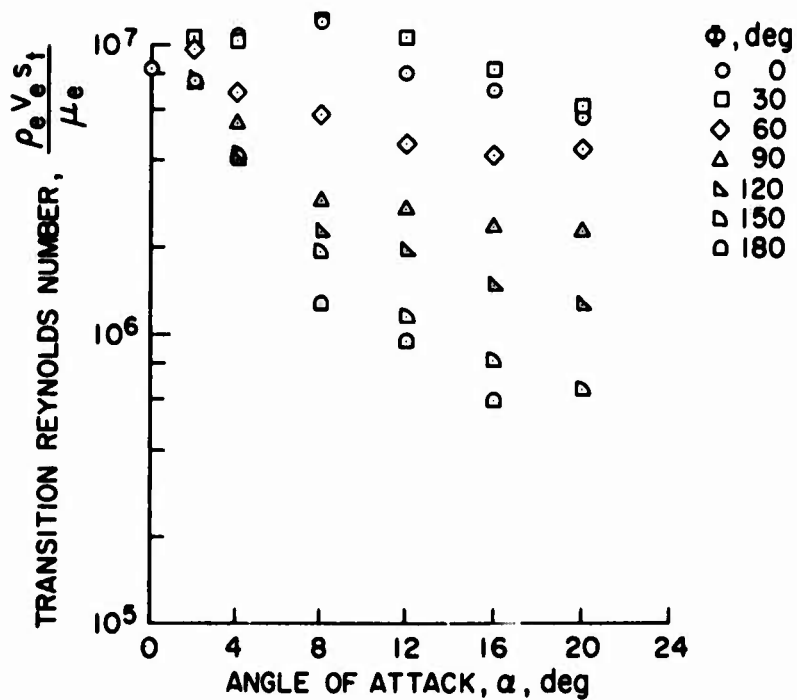
(b) $\theta_c = 5^\circ$, $M_e = 6.6$

Figure 2. Concluded



(a) Boundary of transition

Figure 3. Effect of angle of attack on transition;
 $\theta_c = 15^\circ$, $M_\infty = 7.4$



(b) End of transition

Figure 3. Concluded

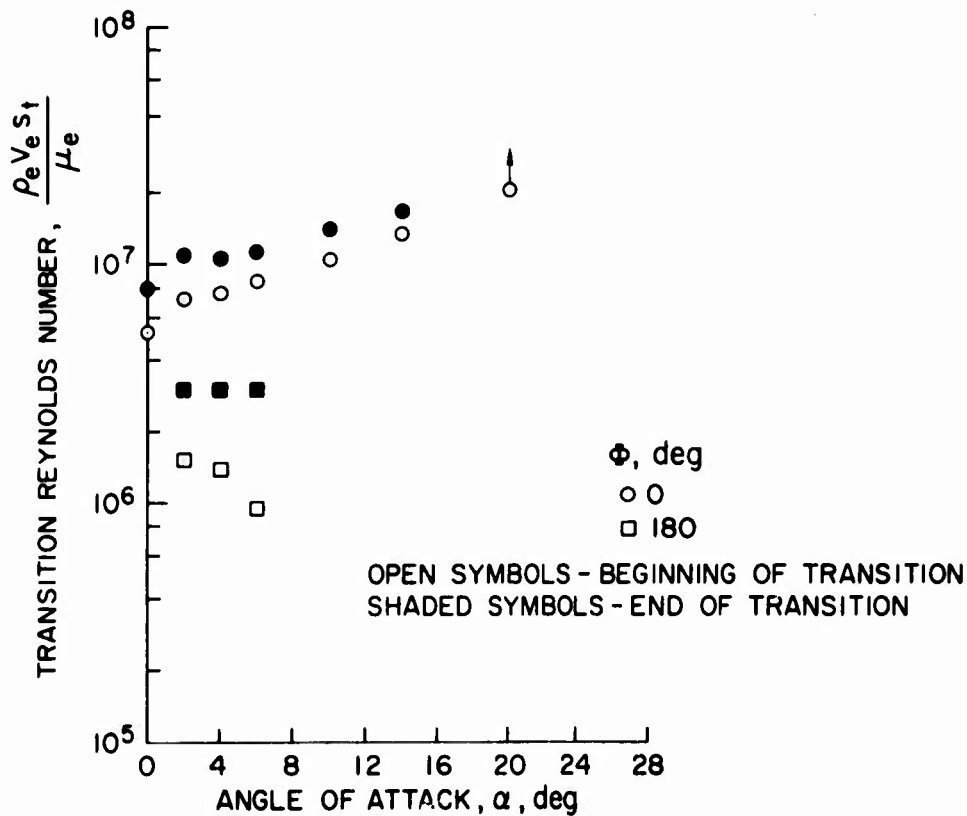


Figure 4. Effect of angle of attack on transition; $\Theta_c = 5^\circ$, $M_\infty = 7.4$

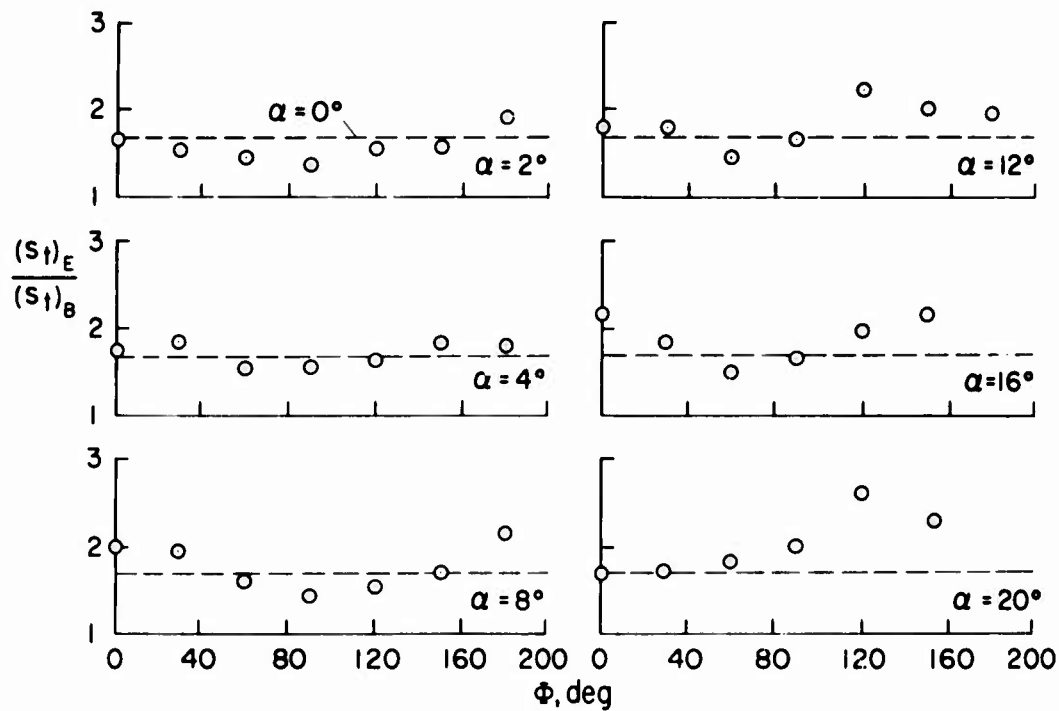


Figure 5. Effect of angle of attack and meridian angle on the length of the transition region; $M_\infty = 7.4$, $\Theta_c = 15^\circ$

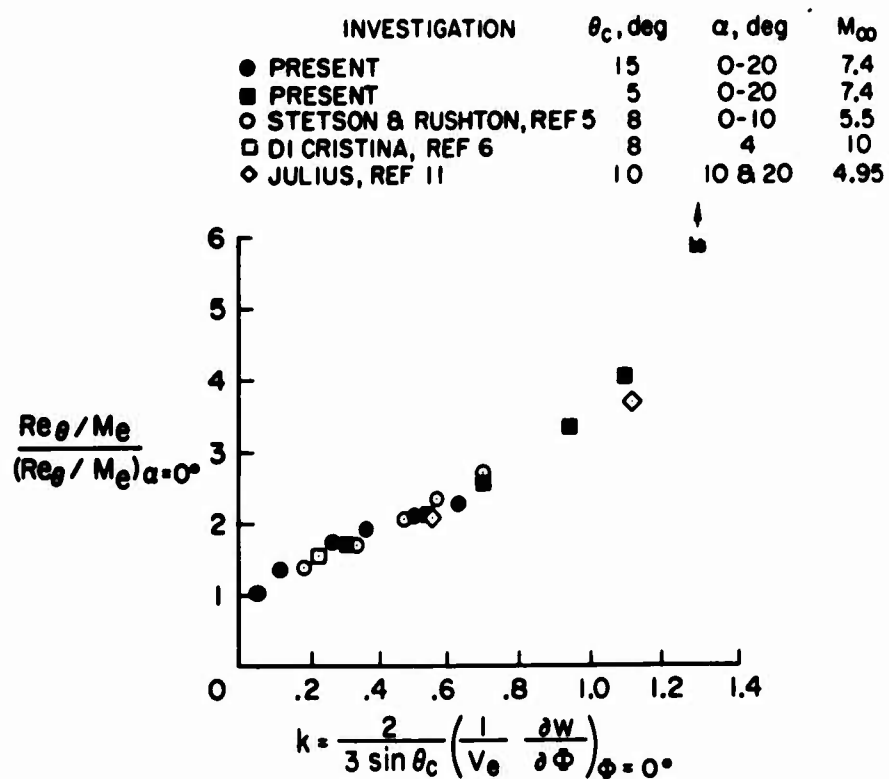


Figure 6. Correlation of the beginning of transition;
windward ray of cones

(This page intentionally left blank)

SECTION 5

SOME SPECIAL FEATURES OF BOUNDARY LAYER
TRANSITION ON AEROBALLISTIC RANGE MODELS
(Unclassified)

by J. Leith Potter

ARO, Inc., Tullahoma, Tennessee

ABSTRACT
(Unclassified)

Some points to consider in interpreting data on boundary layer transition obtained by launching 10-deg half-angle cones in an aeroballistic range are discussed. These are: (1) oscillatory motion and finite angles of attack, (2) surface roughness at high unit Reynolds numbers, (3) vibration of the model, and (4) non-uniform surface temperature. The experiments were conducted at free-stream Mach numbers of 2.3 and 5.1, with unit Reynolds numbers of 0.4 to 3×10^6 per inch.

Each of the listed points of discussion is analyzed to the extent feasible with available information. Emphasis is placed on the particular conditions applying in past and current research on boundary layer transition in aeroballistic Range K at the Arnold Engineering Development Center. Under the conditions of the experiments, there was no evidence that any of these four features of range models was a dominant factor in the related experiments which earlier revealed a marked tendency of Reynolds number of transition to increase with range pressure, or unit Reynolds number.

NOMENCLATURE

k	height of roughness element
M	Mach number
N	number of cycles of vibration
p	pressure

*The research reported herein was sponsored by the Arnold Engineering Development Center (AEDC), Air Force Systems Command (AFSC), under Contract F40600-72-C-0003 with ARO, Inc. Reproduction to satisfy the needs of the U. S. Government is authorized.

Re_t	Reynolds number at transition
r_b	cone base radius
r_n	cone nose radius of curvature
s	wetted length measured along surface
T	temperature
U	velocity
W	see Table II
Y	see Table II
y_n	amplitude of vibration after elapsed time τ
y_o	initial amplitude of vibration
α_p	angle of attack of cone in photograph
α_t	total angle of attack of cone
Δ	see Eq. (1)
δ	total boundary layer thickness
ϵ	critical roughness "Reynolds number"
θ_c	cone half-angle
ν	kinematic viscosity
ρ	density

Subscripts

aw	adiabatic wall
k	at height k in the boundary layer, or beginning of roughness (s_k)
o	total, e. g., total temperature
t	transition
w	cone wall
δ	local (inviscid) flow parameter on cone at edge of boundary layer
∞	free-stream

INTRODUCTION

The state of our knowledge of boundary layer transition has been summarized recently in notable reviews by Morkovin (1, 2), Mack (3), and Mack and Morkovin (4). It is a justifiable conclusion after studying these reviews that significant new contributions by experimentalists are necessary and that care must be taken to control and define all factors influencing the transition process in the experimental environment. By far, most previous experimental investigations of transition have been conducted in wind tunnels where it has been generally recognized that coupling between "tunnel" disturbances and flow in the boundary layer under observation almost always made such absolute measurements as local transition Reynolds number, $Re_{\delta, t}$, inapplicable in other environments, even when all of the more obvious dynamic similarity conditions were matched.

Conventional wisdom has led to frequent assumptions that $Re_{\delta, t}$ determined for a model in a wind tunnel must be less than would be found in full-scale free-flight testing, but even that has not always been true. Neither does it seem justifiable to condemn all wind tunnel data, as some have done. When the dominant factor influencing transition has been controlled (e. g., roughness, bluntness, sweep or angle of attack) and results are presented so as to suppress the uncertainty attaching to absolute $Re_{\delta, t}$, useful results may be claimed.

The free-flight range is an experimental facility not widely exploited for boundary layer transition studies, though much used for wake transition observations. This situation is understandable on grounds of convenience and availability, but some rather important information may be obtained from range experiments. The quiet atmosphere of the aeroballistic range appears to offer an opportunity for study of boundary layer transition free of the complex influences of stream turbulence and noise which are known to be present in varying degrees in wind tunnels. In view of the time spent in

wind tunnel experiments and the failure to achieve a commensurate understanding of transition, the possibilities in range experimentation should not be ignored. However, there are some special features of aeroballistic experimentation which present difficulties, and it is appropriate that they be reviewed in the context of their influence on boundary layer transition. The ones discussed in this interim report are:

1. Finite angles of attack and oscillatory motion.
2. Surface roughness under conditions of cold walls and large unit Reynolds number.
3. Vibration of the model.
4. Non-uniform surface temperature.

The discussion is based mainly on experiments reported by Potter (5) and a similar program now in progress at the Arnold Engineering Development Center (AEDC). The current (1971-72) work is aimed at assessment of factors that may contribute to the "unit Reynolds number" influence displayed in reference 5. It involves 10-deg semi-apex-angle, nominally sharp cones at free-stream Mach numbers near 2.3 and 5.1. Cone roughness and vibrational characteristics are being varied, and cone surface condition in flight is being examined with the aid of laser-lighted photography. The two Mach numbers were selected on the basis of stability theory (cf. 3) which suggests that different modes of boundary layer instability are dominant at the two local Mach numbers which are approximately 2.1 and 4.3, respectively.

MODELS AND RANGE SYSTEMS

Data on the models are given in Fig. 1. The 1.75-in. aluminum cones were used to obtain earlier transition data on smooth bodies and for all of the experiments on roughened surfaces. The 2.5-in. cone is now the principal aluminum model; very few launches of the 2.3-in. cone were made.

The aluminum models were fabricated from 7075-T6 alloy and were given a surface finish of $10\text{ }\mu\text{in.}$, rms, or better. A nose radius of 0.005 in. was standard on both aluminum and Lexan^R cones. The latter is a polycarbonate resin which was selected because it would give a cone of appreciably different vibrational characteristics for comparison to the aluminum cone. This was wanted for a study of the possible influence of vibration on boundary layer transition, which is briefly discussed in a later section. At first it was supposed that the Lexan cones would require aluminum tips to prevent ablation, but trial flights in the range proved that an all-Lexan cone surface was feasible. Sabots used with these cones are discussed in the context of their relation to roughening of cone surfaces in a later section.

The aeroballistic range used for this work was AEDC-VKF Range K. This is a 100-ft-long range equipped with six dual-axis shadowgraph systems and a single high-quality schlieren or focused shadowgraph system. The latter, with an effective exposure duration of $0.15\text{ }\mu\text{sec}$, was used to obtain the principal photographic data in this investigation. A laser-front-lighted photographic system, with an effective exposure duration of 20 nano-sec was used to obtain information on cone surface conditions after launch.

A single-stage, 2.5-in. -caliber launcher was used. The muzzle of this gun was located approximately 49 ft from the focused shadowgraph station. The cones were launched without spin, and sabot separation was caused by aerodynamic force on the sabot components.

Noise in the range was monitored by a pair of small microphones, cf. reference 5. Because this subject does not come under discussion in this report, no further information is included.

THE INFLUENCE OF ANGLE OF ATTACK

It is rare that a free-flight model maintains zero angle of attack throughout its flight. Under the best conditions, aeroballistic models may

have near zero average total angle and exhibit amplitudes of only one or two degrees. However, the typical range is equipped with only a few schlieren or shadowgraph stations of the high quality needed for photographing boundary layer transition, and the photographic data on the models launched inevitably will include a random distribution of angles. Note that one must distinguish between the total angle and the angle in the plane of the photograph. They usually will be different. The range pressures in transition work usually are relatively high, which aids in damping the model motions, but the observation station for transition studies on high-speed, sharp-nosed models usually must be located rather near the launcher to obtain data prior to ablation of the model. Thus, finite and variable angles of attack must be expected.

For the experiments discussed herein, Fig. 2 is typical. The angles in two planes are plotted as a function of length along the range, measured from the first to the last of six dual-axis shadowgraph stations. The parallel-light, single-axis shadowgraph station was located at 5 ft on the length scale given. This typical case is characterized by an average velocity of approximately 5700 ft/sec, a half-cycle of motion in roughly 17 ft, and a maximum amplitude somewhat under 2 deg. The wetted length of the conical model upstream of transition in this case was slightly under 5 in. Thus, there was a change in angle of attack of 2 deg in 17 ft of flight or 0.0029 sec, giving a rate of change of 690 deg/sec. In terms of wetted-length-to-transition, the velocity was 13,700 lengths/sec. This enables expressing the oscillatory motion as $690/13,700 = 0.05$ deg/wetted length. If we assume that the change in angle of attack during a time corresponding to flow from stagnation point to transition location is crucial, then this information seems to warrant the tentative assumption that the oscillations of the models, per se, in these experiments were of low enough frequency to be ignored as a factor in boundary layer transition. The margin of safety here may not be large. There is reason to suspect that as little as $0.05 \theta_c$ deg per wetted length may be significant for slender, sharp cones. This warning is based on the

data to be discussed next, which show important changes in length-to-transition, s_t , when a cone under conditions such as these is tested at small angles of attack in a wind tunnel.

It could be argued that another length, such as some number of boundary layer thickness, would be more suitable than the length, s_t , which has been used in the preceding discussion. (In this example, total boundary layer thickness midway along the wetted length is calculated to have been approximately 0.005 in.) However, that subject will not be explored any further.

There have been several recent reports on the effects of small angles of attack on transition location. Some of the data are summarized in Fig. 3, and Table I gives supplemental information.

TABLE I. EXPERIMENTS ON EFFECT OF ANGLE OF ATTACK ON TRANSITION

<u>Ref.</u>	<u>θ_c deg</u>	<u>M_∞</u>	<u>T_w/T_{aw}</u>	<u>Re_∞ in.⁻¹ x 10⁻⁶</u>
6	2.87	21.5	~1	1.19
7	8.00	5.5	0.2-0.6	0.11-0.34
8	10.0	6.9	~0.5	0.38
9	5.0	8.0	~0.4	1.14
10	8.0	10.2	~0.3	0.175
11	10.0	6.0	~0.86	1.10

For comparison, the present conditions are:

10.0	5.1	~0.18	0.6-4.0
10.0	2.4	~0.50	0.6-1.7

The authors of reference 7 ignored the possibility of a unit Reynolds number influence in drawing the curve reproduced in Fig. 3, i. e., they compared points for $\alpha = 0$ and $\alpha \neq 0$ which did not correspond to constant U/ν . The curve marked 7a represents the result of our effort to adjust the results

of reference 7 on the basis of an assumed $Re_t \sim (U/\nu)^{1/2}$ relation. It is shown only to indicate qualitatively how much influence may have existed.

The curves marked 10 and 10a represent the extremes of the data of reference 10. Curve 10 represents the angle $\phi = 0$ where ϕ is measured, as a roll angle, circumferentially from either the windward or leeward "stagnation" line on the cone surface. Curve 10a normally, but not always, represents $\phi = 90$ deg. The case $\phi = 90$ deg was not always the extreme; sometimes it was $\phi = 72$ deg.

Table I shows that some of the conditions represented in Fig. 3 are at least roughly comparable to the Mach 5 phase of the present investigation. The roles of Mach number and even cone angle cannot be easily seen, probably because of experimental scatter and the influence of additional factors. Some of the referenced material shows evidence that nose bluntness and Reynolds number also are factors to consider in correlating such data. Note that s_t does not vary as would be expected on the basis of changes in local unit Reynolds number when α varies. Apparently cross-flow effects dominate. Notice also that DiCristina (10) is the only one of these investigators who has given data for various circumferential angles, i. e., outside the plane of symmetry. His data for $0 \leq \phi \leq 90$ deg are represented by the shaded areas in Fig. 3. This is very important in the present case because, in the range data, it is rare for the total angle of attack, α_t , to equal the angle in the plane of the photograph, α_p .

Ward's results (11) are of interest because the experimental conditions, M_δ , θ_c , r_n/r_b , and $(U/\nu)_\delta$, were close to the present Mach 5 case. We have made a modification to Ward's result which consists of refairing his curves between ± 1 deg, as shown in Fig. 4a. The result is not in conflict with Ward's data, and it seems to agree better with the present range data.

The original curve from reference 11 is presented here as Fig. 4a, where the modification made by the present author is shown. For greater clarity and convenience, the portion of the modified curve for very small angles is redrawn with an expanded scale in Fig. 4b. The precision of the data does not justify the scale in Fig. 4b, but it does aid in making self-consistent data corrections.

Turning again to Fig. 3, it becomes clear that data for the lee side involve a highly uncertain correction for angle of attack. At $\alpha / \theta_c = 0.07$ on the lee side, corresponding to 0.7 deg for the 10-deg cones, the spread between the various curves is around ± 10 percent. And it rapidly worsens as angle increases. A more favorable picture is presented by the windward case if we are content to ignore the three most extreme curves. Then, we see that the spread of the data from references 7, 10, and 11 is less than ± 8 percent for $\alpha / \theta_c \leq 0.65$, or $\alpha \leq 6.5$ deg in our experiments. In fact, the curve from reference 6 may be included, and the spread is no worse than ± 10 percent at $\alpha / \theta_c = 0.4$, or 4 deg for a 10-deg cone. Bearing in mind that we particularly need the information from reference 10, it is fortunate that those data for all ϕ 's between 0 and 90 deg away from the windward line of symmetry are contained within the boundaries just noted. Considering the combined uncertainties of locating transition "points" in the photographs, the evident disagreements in Fig. 3, and the inaccuracy in measuring α_t and α_p , it appears that a reasonable course of action for us is to accept roughly ± 10 percent uncertainty in the correction and to:

- (a) use windward s_t measurements for $\alpha_t \leq 2$ deg;
- (b) discard leeward s_t measurements for $\alpha_t \geq 0.7$ deg;
- (c) correct the retained s_t values using the curve of Ward (11), as modified;
- (d) use α_p as the α in Fig. 3 without regard for the fact that, in general, $\alpha_p \neq \alpha_t$;

- (c) use only cases where $\alpha_p < 1.5$ deg and ignore the corresponding small variations of local Mach and Reynolds numbers from the nominal M_δ and $(U/\nu)_\delta$ corresponding to α_p

(Note that α 's are absolute angles in the foregoing listing and hereafter.)

We choose to use Ward's (modified) curve rather than DiCristina's more complete results because it is seen in Fig. 3 that Ward's curve lies in among DiCristina's windward data, being close enough to any of DiCristina's curves to allow us to ignore the difference between α_p and α_t . That is, we do not attempt to determine a correction for the specific circumferential angle represented by a photograph where $\alpha_p \neq \alpha_t$ because any error incurred seems likely to be within the scatter and uncertainty arising from other factors. On the lee side, Ward's modified curve lies near the middle of all the curves in Fig. 3 for $\alpha/\theta_c < 0.07$. Furthermore, the aeroballistic range data for Mach 5 suggest that, if Ward's windward curve is used, then the best agreement between transition lengths is obtained when Ward's leeward curve also is used. Finally, we note that the Reynolds number of Ward's experiment is within the variation of that parameter in the present free-flight experiments, cone angles and bluntness ratios (r_n/r_b) are nearly equal and Mach numbers are close for the present Mach 5 case.

SURFACE ROUGHNESS

Because of the typically higher local unit Reynolds number, cold walls ($T_w = T_{aw}$) and consequently thin boundary layers, it has been suggested that transition data from aeroballistic ranges may be affected by surface roughness. This feeling is reinforced in some persons who also feel that transition Reynolds numbers reported from range experiments "should" be larger if the ambient conditions are less disturbed than those in wind tunnels. Although a method exists for predicting the influence of roughness on transition (ref. 12), it was thought best to conduct some experiments under actual

aeroballistic range conditions. Preliminary results may be reported at this time.

Cones otherwise identical to the 1.75-in. models used in the present investigation and that of reference 5 were deliberately roughened, as sketched in Fig. 5. Considering that circumferential machine tool marks, or grooves, seemed to be the most general form of roughness encountered on conical bodies, the desired roughness was created simply by changing cutting tool speed. That produced varying degrees of screw-thread type of roughness which was measured in the usual manner with a profilometer. The shortcomings of such devices for surface roughness measurements are well known. Mainly, the objections are the possible scratching of the surface by the stylus and the inordinately large radius of the profilometer stylus ($\sim 500 \mu\text{in.}$) compared to the smaller dimensions of the roughness. A well-finished cone surface registered less than $10 \mu\text{in.}$, rms, but one must assume that the profilometer stylus could not penetrate to the bottom of surface defects with transverse widths less than stylus diameter, cf. reference 13. Whether such types of roughness are of any importance is another subject to consider. It is probable that defects of this scale did not matter in the experiments discussed herein.

If it had developed that roughness heights of the order of $100 \mu\text{in.}$, rms, or less were critical, efforts to find a more precise measurement method were planned. As it has turned out, the data from our study of machining-type roughness on cones at Mach 5 in the aeroballistic range show no significant influence of such roughness when the profilometer reading was less than approximately $250 \mu\text{in.}$ These results are shown in Fig. 6.

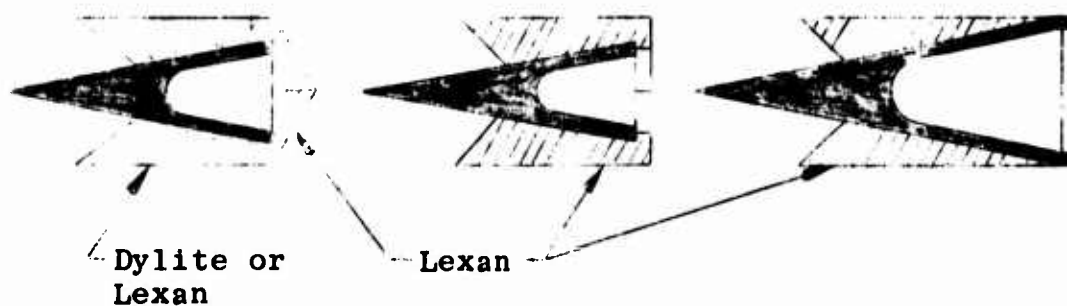
For comparison, Fig. 6 also includes a curve giving the estimated influence of the roughness according to the method of Potter and Whitfield (12). The calculations were made on the basis that effective roughness height, k , was the rms value given by the profilometer and $s_k = 1.5 \text{ in.}$ Tool marks were treated as two-dimensional roughness in the calculation.

It is interesting to observe the sensitivity exhibited in the 300- to 500- μ in. region of Fig. 6. This is entirely consistent with the predictive method (ref. 12) which is based on a critical Reynolds number of roughness, ϵ , which changes from 300 to 4500 as the Mach number, M_k , in the boundary layer at the height, k , changes from 0.5 to 2. It is clear that the inaccuracy of calculations of boundary layer profile quantities, combined with inaccuracy of determinations of roughness height and transition location makes close comparisons in Fig. 6 unwarranted. A large amount of experimental scatter is not surprising either.

It must be remembered that it is surface condition in flight at the observation station which really matters. Thus, we have used laser-front-lighted photography of the cones in flight as a means for identifying any cones with visible defects such as roughened, bent, or ablated surfaces. The technique, as applied to high-speed free-flight ablation research, has been described by Dugger, Enis and Hill (14).

We have used two basic types of sabots in this work. In the prior work (ref. 5) and part of the current investigation, closed-base sabots were used. For all of the 2.3- and 2.5-in. aluminum cones used in the study under way, open-based sabots were used. The following sketch shows the principal features of these designs, all of which were used with a gun of 2.5-in. caliber.

Base:	Closed	Open	Open
Cone			
Diameter:	1.75 in.	1.75 in.	2.50 in.



One sees that under load from the pressure of the gun gas the sabot pushes on the cone if the sabot is closed-base. Masses and base areas of the open-based sabot for sub-caliber cones are adjusted so that the cone pushes on the sabot. For full-caliber cones and open-based sabots, it is obvious that the cone pushes on the sabot during launch. The point of this discussion is that launch loads are great and the cone wetted surface may be roughened if there is sufficient interaction as the cone presses into the open-based sabot. We have developed open-based sabots because there is evidence that they lead to less disturbed launches and lower angles of attack after the sabot separates from the cone.

Aside from a few isolated cases of damage in launch, the potentially most important finding has been that interaction between cone and sabot during launch from a gun may produce a discolored area on the cone surface, as seen in laser-front-lighted photographs. An example is Fig. 7.

Cones in these experiments were made from either 7075-T6 aluminum alloy or Lexan. The latter was used for the cones in the phase of the study discussed in the following section. The open-based sabots for the aluminum cones and the closed-base sabots for the Lexan cones were of Lexan, while the major portion of the closed-base sabots interacting with the surfaces of the other aluminum cones was Dylite [®]. The latter is a soft plastic much used for inexpensive ice chests and packaging. During the experiments of reference 5, closed-base sabots made of Lexan were used.

Laser-front-lighted photography of static aluminum cones subjected to simulated launch loadings in open-based sabots revealed that the discolored area of Fig. 7 could be approximated with roughnesses measuring only 15 μ in., rms. It was also found that the inner surfaces of the Lexan sabots contacting the cones were characterized by profilometer readings of the order of 100 μ in., rms. Therefore, it was decided to require inner Lexan sabot surfaces to be finished to the order of 32 μ in., rms, which is

deemed about the best to be expected on a routine basis from ordinary lathe work on Lexan. Then, it seemed a safe assumption that any scuffing or embossing due to the cone pressing against the sabot would be less than $32\text{ }\mu\text{in.}$, rms, particularly since the aluminum is much the stronger of the two materials. After instituting this step, the laser light produces photographs showing smooth-appearing cones in flight.

The Dylite foam is so soft, in comparison to aluminum that any interaction under launch loading should not appreciably roughen the aluminum cones. In addition, the closed-base sabot causes the base of the cone to carry the load, rather than the cone wetted surface, and this lessens the likelihood of surface embossing.

In view of Fig. 6 and these other results, it is concluded that surface roughness has not significantly affected the data presented in reference 5, where closed-base sabots were used. And further, under the controls imposed since the laser-lighted photography system became available, we believe roughness can be regarded as a negligible factor in relation to the data for any of the so-called smooth cones under conditions where the method of reference 12 predicts no influence.

THE INFLUENCE OF MODEL VARIATION

The possible influence of model vibration was examined by comparing transition results obtained from launching cones of two materials under otherwise similar conditions. The materials were chosen on the basis of their being compatible with the rigors of range operations while having appreciably different vibrational characteristics. If we chanced to make a significant change in transition location by this variation in cone vibrational behavior, it at least would indicate the need for more careful study. Seeing no change does not prove that cone vibration is not a factor, but the experiment seemed worthwhile.

All the previous work, as well as the current extension, involved aluminum cones. The only readily usable material offering significantly different vibrational characteristics appeared to be Lexan. Table II shows relevant data on the two materials.

TABLE II. FREQUENCY AND AMPLITUDE DATA

<u>Material</u>	<u>W</u>	<u>Y</u>
Aluminum 7075-T6	1	1
Lexan	0.28	3.3

$$W = (E/\rho)_{\text{Lexan}}^{1/2} / (E/\rho)_{\text{aluminum}}^{1/2}$$

= frequency ratio

$$Y = (\sigma_y/E)_{\text{Lexan}} / (\sigma_y/E)_{\text{aluminum}}$$

= amplitude ratio

E = Young's modulus of elasticity

ρ = material density

σ_y = yield strength in tension

Laboratory experiments have essentially confirmed the computed frequency ratio in Table II. These experiments took two forms. First, the 1.75-in. -diam aluminum and Lexan cones were simulated by models in the manner shown in Fig. 8.

The assumption was made that the cone tip in free flight would tend to vibrate as if the cone were fixed at its center of gravity, as in Fig. 8. The length of 3.013 in. that the cone extends from the support collar also was the distance from the tip to the center of gravity of the 1.75-in. free-flight cone. Strain gages were attached to the base of the cone and wired to measure bending stress. The collar was suspended from wires and struck with a hammer to induce vibration in the cone.

Bending strain at the base of the cone simulating the range models was measured with two strain gages which formed adjacent arms of a four-equal-arm bridge circuit as shown in Fig. 9. The bridge was powered from a 6-volt battery. Strain, represented by the bridge output, was amplified using a differential-type d-c amplifier and was recorded using a preamp and an oscilloscope. A 3-volt common mode voltage was provided by a resistance voltage divider so that zero voltage would appear at the amplifier inputs with the bridge balanced. The oscilloscope was triggered internally from gage output. The strain recording system was calibrated by unbalancing the bridge circuit with fixed resistors paralleled with one arm of the resistance bridge.

Oscilloscope traces as shown in Fig. 10 were obtained when the cones were struck with a large ball bearing. The lower frequency and greater amplitude of the Lexan cone is obvious. It should be noted that the so-called Lexan cone is not truly representative of a cone made only from Lexan; for aerodynamic stability it was necessary to insert internal metal ballast in the fore part of the cone. This affected the vibrational characteristics, and it is the ballasted cone which is represented in Fig. 10. Apparently, the ballast acted as a damper because it reduced the measured frequency.

The oscilloscope traces were read on a film reader to determine frequency and the logarithmic decrement,

$$\Delta = (1/N) \ell_n (y_0/y_n) \quad (1)$$

In Eq. (1) N is the number of cycles, y_0 is the original amplitude, and y_n is the amplitude after the N cycles. We obtained $\Delta = 0.047$ for the aluminum cone. The ballasted Lexan cone did not give a constant Δ . The value was lower at late times but was approximately constant at 0.3 for about 8 msec after being struck.

The calculated natural frequency of the fixed-base aluminum cone is 7960 Hz, but the measured frequency was only 6880 Hz. Part of the

discrepancy may be attributed to the fact that the collar does not fully represent a fixed base for the cone. The ballasted Lexan cone experimentally yielded 1250 Hz and a wholly Lexan cone gave 2060 Hz. Therefore, rather than the computed ratio of Lexan-to-aluminum frequencies, $W = 0.28$, which appears in Table II, or the experimentally determined $W = 0.30$, both of which apply to wholly Lexan cones, we have $W = 0.18$ for the ballasted Lexan cones actually used for comparison with the aluminum cones. While we cannot say if this variation in cone vibrational frequency is significant in regard to boundary layer transition under the circumstances studied, it is at least large enough to be interesting.

The time required for a given amplitude change is given by

$$\tau = [1/(\Delta f)] \ell_n (y_0/y_n) \quad (2)$$

where f is the frequency in Hz. Because it would seem very likely that any cone vibration is induced early within the launcher, the time elapsing between, say, the start of motion within the launcher and arrival at the viewing station is relevant insofar as the cone vibration amplitude is concerned. In the case of the Mach 5 experiments, this (average) time was 14.4 msec and for the Mach 2 launches it was 27.9 msec. Therefore, if the initial maximum amplitude, y_0 , of the cone tip were known, Eq. (2) and these input data would permit a calculation of the amplitude, y_n , at the focused shadowgraph station. We cannot make this calculation because y_0 is not known, but an upper limit may be placed on it. For the aluminum cone, it is calculated that a deflection of the tip of 0.065 in. would have caused the metal to yield. No such bending was ever observed in flight so it is safe to assume that y_0 did not attain that magnitude. Let us assume then, as an example, $y_0 \leq 0.06$ in. Substituting into Eq. (2) the quantities

$$\tau = 14.4 \text{ msec,}$$

$$\Delta = 0.047,$$

$$f = 6880 \text{ Hz, and}$$

$$y_0 \leq 0.06 \text{ in.}$$

we obtain $y_n \approx 0.00056$ in. for the aluminum cone. Concerning the ballasted Lexan cone, we use

$$\tau = 14.4 \text{ msec,}$$

$$\Delta = 0.3,$$

$$f = 1250 \text{ Hz, and}$$

$$y_0 \approx 3.3 (0.06) = 0.20 \text{ in.}$$

to obtain $y_n \approx 0.00091$ in. Although the Lexan cone may start with more than three times the tip deflection of the aluminum cone, it would be expected to have roughly 1.6 times as much tip deflection at the viewing station.

Because of interest in possible higher vibrational modes, a second type of experiment was conducted with one of the 1.75-in. aluminum cones of the type actually launched. It was suspended by a string at its center of gravity and struck with a hammer. A microphone and recording system of the type used to monitor noise in the range recorded the result. Frequencies of 7680 and 7180 Hz could be identified. Higher modes could not be found by this means, but it was concluded that any higher modes were associated with very much lower amplitudes.

By comparing transition on aluminum and ballasted Lexan cones, we are seeing the effect of a reduction of vibrational frequency from 6880 to 1250 Hz, coupled with a corresponding increase in maximum possible tip vibrational amplitude by a factor of 1.6. It is believed that there was a small amount of nose tip ablation on the Lexan cones. This is discussed in the following section. At this time sufficient Mach 5 launches have been carried out so that we may report tentatively that no significant difference in transition Reynolds numbers has been found. Six ballasted Lexan cones have been launched; four had $Re_{\delta, t}$ above the level for aluminum and two had $Re_{\delta, t}$ below that level. The average result is

$$\frac{Re_{\delta, t} (\text{Lexan})}{Re_{\delta, t} (\text{aluminum})} = 1.05$$

which cannot be regarded as significant because it is within the experimental scatter.

It may be noted that a recent wind tunnel experiment by Olson et al. (15) revealed no influence of model vibration on transition Reynolds number. In that situation, frequencies of 2900 to 82,000 Hz and peak-to-peak amplitudes of 40 to 1500 μ in. were explored. The authors believed that artificial roughness heights equal to the vibration amplitudes would have tripped their boundary layer, and they concluded that vibration in their case was less effective as a trip than fixed surface roughness. Perhaps this should not be surprising. Unless a sensitive mode of vibration were chanced upon, the surface deflections owing to vibration would take the form of gentle waviness rather than abrupt discontinuities in the nature of boundary layer trips.

NON-UNIFORM WALL TEMPERATURE

A source of potential influence on transition under range conditions is the non-uniform surface temperature arising from aerodynamic heating. A hot nose will be combined with a relatively unheated afterbody, and the boundary layer profile will reflect this. Rhudy (16) has made an illustrative calculation of the influence of a hot leading edge section with $T_w/T_o = 0.8$ followed by a cooled plate with $T_w/T_o = 0.2$. He shows that, for $M_\delta = 6$ and $(U/\nu)_\delta = 1.1 \times 10^6 \text{ in.}^{-1}$, it takes a distance of approximately $600 \delta_j$ for the product ρu in the boundary layer at the critical height $y/\delta = 0.9$ to attain the profile that is calculated for a plate with $T_w/T_o = 0.2$ over its entire length. The symbol δ_j represents boundary layer thickness at the discontinuous change of wall temperature. Apparently there have been no experiments to investigate the seriousness of the effect of non-uniform T_w on transition.

In the range investigations conducted by the author, calculations of stagnation point and afterbody temperatures have been made. It was calculated that Lexan cone tips would melt under the Mach 5 conditions, and yet no evidence of tip blunting was seen. Thus, it is inferred that the calculated

temperature increases were too great, but that a small amount of localized ablation occurred. Inspection of the laser-lighted photographs of Lexan cones in flight revealed small decreases in length and faintly cusped tip shapes. However, the laser station was 32 percent further downrange than the focused shadowgraph and ablation would have been much less at the shadowgraph where transition was determined. If we take a published melting temperature of roughly 550°K for Lexan, it follows that the nose tips of the Lexan cones were about twice the temperature of the skirts which heat negligibly in the brief flight. Our calculation method yields a maximum tip-to-skirt temperature ratio of roughly 2:1 for the Mach 5 aluminum cones as well. At Mach 2 these ratios are much nearer unity.

The calculated boundary layer thickness at, say, 100 nose radii or 0.5 in. from the stagnation point may be taken as a very conservative (i. e., large) value for Rhudy's δ_j in the present case. Then, in keeping with his results, we may infer that the cone boundary layers at the transition locations should be essentially free of "hot-tip" influence when distance to transition, s_t , is greater than $600 \delta_j$. On this basis, all of our data correspond to $s_t/\delta_j > 2000$ for the conditions encountered. Coupled with the lesser tip-to-afterbody temperature ratio and the conservative nature of our comparison with the results in reference 16, the hot-tip effect is not an obvious factor in the present work. Until other data are available, no more may be said.

The rather low wall-to-adiabatic recovery temperature ratios, T_w/T_{aw} , are important factors in high-speed range transition data. In the work of reference 5, and in the current work:

$$T_w/T_{aw} = 0.18 \text{ at Mach 5}$$

$$T_w/T_{aw} = 0.50 \text{ at Mach 2.}$$

These average values are based on $T_w = 300^\circ\text{K}$ and laminar-flow recovery factors.

CONCLUDING REMARKS

A major incentive for the analysis of these four possible factors in regard to transition data from aeroballistic ranges has been the desire to learn if the range pressure or unit Reynolds number influence shown in reference 5 could have been caused by conditions peculiar to the range operations. In that research it was found that

$$Re_{\delta,t} \sim (U/\nu)_{\delta}^n$$

with $n \approx 0.6$. At this time, at least, there seems to be no conclusive indications that any of these conditions were significant. That is, we have found no reason to suspect that either the U/ν dependence or the absolute levels of $Re_{\delta,t}$ were importantly affected by the four factors discussed. It is possible that a general, roughly 10 percent increase in $Re_{\delta,t}$ values of the earlier work will result from applying the correction for angle of attack described herein.

The current research program is not completed and these results are tentative. However, there is no reason to expect that they will be altered in the near future. Recent experiments have added data points confirming the major conclusions of reference 5 for Mach 5 and indicating similar results at Mach 2.

In closing, the help of colleagues in the Aerospace Instrumentation and the Aeroballistics Branches should be recognized. In particular, E. J. Sanders, J. R. DeWitt, and R. P. Young have made specific contributions to the experimental program.

REFERENCES

1. M. V. Morkovin, Critical Evaluation of Transition from Laminar to Turbulent Shear Layers with Emphasis on Hypersonically Traveling Bodies, AFFDL-TR-68-149 (1968).
2. M. V. Morkovin, In Viscous Drag Reduction, Plenum Press, pp 1-31 (1969).

3. L. M. Mack, Boundary Layer Stability Theory, Jet Propulsion Laboratory JPL 900-277 Rev. A (November 1969).
4. L. M. Mack and M. V. Morkovin, AIAA short course notes on boundary-layer stability and transition, 1969 (unpublished).
5. J. L. Potter, Observations on the Influence of Ambient Pressure on Boundary-Layer Transition, AIAA Journal, Vol. 6, No. 10, pp 1907-1911 (October 1968).
6. M. C. Fischer and D. H. Rudy, Effect of Angle of Attack on Boundary-Layer Transition at Mach 21, AIAA Journal, Vol. 9, No. 6, pp 1203-1205 (June 1971).
7. K. F. Stetson and G. H. Rushton, Shock Tunnel Investigation of Boundary-Layer Transition at $M = 5.5$, AIAA Journal, Vol. 5, No. 5, pp 899-906 (May 1967).
8. M. C. Fischer, An Experimental Investigation of Boundary Layer Transition on a 10° Half-Angle Cone at Mach 6.9, NASA TN D-5766 (1970).
9. P. C. Stainback, Effect of Unit Reynolds Number, Nose Bluntness, Angle of Attack and Roughness on Transition on a 5° Half-Angle Cone at Mach 8, NASA TN D-4961 (1969).
10. V. DiCristina, Three-Dimensional Laminar Boundary-Layer Transition on a Sharp 8° Cone at Mach 10, AIAA Journal, Vol. 8, No. 5, pp 852-856 (May 1970).
11. L. K. Ward, Influence of Boundary Layer Transition on Dynamic Stability at Hypersonic Speeds, Transactions of the Second Technical Workshop on Dynamic Stability Testing, Arnold Engineering Development Center, Vol. II (April 1965).
12. J. L. Potter and J. D. Whitfield, Effects of Slight Nose Bluntness and Roughness on Boundary-Layer Transition in Supersonic Flows, Journal of Fluid Mechanics, Vol. 12, Part 4, pp 501-535 (1962).
13. M. E. Wilkins and J. F. Darsow, Finishing and Inspection of Model Surfaces and Boundary-Layer-Transition Tests, NASA Memo 1-19-59A (February 1959).
14. P. H. Dugger, C. P. Enis and J. W. Hill, Laser High-Speed Photography for Accurate Measurements of the Contours of Models in Hypervelocity Flight within an Aeroballistic Range, Proceedings of the Technical Program, Electro-Optical Systems Design Conference, New York (September 1970).

15. L. E. Olson, G. M. Gregorek and J. D. Lee, The Influence of Artificially Induced Turbulence upon Boundary Layer Transition in Supersonic Flows, Aerospace Research Labs ARL 71-0022 (January 1971).
16. J. P. Rhudy, Effect of Uncooled Leading Edge on Cooled-Wall Hypersonic Flat-Plate Boundary-Layer Transition, AIAA Journal, Vol. 8, No. 3, pp 576-577 (March 1970).

Not to Scale. All Dimensions in Inches

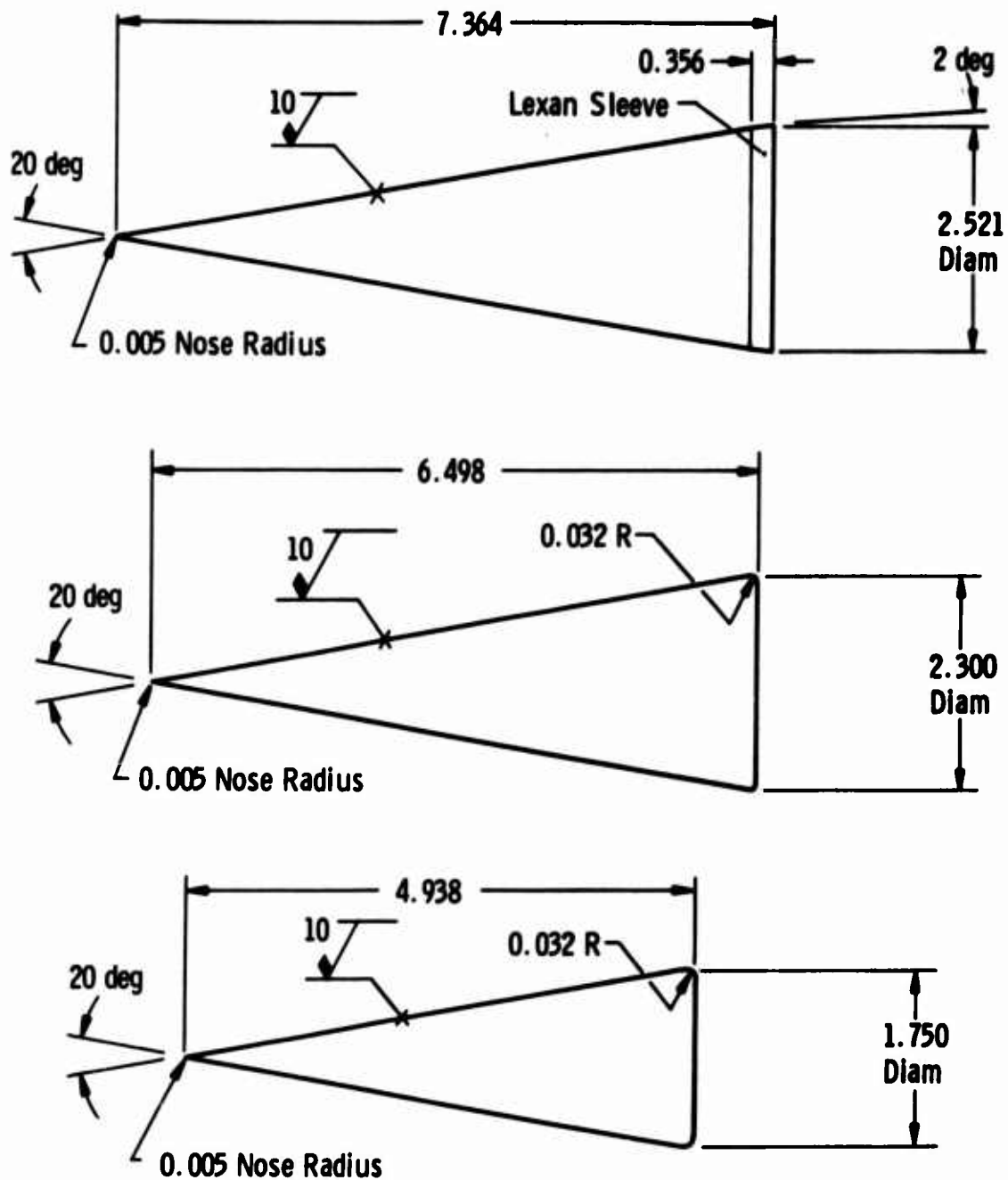


FIG. 1. CONES USED IN EXPERIMENTS (Except as noted on the 2.5-in. cone, all 2.5- or 2.3-in. cone surfaces were aluminum. The 1.75-in. cones were either aluminum or Lexan.)

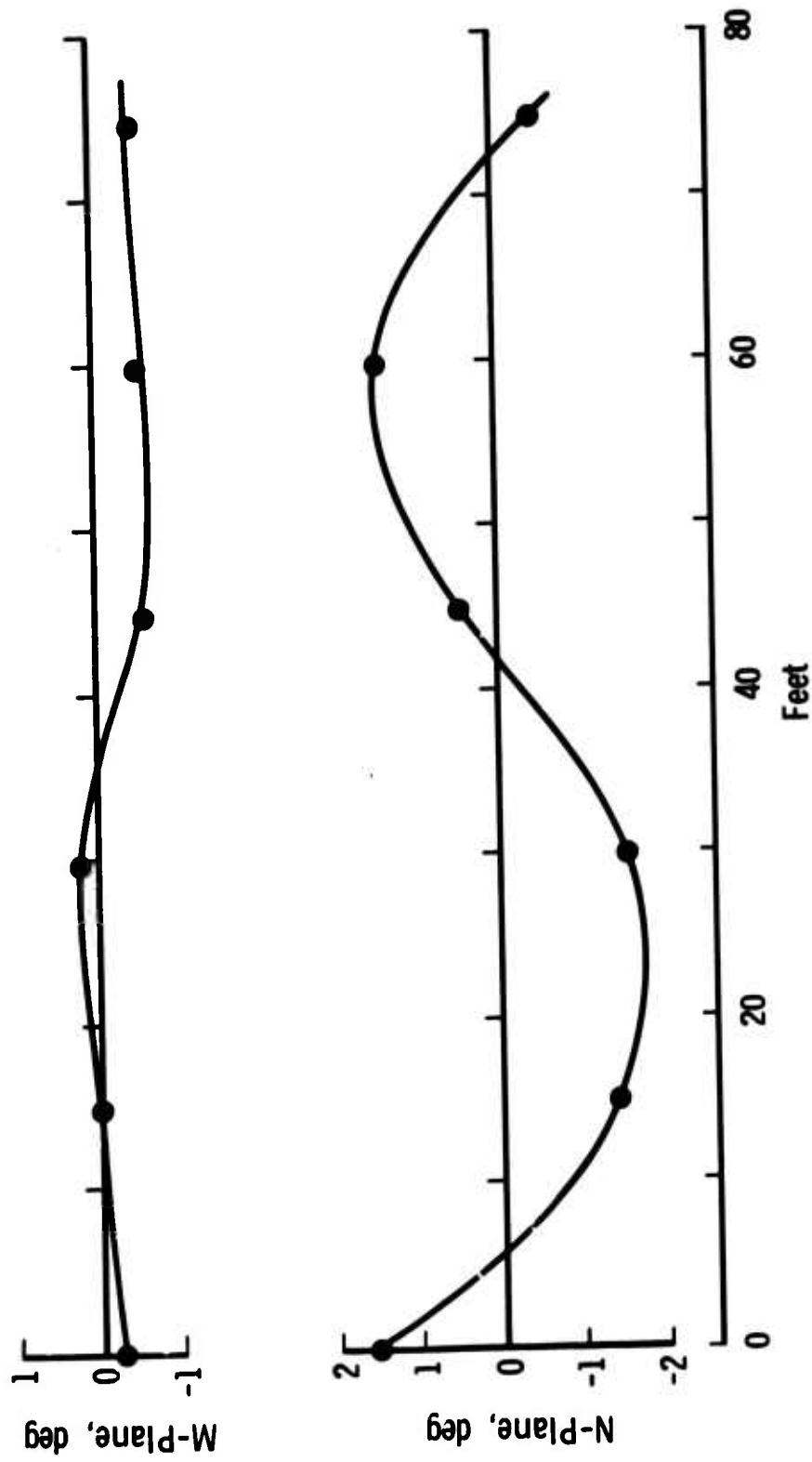


FIG. 2. TYPICAL CONE TRAJECTORY.

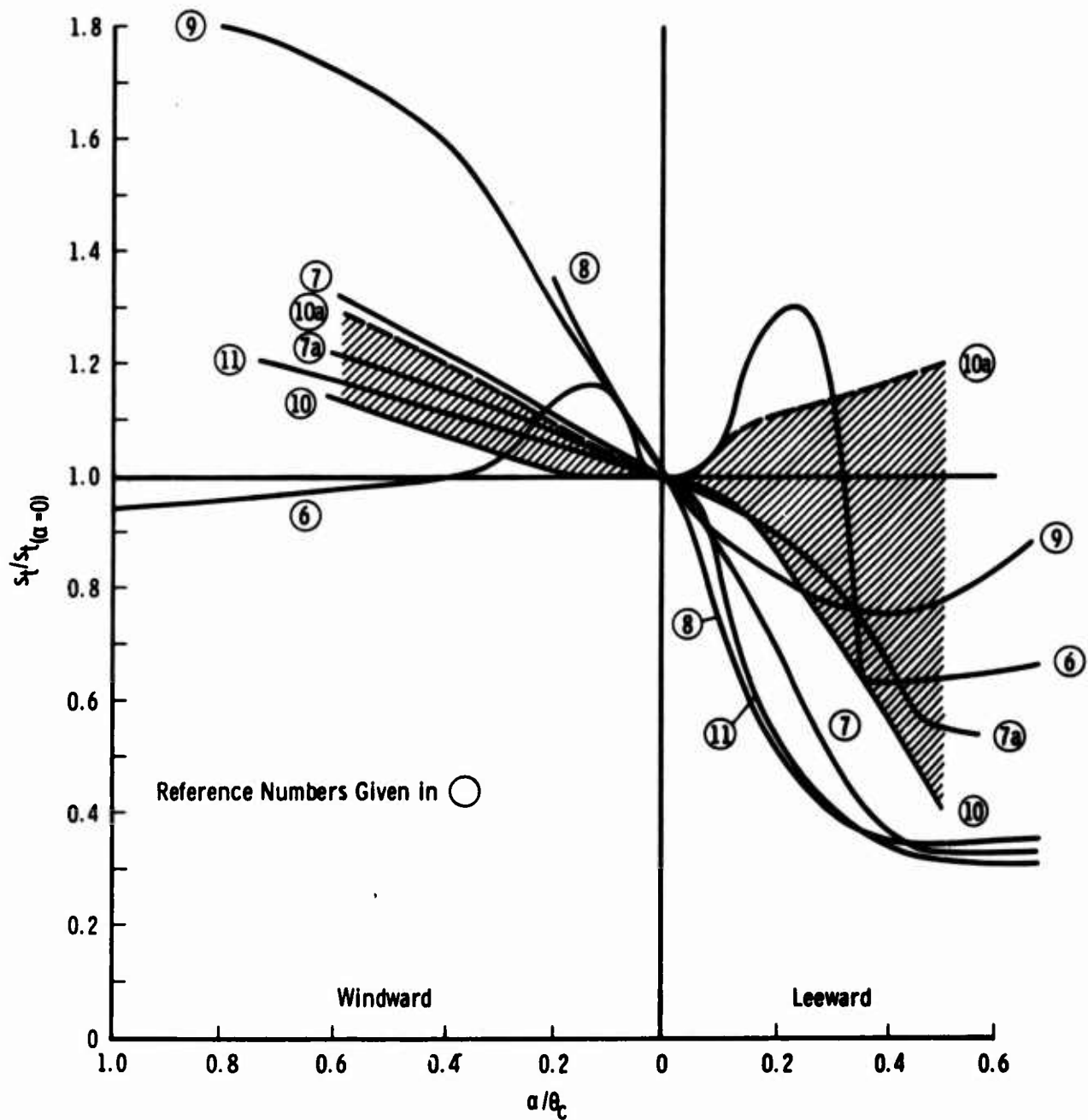


FIG. 3. SOME PUBLISHED DATA ON THE INFLUENCE OF ANGLE OF ATTACK ON TRANSITION LOCATION.

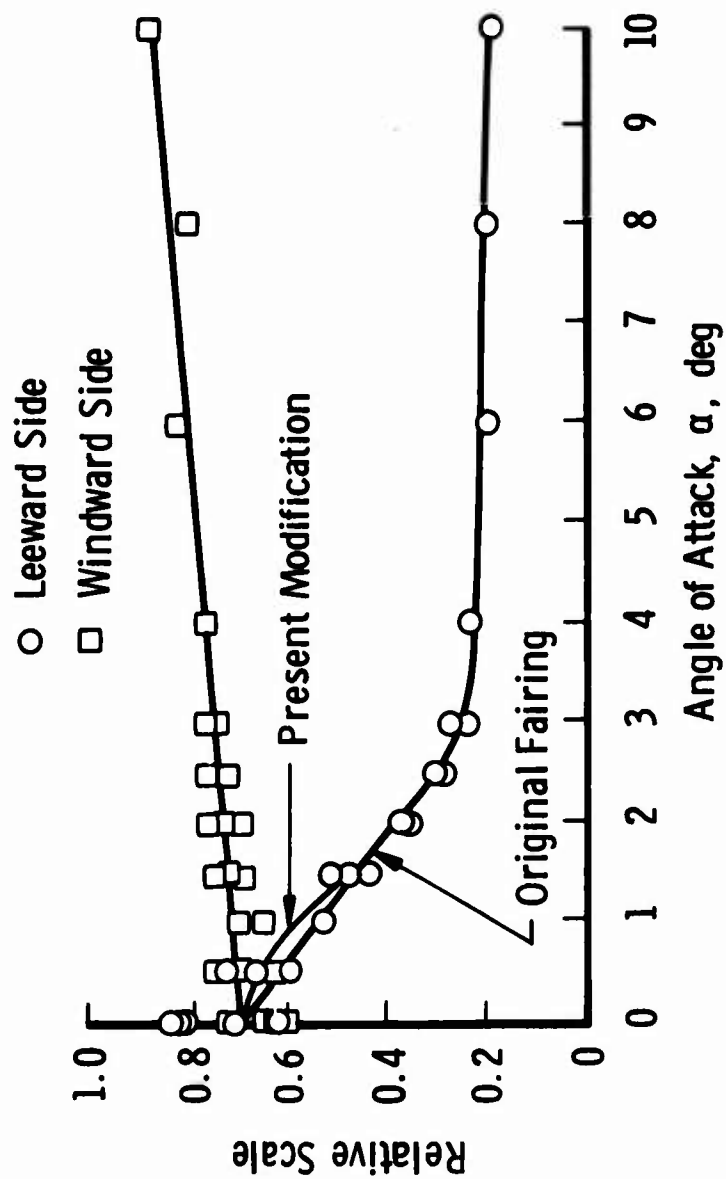


FIG. 4a. EFFECT OF ANGLE OF ATTACK ON TRANSITION LOCATION, FROM WARD (11).

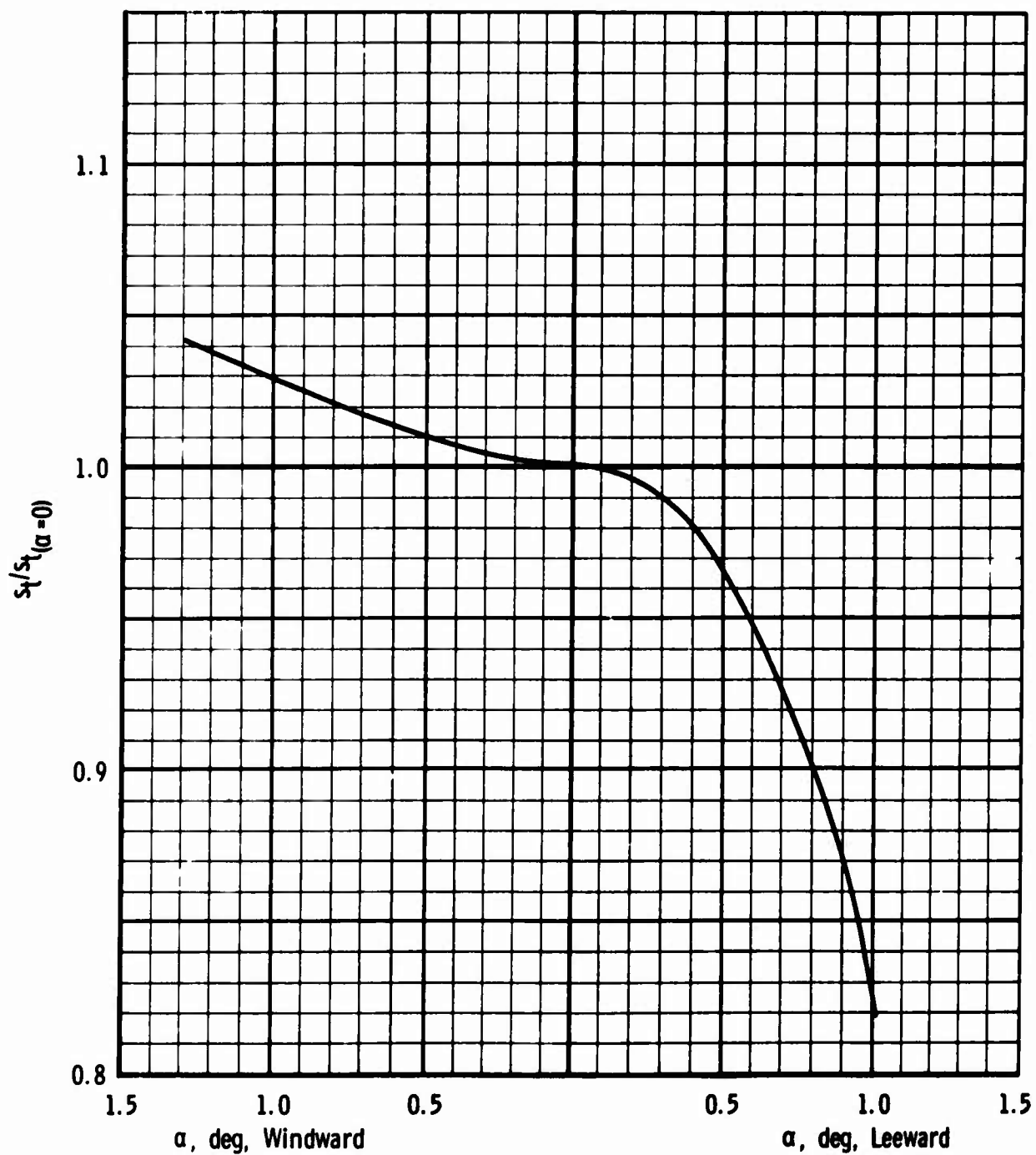
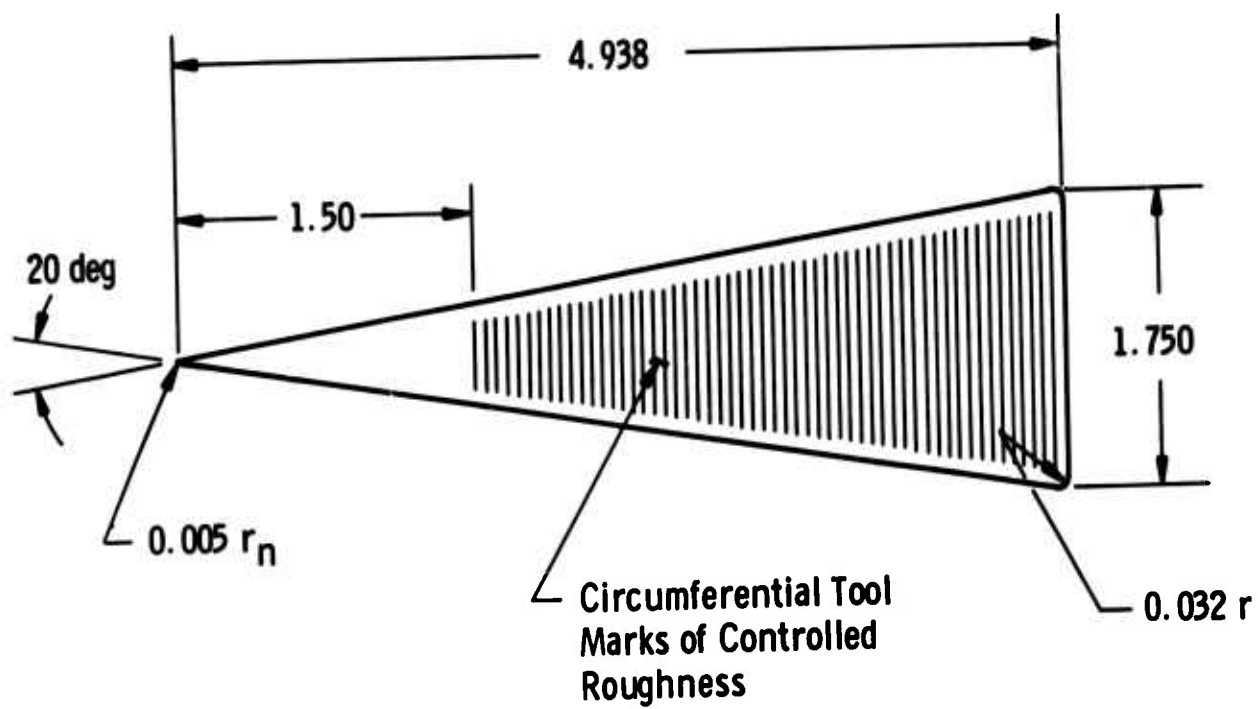


FIG. 4b. WARD'S (MODIFIED) DATA FOR 10-DEG SEMI-ANGLE CONE.



All Dimensions in Inches

FIG. 5. ROUGHENED CONE.

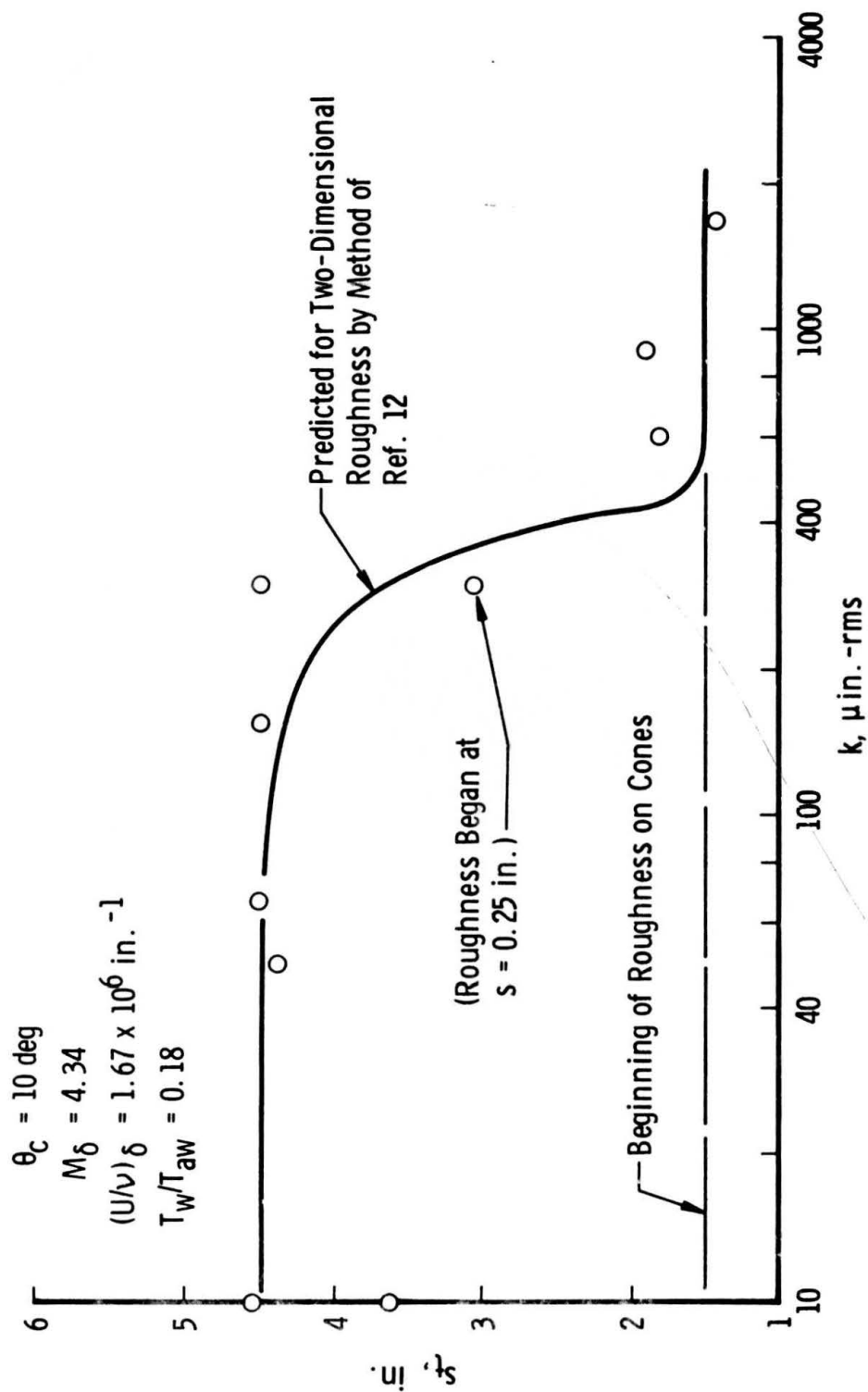


FIG. 6. EFFECT OF SURFACE ROUGHNESS.

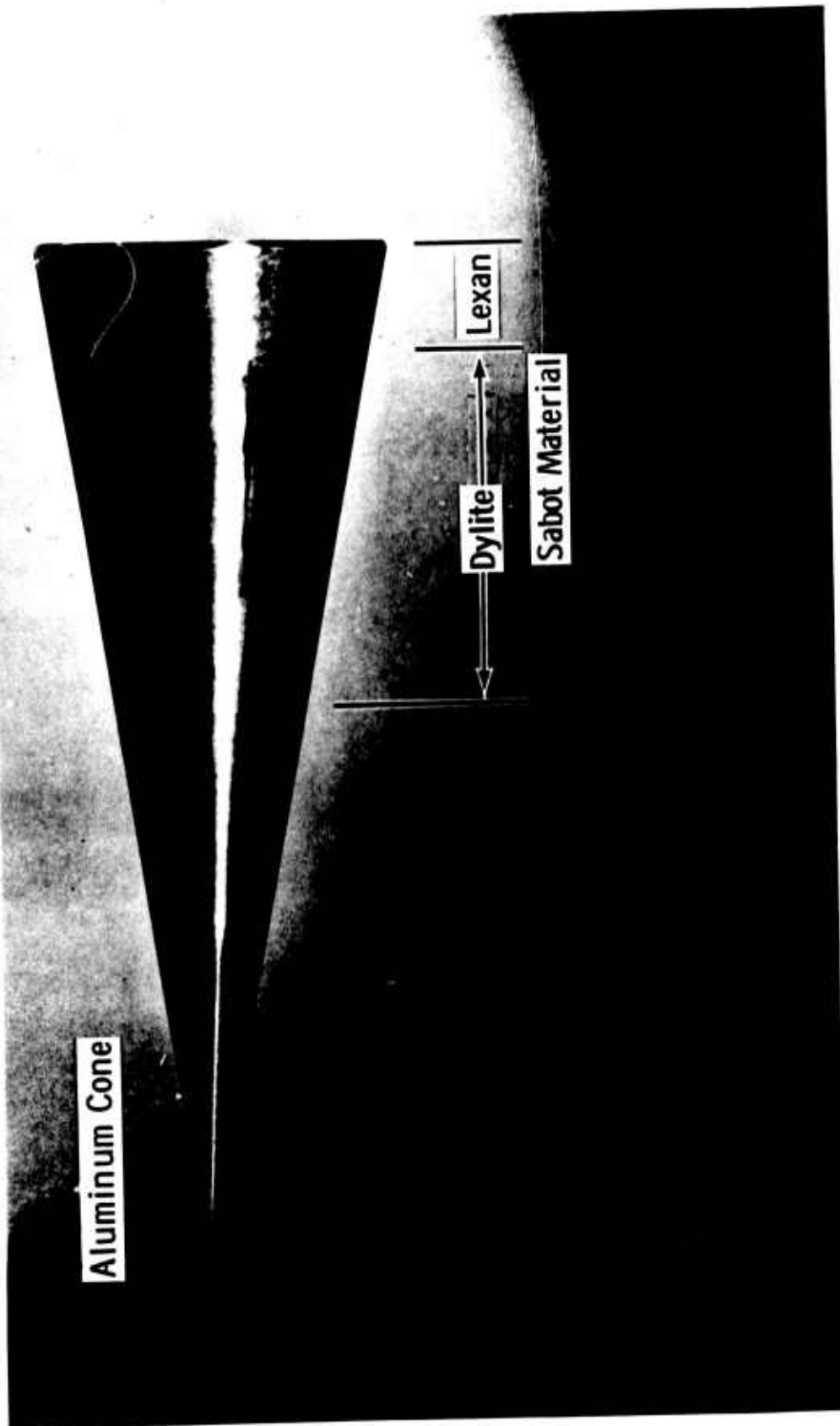


FIG. 7. LASER-FRONT-LIGHTED PHOTOGRAPH OF CONE IN FLIGHT AT MACH 5. Sabot was closed-base type fabricated from Lexan and Dylite.

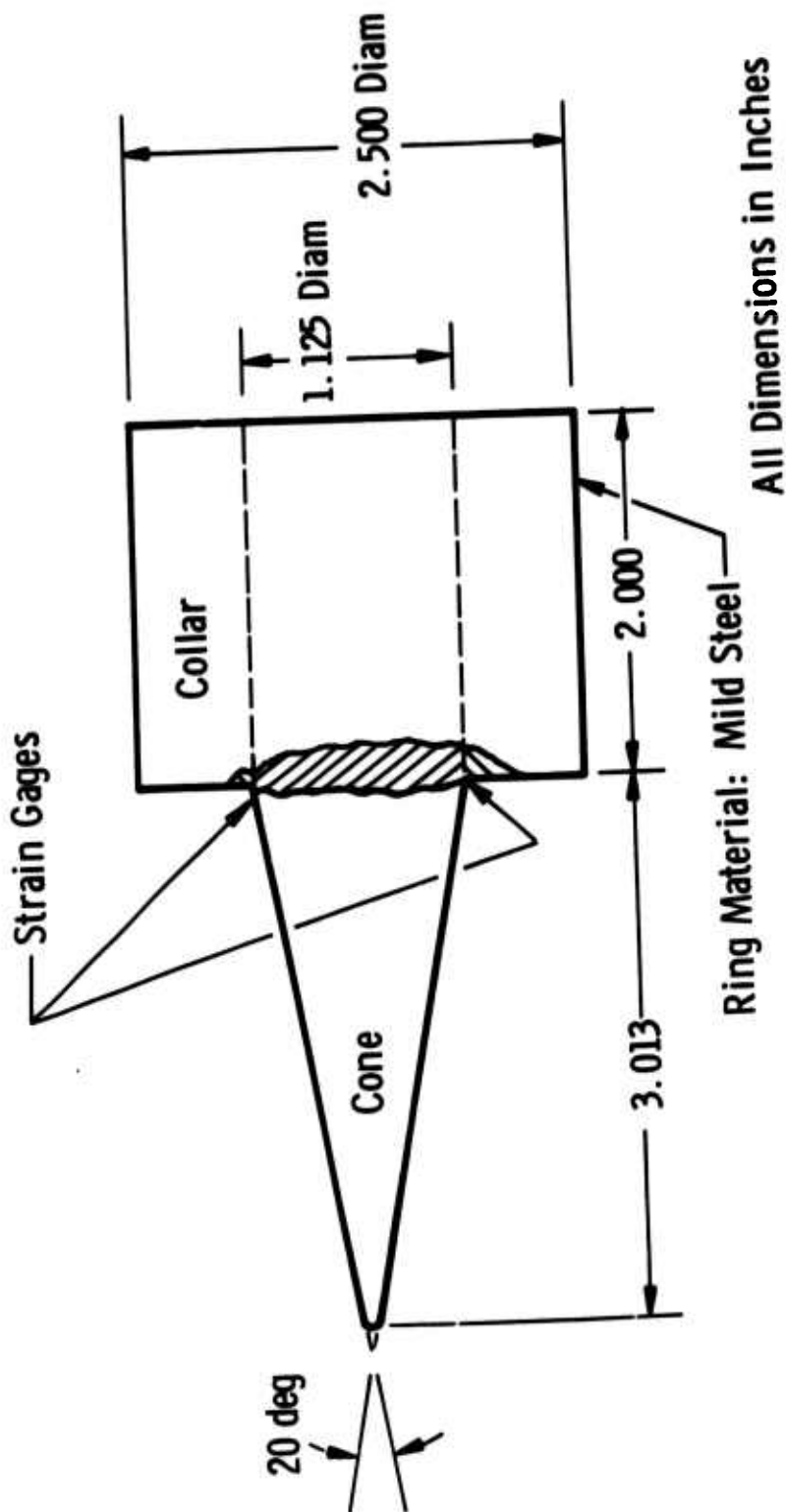
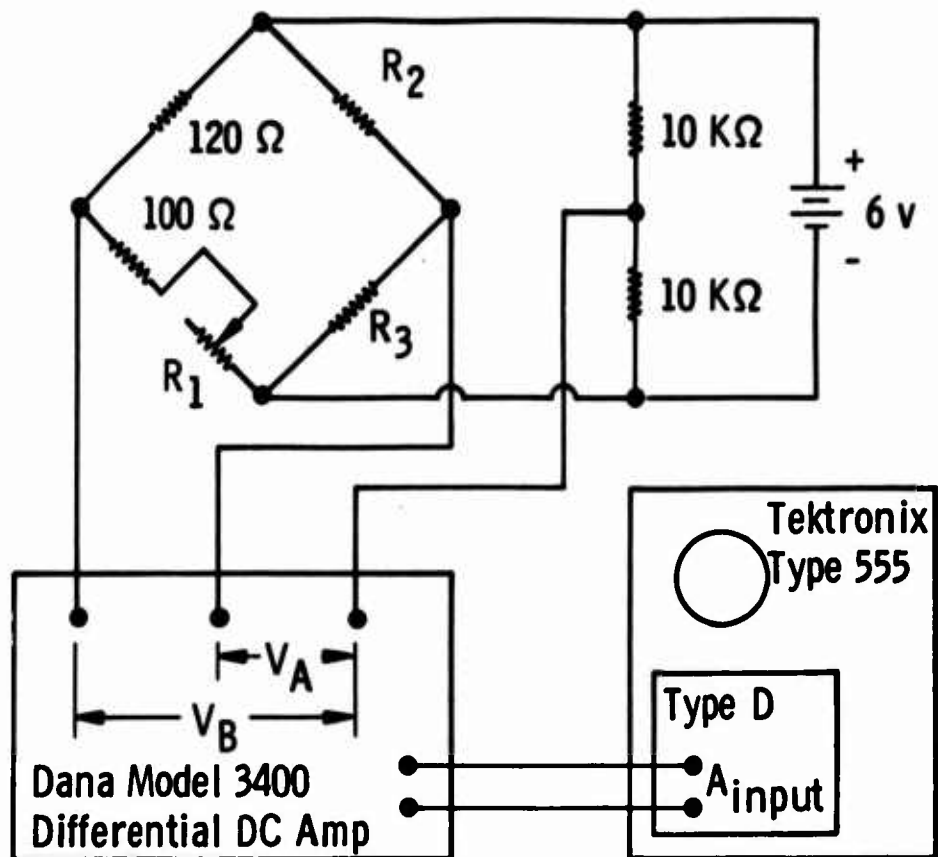


FIG. 8. APPARATUS FOR STUDYING VIBRATIONAL CHARACTERISTICS OF ALUMINUM AND LEXAN CONES.



- Notes: (1) R_1 is a $25\ \Omega$, carbon potentiometer.
 (2) R_2 and R_3 are SR4 Type FAE-03N-1256 strain gages.
 (3) Bridge output is $V_A - V_B$.

FIG. 9. STRAIN MEASUREMENT APPARATUS.

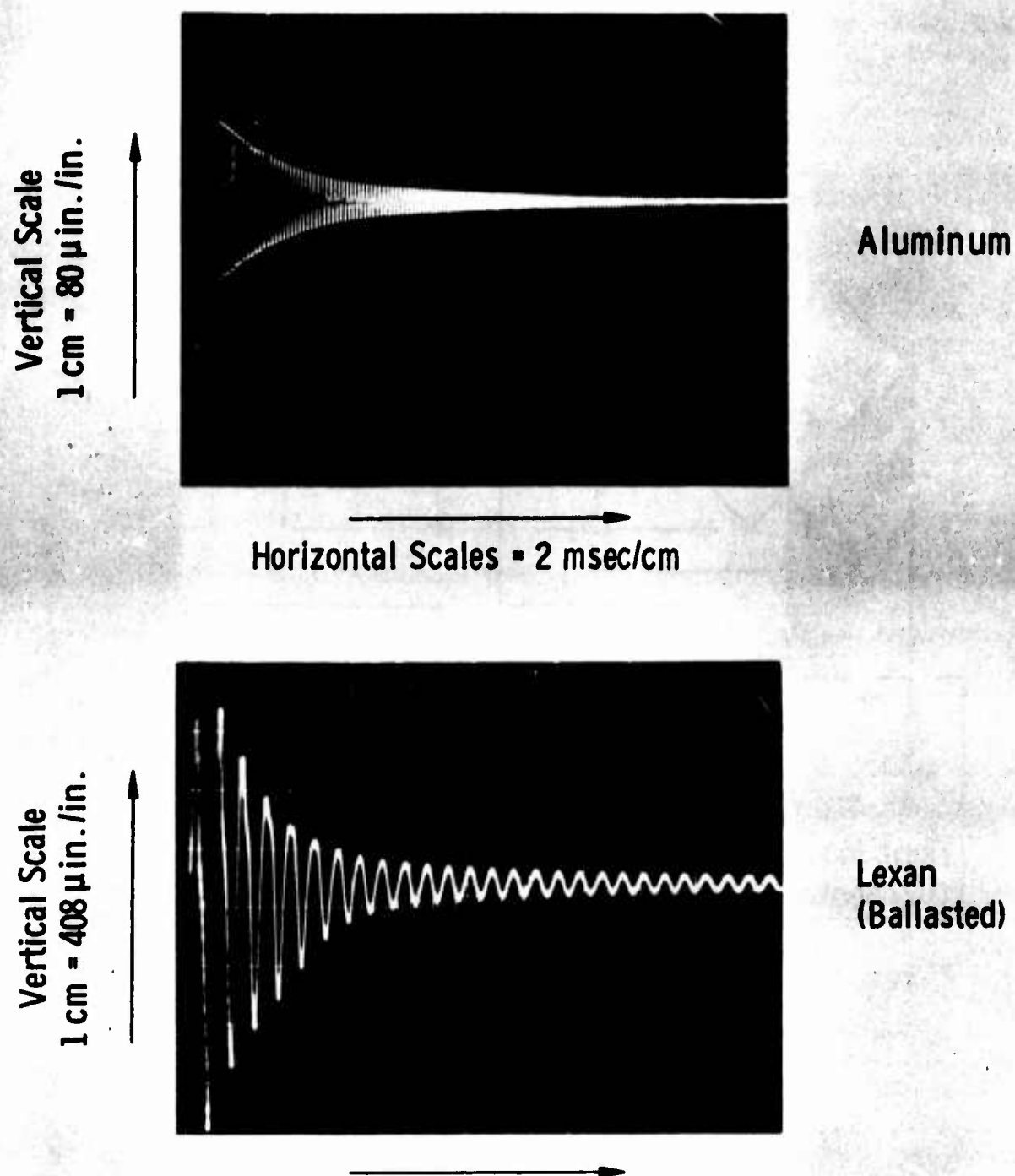


FIG. 10. VIBRATIONAL RESPONSE OF ALUMINUM
AND LEXAN CONES.

SECTION 6

HYPERSONIC SIMULATION FOR LIFTING

BODY TRANSITION STUDIES*

(Unclassified)

By

S. R. Pate**

and

J. C. Adams***

ARO, Inc.

Arnold Air Force Station, Tennessee

For Presentation at the

Boundary Layer Transition Specialists Workshop

Sponsored by the Aerospace Corporation

San Bernardino, California

November 3-5, 1971

*The research reported herein was sponsored by the Arnold Engineering Development Center (AEDC), Air Force Systems Command (AFSC), U. S. Air Force, under Contract F40600-72-C-0003 with ARO, Inc., contract operator, AEDC. Further reproduction is authorized to satisfy needs of the U. S. Government.

**Supervisor, Impulse Tunnels and Dynamics Section, Aerodynamics Projects Branch, Aerodynamics Division, von Karman Gas Dynamics Facility, Arnold Air Force Station, Tennessee.

***Supervisor, Project Support and Special Studies Section, Aerodynamics Projects Branch, Aerodynamics Division, von Karman Gas Dynamics Facility, Arnold Air Force Station, Tennessee.

HYPERSONIC SIMULATION
FOR LIFTING BODY TRANSITION STUDIES
(Unclassified)

By

S. R. Pate and J. C. Adams

ARO, Inc.

Arnold Air Force Station, Tennessee

ABSTRACT

Similitude requirements for boundary-layer transition on lifting bodies at hypersonic speeds are discussed. Particular attention is focused on boundary-layer crossflow instabilities and similarity requirements. The critical crossflow Reynolds number concept is extended to lifting bodies at hypersonic conditions by applying a theoretical three-dimensional boundary-layer solution in conjunction with the critical crossflow Reynolds number criteria to correlate entrained vortex formations on sharp cones at angles of incidence under cold wall conditions. A strong influence of wall temperature ratio (T_w/T_0) on the critical crossflow Reynolds number is predicted. The relevance of using wind tunnel transition data, particularly from lifting bodies and Space Shuttle Orbiter configurations, to predict atmospheric flight values is discussed. Recent experimental data illustrating the adverse effects of very small amounts of unintentional surface roughness on lifting body transition locations are included.

NOMENCLATURE

l	Characteristic length ($l = 21.35$ -in. for MDAC STS Orbiter)
\dot{q}	Heat transfer rate
\dot{q}_{ref}	Stagnation heat transfer rate based on nose radius of 0.132 in. A 1-ft. radius sphere scaled to 0.011 model scale (MDAC model scale) corresponds to a radius of 0.132-in.
M_∞	Free-stream Mach number
Re_t	Transition Reynolds number based on x_t and local flow condition at edge of boundary layer
Re_∞	Free-stream unit Reynolds number
$Re_{\infty, l}$	Reynolds number based on free-stream condition and characteristic length
$Re_{\infty, st}$	Transition Reynolds number based on s_t and free-stream conditions
s	Surface distance measured from model nose apex
s_t, x_t	Location of boundary layer transition as measured from nose apex
T_O	Tunnel reservoir temperature, °K
T_w	Model wall temperature, °K
U_e	Local flow total velocity at edge of boundary layer
w_{max}	Maximum value of velocity in crossflow profile
x	Axial distance from model nose or wing leading edge
α	Angle of attack, degree
Γ	Sweep angle, degree
δ	Boundary layer thickness
δ_v	Cone half angle, degree
ϵ_i	Inviscid outer edge upwash angle
ϵ_s	Surface upwash angle (viscous)
ϵ_{vortex}	Entrained vortex upwash angle

μ_e	Local viscosity at outer edge of boundary layer
ρ_e	Local flow density at outer edge of boundary layer
ϕ	Model circumferential location, degree
x_{max}	Crossflow Reynolds number $x_{max} = \left(\frac{\rho_e v_{max} \delta}{\mu_e} \right)$

I. INTRODUCTION

In light of published results on the dominating influence of facility generated disturbances on boundary layer stability and transition (Refs. 1-6) one might conclude that a meaningful estimate of flight transition based on ground test data is impossible. This could very well be true for some basic and simple configurations such as a flat plate and sharp cone at zero incidence (Refs. 4-6). However, it cannot be established a priori for more complex geometries where other factors such as crossflow velocities or surface irregularities are present. The flow processes created by these three-dimensional flow fields have the potential for dominating the transition process irrespective of the tunnel disturbance levels. Lifting bodies, which include basic hypersonic shapes as well as complex configurations such as the NASA Space Transportation System (STS) Orbiter, when operated at angles of attack will experience boundary-layer crossflow velocities and instabilities which can dominate the transition process and promote early transition. Also the laminar boundary layer on the windward side of hypersonic lifting bodies at high angles of attack can become relatively thin and easily tripped by unintentional surface irregularities or protuberances.

The present paper extends the critical crossflow Reynolds number concept of Ref. 7 to include the correlation of entrained vortex formation in the three-dimensional laminar boundary layer on sharp slender cones at angle of attack under hypersonic flow conditions. Recent transition data taken in the VKF hypersonic

wind tunnels on the McDonnell-Douglas (MDAC) STS Orbiter configuration at high angles of attack are presented. Simulation requirements for hypersonic lifting bodies and the relevance of using experimental data from ground test facilities to predict the location of atmospheric flight values are discussed.

II. CROSSFLOW PARAMETERS AND SIMULATION REQUIREMENTS

The de-stabilizing effect of wing sweep and the resulting spanwise pressure gradient on the three-dimensional laminar boundary layer was first reported in Ref. 7. This type dynamic instability is related to the inflection point in the crossflow velocity component (w) that is normal to the outer-edge flow streamline, as illustrated in Figs. 1 and 2. It was established in Ref. 7 that the onset of instabilities and the development of transition could be correlated directly with a finite and specific critical crossflow Reynolds number, x_{\max} .

The crossflow Reynolds number (x_{\max}) is defined by

$$x_{\max} = \frac{(\rho_e) (w_{\max}) (\delta)}{\mu_e} \quad (1)$$

where subscript e denotes local inviscid edge value, δ denotes the boundary-layer thickness, and the velocity component w_{\max} is the maximum crossflow component of the three-dimensional boundary-layer velocity profile in streamline coordinates as illustrated in Fig. 1.

For a given characteristic length Reynolds number $Re_{\infty, l}$,

Mach number, and T_w/T_o value the crossflow Reynolds number can be expressed in the following functional relationship form (Refs. 7-8):

- a. Given two-dimensional swept-wing geometry with an adiabatic wall

$$\left[\frac{x_{\max}}{\sqrt{Re_{\infty, l}}} \right] = f \left(\frac{x}{l} \right) \quad (2)$$

$$\left. \begin{array}{c} M_{\infty} \\ \Gamma \\ \alpha \end{array} \right\} = \text{const.}$$

- b. Given sharp cone at angle of attack with a non-adiabatic wall

$$\left[\frac{x_{\max}}{\sqrt{\frac{x}{l}}} \right] = f(\phi, T_w/T_o) \quad (3)$$

$$\left. \begin{array}{c} M_{\infty} \\ Re_{\infty, l} \\ \alpha \end{array} \right\} = \text{const.}$$

Aerodynamic crossflow simulation requires both dynamic and geometric similarity; these requirements are satisfied when geometric similarity exists and

$$(Re_{\infty, l})_{\text{Tunnel}} = (Re_{\infty, l})_{\text{Flight}} \quad (4)$$

in addition to duplication of vehicle attitude, Mach number, and T_w/T_o ratios.

III. CORRELATION OF TRANSITION WITH A CRITICAL CROSSFLOW REYNOLDS NUMBER (x_{\max})

Owen and Randell (Ref. 7) investigated the destabilizing effect of wing sweep and the resulting spanwise pressure gradient on the subsonic laminar boundary layer. They determined that at subsonic speeds boundary layer instability occurred at $x_{\max} \approx 125$ and transition occurred at a critical value $x_{\max} \approx 175$.

Chapman (Ref. 8) investigated analytically the effects of crossflow on transition on swept circular leading edges at hypersonic speeds ($M_\infty = 4$ and 7). He determined that the critical crossflow Reynolds number criteria established by Owen and Randall (Ref. 7) for subsonic flow were also apparently applicable up to a free-stream Mach number of 7. Chapman did not investigate theoretically the flow downstream of the circular leading edge because of the complexity of the three-dimensional compressible boundary-layer equations. The crossflow velocity ratio

$$\beta = \left(\frac{w_{\max}}{U_e} \right)$$

distribution was shown to increase with distance from the stagnation point, and the crossflow Reynolds number reached a maximum value at the 60-deg location. Chapman analyzed experimentally heat transfer rate data on yawed cylinders from several sources and concluded that transition occurred in the nose regions when $x_{\max} \approx 175$.

Pate (Ref. 9) investigated transition on sharp leading edge swept wings in supersonic flow both experimentally and analytically

using an integral method. His results showed that even on very thin wings (3% thick biconic wing section) the crossflow at wing swept angles of 24-, 36-, and 50-degrees was sufficient to produce critical crossflow Reynolds numbers leading to boundary-layer transition.

The crossflow phenomenon is illustrated graphically in Fig. 3 for a blunt-nose swept geometry. The maximum crossflow Reynolds number will increase in the nose region when the free-stream Reynolds number or wing sweep is increased. When the critical crossflow Reynolds number (x_{max}) is reached, transition will jump from somewhere in Region #2 to the $x_{max} \approx 175$ station in Region #1.

The critical crossflow phenomenon is applicable to the flow on the windward surface of lifting bodies and at the critical flow condition it would be possible for a completely laminar boundary layer to become instantaneously turbulent.

Maximum crossflow Reynolds numbers that have been determined experimentally (Refs. 7, 8, and 9) over the Mach number range from 0 to 7 are correlated with respect to boundary-layer transition in Fig. 4. A critical value of approximately 175 appears to represent the data fairly well. Therefore, it can be assumed that with a fair degree of certainty that a crossflow Reynolds number of about 175 is sufficient to cause boundary-layer transition because of the crossflow instability phenomenon. Based on these results the following general criteria are accepted:

x_{\max}	<	100	Laminar Boundary Layer
$100 \leq x_{\max}$	\leq	200	Vortex Formation and Transitional Boundary Layer
x_{\max}	>	200	Turbulent Boundary Layer

IV. TRANSITION AND CROSSFLOW REYNOLDS NUMBERS ON A SUPERSONIC SWEPT WING

Experimental transition Reynolds number (Re_t) and predicted transition Reynolds numbers (Re_x), corresponding to the surface locations for various theoretical critical crossflow Reynolds number (x_{\max}), values taken from Ref. 9 are presented in Fig. 5. The crossflow Reynolds number distributions were determined using an integral method and have the functional form expressed in Eq. 1. There are two significant results shown in Fig. 5. First: large crossflow Reynolds numbers can occur even on very thin (3% thick) supersonic airfoils and the experimentally measured beginning of transition locations are reasonably close to the wing stations corresponding to a critical crossflow Reynolds number of 150. Second: it is necessary when conducting wind tunnel crossflow dominated transition experiments, for the purpose of establishing atmospheric flight values, to have complete geometric similarity and to conduct the tunnel tests at the simulated flight Reynolds number based on a characteristic length as discussed in Section II.

V. PREDICTION OF UPWASH ANGLES AND ENTRAINED VORTICES LEADING TO TRANSITION

5.1 ANALYTICAL APPROACH AND SCOPE

The analytical tools applied in the present section utilize implicit finite-difference integration of the governing three-dimensional laminar boundary-layer equations for supersonic or hypersonic flow over a sharp cone at incidence following McGowan and Davis (Ref. 10). Inviscid edge conditions are input to the boundary-layer analysis following the numerical procedure of Jones (Ref. 11) for solving the problem of steady supersonic or hypersonic inviscid flow around sharp cones at incidence. The three-dimensional turbulent boundary-layer analysis follows Adams (Ref. 12) and is based upon the three-dimensional invariant turbulence eddy viscosity model developed by Hunt, Bushnell, and Beckwith (Ref. 13).

The theoretical study reported herein is devoted to analysis of experimental data presented by McDevitt and Mellenthin (Ref. 14) concerning measured upwash patterns and entrained vortex formation on sharp cones at incidence in the NASA Ames 3.5-foot Hypersonic (Air) Tunnel under cold wall ($T_w/T_0 = 0.3$) conditions. Figure 2 gives the pertinent sharp cone geometry and nomenclature.

5.2 ORIENTATION OF ENTRAINED VORTICES

Three-dimensional compressible boundary-layer stability theory (following Refs. 15 and 16) has been applied to determine

neutral, purely inviscid oscillations forming a stationary wave. The assumption is made, based on qualitative agreement between other published experiments and theory (see Ref. 17, for example) that the direction of the observed stationary entrained vortices caused by three-dimensional boundary-layer crossflow instability is equal to the direction of the inviscid stationary wavefronts. Comparisons between experiments and theory for a sharp 10-degree half-angle cone at incidence in a hypersonic $M_\infty = 7.4$ flow are shown in Fig. 6.

The calculated results from three-dimensional inviscid neutral stationary disturbance theory lie some 10 to 15 percent (one to two degrees) below the measured vortex angular orientation at the $\phi = 90^\circ$ location. The reason for the indicated discrepancy in the vortex direction between theory and experiment is not clear, but several assumptions have been made in applying the stability theory to hypersonic flow conditions as discussed by Mack (Ref. 18) and Morkovin (Ref. 19), among others.

Also presented in Fig. 6 are the calculated surface (ϵ_s) and inviscid outer-edge (ϵ_i) upwash angles at the $\phi = 90$ -degree body location. Good agreement between oil-flow measurements and three-dimensional laminar boundary-layer theory is observed for the surface upwash angle. Note the large amount of turning by the laminar boundary layer (the surface upwash angle is approximately a factor of three to four greater than the calculated inviscid outer-edge upwash angle). This is a clear indication of the large amounts of crossflow in the present three-dimensional

laminar boundary layer.

5.3 VORTICES AND TRANSITION ONSET

The exact location at which the stationary vortex system will originate cannot be determined from classical boundary-layer stability theory so that recourse must be taken to application of the maximum local crossflow Reynolds number (x_{\max}) concept discussed in Sections II and III to correlate the onset of vortex formation. Presented in Fig. 7 are the calculated maximum local crossflow Reynolds number distributions around two sharp cones at incidence ($\delta_v = 10^\circ$ at $\alpha = 5^\circ$ and $\delta_v = 15^\circ$ at $\alpha = 5^\circ$) for which McDevitt and Mellenthin (Ref. 14) present photographic documentation of the onset to vortex formation based on an oil-film technique. Note that the data in Fig. 7 are given in laminar boundary-layer similarity format, i.e., x_{\max} is divided by $\sqrt{x/l}$ for a constant $Re_{\infty, l}$ value. From Fig. 7 and the criterion reiterated above, a developed surface plot with lines of constant x_{\max} can easily be formulated with respect to location of onset to vortex formation. Such is presented in Fig. 8 for the two sharp cones at incidence of present interest. Lines of constant $x_{\max} = 100$ and 200 are shown up to the $\phi = 90^\circ$ circumferential location to delineate the region of expected onset to vortex formation. It is extremely difficult to accurately read the McDevitt and Mellenthin photographs with respect to actual initial onset of a vortex streak. Only two such points are presented for the 10-degree sharp cone case. However, for the 15-degree sharp

cone sufficient data are available to form the shaded band shown in Fig. 8. Based on these results it appears that vortex formation may be expected on sharp cones at incidence under conditions where x_{\max} assumes values greater than approximately 150. It is impossible to accurately ascertain if the boundary layer becomes turbulent for $x_{\max} > 200$ based on the McDevitt and Mellenthin data. What is needed here for completeness are heat-transfer measurements in the region of vortex formation and downstream to clearly delineate the state of the boundary layer. However, surface streamline oil-flow data such as shown in Fig. 9 indicate that boundary-layer transition has indeed occurred based on comparison with three-dimensional laminar and turbulent boundary-layer theory. Note that the calculated surface upwash angles are appreciably less in a turbulent flow than in a laminar one. Furthermore, the free-stream length Reynolds number is sufficiently low for this case ($Re_{\infty, l} = 5 \times 10^5$) that one would certainly expect a laminar boundary layer a priori to exist.

It is interesting to observe from Fig. 8 that the maximum crossflow Reynolds number concept, coupled with the three-dimensional laminar boundary-layer analysis, correctly predicts the trend observed in the experimental data of Refs. 20 and 21 in that the transition movement undergoes a much more rapid forward progression on the leeward side than the rearward progression for the windward side of sharp cones at incidence in hypersonic flow.

Another important facet of the crossflow instability phenomenon is the influence of wall temperature level on the

magnitude of the calculated maximum crossflow Reynolds number x_{\max} . As shown very clearly in Fig. 10, increasing wall temperature level at a given circumferential location increases the value of x_{\max} and, hence, makes the three-dimensional laminar boundary layer more susceptible to crossflow instability leading to vortex formation and transition. The reason behind this behavior is that the maximum crossflow velocity is increased by approximately a factor of three, while the boundary layer thickness is increased by approximately a factor of two as the wall temperature level is increased from $T_w/T_o = 0.0$ to $T_w/T_o = 0.90$. Since, from Eq. (1),

$$x_{\max} = \frac{(\rho_e)(w_{\max})(\delta)}{\mu_e} \quad (1)$$

with ρ_e and μ_e being determined by the local inviscid edge conditions (which, of course, are independent of wall temperature level), the above results reveal that the increase of the maximum crossflow Reynolds number with wall temperature level at a given circumferential location, as shown in Fig. 10, is totally because of the sensitivity of the three-dimensional crossflow velocity profile and boundary-layer thickness to changes in the wall temperature level. In general, the hotter the wall, the greater the crossflow velocity and boundary-layer thickness which leads to greater instability (because of increasing crossflow effects) in the three-dimensional laminar boundary layer.

It is very important to recognize from Fig. 10 that severe wall cooling ($T_w/T_o \rightarrow 0$) can render the present sharp cone

($\delta_v = 10^\circ$ at $\alpha = 5^\circ$) scale to three-dimensional crossflow instability over the entire body for the given flow conditions based on a value of $x_{\max} > 150$ required for onset to vortex formation. Recalling the significant influence of transition on static stability characteristics as discussed in Refs. 21 and 22, the results of Fig. 10 give warning that static stability ground testing in hypersonic wind tunnels under hot wall conditions on slender bodies at incidence may not be applicable to cold wall flight conditions because of the crossflow instability phenomenon. Much more work remains to be done in this area before a definite conclusion on this potential problem area in relating ground test results to actual flight conditions can be reached.

VI. EFFECTS OF SURFACE ROUGHNESS ON LIFTING BODY TRANSITION LOCATIONS

Difficulties have been encountered when attempting to intentionally promote early transition at hypersonic speeds because of the relatively large size trip roughness that is required as reported in Refs. 23, 24, and 25. However, the exact opposite appears to be true for hypersonic lifting bodies at high angles of attack and high Reynolds numbers as illustrated by the data in Figs. 11 through 13.

Heat-transfer distributions and transition locations on the MDAC STS Orbiter configuration at $\alpha = 25, 40$, and 60° from the VKI Hypersonic Wind Tunnel B and Hypervelocity Wind Tunnel F are presented in Fig. 11. The Tunnel B data (Figs. 11 and 12a) show

that at $M_\infty = 8$, $Re_{x,l} = 6.6 \times 10^6$, and $\alpha = 40^\circ$ and 60° , 0.025 in. high grit particles spaced randomly at about one-inch intervals over the model windward surface were sufficient to promote boundary-layer transition. The calculated laminar boundary-layer thickness (δ) based on modified yawed-cylinder theory was equal to 0.012 in. at the body location $x/l = 0.1$ for the $\alpha = 60^\circ$ condition of Fig. 12a. The transition-to-turbulence "spikes" due to the roughness grit are clearly discernible in the photograph of the windward surface paint heating patterns shown in Fig. 12a.

During the recent NASA-sponsored MDAC STS Orbiter tests conducted in the VKI Hypersonic Wind Tunnel B, it was found that any surface instrumentation or paint specks which were on the order of 0.010 in. or greater in height could promote boundary-layer transition on the windward surface at incidence. This is illustrated in Fig. 12b where a surface pressure orifice which has been filled and "smoothed" flush with the model surface and an unidentified surface proturbance (possibly a paint speck) caused transition to occur. It was found necessary to use a model with no surface instrumentation gages or ports and to hand-rub the Tempilaq paint after spraying the stycast models before angle of attack heat rate data could be obtained that did not exhibit turbulent "spikes".

Unintentional tripping also occurred in the VKI Hypervelocity Wind Tunnel F tests of the MDAC STS Orbiter as shown by the photograph (thermographic phosphor technique) presented in

Fig. 12c. The turbulent streak that is clearly visible in Fig. 12c originated at the No. 1 surface pressure orifice located at the $s/l = 0.16$ body station. The laminar boundary-layer thickness (δ) was calculated to be 0.014 in. thick at this location for flow conditions of $M_\infty = 10.5$, $\alpha = 40^\circ$, and $Re_\infty = 3.45 \times 10^6$, per foot. The pressure orifice was 0.093 in. in diameter. Surface smoothness measurements performed after completion of the test showed that the discontinuities associated with the surface-mounted contoured heat gages had a maximum height less than 0.001 in.

Transition Reynolds numbers obtained in the VKF Tunnels B and F on the windward ray centerline of the MDAC STS Orbiter configuration at incidence are presented in Fig. 13. The Tunnel F data exhibit the characteristics of a tripped boundary layer (e.g., see Ref. 26). For 20-, 40-, 45-, and 60-degrees angle of attack the boundary layer was evidently tripped by the No. 1 pressure orifice as discussed in the preceding paragraph and/or by surface irregularities further upstream. For the $\alpha = 25^\circ$ condition (see Fig. 11a) the No. 1 pressure orifice was filled and the data indicate that the boundary layer was tripped by the No. 2 pressure orifice except for the $Re_\infty = 0.82 \times 10^6$, per foot condition where the flow over the entire model was laminar.

The experimental data presented in Figs. 11, 12, and 13 clearly illustrate that very small amounts of surface irregularities are apparently sufficient to trip the boundary layer on the

windward surface of lifting geometries at moderate to high angles of attack under high Reynolds number cold wall hypersonic flow conditions. This conclusion should apply to atmospheric flight as well as wind tunnel results.

VII. SUMMARY AND CONCLUDING REMARKS

Experimental and theoretical evaluations of lifting geometries at incidence under hypersonic cold wall conditions have led to the following conclusions regarding viscous flow characteristics and boundary-layer transition:

- (1) Present analytical methods have accurately estimated surface upwash angles and were partially successful in estimating the angular orientation of entrained vortices within the boundary layer on sharp cones at incidence.
- (2) The crossflow Reynolds number (x_{\max}) criteria applied in conjunction with a three-dimensional laminar boundary-layer solution has shown that the onset of vortex formation on sharp yawed cones can be correlated with a specific critical value of the crossflow Reynolds number ($x_{\max} \approx 175$).
- (3) A strong influence of wall temperature ratio (T_w/T_o) on the crossflow Reynolds number has been theoretically predicted with, in general, the hotter the wall, the larger the value of the crossflow Reynolds number.
- (4) These results suggest that ground testing in hypersonic wind tunnels under hot wall conditions on slender cones

at incidence may result in erroneous conclusions relative to transition data. In particular, ground test hot wall data may not simulate cold wall flight conditions for such aerodynamic parameters as static stability coefficients because of the crossflow instability phenomenon promoting premature boundary-layer transition in the hot wall tunnel case which may not be present under cold wall flight conditions.

- (5) The proper simulation parameters for boundary-layer transition dominated by crossflow instability are the characteristic length Reynolds number, vehicle geometry, free-stream Mach number (M_∞) and wall temperature ratio (T_w/T_o) with duplication of model attitude. An adjustment for a "unit Reynolds number effect" between tunnel and atmospheric flight is not applicable for crossflow-dominated transition.
- (6) Experimental hypersonic wind tunnel data obtained on a STS Orbiter configuration under cold wall conditions has shown that very small unintentional surface irregularities (such as pressure orifices and paint specks) can cause boundary-layer transition to occur on the windward ray at moderate to high angles of attack.

REFERENCES

1. G. B. Schubauer and H. K. Skramstad, "Laminar Boundary-Layer Oscillations and Transition on a Flat Plate," NACA Report No. 909, 1948.
2. E. R. Van Driest and C. B. Blumer, "Boundary Layer Transition: Free-Stream Turbulence and Pressure Gradient Effect," AIAA J., Vol. 1, No. 6, June 1963, pp. 1303-1306.
3. J. Laufer, "Aerodynamic Noise in Supersonic Wind Tunnels," J. of the Aerospace Sciences, Vol. 28, No. 9, September 1961, pp. 685-692.
4. S. R. Pate and C. J. Schueler, "Radiated Aerodynamic Noise Effects on Boundary Layer Transition in Supersonic and Hypersonic Wind Tunnels," AIAA J., Vol. 7, No. 3, March 1969, pp. 450-457.
5. S. R. Pate, "Measurements and Correlations of Transition Reynolds Numbers on Sharp Slender Cones at High Speeds," AIAA J., Vol. 9, No. 6, June 1971, pp. 1082-1090.
6. J. M. Kendall, Jr., "Supersonic Boundary Layer Transition Studies," JPL-SPS-37-62, Vol. III, April 1970, pp. 43-47.
7. P. R. Owen and D. G. Randall, "Boundary Layer Transition on a Swept-Back Wing," Royal Aircraft Establishment Memo No. Aero 277, June 1952.
8. G. T. Chapman, "Some Effects of Leading-Edge Sweep on Boundary-Layer Transition at Supersonic Speeds," NASA TN D-1075, September 1961.
9. S. R. Pate, "Experimental and Analytical Investigation of Boundary-Layer Transition on Swept Wings at Mach Numbers 2.5 to 5," AEDC-TR-67-186, October 1967.
10. J. J. McGowan and R. T. Davis, "Development of a Numerical Method to Solve the Three-Dimensional Compressible Laminar Boundary-Layer Equations with Application to Elliptical Cones at Angle of Attack," ARL Report 70-0341, December 1970.
11. D. J. Jones, "Numerical Solutions of the Flow Field for Conical Bodies in a Supersonic Stream," National Research Council of Canada Aeronautical Report LR-507, July 1968.

12. J. C. Adams, "Numerical Calculation of the Three-Dimensional Turbulent Boundary Layer on a Sharp Cone at Incidence in a Supersonic Flow," Paper presented at Workshop on Fluid Dynamics of Unsteady, Three-Dimensional, and Separated Flows, Georgia Institute of Technology, Atlanta, Georgia, June 10-11, 1971.
13. J. L. Hunt, D. M. Bushnell, and I. E. Beckwith, "The Compressible Turbulent Boundary Layer on a Blunt Swept Slab With and Without Leading-Edge Blowing," NASA TN D-6203, March 1971.
14. J. B. McDevitt and J. A. Mellenthin, "Upwash Patterns on Ablating and Nonabating Cones at Hypersonic Speeds," NASA TN D-5346, July 1969.
15. E. Reshotko, "Stability of Three-Dimensional Compressible Boundary Layers," NASA TN D-1220, June 1962.
16. E. Reshotko, "Stability of the Compressible Laminar Boundary Layer," GALCIT Hypersonic Research Project Memorandum No. 52, January 1960.
17. N. Gregory, J. T. Stuart, and N. S. Walker, "On the Stability of Three-Dimensional Boundary Layers with Application to the Flow Due to a Rotating Disk," Phil. Trans. Royal Society (London), Series A, Vol. 248, No. 943, July 1955, pp. 155-199.
18. L. M. Mack, "Boundary-Layer Stability Theory," JPL/CIT 900-277, Rev. A, November 1969.
19. M. V. Morkovin, "Critical Evaluation of Transition from Laminar to Turbulent Shear Layers with Emphasis on Hypersonically Traveling Bodies," AFFDL-TR-63-149, March 1969.
20. V. DiCristina, "Three-Dimensional Boundary Layer Transition on a Sharp 8° Cone at Mach 10," AIAA J., Vol. 8, No. 5, May 1970, pp. 852-856.
21. A. Martellucci and R. S. Neff, "Influence of Asymmetric Transition on Re-Entry Vehicle Characteristics," J. Spacecraft and Rockets, Vol. 8, No. 5, May 1971, pp. 476-482.
22. L. E. Ericsson, "Effect of Boundary Layer Transition on Vehicle Dynamics," J. Spacecraft and Rockets, Vol. 6, No. 12, December 1969, pp. 1404-1409.
23. J. L. Potter and J. D. Whitfield, "Boundary-Layer Transition Under Hypersonic Conditions," AEDC-TR-65-99 (AD 462716), May 1965.

24. J. D. Whitfield and F. A. Iannuzzi, "Experiments on Roughness Effects on Cone Boundary-Layer Transition up to Mach 16," AIAA J., Vol. 7, No. 3, March 1969, pp. 465-470.
25. J. R. Sterrett, et. al., "Transition Fixing for Hypersonic Flow," NASA TN D-4129, October 1967.
26. S. R. Pate, "Supersonic Boundary-Layer Transition: Effects of Roughness and Freestream Disturbances," AIAA J., Vol. 9, No. 5, May 1971, pp. 797-803.

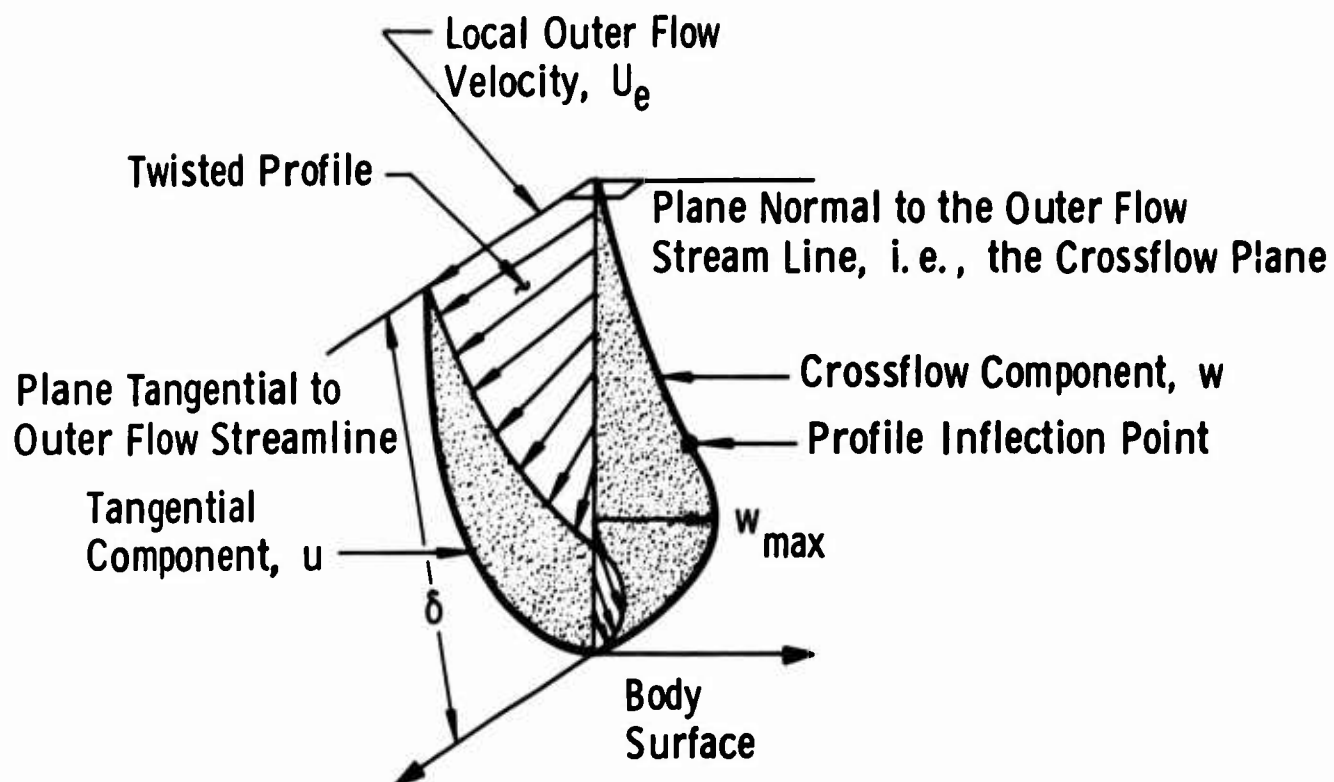


FIG. 1 VELOCITY PROFILES IN THREE-DIMENSIONAL BOUNDARY-LAYER FLOW (FROM REF. 9)

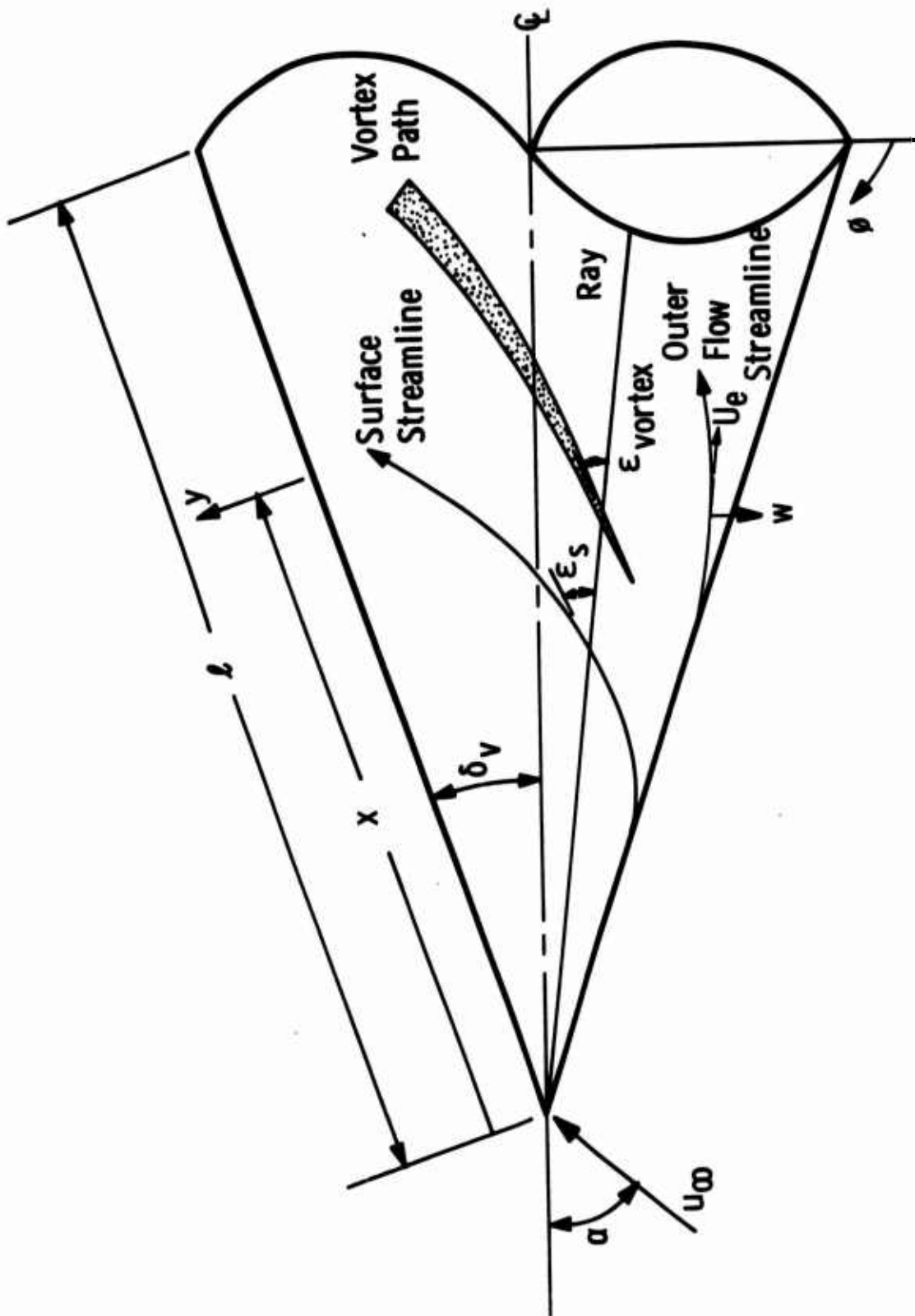


FIG. 2 SHARP CONE GEOMETRY AND NOMENCLATURE

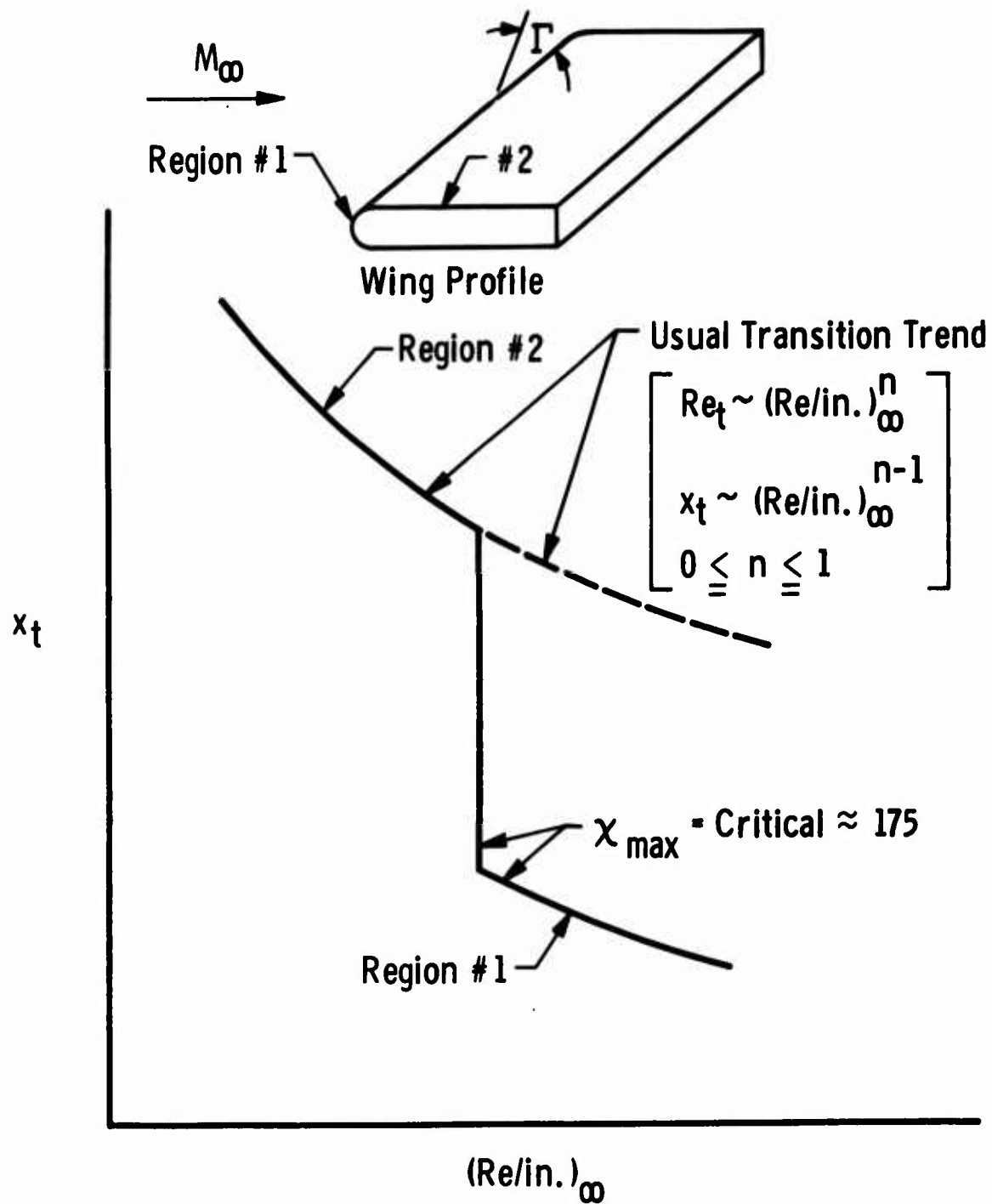





FIG. 3 CRITICAL CROSSFLOW INFLUENCE ON THE BOUNDARY-LAYER TRANSITION PROFILE

<u>Sym</u>	<u>Source</u>	<u>Configuration</u>	<u>Method of Detecting X_t</u>
	Ref. 7	Subsonic Swept Wings	Flow Visualization
	Ref. 8	Yawed Cylinders	Heat-Transfer
	Ref. 9	Supersonic Swept Wing	Surface Pitot Probe

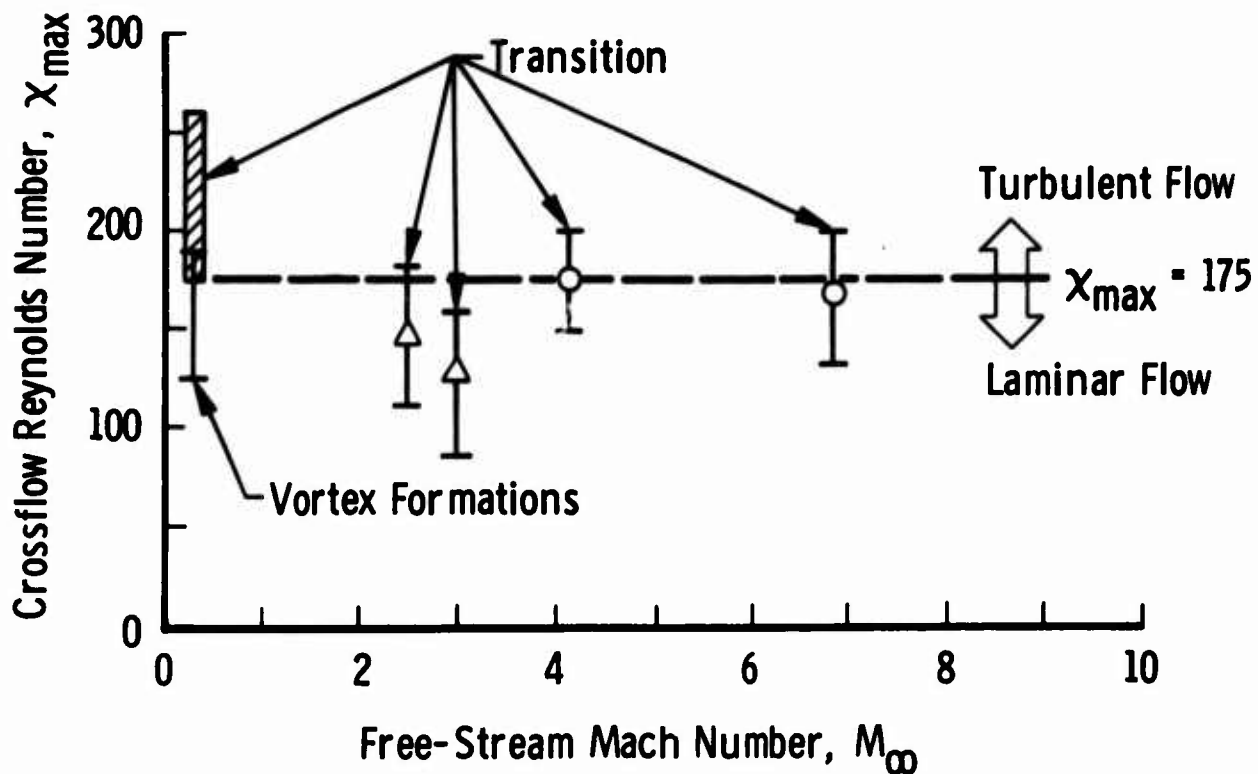
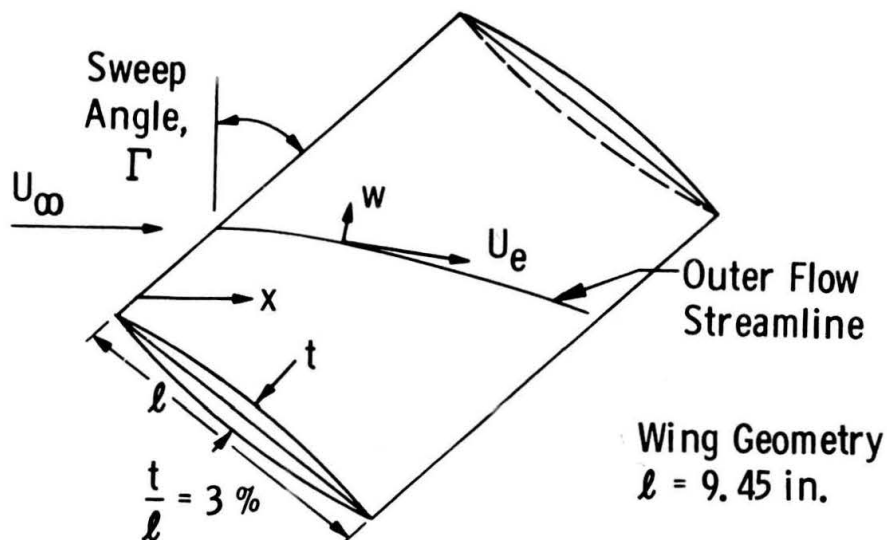


FIG. 4 CORRELATION OF TRANSITION AND CROSSFLOW REYNOLDS NUMBERS



Sym

○ Experimental Data $\left(Re_t = \frac{\rho_\infty U_\infty X_t}{\mu_\infty} \right)$, X_t Corresponds to Beginning of Transition as Measured by a Surface Pitot Probe

— Theory $\left(Re_{\bar{x}} = \frac{\rho_\infty U_\infty \bar{x}}{\mu_\infty} \right)$, \bar{x} Corresponds to Location Where χ_{\max} Critical Occurred

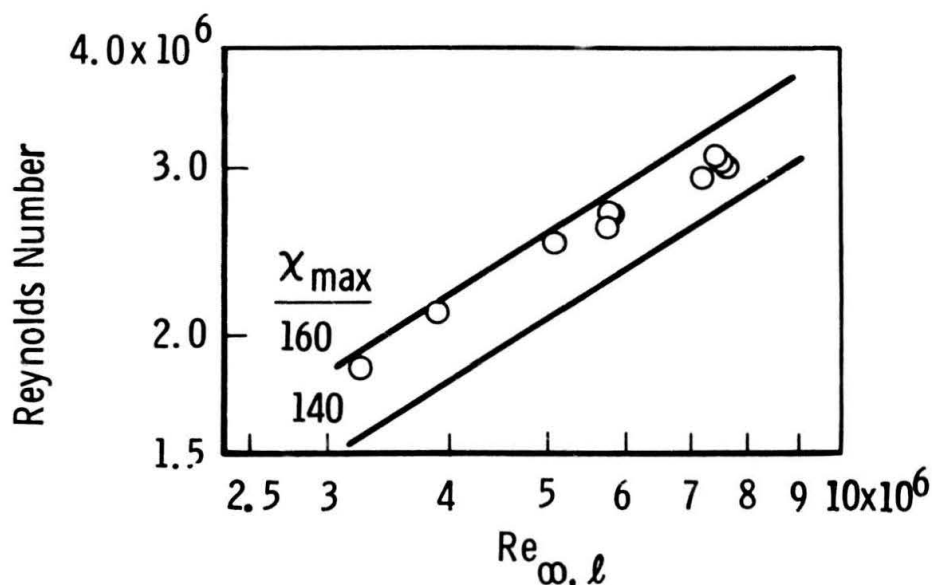


FIG. 5 TRANSITION AND CROSSFLOW REYNOLDS NUMBERS ON A BICONIC THREE-PERCENT-THICK SUPERSONIC AIRFOIL $M_\infty = 3$, $\Gamma = 24$ DEG (FROM REF. 9)

10.0-deg Half-Angle Sharp Cone at $M_\infty = 7.40$,
 $Re_{\infty, L} = 3.0 \times 10^6$, $T_w/T_0 = 0.286$, Air

- Three-Dimensional Laminar Boundary-Layer Theory
- - - Three-Dimensional Inviscid Sharp Cone at Incidence Theory
- ○ Experimental Data from Fig. 15 of Ref. 14
- x Three-Dimensional Neutral Inviscid Stability Theory for Stationary Disturbances

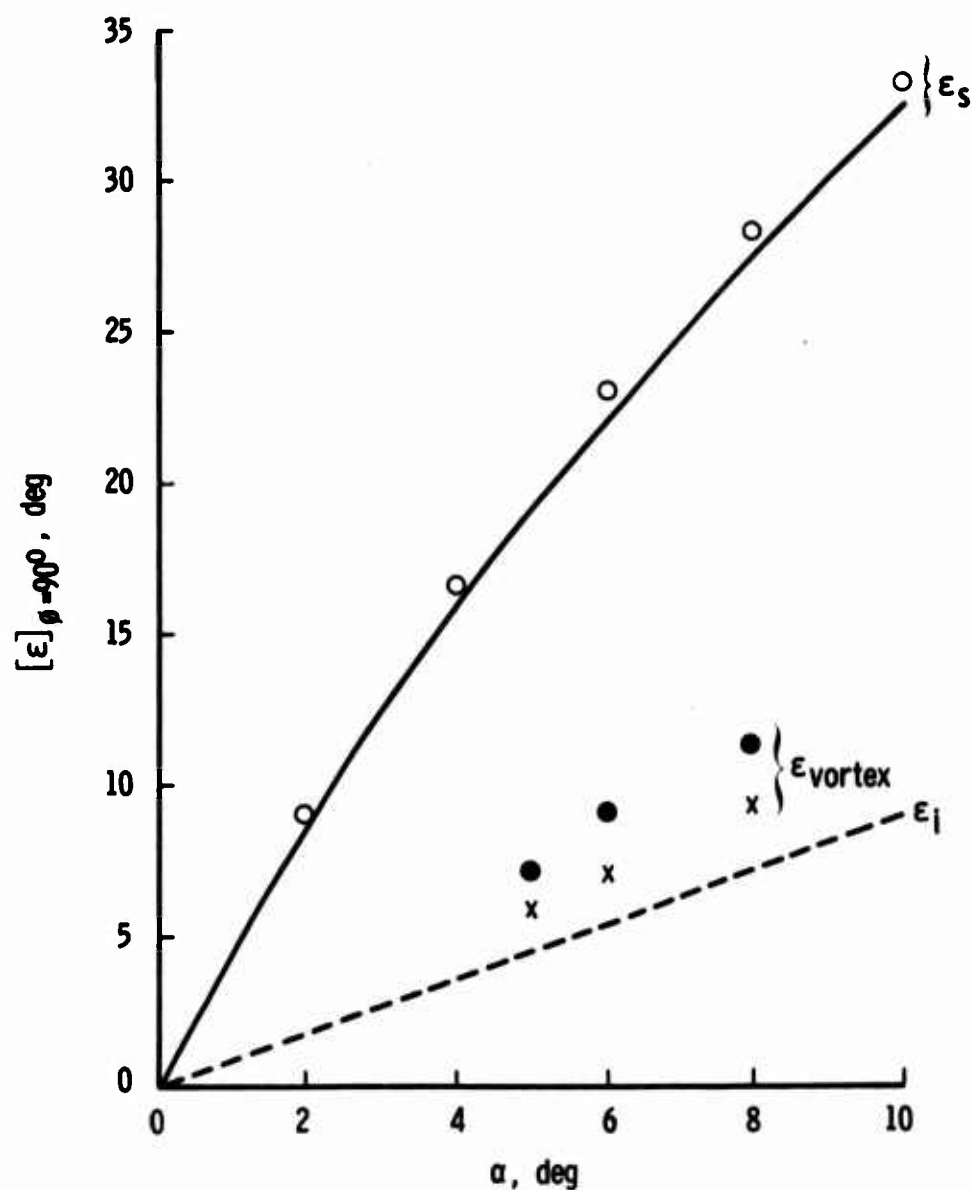


FIG. 6 COMPARISON OF CALCULATED AND MEASURED VORTEX ANGLES AT $\phi = 90^\circ$ ON A SHARP CONE AT INCIDENCE

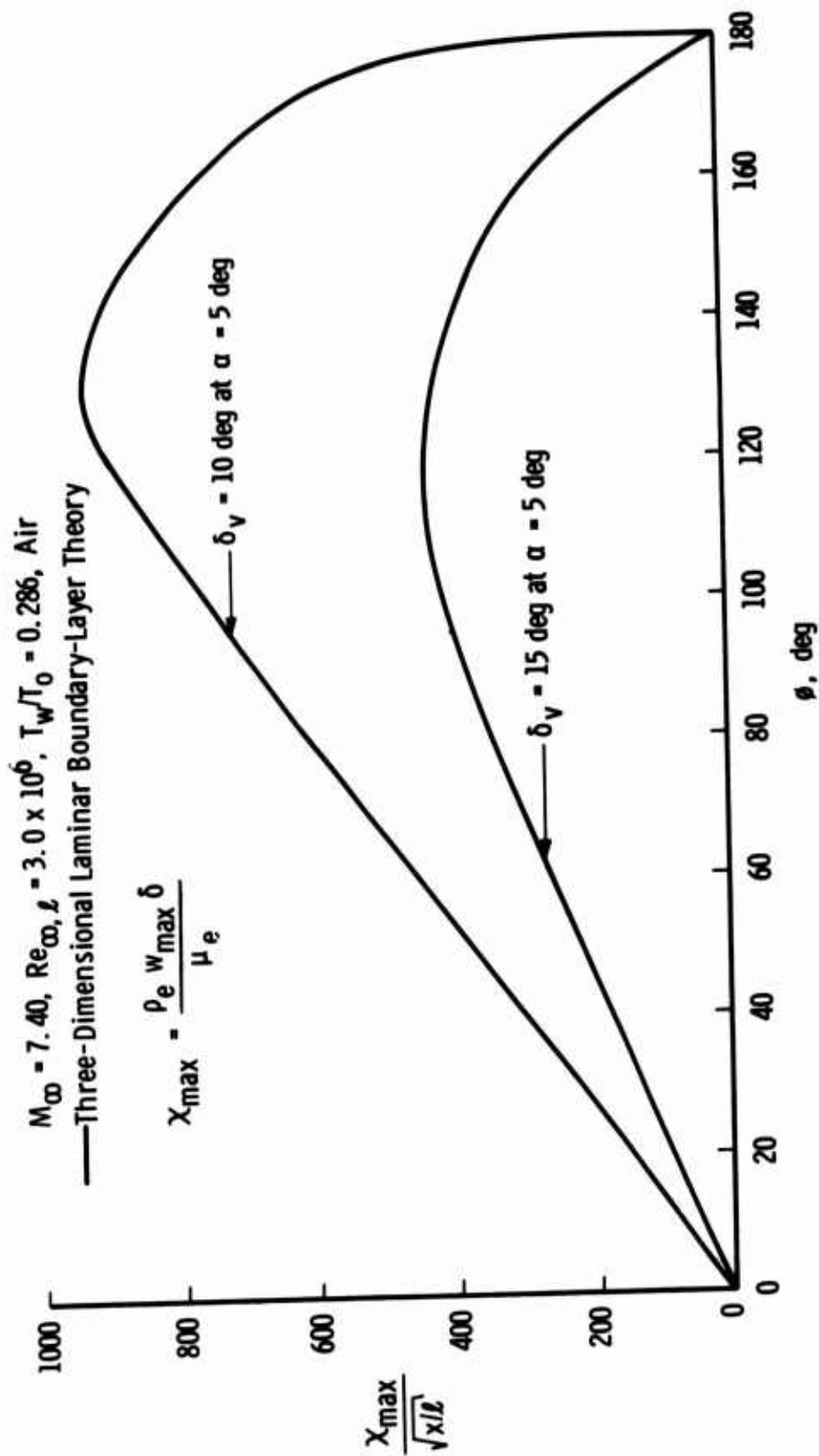


FIG. 7 MAXIMUM CROSS-FLOW REYNOLDS NUMBER DISTRIBUTION ON SHARP CONES AT INCIDENCE

10. 0-deg Half-Angle Sharp Cone at $\alpha = 5.0$ deg
 $M_\infty = 7.40$, $Re_{\infty, \ell} = 3.0 \times 10^6$, $T_w/T_0 = 0.286$, Air

▲ Onset of Vortex Formation Based on Fig. 12 of Ref. 14

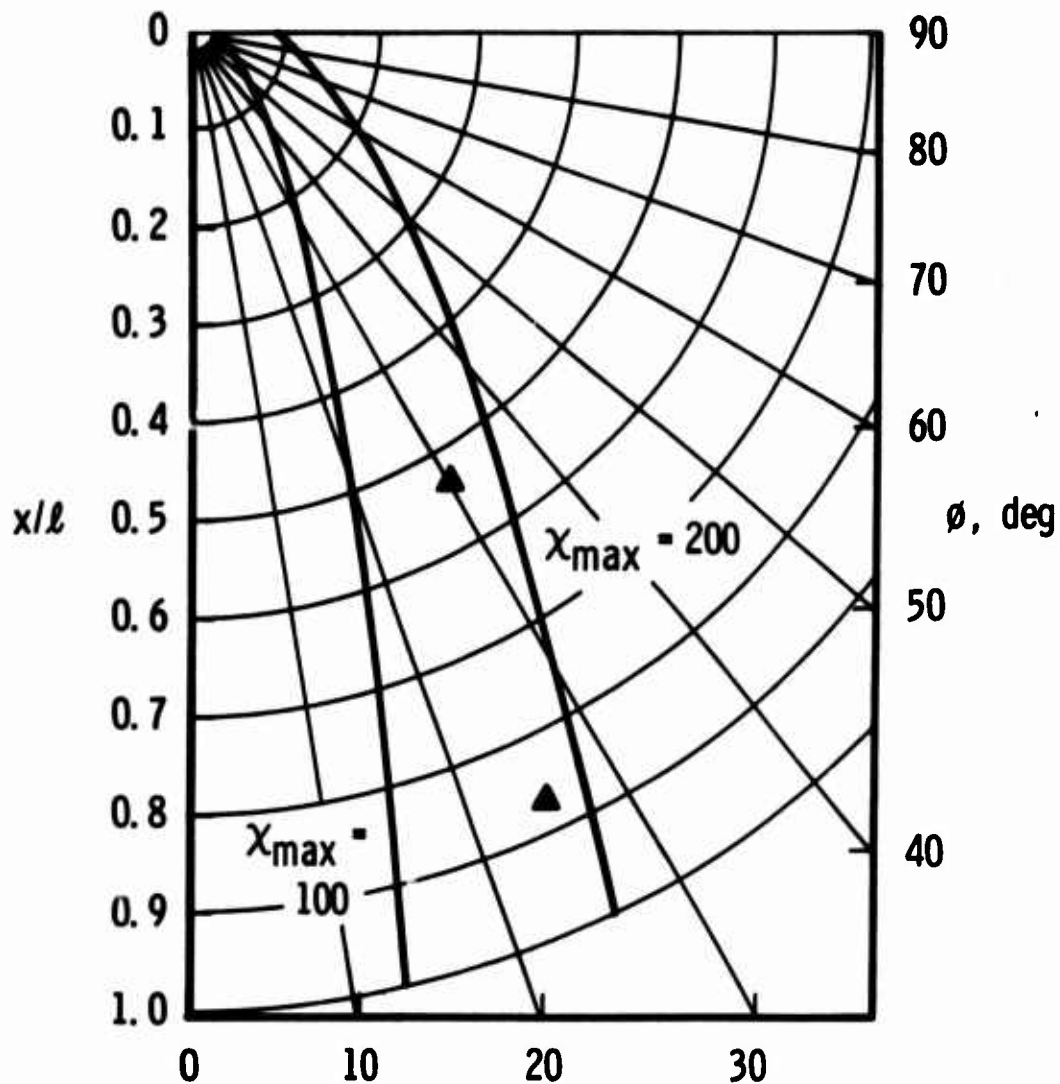


FIG. 8 DEVELOPED-SURFACE PLOT SHOWING ONSET TO VORTEX FORMATION RELATIVE TO LINES OF CONSTANT MAXIMUM CROSSFLOW REYNOLDS NUMBER ON SHARP CONES AT INCIDENCE.

15. 0-deg Half-Angle Sharp Cone at $\alpha = 5.0$ deg
 $M_\infty = 7.40$, $Re_{\infty, \ell} = 3.0 \times 10^6$, $T_w/T_0 = 0.286$, Air

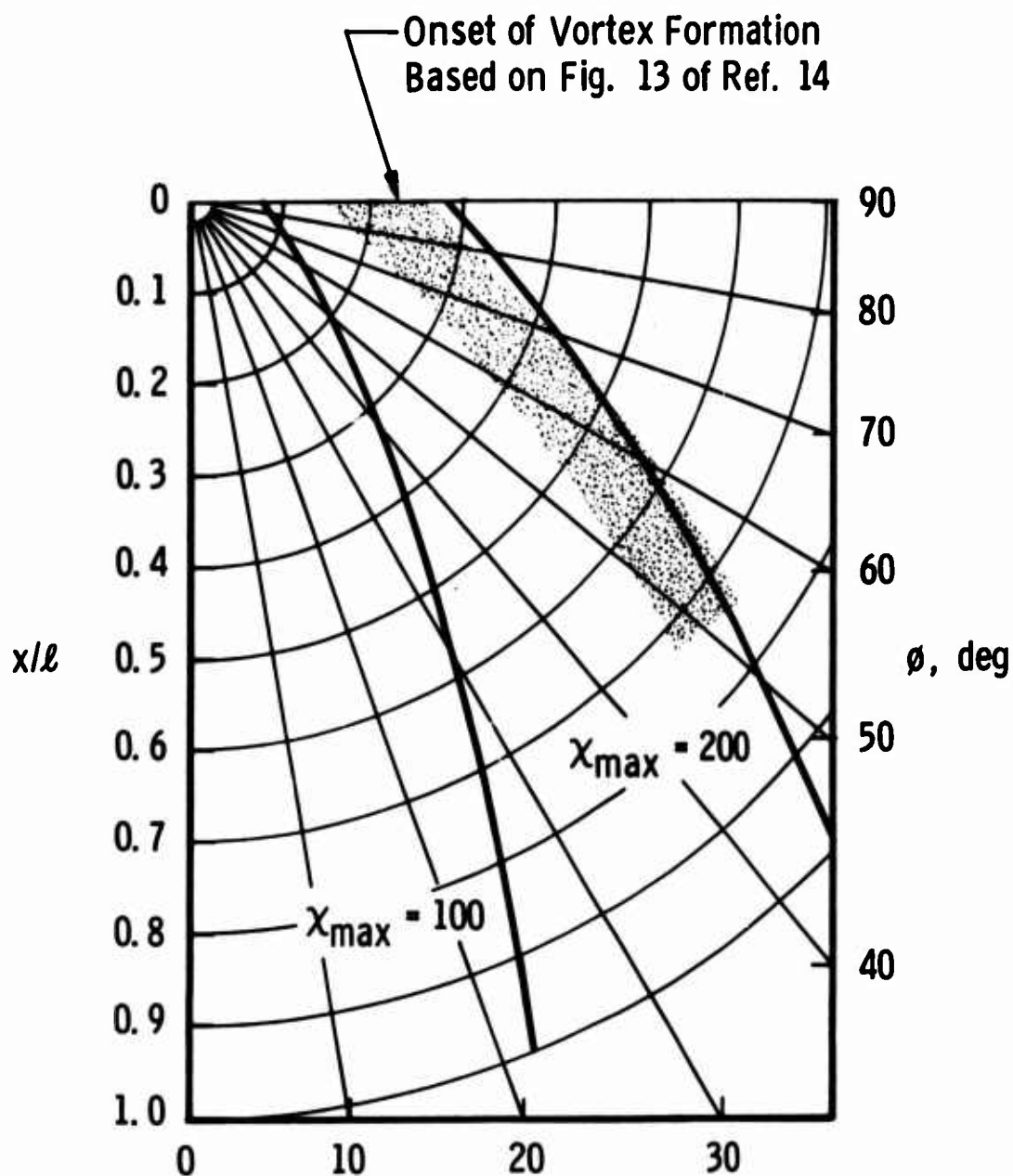


FIG. 8 CONCLUDED

5.0-deg Half-Angle Sharp Cone at $\alpha = 4.0$ deg
 $M_\infty = 7.4$, $Re_\infty, l = 5 \times 10^5$, $T_w/T_0 = 0.3$

● ϵ_s Experimental Data from Fig. 9 of Ref. 14

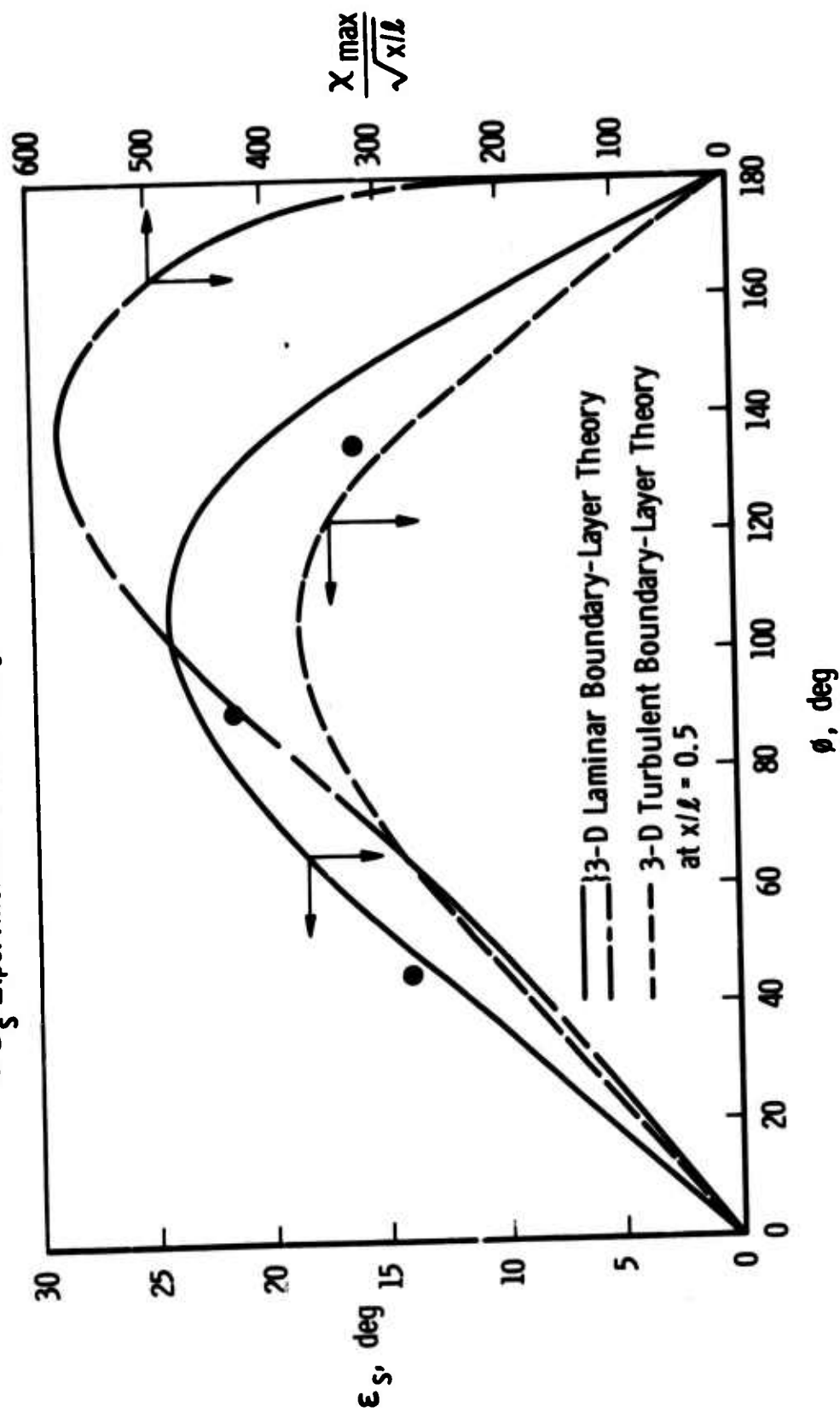


FIG. 9 DISTRIBUTION OF UPWASH ANGLES AND MAXIMUM CROSSFLOW REYNOLDS NUMBER ON A SHARP CONE AT INCIDENCE

10. 0-deg Half-Angle Sharp Cone at $\alpha = 5.0$ deg

$M_\infty = 7.40$, $Re_\infty, l = 5.0 \times 10^5$, Air

— Three-Dimensional Laminar Boundary-Layer Theory

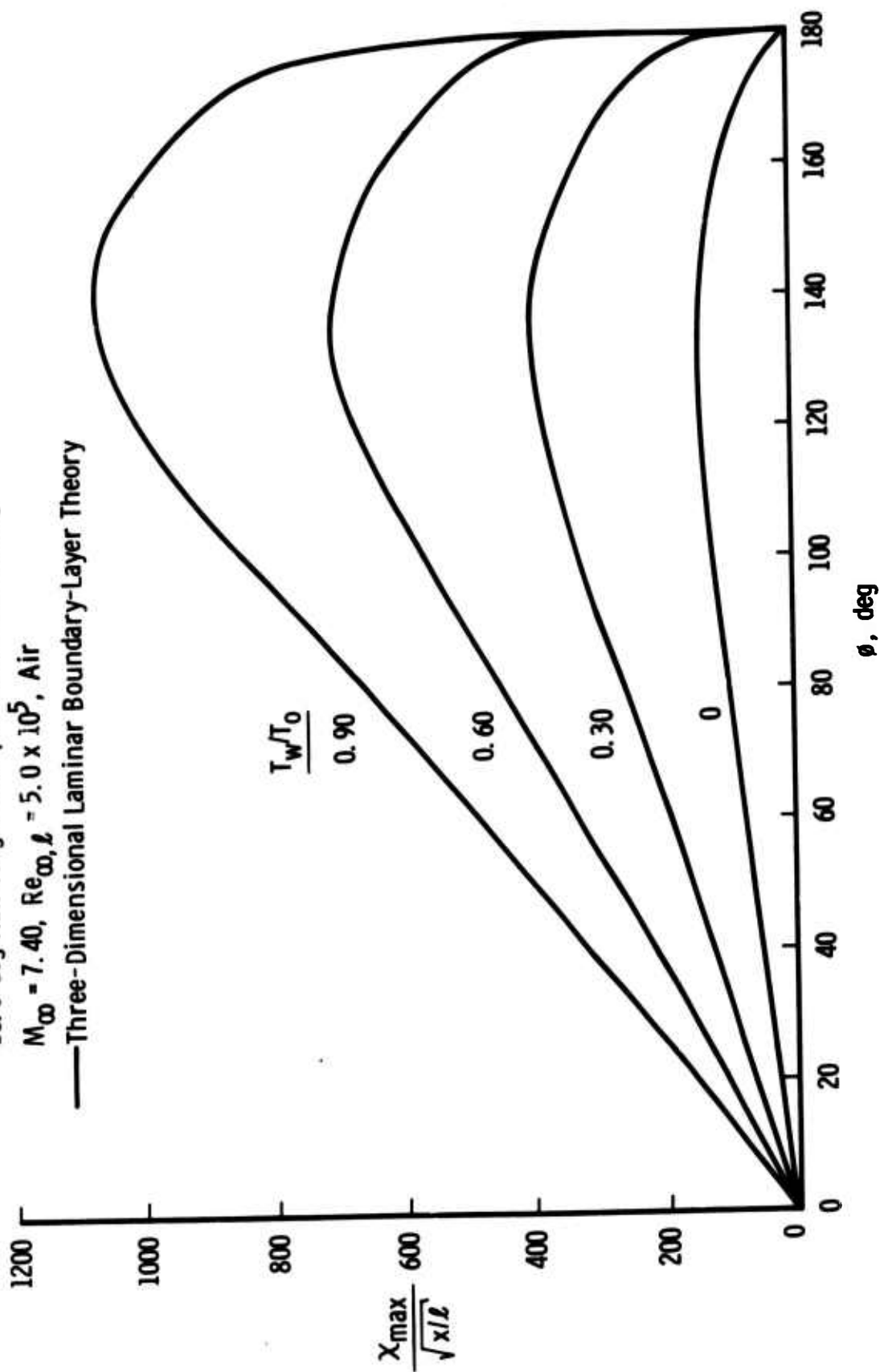


FIG. 10 EFFECT OF WALL TEMPERATURE ON CALCULATED MAXIMUM CROSSFLOW REYNOLDS NUMBER DISTRIBUTIONS ON A SHARP CONE AT INCIDENCE

Sym	M_∞	$Re_\infty / ft \times 10^{-6}$	VKF Tunnel	\dot{q} Method
\diamond	≈ 11.1	0.82	F	Heat Gages
\square	\downarrow	1.1	\downarrow	\downarrow
\triangle	\downarrow	1.7	\downarrow	\downarrow
\circ	\downarrow	3.4	\downarrow	\downarrow

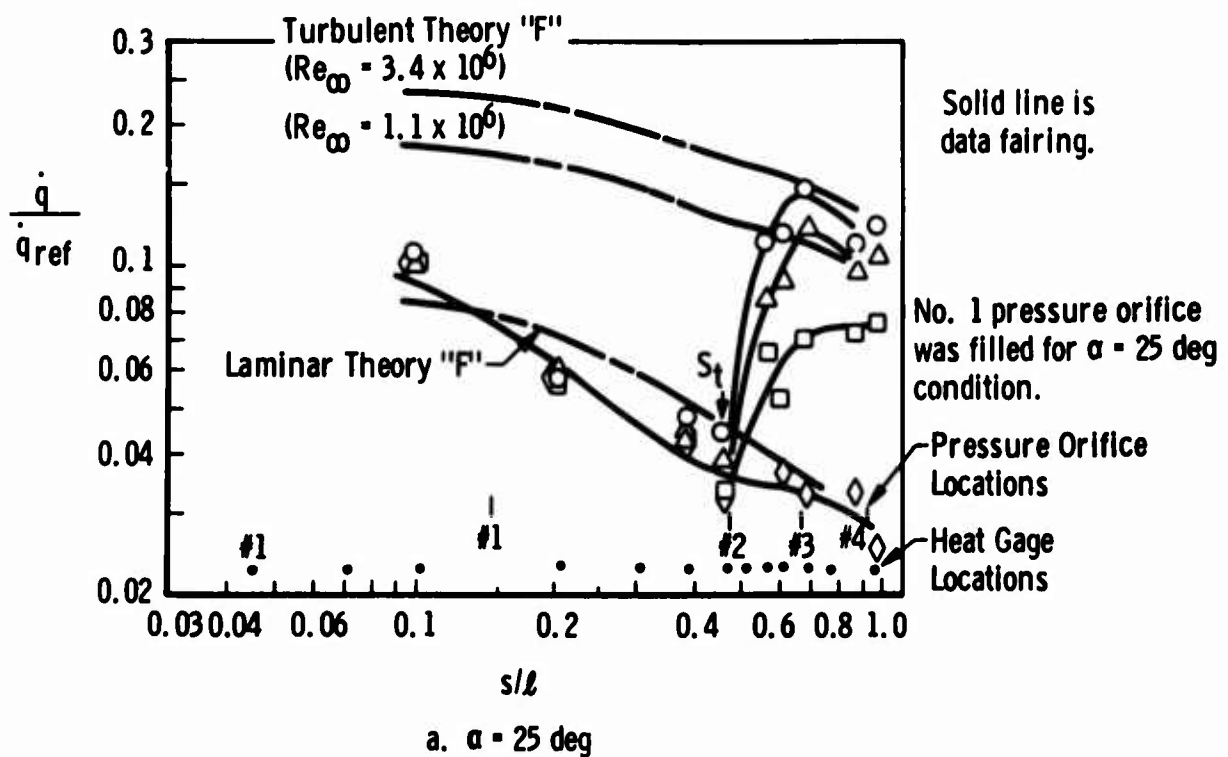


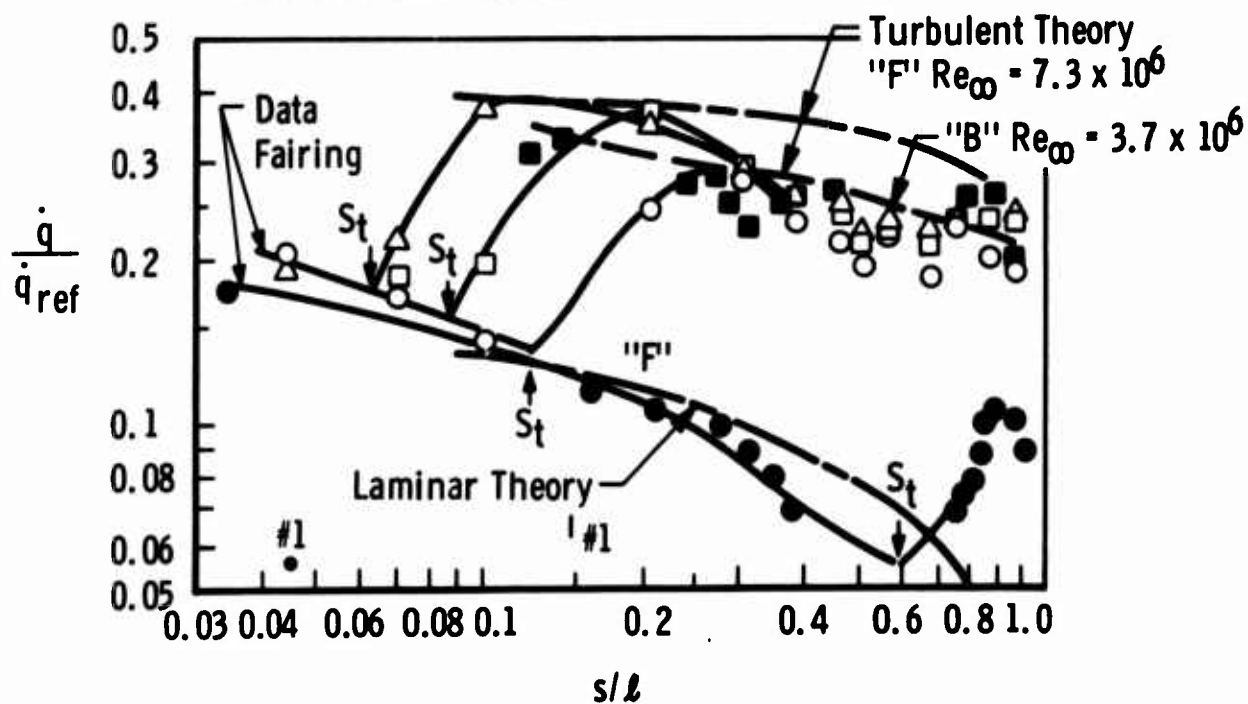
FIG. 11 HEATING DISTRIBUTIONS AND TRANSITION LOCATIONS ON MDAC STS ORBITER IN VKF TUNNELS B AND F

Sym	M_∞	$Re_\infty/ft \times 10^{-6}$	VKF Tunnel	\dot{q} Method
○	≈ 10.5	3.4	F	Heat Gage
□	↓	5.6	↓	↓
△	↓	7.3	↓	↓
●	8	3.7	B	Tempilaq Paint
■	8	3.7	B	" "

*Tripped using 0.025-in. height grit distributed randomly at about one-inch intervals.

No. 1 pressure orifice in Tunnel F model was open.

Tunnel B model had no surface instrumentation and was hand rubbed.

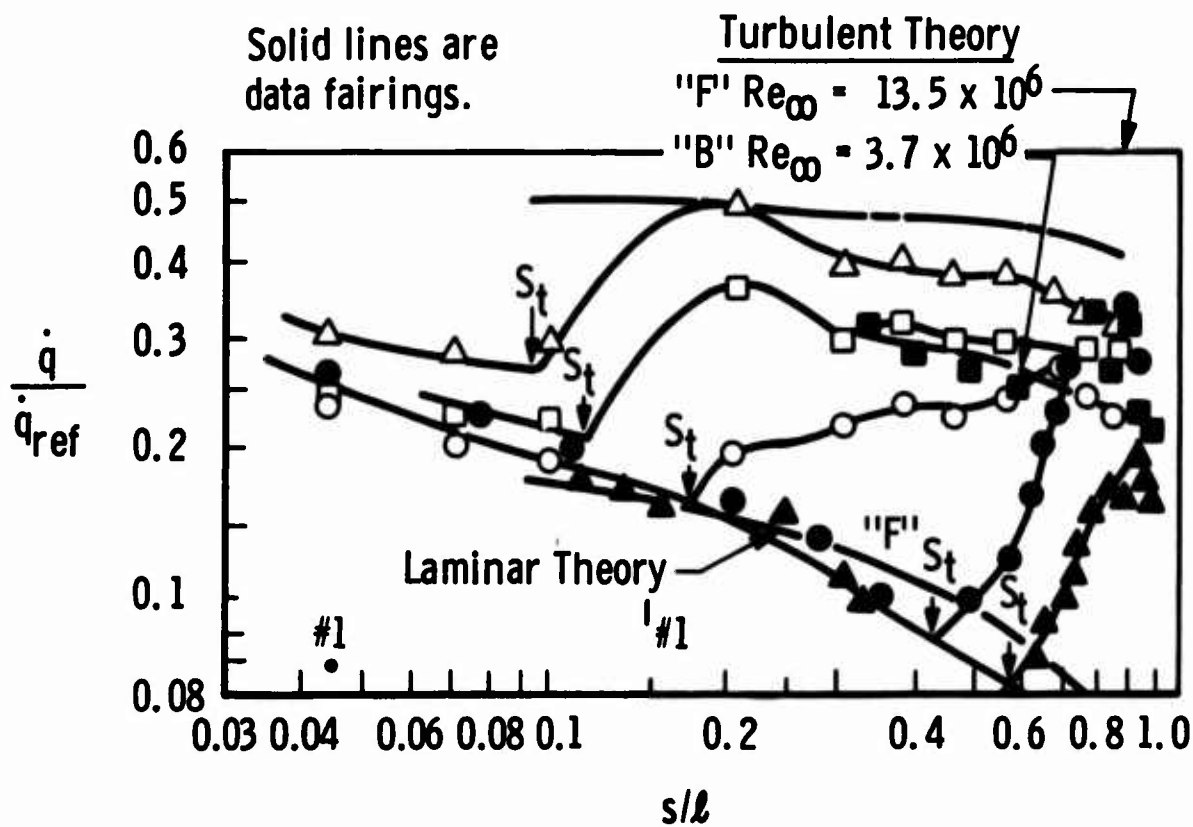


b. $\alpha = 40^\circ$

FIG. 11 CONTINUED

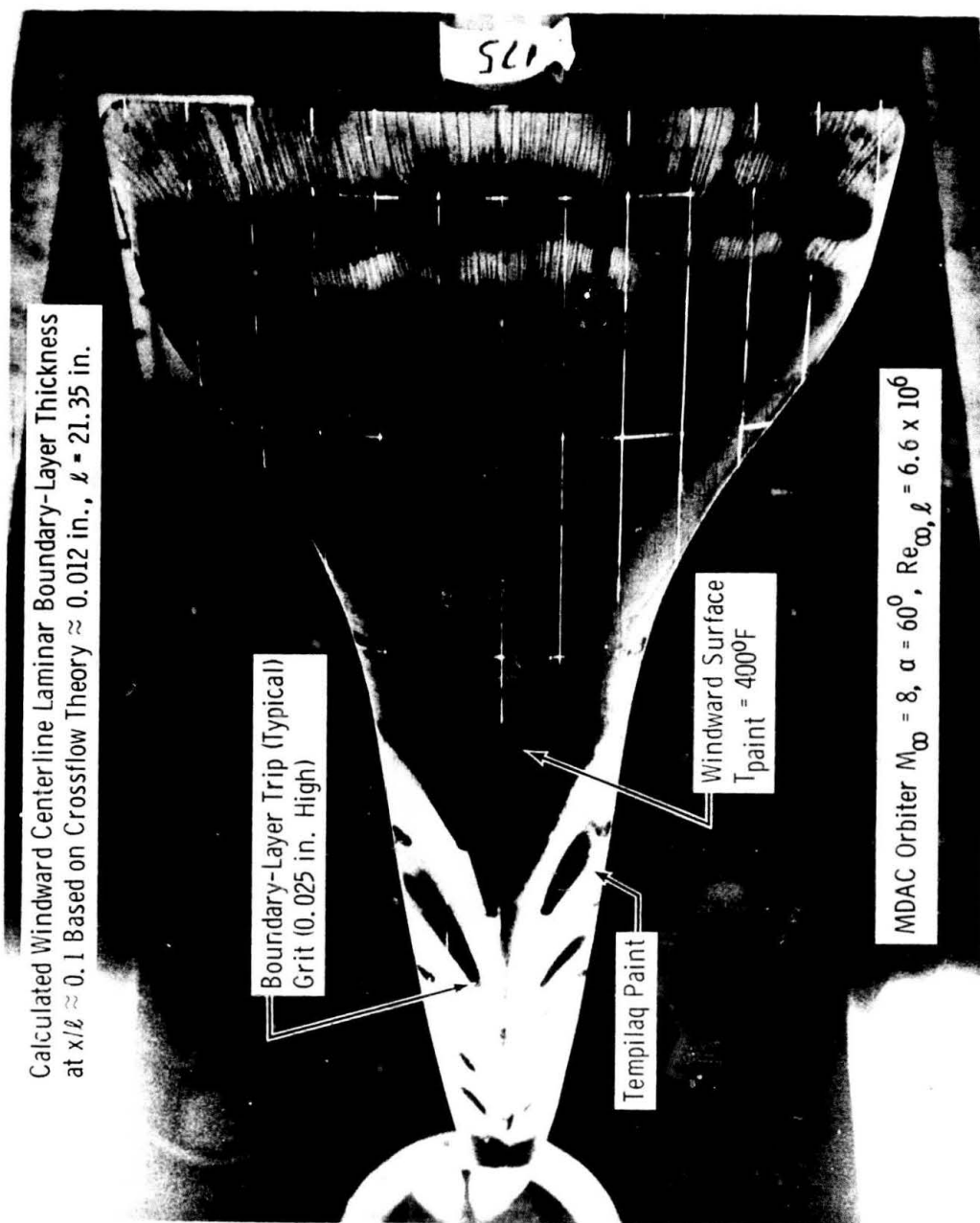
Sym	M_∞	Re_∞/ft $\times 10^{-6}$	VKF Tunnel	\dot{q} Method
○	≈ 10.5	3.3	F	Heat Gage
□	↓	5.8	↓	↓
△	↓	13.5	↓	↓
▲	8	2.52	B	Tempilaq Paint
●	↓	3.71	↓	↓
■	↓	3.71	↓	↓

*Tripped using 0.025-in. height grit distributed randomly at about one-inch intervals.



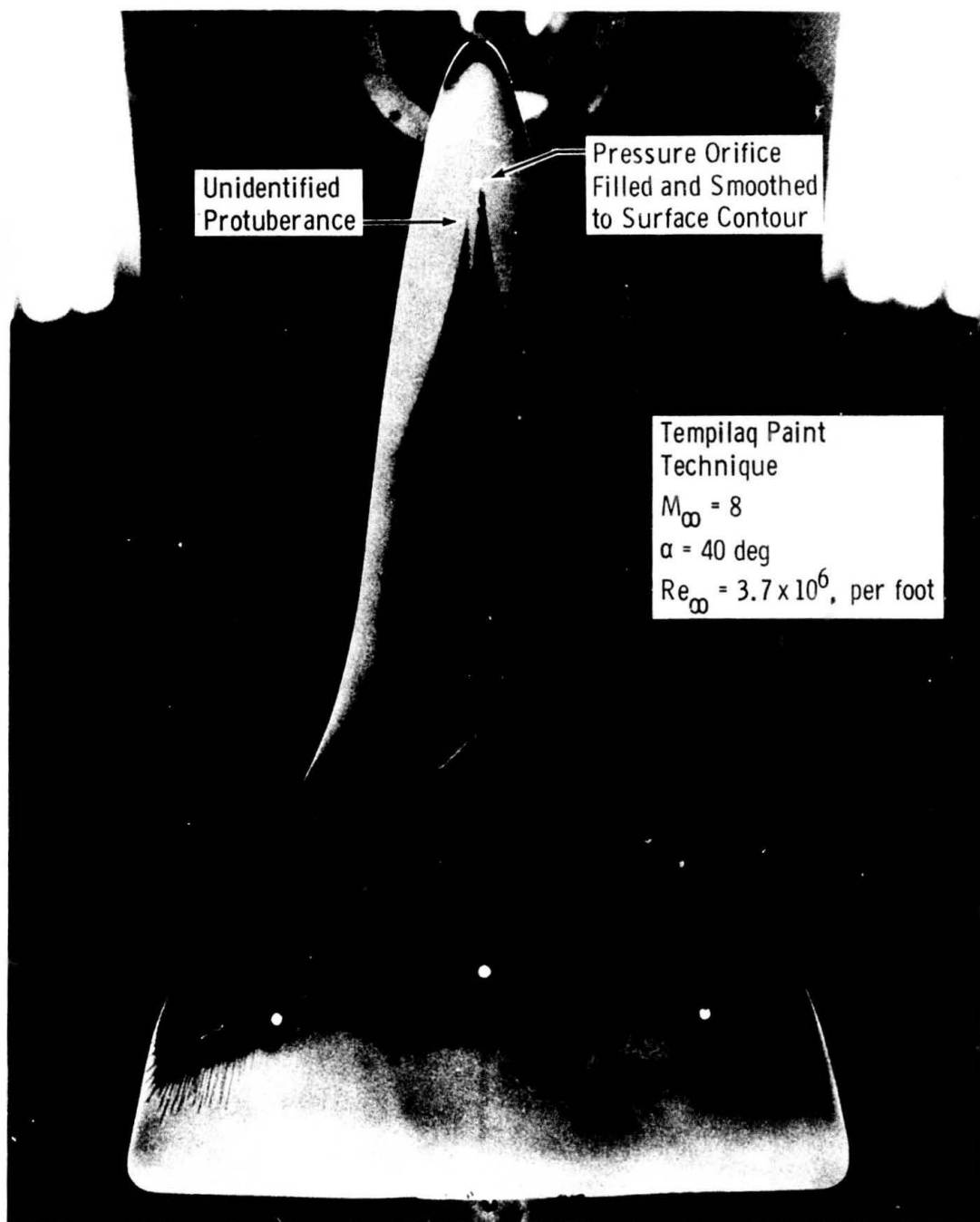
c. $\alpha = 60 \text{ deg}$

FIG. 11 CONCLUDED



a. Photograph of Tempilaq Paint with Distributed Grit, Tunnel B

FIG. 12 OBSERVATIONS OF TRANSITION ON MDAC ORBITER WINDWARD SURFACE IN VKF TUNNELS B AND F

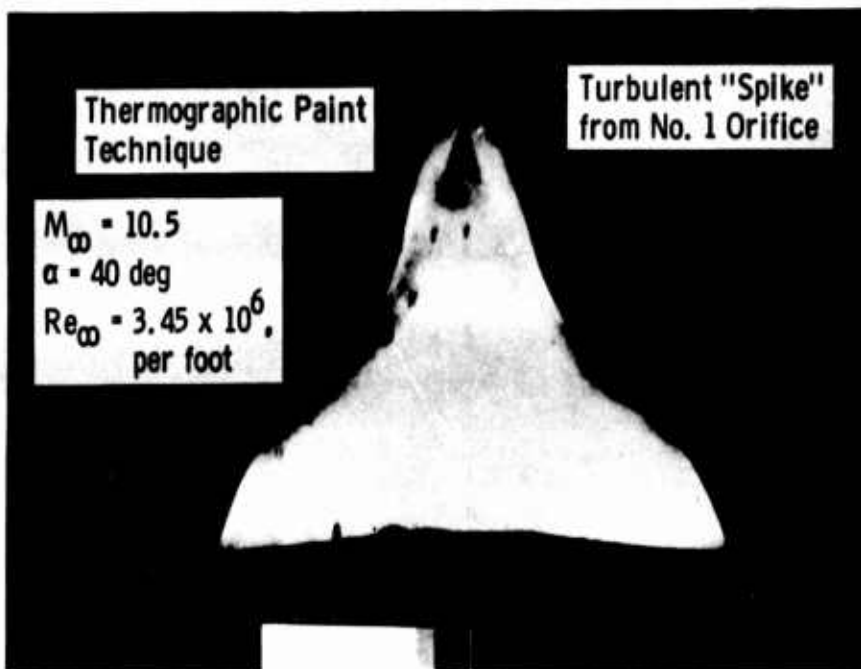


b. Transition Tripping from Unintentional Surface Roughness, Tunnel B

FIG. 12 CONTINUED



Photograph before Run



Photograph during Run

c. Transition Tripping from Unintentional Surface Roughness, Tunnel F

FIG. 12 CONCLUDED

	Sym	α , deg	M_∞	T_w/T_0	VKF Tunnel	Method of X_t Detection	Comments
No. 1 Orifice Filled	▽	25	≈ 10.5	0.24 to 0.15	F	Heat Gages	(Boundary-Layer Unintentionally Tripped)
No. 1 Orifice Open	○	20	↓	≈ 0.24	↓	↓	↓
	△	40	↓	≈ 0.24	↓	↓	↓
	◇	45	↓	≈ 0.21	↓	↓	↓
	□	60.5	↓	0.29 - 0.19	↓	↓	↓
(No Surface Instrumentation	●	20	8	≈ 0.7	B	(Heat Paint	---
Hand Rubbed after Painting)	▲	40	↓	↓	↓	Tempilaq)	---
	■	60	↓	↓	↓	↓	---

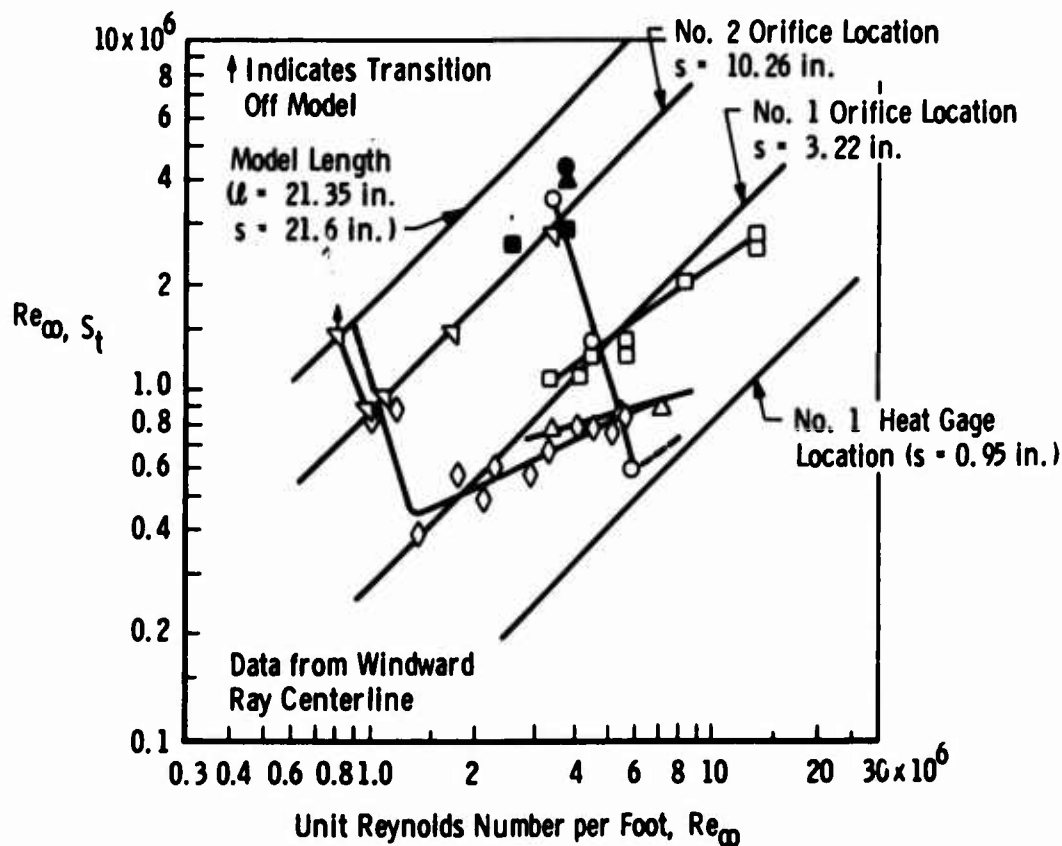


FIG. 13 TRANSITION REYNOLDS NUMBERS ON MDAC STS ORBITER IN VKF TUNNELS B AND F

(This page intentionally left blank)

SECTION 7

EFFECT OF TRANSITION ON THREE-DIMENSIONAL SHOCK WAVE-BOUNDARY LAYER INTERACTION (Unclassified)

R. H. Korkegi

Hypersonic Research Laboratory
Aerospace Research Laboratories
Wright-Patterson Air Force Base, Ohio

ABSTRACT

Shock wave-boundary layer interactions associated with three-dimensional configurations are highly dependent on the nature of the boundary layer. The shock waves are skewed to the flow so that the initial (upstream) part of the interaction may be laminar while far downstream it is turbulent. In between, the transition region is characterized by a well-defined change in the flow separation line from the broad zone of laminar separation to the much narrower one in the turbulent region where the flow may even be unseparated. Oil flow examples are given of shock-wave boundary layer interaction exhibiting transitional cases for blunt fins on flat plates and flow in an axial compression corner.

INTRODUCTION

For two-dimensional shock wave-boundary layer interaction, shock impingement on a surface occurs at a constant spanwise Reynolds number whereby the boundary layer is either laminar, transitional, or turbulent. Extensive experimental evidence shows that a relatively weak shock causes laminar separation whereas a fairly strong shock is required to cause turbulent separation, and the extent of separation is considerably greater for a laminar than for a turbulent boundary layer⁽¹⁾.

In the three-dimensional case, shock waves are generally skewed with respect to the flow direction on a surface so that the shock impingement line may cover a wide Reynolds number range. Thus, a single

shock may interact with a boundary layer which is initially laminar, then transitional, and finally turbulent.

Three-dimensional shock wave-boundary layer interactions occur on many configurations of practical importance such as in inlets of air breathing engines, at wing-body and control surface junctions, and for piggyback configurations. Interactions involving transition may occur on flight vehicles and their components at very high altitudes, or on wind tunnel models tested at Reynolds numbers which are usually much smaller than those encountered in flight.

The purpose of this paper is to identify the effect of boundary layer transition on three-dimensional shock interactions and thus provide the correct interpretation of some anomalous flow patterns.

SHOCK INTERACTION DUE TO BLUNT PROTUBERANCES

The curved bow shock of a blunt protuberance on a body, interacting with the body boundary layer causes widespread separation of a highly three-dimensional nature. As is the case for two-dimensional flow, the extent of separation is considerably greater for laminar than for turbulent interaction^(1, 2).

Figure 1 shows oil flow photographs from the study of Ref. 2 illustrating flow separation due to the impingement of the bow shock of a 3/4 in. diameter blunt fin on a sharp flat plate of 9-inch span at a Mach number of 3 and over a wide range of Reynolds numbers. For the low Reynolds number case of Figure 1A, the interaction is entirely laminar whereas for the high Reynolds number case of Figure 1C, it is totally turbulent and the upstream and lateral extent of interaction is markedly smaller. For the intermediate Reynolds number case of Fig. 1B there is a clear break in the separation line at a Reynolds number of approximately $3/4 \times 10^6$, beyond which it has an inflection and subsequently approaches the turbulent line as indicated by the tracings in the sketch in Figure 1. The initial interaction occurs with a laminar boundary layer. The break is associated with the onset of boundary layer

transition with an attendant decrease in lateral spread of the interaction zone as the boundary layer approaches a fully turbulent state. Note that separation causes a strong disturbance to the flow, and therefore the onset of transition for this case is not necessarily representative of that for flow on an undisturbed flat plate.

Figure 2 illustrates another case of transitional (A) and fully turbulent (B) interaction for the same basic model as in Figure 1 except for a much smaller fin diameter. Figure 2A again shows a break and inflection in the separation line indicative of transitional flow. An additional feature in Fig. 2 is that, somewhat beyond the transition region in Fig. 2A, and at approximately the same position relative to the fin leading edge in Fig. 2B, no further separation is observed. Beyond this point the decreasing strength of the fin bow shock is insufficient to cause separation of the turbulent boundary and, hence, it remains attached with simply a deflection of the streamlines due to shock impingement. The inflection point of the streamlines is slightly upstream of the estimated two-dimensional bow shock shape as shown in the sketch in Figure 2. This difference is probably due to distortion of the bow shock near the plate surface as a consequence of the upstream separated flow region. There is also a plate side-edge effect noticeable in the oil flow photographs, which could cause some distortion of the outboard flow field, but should not affect the center region of interest.

As a final point, the horseshoe vortices generated by the upstream separated flow regions in Figs. 2A and 2B are seen to curve and proceed in a streamwise direction at the point beyond which no further separation occurs.

SHOCK INTERACTION DUE TO AN AXIAL COMPRESSION CORNER

In a compression corner formed by the streamwise intersection of two wedges, embedded shocks, which may be viewed as a distorted

continuation of the individual wedge bow shocks, impinge along the wedge surfaces causing lateral flow separation⁽¹⁾. In the case of sharp-edged wedges with attached bow shocks, the inviscid flow field including the embedded shock impingement line is conical.

A recent study⁽³⁾ over a wide Reynolds number range showed that the lateral extent of interaction due to shock impingement was considerably larger for laminar than for turbulent flow.

Figures 3A and 3B taken from Ref. 3 are oil flow photographs which show the interaction region in the corner of intersecting $9\frac{1}{2}^\circ$ wedges at a Mach number of 3 for a low and a high Reynolds number, respectively.

Reference 3 points out that separation in Fig. 3A is initially due to laminar shock wave-boundary layer interaction, and the break in the separation line at a Reynolds number of approximately $1/2 \times 10^6$ is caused by boundary layer transition. Beyond transition, the interaction region and separation line eventually assume the pattern for fully developed turbulent flow. Figure 3B illustrates turbulent separation with a considerably narrower interaction region. In this figure, the laminar region is so small that it is virtually undetectable near the leading edge of the model. The sketch in Fig. 3 shows that turbulent separation in this case occurs just slightly upstream of the embedded shock wave.

Another example for a model akin to a corner is given in Fig. 4, taken from Ref. 4, which shows transitional separation due to interaction of the bow shock of a 30° wedge on a flat plate at a Mach number of 5.

CONCLUDING REMARKS

Other investigations of supersonic or hypersonic flow over three-dimensional configurations have exhibited similar distortions in separation lines; however, to the author's knowledge, the association of these distortions with boundary layer transition has not heretofore been made.

In general, a three-dimensional shock wave-boundary layer interaction can be viewed locally as a two-dimensional one with cross flow and mass transfer⁽¹⁾--a result of the scavenging vortex in the three-dimensional case. This interpretation is supported by experimental evidence which shows that the extent of a separated flow region is considerably greater for laminar than for turbulent flow for three-dimensional shock wave-boundary layer interaction as well as for the two-dimensional case. Thus, in retrospect, it is reasonable to expect a sharp change in the flow separation line as a skewed impinging shock crosses a region of boundary layer transition. Conversely, a sharp change in an otherwise smoothly curved separation line on a planar surface is most likely indicative of transition because, in the absence of other disturbances in a flow, there is no physical mechanism whereby a shock generator of simple geometry should produce a distorted separation line.

REFERENCES

1. Korkegi, R. H., Survey of Viscous Interactions Associated with High Mach Number Flight, AIAA Journal, Vol 9, No. 5, May 1971, pp. 771-784.
2. Young, F. L., Kaufman, L. G. II, Korkegi, R. H., Experimental Investigation of Interactions between Blunt Fin Shock Waves and Adjacent Boundary Layers at Mach Numbers 3 and 5, ARL 68-0214, Dec 1968, Aerospace Research Labs, Wright-Patterson Air Force Base.
3. West, J. E., and Korkegi, R. H., Interaction in the Corner of Intersecting Wedges at a Mach Number of 3 and High Reynolds Numbers, ARL 71-0241, Oct 1971, Aerospace Research Labs, Wright-Patterson Air Force Base; also paper to be presented at the AIAA 10th Aerospace Sciences Meeting, 17-19 Jan 1972, San Diego.
4. Kaufman, L. G. II, Meckler, L., and Hartofilis, S. A., An Investigation of Flow Separation on Aerodynamic Controls at Hypersonic Speeds, Journal of Aircraft, Vol. 3, No. 6, Nov-Dec 66, pp. 555-561.

A

B

C

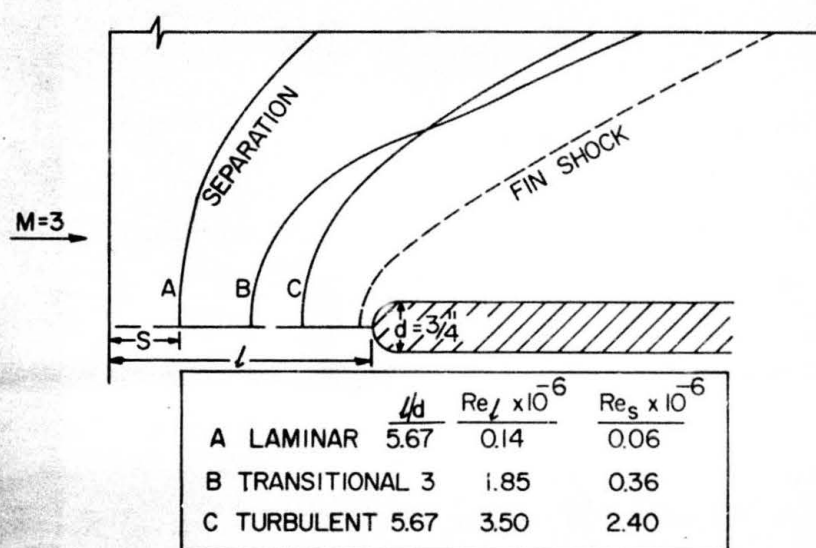


FIG. 1. BLUNT FIN-FLAT PLATE INTERACTION - $d = 3/4$ in.
(oil flow photographs from the study of Ref. 2)

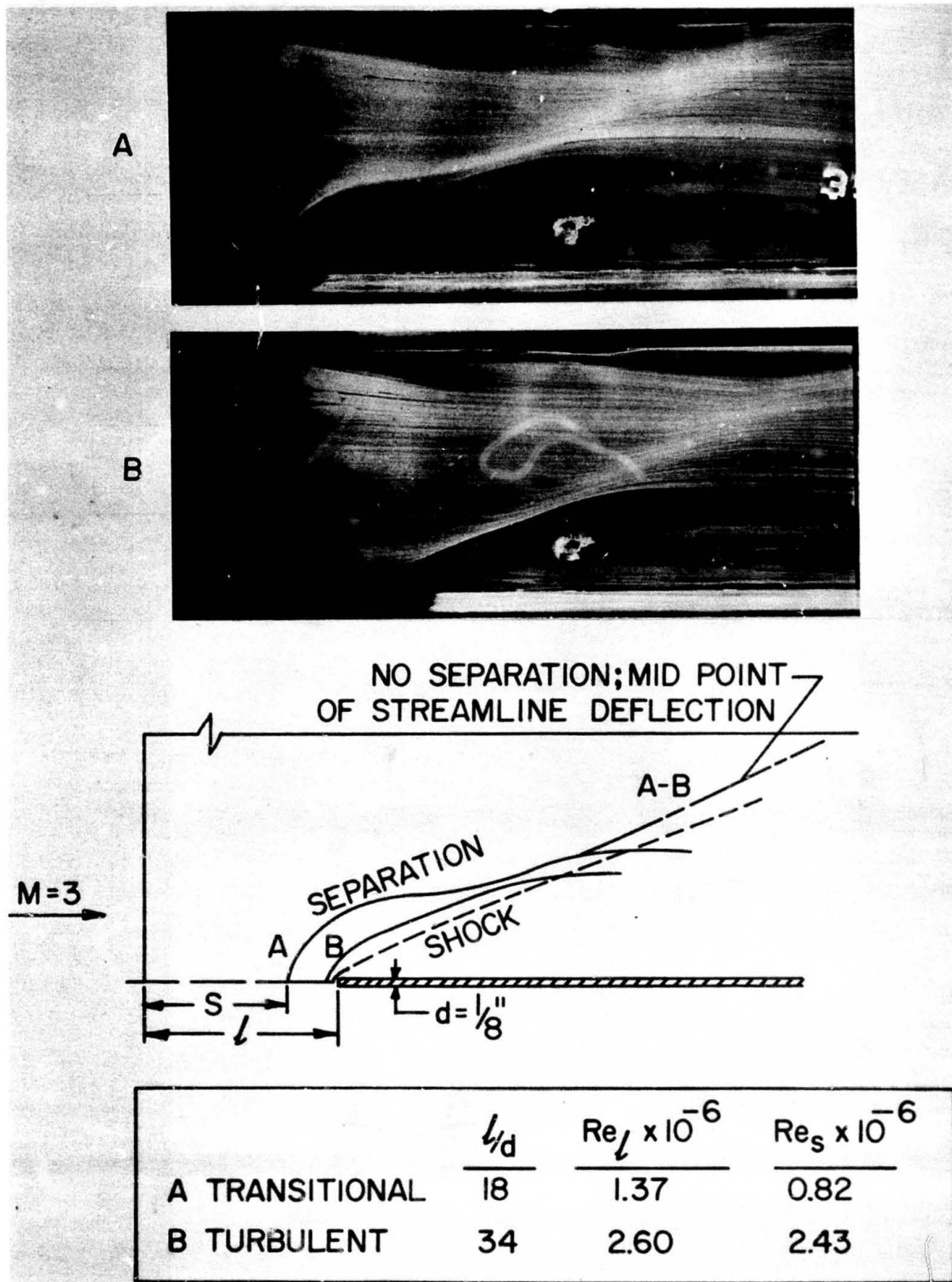
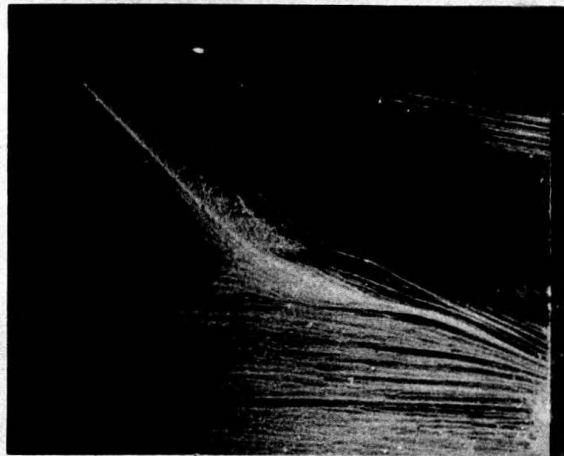


FIG. 2. BLUNT FIN-FLAT PLATE INTERACTION - $d = 1/8$ in.
(oil flow photographs from the study of Ref. 2)



A $Re_l = 1.1 \times 10^6$



B $Re_l = 60 \times 10^6$

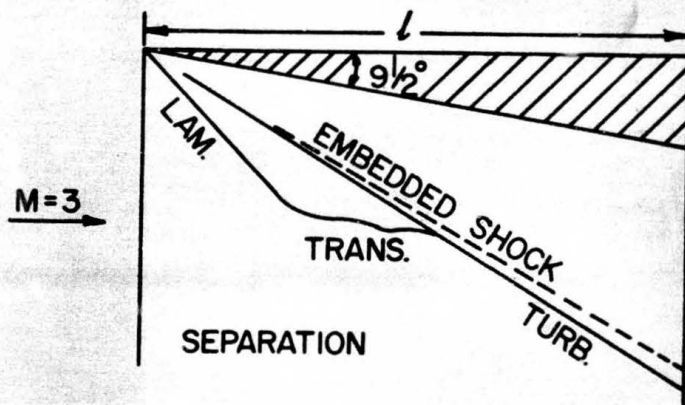
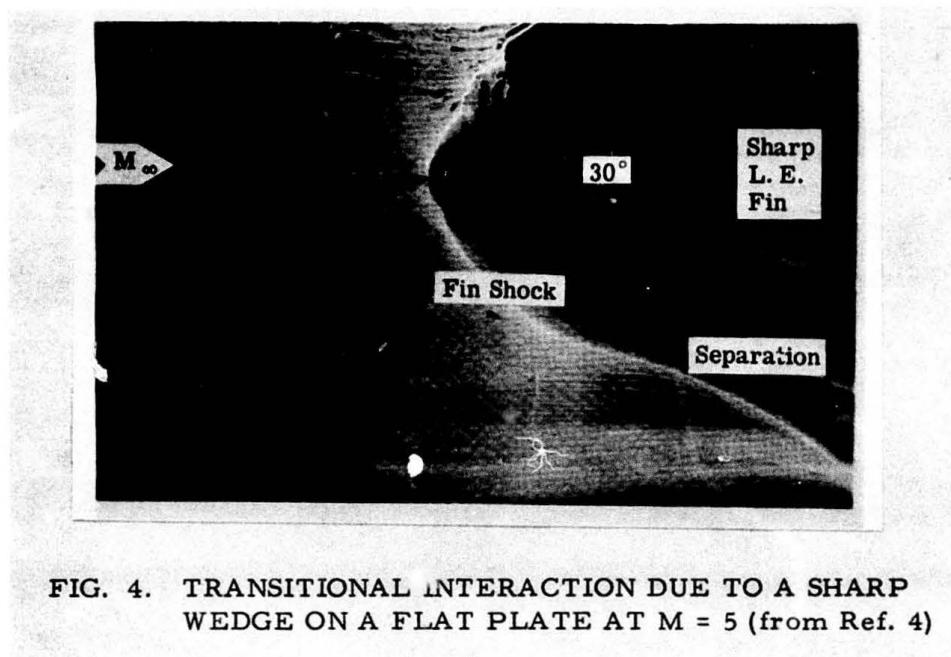


FIG. 3. INTERACTION IN THE CORNER OF AXIALLY INTERSECTING WEDGES (oil flow photographs from Ref. 3)



(This page intentionally left blank)

HYPERSONIC SHOCK TUNNEL TRANSITION STUDIES
(Unclassified)

by D. H. Ross, J. W. Ellinwood and R. L. Varwig

The Aerospace Corporation
Aerodynamics and Propulsion Research Laboratory
El Segundo, California

It is well known that transition Reynolds numbers measured on slender bodies in hypersonic ground test facilities do not correlate with flight observations. This is generally believed to be due to differences in free stream turbulence levels for the two environments. Hence it is important to characterize the free stream turbulence level in hypersonic ground test facilities and to determine the influence of the free stream turbulence on transition. This information might ultimately permit the use of ground test facilities for accurate estimates of flight transition Reynolds numbers.

The Aerospace Corporation program, in this area, consists of three tasks. The first task is to characterize, experimentally, the free stream turbulence in an existing hypersonic shock tunnel. The second task is to apply these data to calculations of linear disturbances in a cone boundary layer stability and mean surface properties. The third task is to experimentally measure mean surface properties on the cone and then to compare the measured location of transition onset with theoretical predictions. The status of these tasks is described below.

TASK 1. Free stream turbulence measurements. Measurements of free stream turbulence have been made at $M_\infty \approx 15$, $Re/Ft \approx 1.6 \times 10^5 - 1.3 \times 10^6$, in a hypersonic shock tunnel using thin film heat transfer gages. Mean heat transfer, and fluctuations, were recorded on magnetic tape as a function of time. The recorded data was then processed by digital computer and selected stochastic functions of the data were machine plotted. This approach represents an extension of the techniques described in Footnote (1) for the

¹D. H. Ross, "Aerodynamic Noise Investigation in a Short-Duration Shock Tunnel," The Shock and Vibration Bulletin, 37, Part 3, Naval Research Lab. Washington, D.C., January 1968.

measurement and analysis of fluctuating flow properties during the approximately 10 millisecond test time of a short duration facility.

Four configurations of thin-film heat transfer gage were employed: two types of wedge gages, a small conical gage, and a small stagnation gage. (See Fig. 1). This figure also shows a portion of a 4" dia., 11 foot long cone-cylinder body with surface heat transfer gages mounted upon it. The body was used in an early period of the program to measure boundary layer transition. One form of wedge gage made at Aerospace employs a painted conductive strip displaced back from the sharp leading edge. The other gages are sputtered film types with the conductive region at the leading edge of the supporting substrate; these are commercially available DISA probes. They were mounted in the tunnel singly or in groups and operated in a constant current mode. The temperature induced resistance changes of the thin film were sensed as voltage changes and amplified by specially developed wideband operational amplifiers.

The development of high-gain, low-noise wideband data recording and signal conditioning electronics formed an important part of this measurement program. Integrated circuit operational amplifier technology was employed for this purpose. A 2 MHz variable gain (1 to 1000) amplifier was developed in which the integrated circuit was mounted on the end of a wafer switch and the passive components selected and switched in for each gain to give optimum bandwidth. Based upon this amplifier, an active analog filter was developed to convert the parabolic temperature time history of the thin film surface gage to a step function whose amplitude represents the heat transfer to the gage. This circuit has a high frequency limit of about 1 MHz, compared to 20-30 KHz for previous passive analog circuits, and represents a net gain in signal strength in excess of 50 dB over the passive networks. This active analog circuit can also be considered to be a compensated amplifier (as in standard constant current hot-wire anemometer practice) with a 10 dB per decade rising characteristic in frequency space.

For each test of a given gage the same output signal was split and amplified or processed ten different ways and recorded on ten wideband FM channels (0 - 400 KHz) of an Ampex FR-1800H magnetic instrumentation recorder. Both the temperature level and fluctuations were recorded. The temperature level was amplified, while this signal was high pass filtered to remove the

mean level and then the resulting fluctuations amplified one or two orders of magnitude more than the mean signal. The same procedure was used with both active and passive heat-transfer analog networks to yield the overall and fluctuating heat transfer values.

The gage surface temperature output of an Aerospace wedge gage for Test 737 will be used to illustrate typical results. Test conditions were $M_\infty = 14.1$ and $Re/Ft = 1.6 \times 10^5$. The gage position was in the test cone $4-3/4^\circ$ from the tunnel centerline. Figure 2 shows a scope photo of the temperature-time traces for four gages mounted in a rake; the following results refer to the lowest trace. The time scale is 2 ms/division, and the signal has been amplified by a gain of 400 prior to recording and display on the scope. The signal was split and, after passing through an 800 Hz high pass (passive) filter to remove the mean signal, was amplified to an overall gain of 20,000 and recorded to determine the signal fluctuations. Figure 3 shows a scope trace of this signal played back from the analog tape and recorded in a scope photo with a time expansion of 10 compared to Figure 2. The time scale is 0.2 msec/div and the amplitude is 0.5 volts/div. (A 150 KHz low pass filter was used in obtaining the playback scope trace). Figure 4 depicts the overall analog-processed heat transfer signal in the upper trace, and a filtered and re-amplified fluctuating signal in the lower trace. The levels of Q_{RMS}/Q_{Mean} range from 1.5% to 3.0% for the tests reduced to date.

The wideband analog magnetic tapes were played through a wideband A to D converter in the Aerospace Data and Computation Center, resulting in a digitized standard format tape. This tape then served as input for a series of digital computer wave analysis programs on CDC 6600 and 6400 computers. A power spectral density plot of the heat transfer fluctuations of Figure 4 is displayed in Figure 5.

TASK 2. Stability theory calculations. A computer program describing the effect of linear disturbances on a hypersonic boundary layer is being developed along lines similar to the program of L. Mack (NASA). The eighth-order system of perfect gas, parallel-flow equations is again integrated from the outer edge to the surface, but the surface conditions are satisfied by iteration logic slightly different from Mack's. The program development is at a stage where neutral stability curves can be generated at any Mach number.

The only results to date have been at Mach number 4.5, to enable comparison with Mack's results at that speed. These results (Fig. 6) show that our program works well at low wave number or frequency and shows that Mack's results are reproducible. Still to be developed is convergence capability at moderately high frequencies. When this is developed we will switch to a Mach number of 11.6 corresponding to experimental cone edge conditions in our shock tunnel. Also to be developed are integrations of fluctuation correlations that reveal changes in mean properties at the surface. Effects of free stream disturbances on boundary layer development will then be investigated.

TASK 3. Cone surface measurements. Heat transfer measurements have been made on the surface of a ten foot cone of half angle 5° mounted in the hypersonic shock tunnel. Results for $M_\infty \approx 15$ and $Re/Ft = 1.5 \times 10^6$ are shown in Fig. 7. The entire transitional flow regime is contained on the cone surface and can be probed further. The unit Reynolds number can be lowered a factor of two and still have natural transition begin on the cone. These measurements of mean heat transfer will be compared with the theoretical predictions based on correlations of the linear disturbances, when the latter are available.

CONCLUSION

It has been demonstrated that measurement and analysis techniques have been developed to measure the free stream turbulence environment of a hypersonic shock tunnel in terms of the heat transfer to a thin film resistance gage. It has also been shown that laminar, transitional and fully developed turbulent boundary layers can be produced on the surface of a conical model positioned in that tunnel. It is planned to extend the mean and fluctuating measurements over a wider range of parameters in the free stream and within the boundary layer of the cone. In addition, efforts continue to utilize machine computation results of linear stability theory to account for significant features of the measurements and to help elucidate the role of facility free stream turbulence in the transition process.

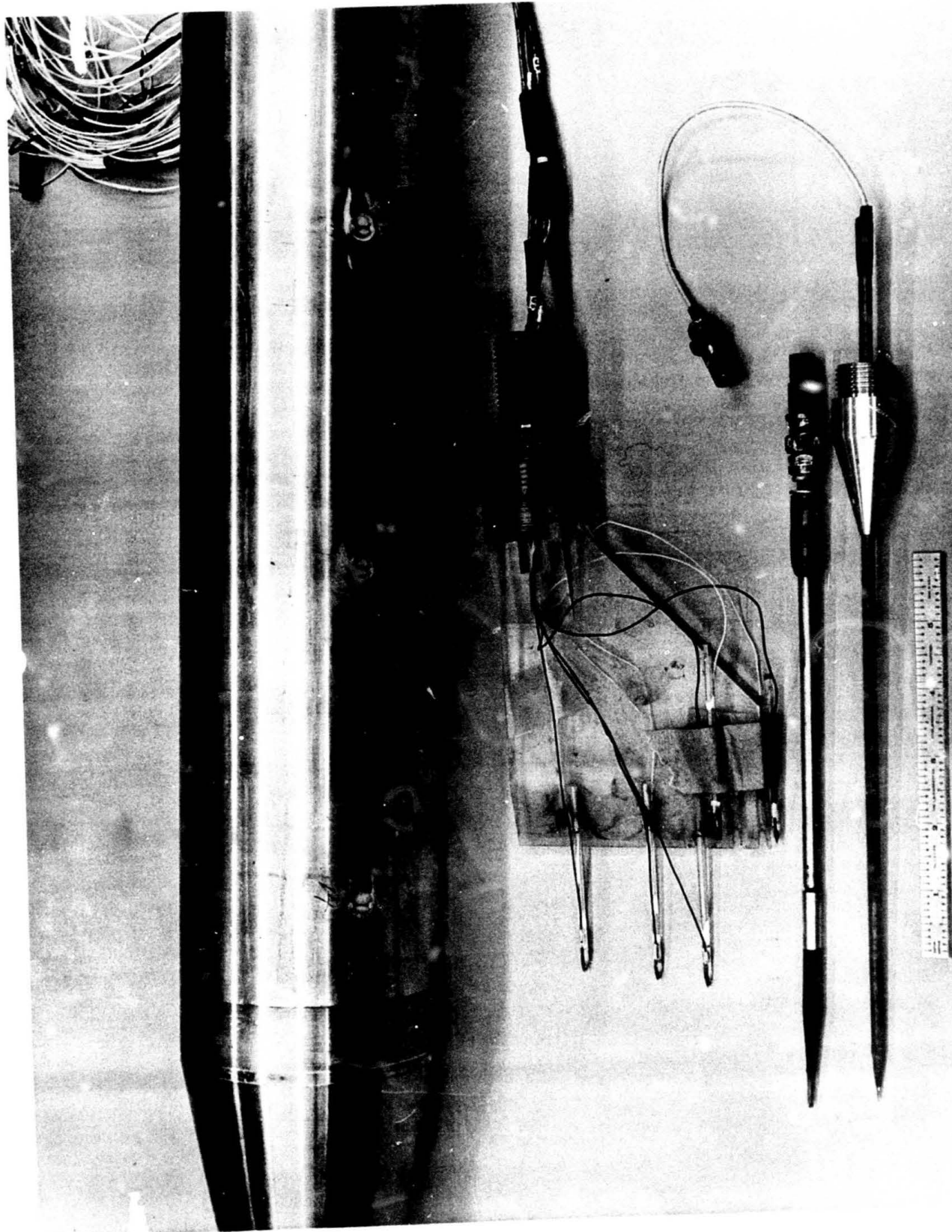


FIG. 1. HOT-FILM PROBES AND CONE-CYLINDER MODEL. Individual hot-film probes and a rake of probes appear at the bottom, and a 4 inch diameter cone-cylinder model with surface mounted film gages is shown at the top of this photo.

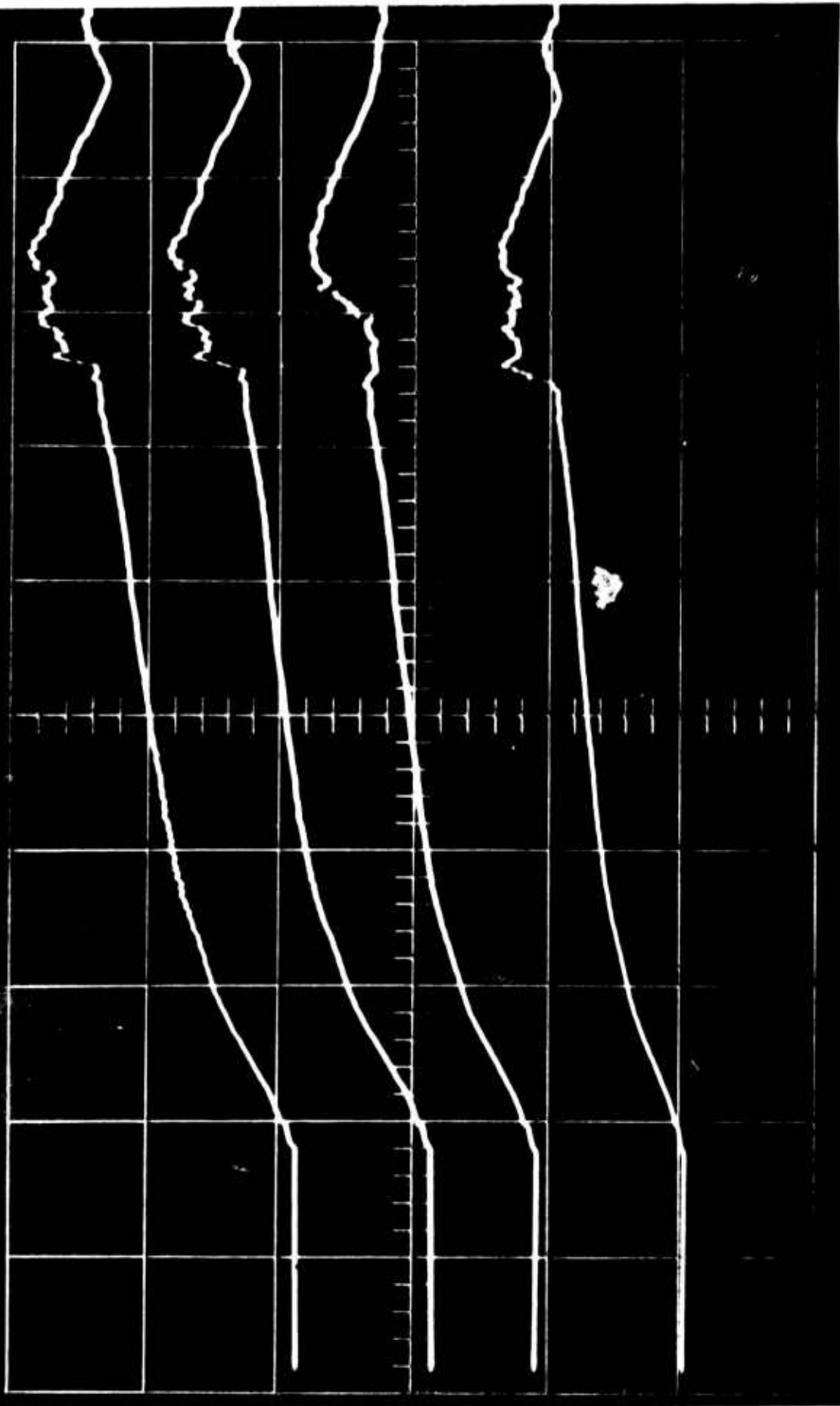


FIG. 2. SURFACE TEMPERATURE TRACES. The roughly parabolic temperature-time traces from an array of four probes appears with a time scale of 2 msec per large division.

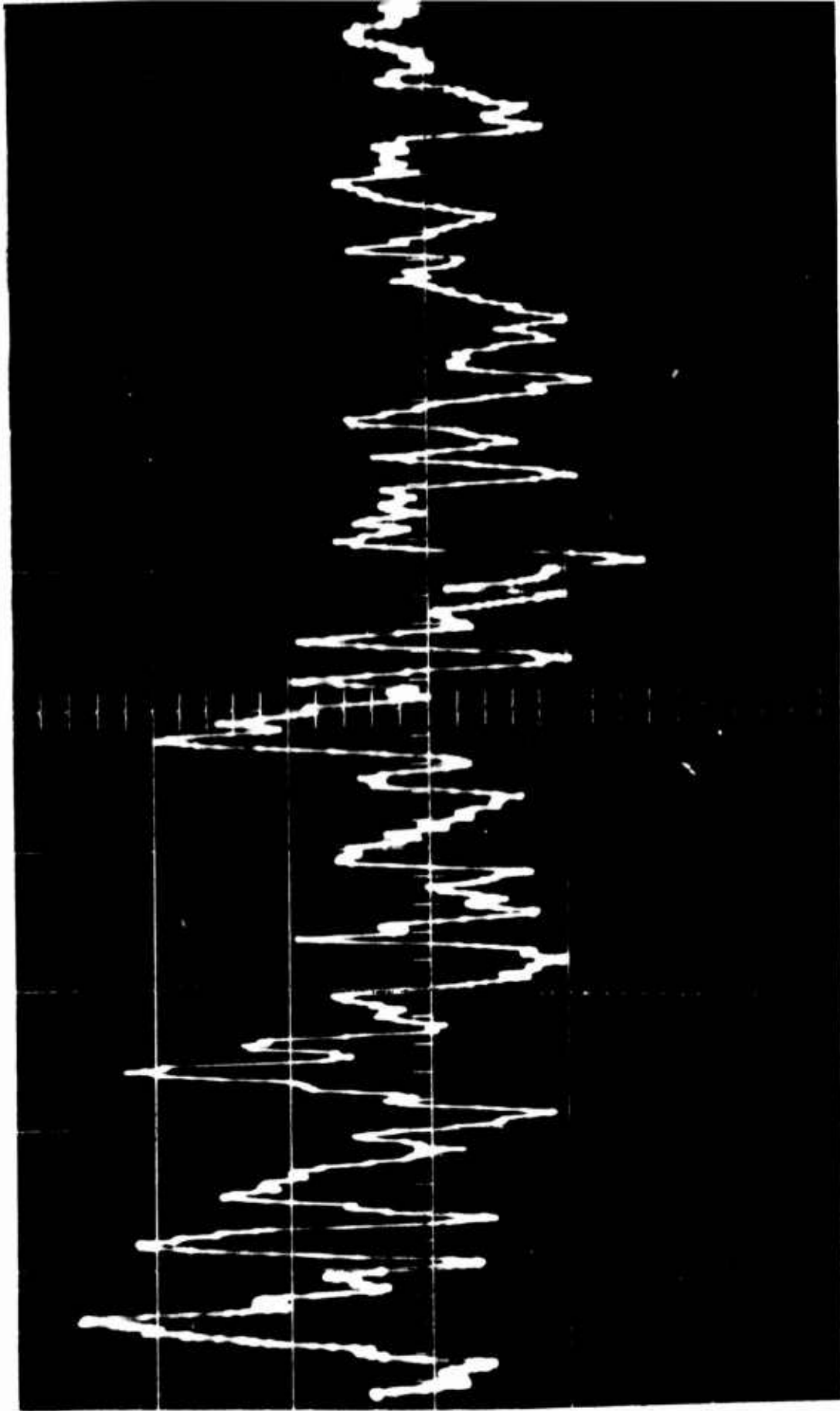


FIG. 3. EXPANDED TRACE SHOWING PROBE TEMPERATURE FLUCTUATIONS. High pass filtered and re-amplified signal showing fluctuations is signal of Fig. 2 at time scale of 0.2 msec per large division.

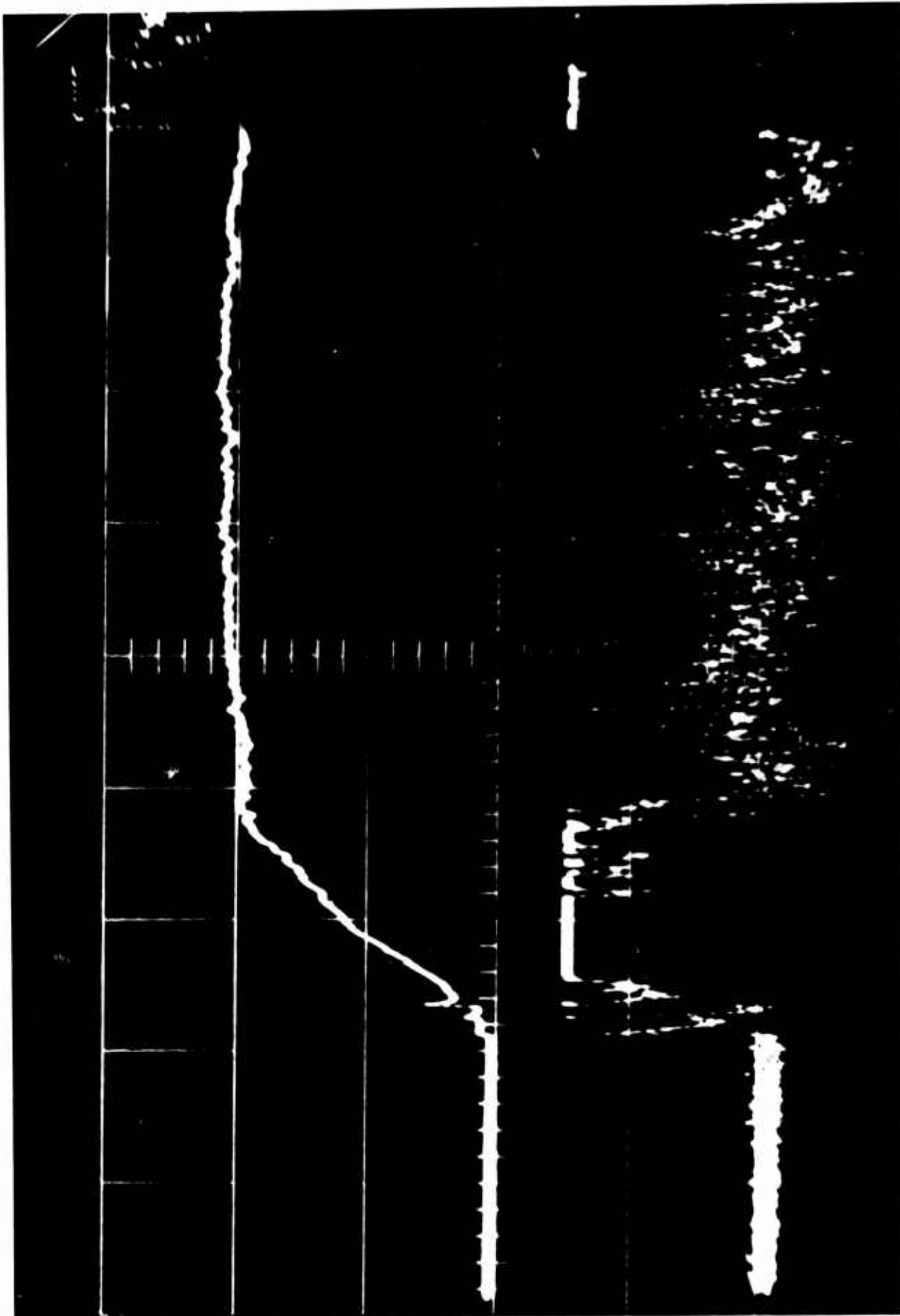


FIG. 4. ANALOG PROCESSED HEAT TRANSFER AND FLUCTUATIONS. Upper trace represents mean heat transfer to wedge probe and lower trace the amplified fluctuations. Time scale 2 msec per large division.

PERSONIC SHOCK TUNNEL FREE STREAM TURBULENCE

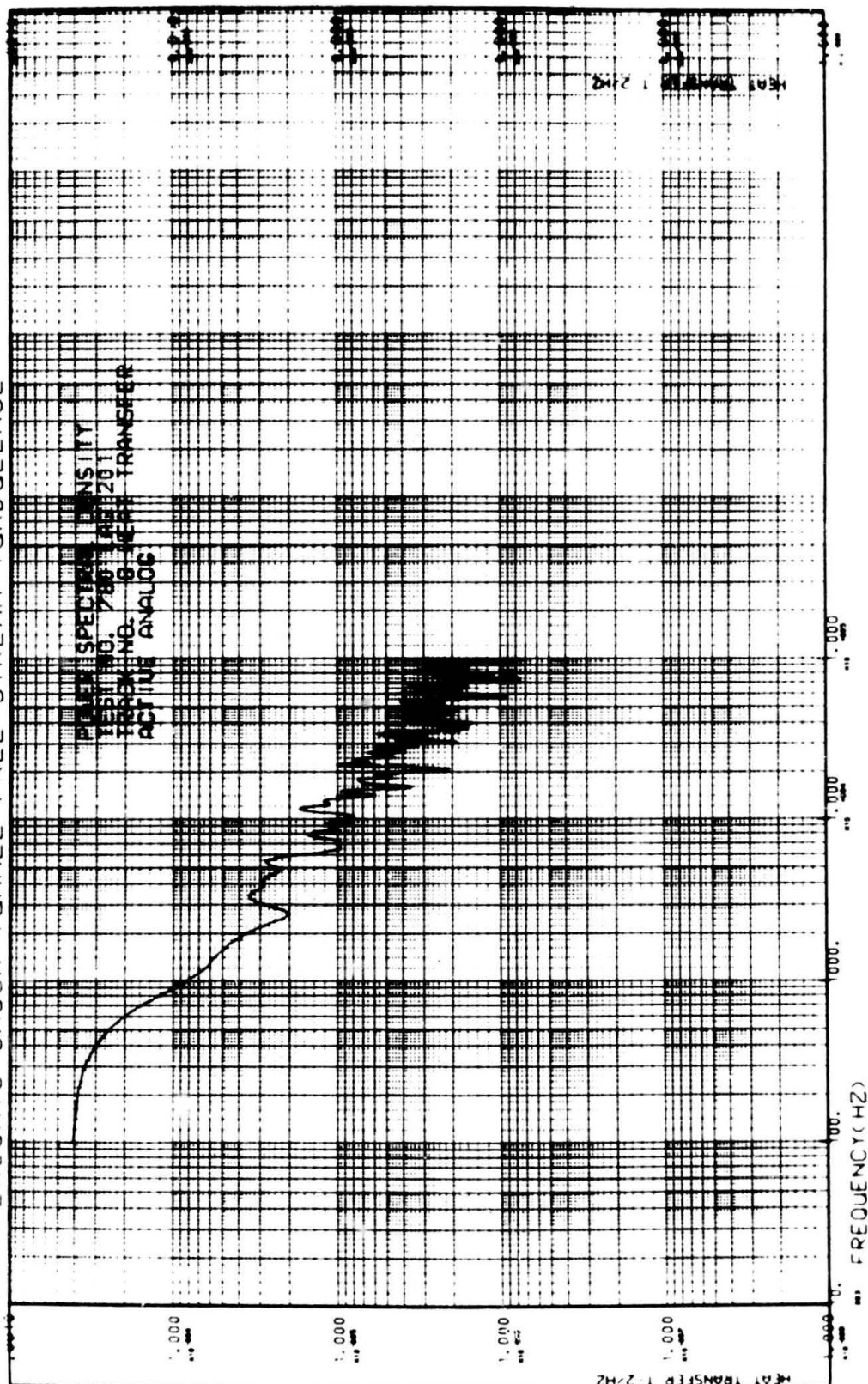


FIG. 5. POWER SPECTRUM OF FREE-STREAM TURBULENCE. (Q^2/Hz) vs frequency in free stream $M_\infty = 14.1$.

COMPRESSIBLE STABILITY THEORY $M = 4.5$

UNYAWED DISTURBANCES
INSULATED FLAT PLATE

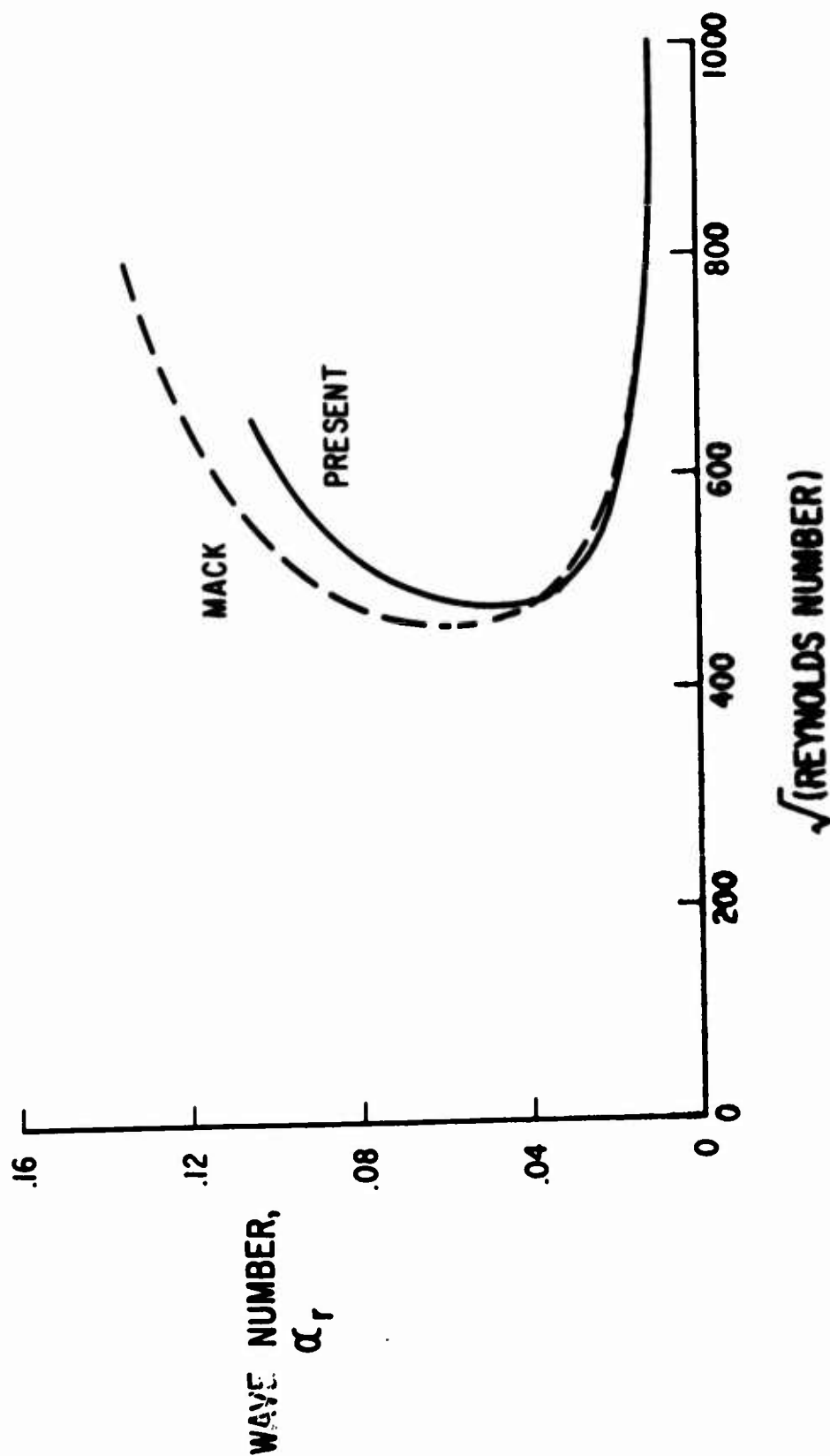


FIG. 6. STABILITY DIAGRAM. Comparison of neutral stability curves as computed by Mack and by Ellinwood.

CONE TRANSITION MEASUREMENTS

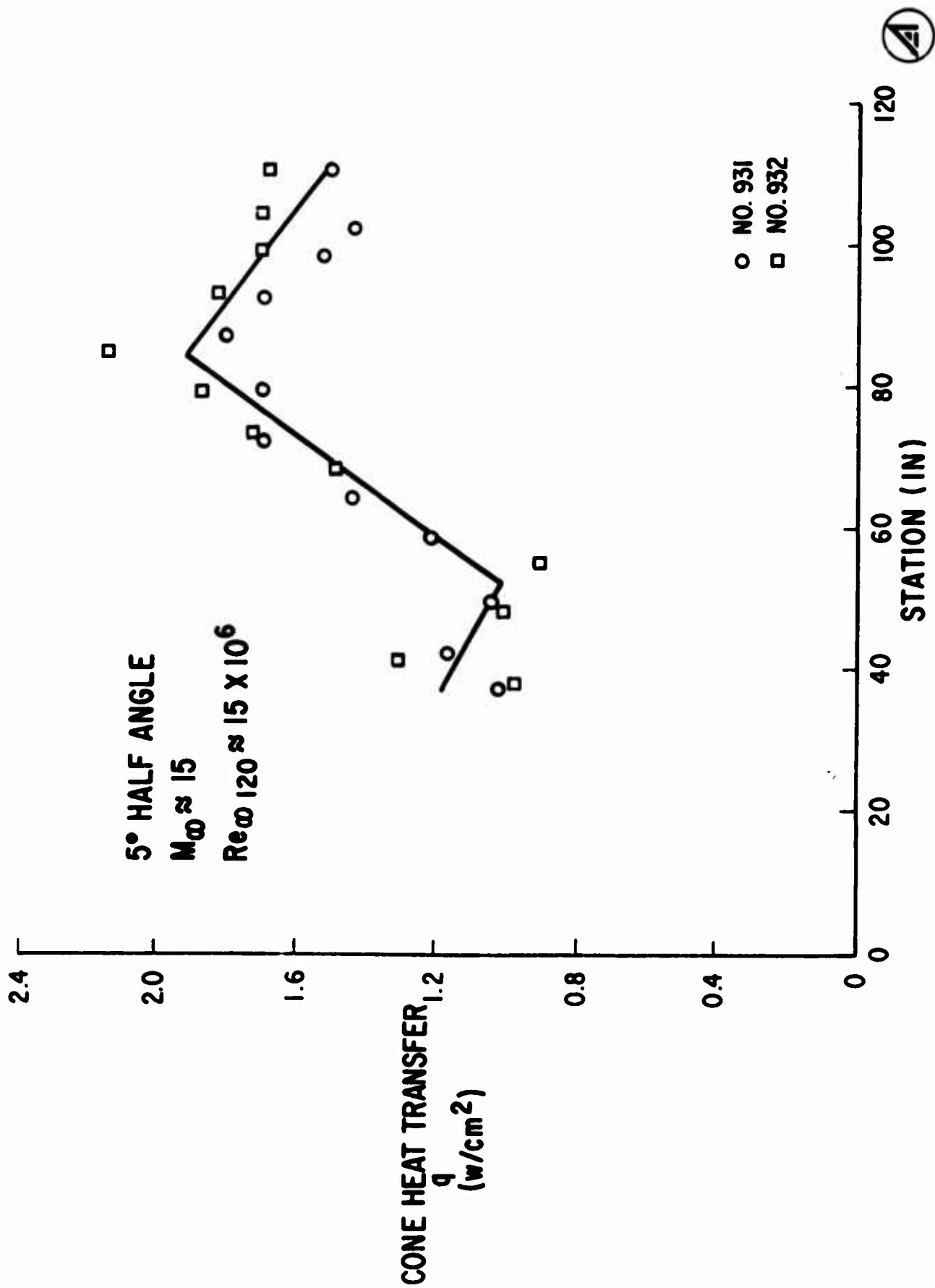


FIG. 7. STEADY STATE HEAT TRANSFER ON CONE MODEL. The laminar, transitional, and turbulent boundary layer regimes are shown.

(This page intentionally left blank)

SECTION 9a

OPEN QUESTIONS - TRANSITION TO TURBULENCE AT HIGH SPEEDS, 1971* (Unclassified)

by Mark V. Morkovin

MMAE Dept., Illinois Institute of Technology, Chicago, Ill. 60616

ABSTRACT (Unclassified)

The shock of the 1967 Boundary-Layer Transition Study Group Conference (AF Rpt. No. BSD-TR-67-213, Vols. I-IV, W. D. McCauley, Editor) started many repercussions in our national attempt to cope with the dilemmas it bared. From the vantage of the author's 1971 reevaluation of the scientific and practical problems (Ref. 5), a succinct recapitulation of the salient aspects of transition is first presented. The up-to-date unclassified information is then compressed into twenty-two observations which are quite inconsistent. Four groups of targets for longer-range transition research are then identified and speculated about. The main objective of the paper is to provide concise background information and some stimulus for the discussions of the various Committees at the Workshop.

*Supported under USAF OSR-Themis Contract F 44620-69-C-0022, Mechanics Division.

INTRODUCTION

For supersonic and hypersonic vehicles the absence or occurrence of transition to turbulence often becomes a primary design consideration. Yet testing facilities cannot duplicate the corresponding environmental design conditions and the designer must rely on extrapolations, generally with several parameters varying simultaneously. This "working paper" attempts to clarify what type of information appears currently most desirable for longer-range objectives of rational design for transition.

Most of the information, on which the paper rests, has been described and documented in the USAF sponsored "CET" (Ref. 1, which has an Index), in "MM" (Ref. 2)*, and in Mack (Ref. 3), where the reader will find specific details and references. Newer information has been compiled for a briefing to the NASA Advisory Research Subcommittee on Fluid Mechanics (unpublished) and for the forthcoming volume of Advances in Aerospace Sciences, edited for Pergamon Press by D. Küchemann (Ref. 5).

CET (Ref. 1) represented an approximate 1968 consensus of some sixty researchers in high-speed stability and transition, experimental and theoretical. The groundwork for that consensus was laid here at the Aerospace Corporation in 1967: Ref. 6. This paper succinctly recapitulates key concepts and findings of the earlier consensus, weaves in the newer data, and speculates about the consequences and prospects. Perhaps it will be of use for the deliberations of the Committees at this Workshop. For that purpose each subtopic is numbered separately for easy specific reference.

1. FACTORS IN HIGH-SPEED TRANSITION

(1.01) Boundary-Layer (BL) instabilities comprise a group of runaway phenomena in which disturbances are selectively amplified by factors of 100 - 10,000 before self-regenerative wall turbulence sets in.

(1.02) Criteria for self-regeneration of wall turbulence (intensity, scale, phase relations; existence of minimum Reynolds numbers, R_{min} , for guaranteed growth or decay; relaminarization of turbulent shear layers) are barely discernible at low speeds and completely unknown at high speeds.

*The Mack-Morkovin lectures are now available on tape, with all the supporting material: Ref. 4.

(1.03) Theory and experiment indicate a multiplicity of competing runaway modes (generalized Tollmien-Schlichting waves - 2Dim. TS mode; Mack's higher "acoustic" modes; oblique waves in 2D boundary layers, more unstable at supersonic speeds; modes associated with streamwise vorticity of mean shear layer - cross-flow modes; nonlinear vorticity stretching and deformation of 3D patterns behind roughness; vorticity stretching in accelerated layers; etc.) each of which can dominantly or cooperatively with others grow to the self-regeneration threshold and generate a local turbulent spot at a position x, z, t , (y being normal to BL and z spanwise). See the instability-transition flow chart in Fig. 1.

(1.04) The relative distribution of unsteady free-stream disturbances (vorticity \equiv turbulence; temperature-density-entropy spottiness; sound) and their relative 3D spectra (characteristics which are extremely difficult to measure) apparently determine which of the modes dominate the growth to transition in a particular boundary layer at a given Mach number, M , Reynolds number, R , cooling ratio, H_w/H_r (enthalpy or temperature at wall to that at recovery conditions), for a given streamwise and lateral pressure gradient, three-dimensionality of the mean layer, wall ablation or transpiration rate, \dot{m} ; etc.

(1.05) The process of assimilation of the free-stream vorticity, entropy fluctuation, or sound, into the various unstable modes (1.03) (BL receptivity or transfer function) remain essentially unexplored, theoretically or experimentally.

(1.06) The parameters or Operation Modifiers, (Fig. 1), cited in (1.04): M , R , H_w/H_r , $p(x)$, $p(z)$, 3Dity, \dot{m} , etc., determine the mean BL profiles, and through them, (often rather sensitively) the amplification rates of the different competing runaway modes of (1.03). For small (linearizable) disturbances, amazingly rich functional dependence on M , R , and H_w/H_r , of the selective amplification rates has been partially charted by Mack (Ref. 3) for $M \leq 10$ (quasi-parallel assumption) and quantitatively verified on an adiabatic flat plate at M of 4.5 by Kendall in the acoustically aseptic Jet Propulsion Laboratory supersonic wind tunnel. (No other tunnel currently has acoustically nonradiating laminar sidewalls at R 's of interest.)

(1.07) No comparable high-speed theoretical information exists on the effects of the other operation modifiers, $p(x)$, $p(z)$, $3Dity$, \dot{m} , etc., either singly or in various combinations.

(1.08) Roughness elements, 2D, 3D, single or distributed, are not "true disturbances" but rather passive operation modifiers, which alter the profiles (even causing local separation) and hence the amplification rates of the assimilated free-stream disturbances. At low speeds, single 3D roughness elements may bring about locally unstable motion, which even though vigorous, remains below the threshold of self-regeneration, see (1.02). When the disturbed motion decays, vigorous or not, the roughness effect is called subcritical (with respect to the whole BL, rather than local profiles). A slight increase in unit Reynolds number, R/L , may then cause the local unstable motion to change to a sequence of self-regenerative turbulent spots, growing into a turbulent wedge - the supercritical behavior.

(1.09) At high and low speeds, an increase in wall cooling (decrease in H_w/H_r) which is stabilizing on smooth walls (first mode of the linear theory - see (1.10) - and substantial verification of transition trends at lower M 's) may cause a shift from subcritical to supercritical role of roughness elements. Since the transition distance with increasing cooling then stops growing and starts moving toward the leading edge one speaks of transition reversal in presence of roughness.

(1.10) The cited functional richness of Mack's solutions (1.06) includes a distinctly different response of his higher acoustic modes and the first mode (1.03) to changes in the cooling ratio H_w/H_r . While the first mode is stabilized by cooling, the higher modes actually become more amplified and shift to higher frequencies. Therefore, the input spectra not only influence which competing mode may dominate transition, as in (1.04) but also which mode governs the transition sensitivity to cooling. Reshotko (Ref. 7,8) pointed out on dimensional grounds that it may be difficult to escape the higher modes in steady-flow hypersonic wind tunnels, while they may have little relevance to the boundary layers on bodies in ballistic ranges. If so, one would expect differences of transition behavior with H_w/H_r in these facilities.

(1.11) An additional significant characteristic length enters most of the practical configurations at high speeds: the nose or leading edge

"thickness", which generates a shockwave and, through the subsequent entropy blanket, modifies the mean BL properties until the layer grows sufficiently with x to "swallow" the entropy layer (x_{sw} , the swallowing distance). For such bodies, transition is again sensitive to a combination of functionally distinct Reynolds numbers, and hence to the dimensional unit Reynolds number R/L . (Empirically, small and moderate nose blunting tends to move transition downstream.)

(1.12) Configurations for which B. development is nonsimilar because of geometry, pressure gradient, boundary conditions (e.g. decreasing $H_w(x)$ in the heated-nose effect), etc., essentially harbor additional characteristic lengths which also tend to make Reynolds-number scaling R/L dependent.

(1.13) Once a turbulent spot is formed in laminar surroundings, it moves downstream while growing in all directions. The lateral or transverse growth (contamination) of a turbulent spot or wedge decreases from about 11° semiangle at low speeds to about half the angle at hypersonic speeds. As a nonlinear turbulent process it is essentially R independent, in contrast to the linear amplification region. Two turbulent spots or wedges, growing side by side, apparently grow into each other without an increase in lateral growth rate.

If R_{xB} denotes the Beginning x (nondimensionalized) at which the first turbulent spots are generated, the region over which additional spots are seeded and over which they grow until the laminar patches disappear at R_{xE} (end), may be extensive. The length of the transition region may be significant for design: $R_{xE} - R_{xB} = C R_{xB}$, where C may range from 0.5 to 2.0, with $C \sim 1$ commonly observed in wind tunnels. All the preceding observations are empirical - there is no theory of transverse contamination.

2. INDETERMINACY OF HIGH-SPEED TRANSITION, PARADOXES, AND DISCREPANCIES

(2.01) As a runaway phenomenon of multiple competing modes, (1.03), feeding in an unknown manner, (1.05), on unknown input mixtures of disturbances with nonwhite 3D space-time spectra, (1.04), transition is intrinsically non-deterministic. (By contrast high-Reynolds-number turbulent layers are quasi-deterministic on larger, average scales, except near separation - Ref. 9.) Any

design predictions should take into account in some way the disturbance environments of the operational vehicle and of the facilities from which the transition information is obtained.

(2.02) The mean properties of the BL in question are seldom measured or well enough computed. Hence, additional uncertainties-and causes for discrepancies between experiments - often creep in. (Mack's linear theory (1.06) indicates that amplification rates are occasionally very sensitive to temperature profiles.) In many experiments, especially flight tests, one does not even have information on BL thicknesses δ^* or θ .

(2.03) In a given family of facilities, such as continuous wind tunnels, ballistic ranges, or shock tubes (Ref. 10) the unknown unsteady and steady disturbances tend to evolve in more or less repeatable group patterns - unless willfully modified when testing for sensitivity to disturbances, e.g. Fig. 2, borrowed from Spangler and Wells (Ref. 11). For a given model shape, the large number of potentially independent parameters characterizing the unsteady and steady disturbances (1.04), (2.02), are then hidden. Their combined effects blend with those of the amplification controlling parameters and appear as variations in R_{xB} with M - and with the trouble-indicating dimensional parameter R/L , (stagnation pressure). Observed repetition of "similar" R/L variations creates a temptation to lump the factors (1.02) - (1.07), (1.11), (1.12) into a mythical single "Unit R Effect" and approximate it by the simplest power formula: $R_{xB} \sim (R/L)^n$, n an empirical constant. The pressing needs of the designer may justify such procedures for a current design, but hardly endow it with general research validity.

(2.04) In the same facility the exponent n generally takes on different values even for simple shapes like 2D wedges or hollow cylinders, sharp cones, and wedges with sweepback (the corresponding n variation being roughly from 0.6 to 0.1 in "noisy" hypersonic wind tunnels). This testifies to the fact that R/L variation represents a combined response to many factors.

(2.05) For a given model, transition moves upstream as R/L increases, even for $n \sim 0.6$. Physical considerations make one doubt that the power formula could continue to hold generally: the experiments in a given facility seldom span factors of R/L more than 12-15. In fact, there are

hypersonic wind tunnels (Softley, Ref. 12a,b; Mateer and Larson, Ref. 13; Neal, Ref. 14) where at some operating conditions the R/L dependence disappears while it is present at others. For applications, credible extrapolations (!) rather than interpolations are needed.

(2.06) Since much of high-speed transition research consists primarily of "macroscopic" detection of R of transition (some value between R_{xB} and R_{xE} , depending on technique and facility) as function of M and R/L, for nominally fixed H_w/H_r , and for normal facility constraints, a number of investigators in NASA, ARO, etc., feel that the information is inadequate to separate the "true" M and R variations, i.e. those corresponding to a free-stream without group variation of disturbance parameters. Some feel that the so-called M bucket (minimum of transition R near $M \sim 4$) reflects primarily the ignorance variation with R/L (see MM Sections H and I). Lester Lees does not expect the issues to be clarified until enough of "microscopic" transition research is carried out which would trace the distinct effects of disturbances and amplification rates (CET, Section I).

(2.07) Kendall's evidence from JPL "quiet" tunnel (which can be made willfully noisy by tripping of sidewall boundary layers), the Pate-Schueler 2D correlations (Ref. 15), and Pate's cone correlations, (Ref. 16), make it clear that for $3 < M < 8-10$, transition in wind tunnels tends to be dominated by powerful acoustic disturbances radiated from the turbulent sidewall boundary layers. The intensity, scale, and spectra of this radiation, its interaction with the bow shock wave, and its assimilation within the laminar layer in question (with its own scales and receptivity) certainly depend on M and a number of distinct characteristic lengths. The processes are exceedingly complex as this afternoon's presentations by Kendall and Mack will undoubtedly demonstrate. Earlier evidence indicated that generalized TS waves, etc., (1.03), may be growing in presence of sidewall sound irradiation, but that they are probably not the primary mechanism responsible for "irradiated" transition. The new hot-wire evidence of Kendall, (Ref. 17), seems to point to three-dimensional non-linear processes. Closer quantitative comparisons with Mack's new computations of directly driven, non-TS, disturbance growth, (Ref. 18), will be needed to ascertain which part of the development this new linear theory can match. In "noisy" wind-tunnels for $M > 3$ perhaps one should look to this new

theory rather than to the free TS modes for a rational guide to parameters which govern amplification (or to both?).

(2.08) The "sound-radiator" correlations of Pate and Schueler and of Pate show that, when cast as R_{xNE} (near end of transition) versus R/L , they account for most of the observed power variations, (2.03). Similarly, for a fixed R/L , the M variation appears consistent with expectations. Consequently, one might expect that if the irradiation were removed, the peculiar R/L dependence would disappear for cones and flat plates.

The quantitative verification of Mack's linear theory at M of 4.5 by Kendall, (1.06), was carried out under such circumstances where the r.m.s. pressure fluctuations were in fact decreased by factors from 50 to 100 from the "noisy" conditions for the relevant frequencies above 1000 Hz. While it appeared that these modes, which were stimulated by Kendall on purpose, grew according to the theory, one can only assume that transition would generally take place as a downstream development of such modes if left to itself: "natural" transition was never reached in the "quiet", laminar-sidewall condition.

(2.09) The only way that similar sound disturbances could be affecting a vehicle in atmospheric flight would be through the partially known mechanism of interaction of atmospheric free-stream turbulence and temperature-entropy spottiness with the bow shock (Chapter 3, Ref. 5). It is not presently certain that such atmospheric disturbances of sufficiently large amplitude exist down to the small scales relevant to vehicle boundary layers, CET, Appendix 2. One would be tempted to conjecture that transition Reynolds numbers based on hypersonic-tunnel information are low compared to those in atmospheric flight - unless a new set of effective disturbances took over the dominant seeding role.

(2.10) In 1957, flights in atmosphere revealed the "early blunt-body transition", i.e. transition in the nose region of cooled axisymmetric blunt bodies, which was previously considered stable on the basis of the usual linear theory. It is still the implication of CET Refs. 17, 140, 222-223, that unless surface roughness is reduced below 5 microinches r.m.s., a designer should expect transition at Reynolds numbers (based on momentum thickness θ) of 150-250 for free-stream R/L on the order of 10^8 /inch in flights with sub-

stantial cooling. (This is often called the blunt-body limit.) Apparently, there is enough energy in atmospheric free-stream disturbances at small enough scales to excite the nose boundary layer, made three-dimensional by roughness, and possessing high density near the wall because of cooling. While one can conjecture that the dominant destabilizing effect is one of stretching of streamwise vorticity disturbances, the mechanism remains unknown and outside of the realm of the generalized Orr-Sommerfeld equations. Such transition mechanisms not corresponding to linear theory will be referred to as bypasses.

(2.11) Clearly, a designer must document experimentally all the bypasses which can possibly be present for his configuration before he can rely on linear theory, even for guidance. Systematic "spoiler" testing in ground facilities with on-purpose roughness, non-uniformities etc., somewhat larger than realistically anticipated to occur in the unclement flight environment, is in order. Only after such preparation are the usually much less informative flight tests indicated - for checking environmental conditions not otherwise obtainable.

(2.12) Flight tests in ballistic ranges (cleared of dust; with long settling time) by and large remove the combination of free-stream disturbances plaguing the hypersonic wind tunnels. In accordance with (2.08), one would expect a substantially increased R_{xB} , unless another bypass rose out of the "noise level", as the front-runner disturbances are discarded. Potter's results (Ref. 19) on 20° total-angle cones with 0.005 inch nose radius, however, exhibit lower transition Reynolds numbers, CET, Section IV, 3. Furthermore, Potter observed an R/L variation similar to those in wind tunnels, even though the dominant turbulent radiation of Pate and Schueler, with its R/L dependence, was not present. The dilemma of the lower transition R and the $(R/L)^n$, $0.6 < n < .7$, variation of Potter remain unreconciled. (Two factors may be relevant: the cones were rather cold, T_w/T_f of 0.18, and the unit Reynolds number moderately high, R/inch of $1.22 \cdot 10^6$.) One could speculate with respect to the possibility of transition reversal, (1.09), nose disturbances, (see Jedlicka, CET, Ref. 114), and other so-called auto-disturbances in highly stressed models.

Sheetz' independent verification of the R/L effect of Potter in the NOL Ballistic Range was cut off after six shots, Ref. 20. The contrast between

Potter's results and Sheetz' small sample is tabulated below in terms of local properties at edge of BL.

	M_e	$R/in \times 10^{-6}$	T_w/T_r	Nose rad.	Cone angle	R/L power, n
Potter	4.4	0.7 - 4.3	0.18	0.005 in.	20° total	.6 - .7
Sheetz	6.9	1.1 - 11.6	0.11	0.001 in.	10° total	.2+

Since the techniques of determining R_{tr} appear similar, the substantial difference in the R/L sensitivity poses further questions as to its causes. Potter will undoubtedly have wiser comments on this in his presentation (Ref. 21) than any speculations the author might adduce.

(2.13) Strong arguments have taken place between experimenters as to whether transition is sensitive to the cooling ratio H_w/H_r at M 's > 6.5 (CET pp 50-52 and Chapter 9, Ref. 5). Little sensitivity is found in near-continuous hypersonic tunnels, where, however, transition is likely to be dominated by sidewall sound, e.g. Sanator et al, Ref. 24. A partial collection of published temperature-sensitive transition data is shown in Fig. 3. It includes the "insensitive" sample of Sanator et al, the recent information of Mateer (Ref. 22) and Maddalon (Ref. 23), as well as a typical "re-reversal" behavior of Richards and Stollery (ref. 25) and Wisniewski and Jack (Ref. 26). In the NOL ballistic ranges transition reversals - for highly polished bodies, but cold and at relatively high R/L values - are inferred for the full explored range $0.02 \leq H_w/H_r \leq 0.26$. Sheetz' newly discovered R/L sensitivity (2.12) is mild so that the transition reversal of his earlier experiments (Ref. 27) apparently remains.

The cluster of points near T_w/T_r of 1.1 on the extended Maddalon curve in Fig. 3 indicates a new type of reversal - with heating, which is also implicit in the work of Wagner et al (Ref. 28) in the same $M \sim 20$ helium wind tunnel.

(2.14) Rhudy and Whitfield (Ref. 29) raised the possibility that some of the reversals in Fig. 3, e.g. those in gun tunnels and ballistic range, might be associated with the time-dependent gradient of wall temperature $T_w(x)$, as per factor (1.12), an effect not specifically investigated at supersonic speeds. Controlled hot-lip experiments at low speeds (McCroskey and Lam, Ref. 30; Cebeci and Smith, Ref. 31) demonstrate that the effects

can be large - but stabilizing! In effect, the wall farther downstream was absorbing the heat liberated at the nose. Cebeci and Smith used a non-similar boundary-layer program to generate the evolving profiles (just like Rhudy) and tackled the stability problem on a quasi-parallel, x-independent basis. The linear theory confirmed well the experiments!

(2.15) It was thought of interest to relate the Wisniewski-Jack double reversal to published unclassified flight-test information on cones, which are presumably free of acoustic irradiation: Fig. 4. The same information in terms of local Re_{tr} and local M is presented in Fig. 5, this time compared to tests on the same 5° ^{cone} total-angle in six different wind tunnels. Discussion and more specifics of the reversals of the Merlet-Rumsey and Rumsey-Lee flights are found on pp 48-49 of CET. As related on p 47 of CET, a series of flight tests with different degrees of high surface polish convinced the NACA personnel that even 6-10 microinches, r.m.s., of surface roughness could have substantial effects on transition. The reversals were suspected to be such effects. It would be interesting to have the different roughness correlations applied to these cases.

(2.16) It has been hoped that if regions of overlap of M , R , and T_w/T_r can be achieved between ground facilities, much could be learned and explained. Lemcke, Naysmith, Picken, and Thomann (Ref. 32) and Naysmith (Ref. 33) report agreement of laminar and turbulent heat transfer rates but not of R_{tr} between the flight of Jaribu MK.2, a parabolic-nose vehicle, and wind-tunnel tests at the Swedish FFA, despite "almost perfect aerodynamic simulation" at $M_\infty = 7.17$! For that condition, the flight T_w in the laminar region hovered around $0.37 \cdot T_t$ and R_∞ (based on 0.5 ft. diameter) was 5.32×10^6 while in the tunnel T_w/T_t were 0.43 and 0.32, and R_∞ was 5.10^6 . R_{tr} (based on local conditions) in the presumably acoustically contaminated tunnel, even at $\alpha = 5^\circ$ remained above 10^6 , while in flight R_{tr} was below $0.5 \cdot 10^6$, i.e. extremely low with respect to any values in Figs. 4 and 5. Since the actual flight model was tested in the tunnel (using the flight sensors) the surface roughness were "the same". The biggest difference was in the stagnation temperature T_t : flight $2115^\circ K$ vs. tunnel $700^\circ K$. The authors make an indirect, fairly plausible case for the vibration of the rocket-motor as the culprit. See further discussion in Section 9.9 of Ref. 5.

(2.17) Yet another high-Mach number flight program ($M_\infty > 10$, unspecified; $M_e \sim 6.1$) did not produce very high transition Reynolds numbers: Sherman and Nakamura (Ref. 34). A series of four shots of identical, beryllium-skinned, graphite-tipped cones of total angle of 44° , following "identical" unspecified trajectories, registered the following history. "Transitional flow began at the aft end of the vehicle" ($R_{tr} \sim 5.3 \pm 0.7$; $R/ft \sim 1.6 \times 10^6$; $R_\theta \sim 850 \pm 60$; $M_e = 6.2 \pm$; $T_w/T_r \sim 0.09$; all based on local values) "and moved forward along the conical surface at a decreasing (i.e. non-constant) value of the local Reynolds number", reaching the front measuring station for: $R_{tr} \sim 3.2 \pm 0.2$; $R/ft \sim 2.6 \times 10^6$; $R_\theta \sim 660 \pm 30$; $M_e = 6.1 \pm$; $T_w/T_r \sim 0.12$; see Figs. 4 and 5. Could this represent the re-reversal leg of Wisniewski-Jack, Richards-Stollery mark of Z? Again, the freedom from acoustic irradiation, which poisons the tunnels, did not raise R_{tr} to the high levels one might expect...

(2.18) Obviously, there are problems with understanding and predicting transition on cones (at zero angle of attack) and on wedges. And yet these simple shapes are not amenable to many designs, e.g. those of lifting-entry vehicles. Figure 6 borrowed from the recent Young, Reda, and Roberge study (Ref. 35) the Multipurpose Reusable Spacecraft at Mach 10 demonstrates a special effect such as may unexpectedly develop for non-simple geometries. At $\alpha = 10-20^\circ$, the spherical nose flaring out into a flat bottom accentuates the formation of a local minimum of shock inclination, which occurs even on pure sphere cones as shown by L. N. Wilson (Ref. 36). The larger shock decelerations away from this minimum inclination produce a relative subsonic jet of faster fluid at the minimum; a jet, which can be seen traveling (as a density maximum) toward the body along the 3D streamlines in Fig. 28. The "Ames effect" (for Seiff, Sommer, Canning, Cleary and Larson from Ames Research Center who spoke to deaf ears for years) consists then of the transition of this highly unstable relative jet and of the contamination of the boundary layer (Coles' effect: Section 6.2 of Ref. 5) for angles for which the jet streamlines come close enough to the body. The observed Reynolds numbers of transition (causing severe heating) were extremely low despite the usually beneficial hypersonic effects at Mach 10. In fact any chief engineer who would have gambled a design on the best predictions and correlations would have probably lost his

vehicle - see the educational Fig. 15 of Young et al.

(2.19) Even at zero angle of attack, the approach to the effects of pressure gradients is hardly rational. In fact, not even the linearized stability theory teaches one how to separate the effect due changes in M_e and due to the alterations in mean profiles. The concept of the entropy-swallowing distance has been very fruitful for small blunting radii (Section 5.2 of Ref. 5) but non-empirical estimates of the optimal effect and any characterization of the adverse blunt-body effect are lacking.

Michel and Schmitt (Ref. 37) present a systematic study of 3 cone-cylinders and 3 ogive-cylinders at $T_w/T_t = 0.36$, $M_\infty = 6.9$ (see their Figs. 6, 9, 13-15). There are differences due to mismatched gradients but the local R_{tr} values correlate quite well on the basis of local M_e for fixed R_∞/cm of $0.3 \cdot 10^6$. The adverse effect of the bluntness is clearly indicated in their Fig. 15.

Softley's empirical scheme (Ref. 38) for estimating optimal blunting and his comparisons with cones in pressure gradients are described on p. 62 of CET. An intriguing postponement of transition when the nose of a hollow cylinder was made to protrude into a region of considerable negative pressure gradient in the tunnel was reported by Bertram (Ref. 42) on his p. 23.

(2.20) The first case of relaminarization ever was observed and documented by Sternberg (Ref. 39), see also pp. $G_8 - G_{11}$ of MM, Refs. 2 and 4, and Sections 3.8 and 3.9 of Ref. 5. Apparently the Michel-Schmitt bodies did not reach the relaminarization conditions but other bodies are likely. Similar relaminarization (often only local) exists in the high accelerations in wind tunnel nozzles, e.g. Amick, Ref. 40, and Winkler and Persh, Ref. 41. A "quiet" supersonic tunnel must either sustain the relaminarization throughout (e.g. the JPL wind tunnel) or suck away the final turbulent boundary layer.

(2.21) Thus the pressure-gradient effects can be studied on the sidewalls of some supersonic and hypersonic tunnels at very low unit Reynolds number. Apparently the largest sidewall Reynolds numbers (based on distance from the throat) thus far achieved with laminar boundary layers are on the order of 5×10^6 at M of 4.5 at JPL ($R/L \sim 0.05 \times 10^6/\text{inch}$) and 13×10^6 at $M = 18.7$ in the Langley unheated 22 inch helium tunnel ($R/L \sim 0.17 \times 10^6/\text{inch}$) - Wagner et al, Ref. 28. Using hot wires, Wagner et al documented that as the

sidewall boundary layer of the M 20 helium tunnel goes through transition at a given x, when R/L increases, the dimensionless pressure fluctuations at the downstream tunnel centerline position, to which the x station radiates, rise rapidly and then slowly subside as R/L continues to rise.

(2.22) It is this subsidence which is apparently responsible for the n-power rise, (2.03), of R_{xB} at beginning of transition on models inserted into supersonic and hypersonic tunnels. This trend is present on a wedge model (local M_e) in the above M~20 helium tunnel. However the shift to the extra high R_{xB} corresponding to a truly laminar sidewall layer at low R/L values were not reached (as they were at JPL at M of 4.5), even though the pressure fluctuations in the empty tunnel were substantially lower. (Perhaps the subsonic turbulent boundary layers are not perfectly relaminarized in the nozzle region leading to the possibility of very long transitional stretches with nondense turbulent spots as in the case of Jedlicka et al, Ref. 114 of CET, also with high accelerations.)

3. SPECULATIONS ON POSSIBLE TRANSITION RESEARCH AND DEVELOPMENT

The first two pages of Appendix: "Major Open Questions Relevant to Applications" were discussed, with sketches, on pp. J₁-J₄ of MM Ref. 2 and on the cassettes, Ref. 4. The possibly presumptuous adjective "relevant to applications" refers to the fact that most of these questions arise when one wishes to extrapolate effects of two or more parameters and discovers that they indicate countertrends in R_{tr} . Generally, these countertrends occur when the responsibility for transition shifts from one of the multiple factors to another. These are also the conditions where a designer needs more guidance - hence the adjective.

The two pages and Sections 1 and 2 represent one man's shopping list for stability and transition research but without indication of priorities. (Further comments can be found on pages 64-66 of CET.) The manner of presentation already imposes some bias and it would be altogether presumptuous to indicate one's subjective priorities.

The third page of the Appendix represents a personal view of the Nature of the Problem as the author understood it when he was associated with the design of the SV-5 Entry Vehicle. The philosophy of design for transition is

further discussed in Chapters 10 and 11 of Ref. 5.

Among the problems listed in the Appendix and the issues described in Sections 1 and 2 four related groups of problems, with high priority both for urgent engineering applications and for clarification of the basic structure within which other questions can be more meaningfully researched, can perhaps be identified without much controversy.

(I) Resolution of the 1967 San Bernardino dilemma of the M , R , and T_w/T_r variations with new but not especially encouraging information. More specifically:

(Ia) Reconciliation of information from wind tunnels (quasi-continuous and "pulsed"), (2.01)-(2.08), (2.16), (2.18)-(2.22), ballistic ranges (2.02), (2.12), and free atmospheric flight: (2.01), (2.02), (2.10), (2.15)-(2.17).

(Ib) Full clarification of the increasingly more irritating phenomena of reversal of transition with cooling, see (1.09), (2.13), (2.14), (2.15), and Figures 4 and 5.

(II) More consistent conceptual framework, especially

(IIa) Clarification of the role and limits of existing linear theory, e.g. with respect to temperature effects, including entropy-layer and hot-lip effects (2.14).

(IIb) Identification and classification of transition "bypasses" of linear theory, e.g. (2.10), (2.11), acoustic irradiation in tunnels (?).

Note: basic research on (IIa) and (IIb) at low speeds is far from complete, and even there the role of nonlinearity remains confused, CET pp 8-10, and Chapters 3, 4, and 10 of Ref. 5.

(III) Sound approach to streamwise pressure gradients which should probably lean on both the concepts of physical mechanisms and of linear theory - see (2.18), (2.19), and relaminarization (2.20). Variable heat transfer and ablation often complicate these effects and need to be tackled in due course.

(IV) Same objectives for cross-flow gradients, which are likely to have additional instability mechanisms (judging by low-speed linearized theory for flows with streamwise vorticity, see Chapter 7 of Ref. 5). Sporadic evidence of formation of streamwise vortices, especially in presence of sweepback, edge-unevenness, local separation and/or ablation, calls attention to the implications

of this phenomenon.

These broad categories encompass many, many problems and forbiddingly many variables and parameters. The task of characterizing adequately the mean profiles for I-IV alone is a formidable problem. Current design clearly cannot wait for the broad, longer-range approach. One needs to take the correlation road, but with circumspection. For a given design with strong "family constraints" on the parameters (e.g. due to special trajectories such as those of Ref. 34), the procedure may well be safe, but one would be wise to evaluate the risks carefully and keep in mind the possibilities of unexpected effects such as those encountered on Jaribu, (2.16), and on the Multipurpose Reusable Vehicle, (2.18). And the basic question remains: which ground facilities can be relied upon for the design estimates?

That question alone suggests that the longer-range program has to be pursued as well. But where is the best pay-off? If a "quiet tunnel" with high enough R/L could be successfully designed and built at a Mach number 10-15, its laminar operation might well (or might not) validate the results from other hypersonic tunnels which are currently suspect. The implications of the published experiences in the Langley M20 helium tunnel, (2.20)-(2.22), make the author currently less optimistic as to the prognosis. Hopefully the report of E. Reshotko and his Committee at this Workshop can shed some better light on the prospects of the quiet tunnel.

In his recent academic ignorance of flight results the author would like to ask a question which has been bothering him with respect to the incomplete information of Figs. 3-5. Can hypersonic vehicles with high cooling, say $H_w/H_r < 0.3$ consistently reach the high values of R_{tr} which linear theory would indicate? Without and with ablation? If not, would not this fact point to the temperature sensitivity as the key problem? For what conditions is the achievement of high R_{tr} "spoiled"? Judging by the available information: this occurs for high cooling, relatively high R/L, and small roughness combinations of conditions, (2.10), (2.12), (2.15)-(2.17). Such conditions have been little explored experimentally* and the cognoscenti of the various facilities can perhaps feel challenged and encouraged to devise telling experiments for such combinations

*The kinematic viscosity based on wall values may be more significant for correlations in such cases.

of conditions. If the above premise is correct, any information gleaned from such efforts may well have an important bearing on target category I. But these speculations belong more appropriately to the Committee sessions on Friday, which hopefully can lean on the projections of facts in Sections 1 and 2 herein.

REFERENCES

1. M. V. Morkovin, Critical Evaluation of Transition from Laminar to Turbulent Shear Layers with Emphasis on Hypersonically Traveling Bodies, AFFDL TR 68-149 (March 1969).
2. L. M. Mack and M. V. Morkovin, High-Speed Boundary-Layer Stability and Transition, Notebook for the AIAA Professional Study Series, AIAA (June 1969).
3. L. M. Mack, Boundary-Layer Stability Theory, Jet Propulsion Laboratories, Tech Report 900-277 (1969).
4. L. M. Mack and M. V. Morkovin, High-Speed Boundary-Layer Stability and Transition, 9 cassettes, two reference texts, and a notebook with annotated slides, AIAA Educational Programs (October 1971).
5. M. V. Morkovin, Critical Evaluation of Laminar-Turbulent Transition and High-Speed Dilemma, Vol. 13 of Progress in Aerospace Sciences, D. Kuchemann, Editor, Pergamon Press (1972).
6. W. D. McCauley, Editor, Proceedings, Boundary Layer Transition Study Group Meeting, Vols. I-IV, AF Report No. BSD-TR-67-2113, Aerospace Corporation, San Bernardino, California (August 1967).
7. E. Reshotko, Stability Theory as a Guide to the Evaluation of Transition Data, AIAA Journal, Vol. 7, pp 1086-92 (1969).
8. E. Reshotko, Boundary-Layer Stability and Transition, Proceedings, Conference on Boundary Layer Concepts in Fluid Mechanics, Univ. of Massachusetts (July 1969).
9. S. J. Kline, M. V. Morkovin, G. Sovran, and D. J. Cockrell, Calculation of Turbulent Boundary Layers - 1968 AFOSR-IFP- Stanford Conference, Proceedings, available from Mech. Eng. Dept. Stanford Univ.
10. M. V. Morkovin, Lessons from Transition of Shock-Tube Boundary Layers, in these Proceedings.
11. J. G. Spangler and C. S. Wells, Jr., Effects of Freestream Disturbances on Boundary-Layer Transition, AIAA Journal, Vol. 6, pp 543-545 (1968).
12. E. J. Softley, B. C. Graber, and R. E. Zempel, (a) Experimental Observation of Transition of the Hypersonic Boundary Layer, AIAA Journal, Vol. 7, pp 757-762 (1969); (b) Boundary-Layer Transition on Hypersonic Blunt, Slender Cones, AIAA Paper 69-705 (June 1969).
13. G. G. Mateer and H. K. Larson, Unusual Boundary-Layer Transition Results on Cones in Hypersonic Flow, AIAA Journal, Vol. 7, pp 660-664 (1969).

14. L. Neal, Jr., A Study of the Pressure, Heat Transfer, and Skin Friction on Sharp and Blunt Flat Plates at Mach 6.8, NASA TN D-3312 (1966) especially p 15 and Fig. 20.
15. S. R. Pate and C. J. Schueler, An Investigation of Radiated Aerodynamic Noise Effects on Boundary-Layer Transition in Supersonic and Hypersonic Wind Tunnels, AIAA Journal, Vol. 7, p 450 (1969).
16. S. R. Pate, Measurements and Correlations of Transition Reynolds Numbers on Sharp Slender Cones at High Speeds, AIAA Journal, Vol. 9, p 1082 (1971).
17. J. M. Kendall, Jr. JPL Experimental Investigations, in these Proceedings, also: Supersonic Boundary-Layer Transition Studies, Jet Propulsion Laboratories Space Program Summary, Vol. III, pp 37-62 (April 1970).
18. L. M. Mack, Progress on Compressible Boundary Layer Stability Computations, in these Proceedings.
19. J. L. Potter, Observations on the Influence of Ambient Pressure on Boundary-Layer Transition, AIAA Journal, Vol. 6, pp 1907-1912 (1966,
20. N. W. Sheetz, Jr., Ballistics Range Experiments on the Effect of Unit Reynolds Number on Boundary-Layer Transition, Proceedings, 8th Navy Symposium on Aeroballistics, p 201 (May 1969).
21. J. L. Potter, Some Special Features of Boundary Layer Transition on Aeroballistic Range Models, in these Proceedings.
22. G. G. Mateer, Effects of Wall Cooling and Angle of Attack on the Boundary-Layer Transition of Sharp Cones at Mach Number 7.4, in these Proceedings.
23. D. V. Maddalon, Effect of Wall-to-Total Temperature Ratio on Transition Reynolds Number at Mach 6.8, AIAA Journal, Vol. 7, p 2355 (1969).
24. R. J. Sanator, J. P. DeCarlo, and D. T. Torrillo, Hypersonic Boundary Layer Transition Data for Cold Wall Slender Cone, AIAA Journal, Vol. 3, p 758 (1965).
25. B. E. Richards and J. L. Stollery, (a) Further Experiments on Transition Reversal at Hypersonic Speeds, AIAA Journal, Vol. 4, p 2224 (December 1966); (b) Transition Reversal on a Flat Plate at Hypersonic Speeds, AGARDograph 97, p 483 (1965).
26. R. J. Wisniewski and J. R. Jack, Recent Studies on the Effect of Cooling on Boundary Layer Transition at Mach 4, Journal of Aerospace Science, Vol. 28, p 250 (1961).
27. N. W. Sheetz, Jr., Ballistics Range Boundary-Layer Transition Measurements on Cones at Hypersonic Speeds, Proceedings, Viscous Drag Reduction Symposium, C. S. Wells, Jr., Editor, Plenum Press (February 1969).

28. R. D. Wagner, Jr., D. V. Maddalon, and L. M. Weinstein, Influence of Measured Free-Stream Disturbances on Hypersonic Boundary-Layer Transition, AIAA Journal, Vol. 8, p 1664 (1970).
29. J. P. Rhudy, Effect of Uncooled Leading Edge on Cooled-Wall Hypersonic Flat-Plate Boundary-Layer Transition, AIAA Journal, Vol. 8, p 576 (1970).
30. W. J. McCroskey and S. H. Lam, The Temperature-Vorticity Analogy in Boundary Layers, Int. Jour. Heat Mass Transfer, Vol. 9, p 1205 (1966).
31. T. Cebeci and A. M. O. Smith, Investigation of Heat Transfer and of Suction for Tripping Boundary Layers, Jour. Aircr., Vol. 6, p 450 (1968) discussion by W. J. McCroskey and reply, ibid, p 285 (1969).
32. B. Lemcke, A. Naysmith, J. Picken, and H. Thomann, Comparison of Heat Transfer Measurements in Free Flight and in Wind Tunnel at M=7 at Similar Reynolds Numbers and Temperature Ratios, Proceedings 7th Congress Int. Council Aeron. Sci., Rome (1970).
33. A. Naysmith, Measurements of Heat Transfer Rates and Boundary-Layer Transition on a Blunt-Nosed Body of Revolution in Free-Flight at Supersonic and Hypersonic Speeds, Roy. Airc. Establishment, UK, TR 70096 (1970).
34. M. M. Sherman and T. Nakamura, Flight Test Measurements of Boundary-Layer Transition on a Non-Ablating 22° Cone, Journal Space. Rockets, Vol. 7, p 137 (1970).
35. C. H. Young, D. C. Reda, and A. M. Roberge, Hypersonic Transitional and Turbulent Flow Studies on a Lifting Entry Vehicle, AIAA Paper No. 71-100, (January 1971).
36. L. N. Wilson, Inflection in Bow Shock Shape at Hypersonic Speeds, AIAA Journal, Vol. 5, p 1532 (1967).
37. R. Michel and V. Schmitt, Résultats sur la Région de Transition de la Couche Limite en Hypersonique, l'Aéronautique et l'Astronautique, No. 19, p 42 (March 1970).
38. E. J. Softley, Boundary Layer Transition on Hypersonic Blunt Slender Cones, AIAA Paper 69-705 (June 1969).
39. J. Sternberg, The Transition from a Turbulent to a Laminar Boundary Layer, Ball. Res. Lab. Aberdeen Proving Grounds, Report No. 909 (1954).
40. J. L. Amick, Extension of the Operating Range of a Low-Turbulence Hypersonic Wind Tunnel, Proposal to ARL, Wright Patterson AFB by University of Michigan (June 1968).
41. E. M. Winkler and J. Persh, NOL Hypersonic Tunnel No. 4: Experimental and Theoretical Investigation of the Boundary Layer and Heat Transfer Characteristics of a Cooled Hypersonic Wedge Nozzle at a Mach Number of 5.5, NAVORD Report 3757 (July 1954) especially Figure 1.

42. M. Bertram, Exploratory Investigation of Boundary-Layer Transition on a Hollow Cylinder at a Mach Number of 6.9", NACA Tech Report 1313 (1957).

APPENDIX

MAJOR OPEN QUESTIONS

relevant to applications

*Early blunt-body transition

Non-quasi-parallel stability theory including vorticity stretching

*Effect of nonsimilarity, e.g. Whitfield's hot-lip effect

** R_{tr} sensitivity to H_w/H_r , $M > 6$ $\left\{ \begin{array}{l} \text{Ball range; gun tunnel} \\ \text{more conventional tunnels} \end{array} \right.$

**Reversal with cooling for "smooth" bodies $\left\{ \begin{array}{l} \text{blunt} \\ \text{flat} \end{array} \right.$

** R_{tr} rereversal with high cooling

**Unit R effects $\left\{ \begin{array}{l} \text{Wind tunnel Pate \& Schueler} \\ \text{Ballistic range Potter, Sheets} \end{array} \right.$

*Existence of "bypasses" \leftarrow flight

*What part of R_{tr} variation is M-effect?
and what part is R/L-effect?

*Role of favorable $\partial p / \partial x$ at $M > 1$

**Role of streamwise vorticity at supersonic and hypersonic M's - 3D BL's

sweep; α
protuberances
spanwise nonuniformities

* \dot{m} (transpiration, ablation)

*Interactions of \dot{m} and H_w/H_r effects
(cf. countertrend (6)^rp J-2 of MM)

*Interactions of \dot{m} and cross-flow effects

*Interaction of cross-flow and H_w/H_r effects

Free-stream disturbance fields + their variations
and

Receptivity of B.L to all disturbance modes

MM page (Ref. 2)

CET page (Ref. 1)



p 24, 46-47

MM: H-9 to H-11

MM: H-9

pp 23-28

p 25, Fig. 11

MM: H-8, H-9

p 46

p 49-52

p 51

MM: Section H, I

p 59

MM: G-2, G-21

MM: H-17 to H-20

MM: Section I

MM: F-35

pp 40-45

MM: F-28, H-2, H-14-17

MM: F-19, F-20

p 66

Figs. 32, 33

MM: H-4, H-5

pp 26-28

MM: Section G

pp 23, 27, F-37

Interaction of bow-shock with modal disturbances

p 96
MM: G-11 to G-14

*Variation of transverse contamination with M

MM: F-19, F-20

**Nature of turbulent BL's at high M's

p 66
MM: F-1, H-12

See also Index of Ref. 1 and Table of Contents of Ref. 5.

NATURE OF PROBLEM:

MULTIPLE RUNAWAY PHENOMENA, COMPETING

UNKNOWN INPUTS

TOO MANY PARAMETERS

BASE FLOWS (= MEAN PROFILES) POORLY PREDICTABLE, YET
AMPLIFICATION-CONTROLLING

INSUFFICIENTLY KNOWN CRITERIA FOR TURBULENCE SELF-REGENERATION,
ESPECIALLY FOR LARGE M'S

NECESSITY OF EXTRAPOLATION OF INFORMATION FROM LIMITED GROUND
FACILITIES

NUMBER OF SUFFICIENTLY CONTROLLED EXPERIMENTS FORMS TOO SMALL
A SET OF SAMPLES FOR ANY SCIENTIFIC PROBABILITY STATEMENTS

NEED FOR THEORETICAL (LINEAR) AND CONCEPTUAL (INCLUDING NONLINEAR
EFFECTS) FRAMEWORK TO GUIDE JUDGMENTS OF NON-STATISTICAL
PROBABILITIES

DESIGN ASSESSMENTS OF RISKS OF SUCH PROBABILITIES

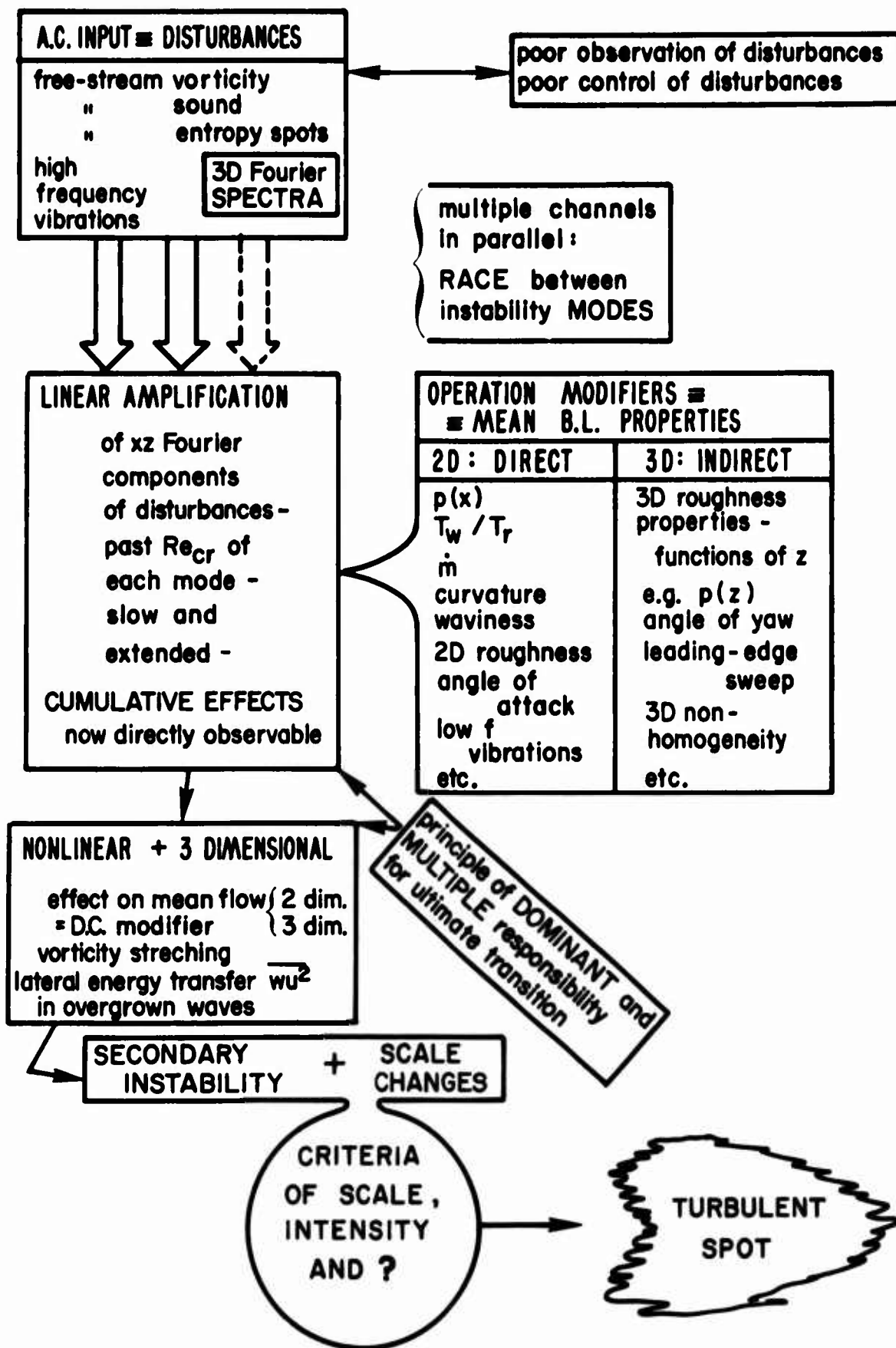


Fig. 1 - Laminar Boundary Layer As A Linear And Nonlinear Operator

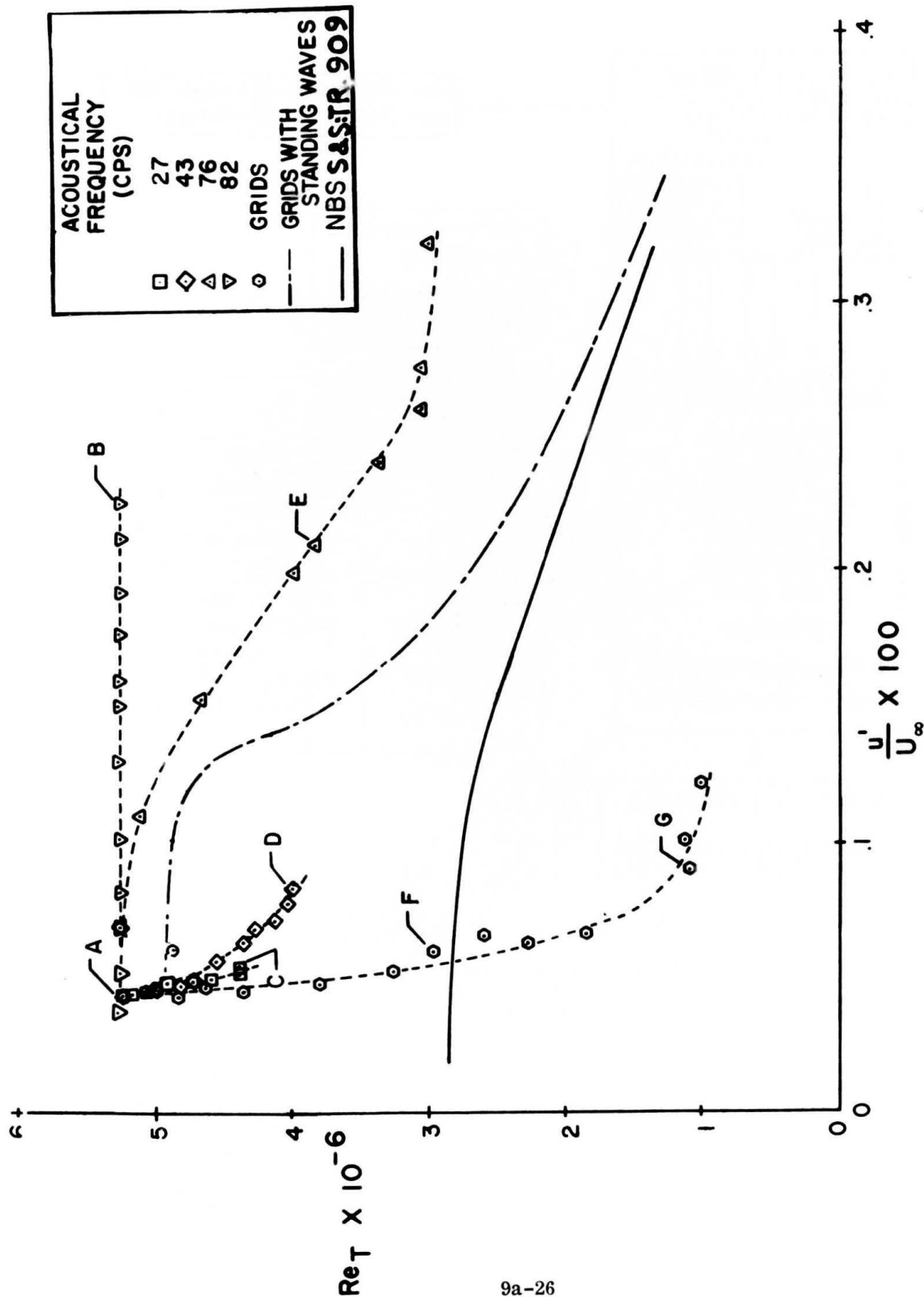
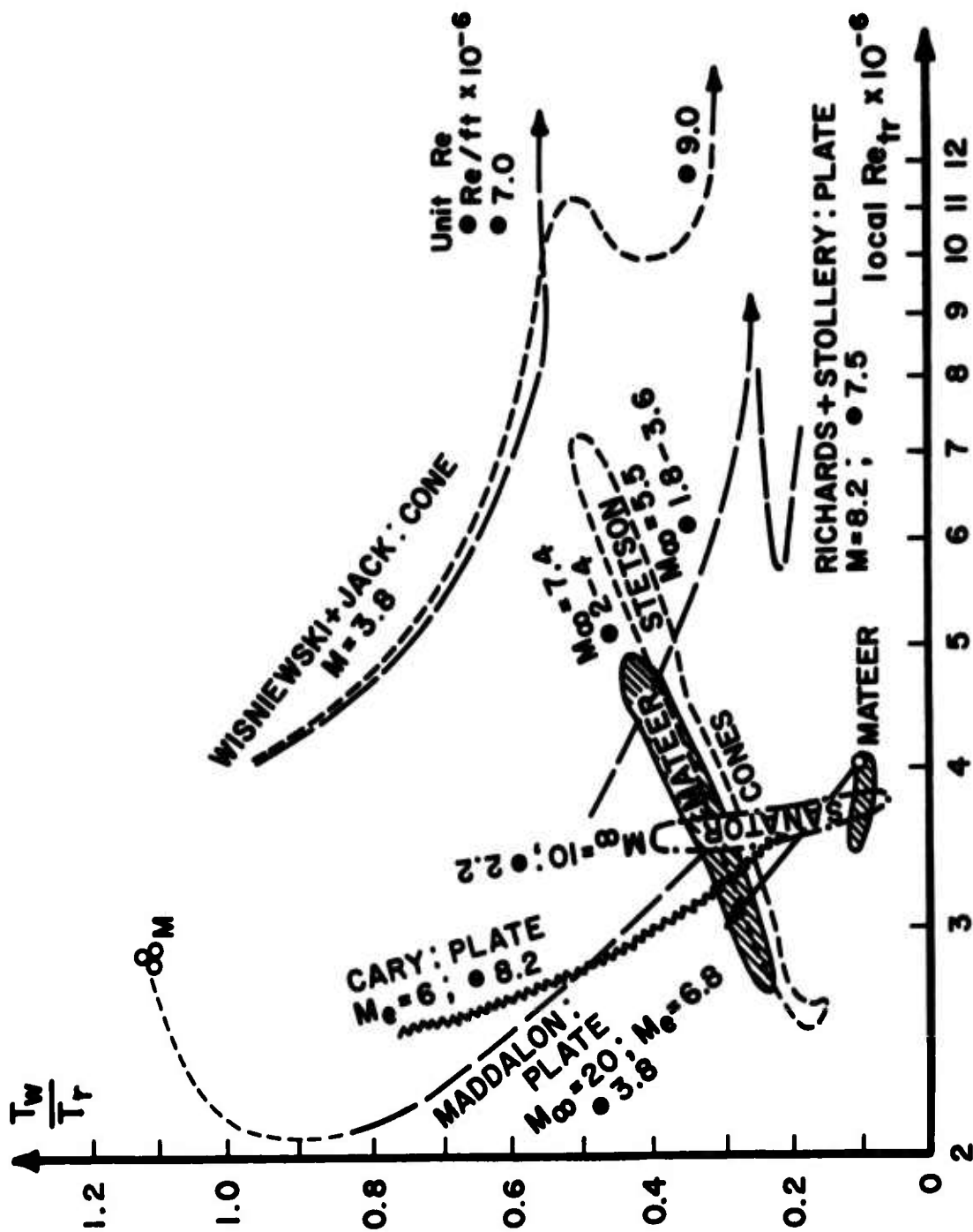
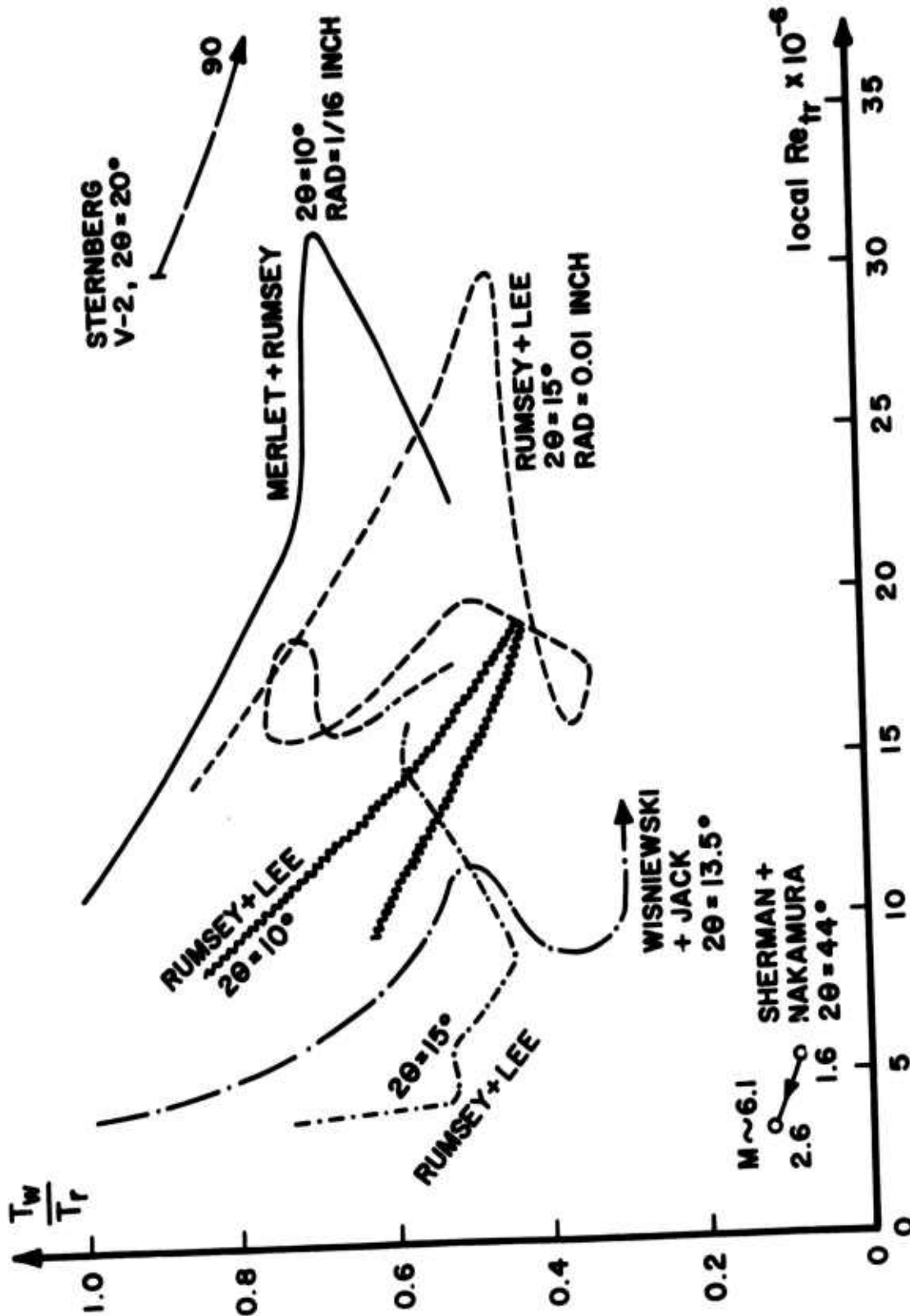


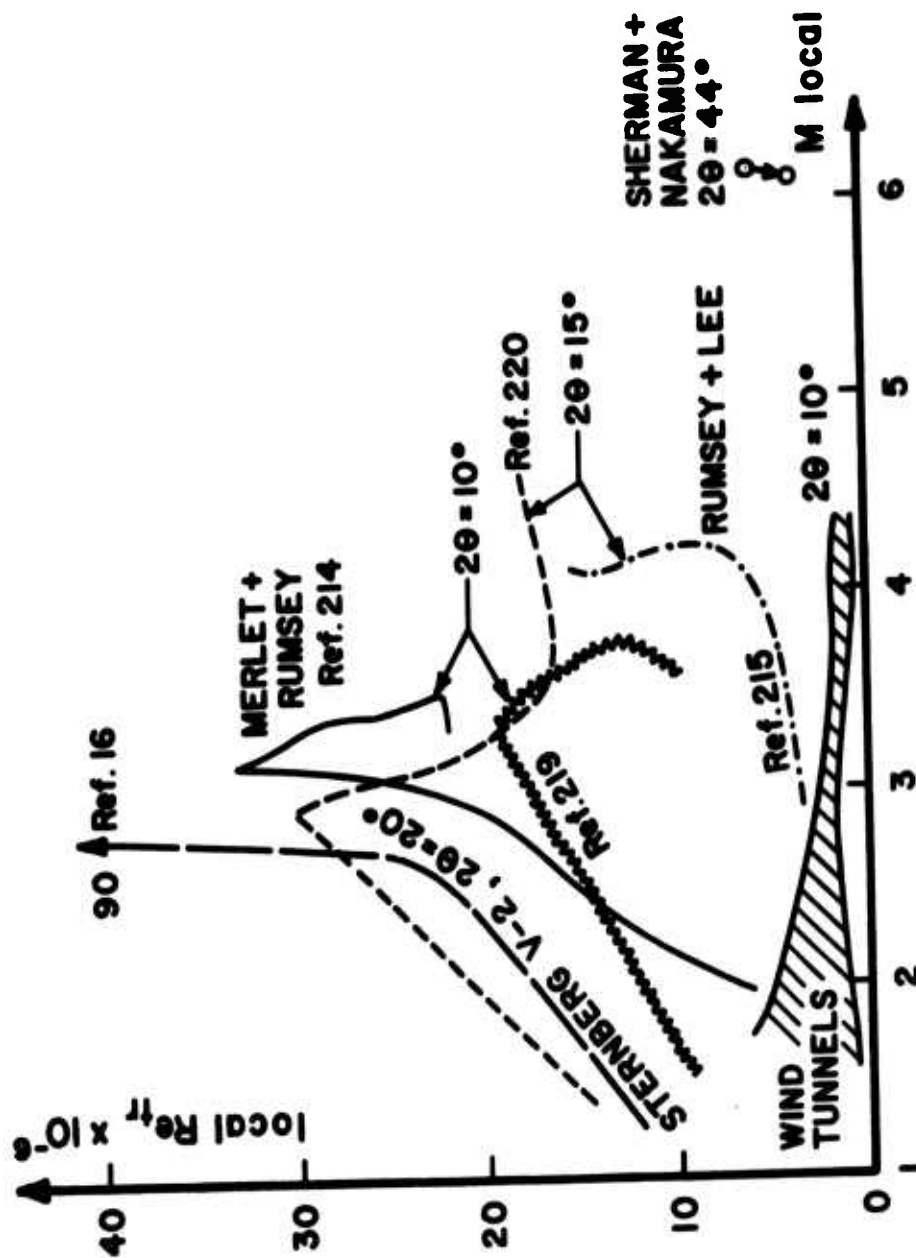
Fig. 2. Transition Reynolds number as function of free-stream disturbance intensity. ($U_0/\nu = 2.4 \times 10^5/\text{ft}$; $U_0 = 38.5 \text{ fps}$).
From Spangler and Wells, Ref 11.



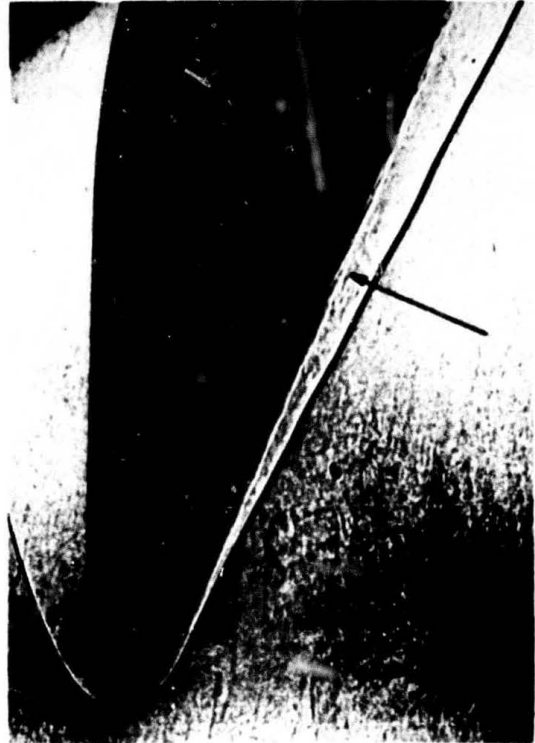
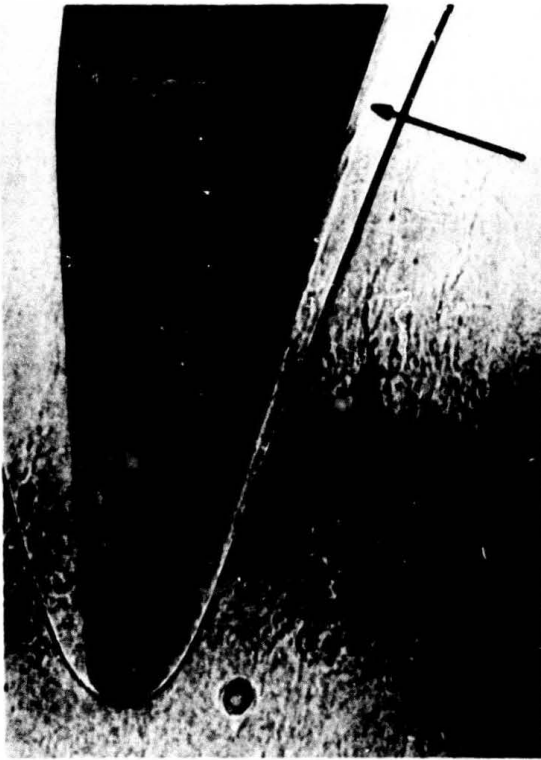
3. Transition Sensitivity to Cooling in Various Wind Tunnels



4. Transition on Cones in Flight in Terms of Local Reynolds Number and Local Cooling Ratio.



5. Transition on Cones in Flight in Terms of Local Mach Number and Local Reynolds Number.



6. Early Transition on Multipurpose Reusable Spacecraft at Mach Ten at Angles of Attack of 0° , 10° , 15° , and 20° .

SECTION 9b

LESSONS FROM TRANSITION OF SHOCK-TUBE BOUNDARY LAYERS*
(Unclassified)

by Mark V. Morkovin

MMAE Dept., Illinois Institute of Technology, Chicago, Ill. 60616

ABSTRACT
(Unclassified)

Experimental observations of transition from laminar to turbulent boundary layers in shock tubes is reviewed. The seemingly contradictory behavior is viewed in the light of transition behavior in other ground facilities. It is concluded that shock tubes may offer a convenient milieu for studying the elusive regime where high cooling is matched with high unit Reynolds number and controllable roughness. However, the nature of the strong disturbances apparently radiating from the region of the contact surface would have to be first explored and understood.

*Supported under USAF OSR-Themis Contract F 44620-69-C-0022, Mechanics Division. This paper was not presented at the Symposium Meeting but is presented here because of general interest.

LIST OF SYMBOLS

a_e	Speed of sound in free-stream
M_e	Mach number at edge of boundary layer (in laboratory coordinates, Sketch 1)
M_s	Shock Mach number
Re	Reynolds number, subscript denoting reference length
Re_{cr}	Critical Re for amplification of infinitesimal disturbances
Re_{tr}	Reynolds number of transition
T_e	Static temperature at edge of boundary layer
T_w	Wall temperature
T_r	Recovery (adiabatic) temperature
\bar{U}_e	Free-stream speed, laboratory coordinates, Sketch 1
U_{tr}	Speed of turbulent front = transition
U_s	Speed of main shock wave
δ	Boundary-layer thickness
δ^*	Displacement thickness, laboratory coordinates

INTRODUCTION

As different as two supersonic wind tunnels may be, they share similar "family constraints" on their free-stream disturbance environment, on the model smoothness and leading-edge characteristics, on the range of attainable temperature ratios T_w/T_r and unit Reynolds numbers at a given Mack number, M , etc. An investigator of transition in a wind tunnel thus has his experiences confined to a more orderly subspace of the transition-parameter phase space (Section 2.3 of ref. 1 and very concisely on p 6 of ref. 2). Unless he exercises special ingenuity in enlarging his experience subspace, the investigator naturally tends to endow his narrower segment of observations and correlations with more general validity - as does his counterpart working with the ballistic range, or another sufficiently different facility. Shock tubes provide still a different set of constraints, and transition behavior on their sidewalls may be useful as shock-therapy for one's sclerotic point of view. It is the purpose of this paper to describe this behavior as observed by different shock-tube practitioners and to relate it to the various facets of transition behavior in wind tunnels and ballistic ranges.

PRECITICAL NATURE OF SHOCK-TUBE TRANSITION

Shock-tube boundary layers avoid the physical obstruction at their leading edges (see Sketch 1) and should therefore be essentially free of the entropy-layer effects (Section 5.2 of ref. 1) and the Ginoux streamwise vorticity effect (Section 7.4 of ref. 1). The laminar boundary layer profiles have been predicted by Mirels (ref. 3) and found in good agreement with measurements of tracer displacements by Gion (ref. 4). In the laboratory coordinate system of Sketch 1, they are more concave than Blasius profiles and should therefore be more stable. Ostrach and Thornton (ref. 5) in effect applied the hypothesis of locally constant base (Section 4.6 of ref. 1 and p 18 of ref. 2; here both quasi-parallel and quasi-steady) and indeed found critical Re_{δ^*} for amplification of 1660 and higher, as compared to about 500 for the Blasius profile. They utilized the Dunn-Lin formulation of the linearized theory (ref. 6) and the computational method of Lees and Lin (ref. 7) which should be adequate for moderate shock pressure ratios yielding subsonic flow behind the leading shock (but probably not for the inference of complete stabilization for cold walls for the reasons detailed by Mack (ref. 8) in the case of normal supersonic

boundary layers).

Lo and behold, the observed transition occurred always for Re_{δ^*} in the region officially stable to infinitesimal disturbances. Furthermore, for increasing shock pressure ratios (for which the Mach number of the shocked fluid increases while simultaneously the wall becomes relatively cooler, i.e. T_w/T_e decreases: the shock-tube family parameter constraint) the recorded transition Re_{δ^*} became orders of magnitude smaller than the theoretical critical Re_{δ^*} - Sketch 2. The magnitude of this contrary behavior recalls that of the blunt-body paradox (Sections 2.2 and 6.3 of ref. 1) although here the theoretical stabilization stems from cooling alone and is not abetted by favorable pressure gradient. Both effects occur when the cooling is matched with relatively high unit Reynolds numbers, conditions which the available roughness criteria do not cover. Ostrach and Thornton concluded that the transition had to be triggered by unknown finite disturbances - a bypass of the Tollmien-Schlichting instability mechanism.

TRANSITION REVERSALS AND RE-REVERSALS IN SHOCK TUBES?

None* of the early experimenters (refs. 9-14) reported seeing Emmons' turbulent spots, either optically or through heat gages with response in microseconds. All evidence indicated a fully turbulent front** encroaching onto a virginal laminar layer some distance downstream from the leading shock, reasonably correlatable in terms three different Reynolds numbers - Ostrach and Thornton's Figs. 1, 5, and 6 in ref. 5. In terms of the rather logical characterization by local boundary layer thickness, Sketch 2, the transition appears again as a mild reversal of the theoretical-temperature (and Mach-number) trend in the data used by Ostrach and Thornton, namely for $T_w/T_e > 0.2$. In terms of the Reynolds number based on the distance which a particle in the free-stream of the shocked gas travels from its initial position until it is engulfed by transition, there is a very mild rise in Re_{tr} as T_w/T_e falls from unity to 0.2. The absence of a geometrical leading edge does remove some ambiguities, but brings forth others such as the choice of the length

*Some of Asbridge's trace wiggles may have been due to spots (ref. 13).

**See Fig. 4 of Hartunian et al (ref. 10b), borrowed from Smith, Glick, Herzberg, and Squire (ref. 15).

most relevant to transition and hence the choice of Reynolds number.

Writing before the advent of the Ostrach-Thornton theory, Hartunian, Russo, and Marrone (ref. 10) preferred not to label the transition behavior for $1 > T_w/T_e > 0.2$ as a transition-trend reversal, probably wisely, wishing to emphasize the differences with the transition reversal with cooling in "normal" supersonic boundary layers (Sections 2.2 and 9.1 of ref. 1, and pp 49-51 of ref. 2). They did feel that the sharp increase in Re_{tr} (however it may be defined) under further supersonic cooling $T_w/T_e < 0.2$ (Sketch 2) may be related to the "complete stabilization by cooling" which was then thought possible (Mack, ref. 8). When the crooked transition cloud in Sketch 2 (or equivalent) is compared to the theoretical trends of Ostrach and Thornton, the stabilization hook is indeed intriguing. Qualitatively it resembles the behavior of very highly cooled "normal" boundary layers in the so-called transition re-reversal (pp 16 and 51 of ref. 2) which is also not understood, if at all fully accepted. As Hartunian et al point out, shock tubes may offer more controllable and less expensive means of studying the combined effects of extreme cooling and high-unit Reynolds numbers (and roughness). They conducted some experiments in argon (for which different parametric combinations obtain) and confirmed their trends with cooling in air.

Hartunian, Russo, and Marrone furthermore focused on the cloud of points in the equivalent of Sketch 2 for $T_w/T_e > 0.2$ and concluded that the scatter could be substantially reduced if one postulated a unit-Reynolds number variation $Re_{tr} \sim (Re/L)^{1/2}$, again reminiscent of wind-tunnel and ballistic-range behavior. The power apparently switched rapidly to zero for $T_w/T_e < 0.2$. That there are disturbances in shock tubes, among them acoustic ones, propagating "on top" of the laboratory free-stream speed \bar{U}_e , there is no doubt. What is somewhat surprising is that this environmental factor would be operative so far below the critical Reynolds number, i.e. without any identifiable amplification process to feed. If the environmental disturbances in shock tubes were particularly inhospitable to laminar flows as the further evidence of Mark and Mirtich (ref. 16), Thompson (ref. 17), Gion (ref. 4), and Thompson and Emrich (ref. 18) indicates, the aforementioned usefulness of the shock tubes for controlled cooling investigations might be impaired. Perhaps the most thorough discussion of shock-tube disturbances is found in Chapter VI of Thompson (ref. 17)

to be augmented by observations of Gion (ref. 4), and Mark and Mirtich (ref. 16).

DISTURBANCE ENVIRONMENT AND NATURAL TRANSITION

Thompson and Gion concentrated on the regime of weaker shocks, the two extreme speeds of Thompson's 23 flow categories reaching barely supersonic Mach numbers M_e of 1.08 and 1.12 (laboratory coordinates). For this range ($T_w/T_e > 0.5$), they report transition Reynolds numbers much higher than the earlier results but still below the theoretical Reynolds number for Tollmien-Schlichting amplification of Ostrach and Thornton. Thompson concludes: "This implies either that the transition mechanism in a shock tube is not one of amplification of infinitesimal disturbances, or that there is some flaw in the application of the theory or in the interpretation of experimental results".

Having discovered early that a downstream facing step (mismatch of metal and glass) of only 0.001 inch in height can and does cause turbulent fronts to propagate downstream at essentially the stream speed \bar{U}_e , Thompson resorted to the "spoiler technique" (Section 3.13 of ref. 1 and p 28 of ref. 2) utilizing two-dimensional and three-dimensional roughness and time-controllable sparks to document various detailed features of transition due to finite disturbances in shock tubes. In contrast to previous shock-tube investigators he found turbulent spots and verified the close resemblance of their characteristics to those of Schubauer and Klebanoff (ref. 19), e.g. the leading and trailing-edge propagation at approximately \bar{U}_e and $0.5 \bar{U}_e$, respectively. Since he operated primarily in the subsonic region, this finding is not surprising, though welcome. However, he could not match the delta-function source distribution of Emmons' spots as proposed by Dhawan and Narasimha (ref. 20) and concluded that there may be more than one primary cause for "natural" spots in shock tubes.

For shock-tube shapes (Hartunian et al: 1.5x2.5 in; Thompson: 3/8x4 in; Mark-Mitrich: circular, 3 in. i.d.) the ratio of the perimeter to the cross-sectional area is usually small, so that transverse influences may be substantial. Perhaps this contributes to the reported absence of spots at high pressure ratios (and to the possibility of "self-ignition" discussed below). First, it is desirable to examine the concept of "natural transition" in shock

tubes. Mark and Mirtich's (ref. 16a) operational definition calls for "...a constant transition time obtained from thin-film gauges at several axial positions...". In other words "natural transition" moves at a speed U_{tr} which is the same as the speed U_g of the generating shock. Such motion of transition might perhaps be described more fittingly as "self-ignition" rather than true "propagation". The concept of "natural shock-tube transition" tacitly implies an identical dominant local disturbance environment (free-stream or wall-conditions) at equal distances behind the shock, identical amplification history, and identical breakdown. If and when such a situation is achieved, it represents "natural transition" only for that particular shock tube, with the particular mode of diaphragm fracture, and under the particular dimensionless smoothness-cleanliness conditions (say referred to a characteristic boundary-layer thickness at the given T_w/T_e).

For instance, it is improbable that the detail dynamics of rupturing diaphragms (which start the shock process) are identical in different shock tubes. This early history is most likely responsible for formations of highly turbulent jets* near the first cracks of the diaphragm and related to the Mark-Mirtich observations of a "central finger", which shortens the duration of laminarity on a model in the middle of the shock tube as against its duration on the walls (ref. 16a). Mark and Mirtich point the finger of suspicion to the highly turbulent irregular region around this usually idealized contact surface (which terminates the column of nearly uniform shocked gas, i.e. the region of meaningful experimentation) as the probable source of large, transition-triggering disturbances. The shock tube flow is such that the acoustic radiation from this region propagates faster than the leading shock ($\bar{U}_e + a_e > U_g$) and can in principle trip the sidewall boundary layer anywhere in the column of the nearly uniform test gas if it is intense enough. In supersonic wind tunnels the acoustic radiation from turbulent boundary layers almost surely causes transition (Kendall, ref. 21 and these Proceedings; Pate and Schueler, ref. 22) so that the precedent beckons. For high pressure ratios and supersonic \bar{U}_e it is even conceivable that it is the nascent, extra vigorous turbulent boundary layer which radiates strongly enough to cause self-ignition

*Special cases of such jets were photographed in unpublished studies of Duff, Hollyer, and Laporte at the University of Michigan in 1952.

of the laminar layer located just downstream on the opposite or even on the same side of the narrow shock tube (see Schlieren photograph - Fig. 4 of Hartunian et al, ref. 10b). Some such finite disturbance mechanisms are evidently needed to explain the T-S precritical transition and the unpublished data alluded to by Mark and Mirtich (ref. 16b): "...for the larger part of our data the time of transition of the boundary layer behind the shock remained constant with axial position along the tube".

FINITE DISTURBANCES, SPOTS AND TRANSITION IN SHOCK TUBES

For all the data actually disclosed by Mark and Mirtich (ref. 16a and b), however, the transition front was very much slower than the shock speed U_s . In the experiments of Thompson (ref. 17) the measured velocities of this front range from 0.89 to 1.09 \bar{U}_e with a mean of 0.97 \bar{U}_e . The tabulated results of Mark and Mirtich (ref. 16b) (which start at the highest pressure ratios of Thompson) in essence extend Thompson's observations of the transition propagation since only two of their runs exceed the cited ratios U_{tr}/\bar{U}_e of Thompson and only by 25%. For what conditions the "self-igniting" mode of transition can take over is not clear. The author conjectures that a combination of high pressure ratios and high unit Re may be needed: M-M list cases at high shock Mach number but at low unit Re for which the behavior follows Thompson, e.g. $M_s = 9.75$, $U_{tr} = 0.91 \bar{U}_e$.

Thompson's results and language imply that (at the lower pressure ratios) there is some amplification process associated with finite-amplitude disturbances, probably still of the Tollmien-Schlichting type*. In analogy with the Schubauer-Klebanoff finding (ref. 19) that strong three-dimensional disturbances do not truly grow like Emmons' spots until they pass the infinitesimal Tollmien-Schlichting Re_{crit} , he searched for experimental evidence of the correlatable onset of such growth of finite disturbances and called it Re_{crit} . This was unfortunate; the clear operational distinction between the concepts warrants distinct names. Actually Thompson's condition corresponds more nearly to the termination of Joseph's (ref. 23) global stability region; see also Section 3.9

*Occasional regular oscillations of T_w indicated by a film gage just before breakdown into a turbulent spot were judged not to be Tollmien-Schlichting waves. Their frequency is much higher, i.e. more like that of the three-dimensional roughness waves in Fig. 24 of ref. 1. For other views of amplification of finite disturbances see Sections 3.9, 4.1, and 6.2 of ref. 1.

of ref. 1. The multipronged results of the Lehigh University research are concisely stated by Thompson and Emrich (ref. 18). By placing two-dimensional and three-dimensional roughness elements at different distances from their monitoring gauges, and by firing sparks of varying strengths at arbitrary times with respect to the local passage of the generating shock, they concluded that (at subsonic M_e) the disturbance, though finite, must reach an appropriate local criterion before turbulence sets in. For instance, a disturbance from a spark will travel downstream at 30-50% of the free-stream speed \bar{U}_e until* the local boundary layer grows to a thickness δ for which $Re_\delta \sim 1600-2000$ ($Re_{\delta*} \sim 400-600$ with slightly more scatter). At such a time the disturbance gives birth to an Emmons spot, the leading edge of which then propagates at \bar{U}_e while the trailing edge continues at approximately $0.5 \bar{U}_e$. The two-dimensional and three-dimensional roughnesses indicated nearly the same conditions for generation of turbulence. According to Schubauer and Klebanoff (ref. 19) and Klebanoff et al (ref. 24) a similar phenomenon occurs in the low-speed Blasius boundary layer at approximately the same Reynolds numbers. For the Blasius layer, however, the conditions nearly coincide with the theoretical Re_{crit} to infinitesimal disturbances whereas here the conditions are utterly Tollmien-Schlichting subcritical (as they are for the blunt-body paradox and for the exploratory low-speed experiments of favorable pressure gradients of Snedeker, Donaldson and Yates, ref. 25). Does the finiteness of the disturbances perhaps override the differences in concavity of the velocity profiles, which are so important for infinitesimal stability?

Asbridge (ref. 13), working with the same shock tube and juncture problems as Thompson, noted that no tripping by wall joints is observed for strong shocks where the free stream is supersonic, $M_e > 1$. Presumably this corresponds to the stabilization of free and separated shear layers at high speeds as discussed in Section 4.4 and Fig. 16 of ref. 1. One would surmise that sparks would remain effective as trippers - the lowest Re_δ values of Thompson in fact occurred at the highest M_e of 0.6 at which he used sparks. No experiments with sparks were reported for supersonic speeds either in shock tubes or in wind tunnels.

*Sparks of maximum available strength damped out completely when fired at small times after the passage of weaker generating shocks: global stability of Joseph (ref. 23)?

The construction of the Thompson-Emrich shock tube afforded shorter running lengths without wall junctures than did that of Hartunian et al (ref. 10) (6 feet to nearest upstream discontinuity). The fact that Thompson reports many runs with much higher Re_{tr} in subsonic M_e runs remains therefore puzzling. One would look for other sources of disturbances to cooperate or to take over the dominant role: the principle of dominant and multiple responsibility of refs. 1 and 2. The author notes that in all four of the highest unit-Re conditions of Thompson (ref. 17) the values were not limited by the wall-joint disturbances as were ten other subsonic conditions listed in his Fig. 28. Furthermore these high-unit Re conditions register noticeably lower values of Re_{tr} . While this trend opposes the usual variation with Re/L , it again focuses on the high-unit Re conditions (with cooling) as perhaps holding the key to the switch in dominant or cooperative disturbances.

Another student of Emrich, E. Gion also documented long laminar runs at Mach numbers M_e below 0.45 while studying in fine detail the structure of the wall boundary layers through the use of dark-field oscillatory-spark micro-photographic tracing of submicron-sized oil drops (ref. 14). In the process he concluded that the scatter of the velocities of the tracer particles in the free-stream and in the laminar boundary layer exceeded by a large margin the inaccuracies of his technique and hence represented a measure of bona fide environmental disturbances. His inferred $\pm 15\%$ u fluctuations are "probably due to pressure waves...from the turbulent boundary layer upstream and from the contact surface". Together with Asbridge's interferometric documentation of mean density variation as function of distance downstream of the generating shock (ref. 13), these measurements constitute the most specific information on the shock-tube disturbance environment at lower pressure ratios (for the given shock tube and geometry). For these conditions, with unit Re on the order of 3-6 million/ft, Gion also found that there was strong evidence of transition being influenced by the mere presence of normal operating debris: dust, diaphragm particles, shreds of sponge (used for cleaning the tube), etc., a presence which was unsuspected until the surface was placed under strong glancing illumination...

RECAPITULATION AND PROSPECTS

The variety of information on transition in shock tubes in this paper can

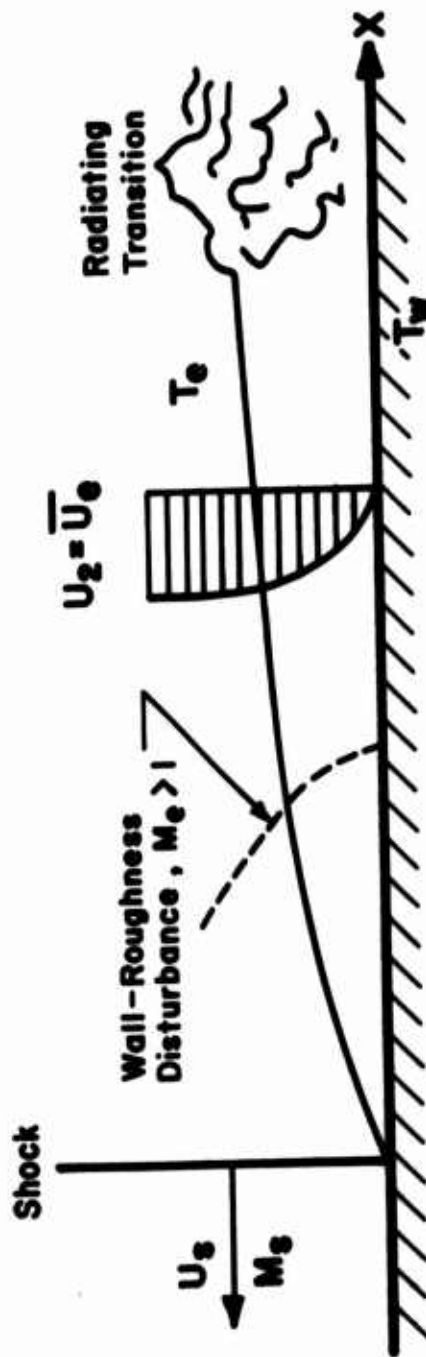
perhaps be better appreciated when one reflects on the fact that it corresponds to a wide range of conditions in Mach number M_e and temperature ratios T_w/T_e . These conditions span the low-speed to moderate supersonic regimes, the latter with very strong cooling. High unit Reynolds number, which is readily achievable in shock tubes, brings forth sensitivity to minute two-dimensional and three-dimensional roughness (including wall joints) at low speeds. At supersonic M_e values, the sensitivity to small three-dimensional roughness may well persist for combinations of high cooling and high unit Re and may contribute to the peculiar variation of transition in Sketch 2.

Since the low-M limit of the Ostrach-Thornton (ref. 5) appears correct, it is unlikely that any numerical difficulties could have spoiled the early trend of their stability limit in Sketch 2 (even if a Mack-type program should modify the high pressure ratio limit). Hence shock tubes almost certainly afford lessons in subcritical transition caused by some finite disturbances. Besides the vorticity generating roughness, the primary suspect, especially at high unit Reynolds numbers, must be the narrow-channel acoustic radiation from the turbulent region surrounding the "contact-surface" and from the boundary layers which have turned turbulent. The latter radiation has been identified as dominant in supersonic and hypersonic wind tunnels so that it well may have a role in shock tubes. The role of the perturbed contact region, however, appears as a novel feature among flow facilities. If shock tubes were to be used for controlled investigations of the troublesome high-cooling, high-unit-Re conditions, the disturbances from this contact region should be investigated first. Since the free stream disturbances in the shocked column of nearly uniform gas consist overwhelmingly of the sound mode, the use of hot-wire techniques in shock tubes (pioneered by the Johns Hopkins group - Kovasznay, Werner (ref. 9), Dosanjh (ref. 26) offers good promise for such a study, both at low and high pressure ratios (see Section 3.11 of ref. 1). Should a new experimental program on transition in shock tubes be undertaken, it would also be desirable to redo the Ostrach-Thornton infinitesimal stability calculations in a Mack framework (ref. 8). This should not only verify the subcritical nature of the observed transition, but also clarify the intricate cooling effects at higher pressure ratios where the equations and computational techniques used by Ostrach and Thornton are probably inadequate.

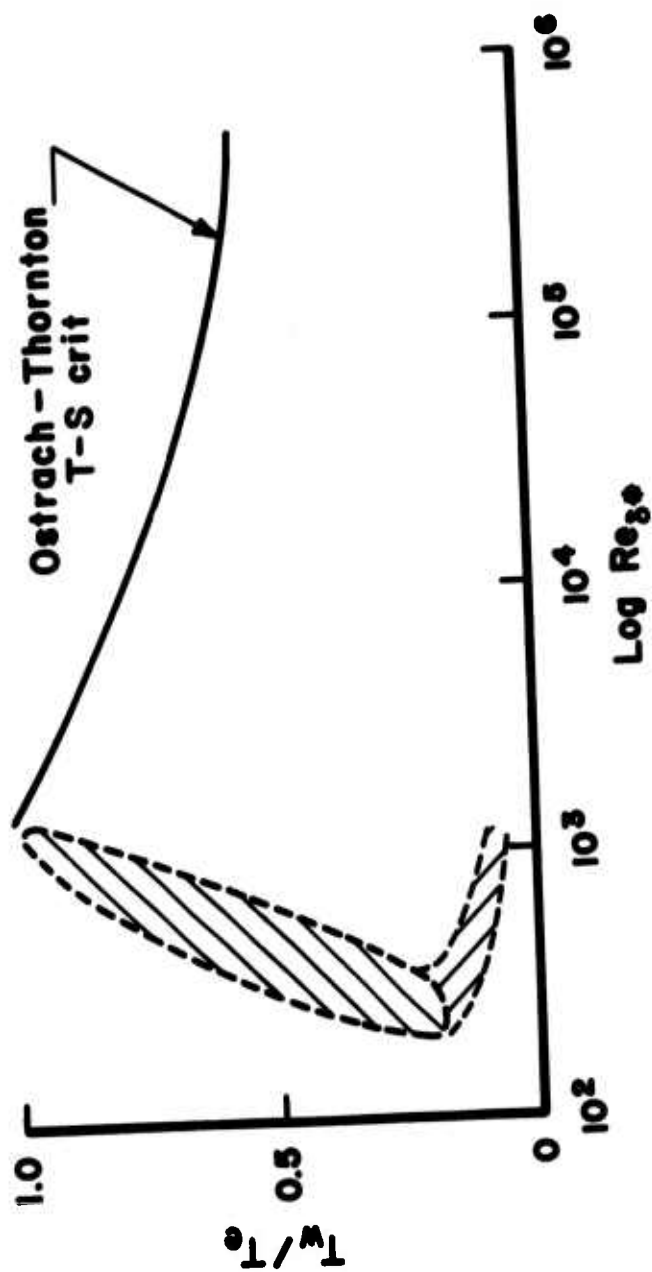
REFERENCES

1. M. V. Morkovin, Critical Evaluation of Laminar-Turbulent Transition and the High Speed Dilemma, Vol. 13 of Progress in Aerospace Sciences, D. Klitchmann, Editor, Pergamon Press (1972).
2. M. V. Morkovin, Critical Evaluation of Transition from Laminar to Turbulent Shear Layers with Emphasis on Hypersonically Traveling Bodies, U.S. AFFDL TR-68-149 (1969).
3. H. Mirels, (a) Boundary Layer Behind Shock or Thin Expansion Wave Moving into Stationary Fluid, NACA TN 3712 (1956), (b) Laminar Boundary Layer Behind a Strong Shock Moving into Air, NASA TN D-291 (1961).
4. E. J. Gion, A Tracer Study of the Shock-Tube Boundary Layer, Inst. of Res., Lehigh Univ., Tech. Rept. 18 (1965).
5. S. Ostrach and P. B. Thornton, Stability of Compressible Boundary Layers Induced by a Moving Wave, Jour. Aerosp. Sci., Vol. 29, p. 289 (1962).
6. D. W. Dunn and C. C. Lin, On the Stability of the Laminar Boundary Layer in a Compressible Fluid, Jour. Aerosp. Sci., Vol. 22, p. 469 (1955).
7. L. Lees and C. C. Lin, Investigation of the Stability of the Laminar Boundary Layer in a Compressible Fluid, NACA TN 1115 (1946).
8. L. Mack, Boundary-Layer Stability Theory, Jet Prop. Lab. Cal. Inst. Tech. Rept. No. 900-277 (1969).
9. J. Werner, Shockwave-Turbulence Interaction - Investigations in a Shock Tube, Ph.D. Thesis, the Johns Hopkins Univ. (1958).
10. R. Hartunian, A. Russo, and P. Marrone, (a) Boundary-Layer Transition and Heat Transfer in Shock Tubes, Proceedings of the Heat Transfer and Fluid Mechanics Institute, Univ. Calif. (1958), Stanford Univ. Press; (b) Jour. Aerosp. Sci., Vol. 27, p. 587 (1960).
11. W. A. Martin, An Experimental Study of the Boundary Layer Behind a Moving Plane Shock Wave, Univ. Toronto, Inst. Aerophys., Rep. 47, (May 1957), shortened in Jour. Aerosp. Sci., Vol. 25, p. 644 (1958).
12. P. B. Gooderum, An Experimental Study of the Turbulent Boundary Layer on a Shock-Tube Wall, NACA TN 4243 (1958).
13. A. R. Asbridge, An Interferometric Study of Shock Tube Boundary Layers, Inst. of Res., Lehigh Univ. Tech. Rept. 14 (1959).
14. A. J. Chabai, Measurement of Wall Heat Transfer and of Transition to Turbulence During Hot Gas and Rarefaction Flows in a Shock Tube, Inst. of Res., Lehigh Univ. Tech. Rept. 12 (1958).

15. W. E. Smith, H. S. Glick, A. Hertzberg, and W. Squire, Schlieren Studies of the Flow Behind Strong Shocks, lecture, Annual Meeting of Div. Fluid Dyn., Am. Phys. Soc. (1954), quoted in ref. 10b.
16. H. Mark and M. J. Mirtich, (a) Transition in Shock-Tube Boundary Layers Phys. Fluids, Vol. 5, p. 251 (1962); (b) Reply to Comments by Emrich and Gion, ibid p. 1487 (1962).
17. W. P. Thompson, An Experimental Study of Turbulent Spots and Wall Roughness Effects in Shock Tube Boundary Layer Transition, Inst. of Res., Lehigh Univ. Tech. Rept. 16 (1963).
18. W. P. Thompson and R. J. Embirch, Turbulent Spots and Roughness Effects in Shock-Tube Boundary-Layer Transition, Phys. Fluids, Vol. 10, p. 17, (1967).
19. G. B. Schubauer and P. S. Klebanoff, Contribution on the Mechanics of Boundary-Layer Transition, NACA Tech. Rept. No. 1289, (1956).
20. S. Dhawan and R. Narasimha, Some Properties of Boundary Layer Flow During the Transition from Laminar to Turbulent Motion, J. of Fluid Mech., Vol. 3, p. 418 (1958).
21. J. M. Kendall, Jr., Supersonic Boundary-Layer Transition Studies, Jet. Prop. Lab. Space Program Summary, Vol. III, pp 37-62, (April 1970).
22. S. R. Pate and C. J. Schueler, An Investigation of Radiated Aerodynamic Noise Effects on Boundary-Layer Transition in Supersonic and Hypersonic Wind Tunnels, AIAA Jour., Vol. 7, p. 450, (1969).
23. D. D. Joseph, On the Place of Energy Methods in a Global Theory of Hydrodynamic Stability, Proc. IUTAM Symposium on Stability of Continuous Systems, Herrenalb, Germany 1969, Springer Verlag (1971).
24. P. S. Klebanoff, G. B. Schubauer, and K. D. Tidstrom, Measurements of the Effect of Two-Dimensional and Three-Dimensional Roughness Elements on Boundary Layer Transition, Jour. Aero. Sciences, Vol. 22, No. 11, (November 1955).
25. R. S. Snedeker, C. duP. Donaldson, and J. E. Yates, A Preliminary Experimental Study of the Behavior of Disturbances Introduced into a Highly Accelerated Laminar Boundary Layer, Aero. Res. Asso. Princeton Rept. to US AFOSR, (October 1970).
26. D. S. Dosanjh, Use of a Hot-Wire Anemometer in Shock-Tube Investigations NACA TN 3163 (December 1954).



Sketch 1. Shock-generated laminar and turbulent boundary layer in laboratory coordinates.



Sketch 2. Local transition Reynolds number as function of the cooling parameter.

(This page intentionally left blank)

UNCLASSIFIED

Security Classification

DOCUMENT CONTROL DATA - R & D

(Security classification of title, body of abstract and indexing annotation must be entered when the overall report is classified)

1. ORIGINATING ACTIVITY (Corporate author)

**THE AEROSPACE CORPORATION
SAN BERNARDINO OPERATIONS**

2a. REPORT SECURITY CLASSIFICATION

UNCLASSIFIED

2b. GROUP

3. REPORT TITLE
PROCEEDINGS OF THE BOUNDARY LAYER TRANSITION WORKSHOP HELD 3 - 5 NOVEMBER 1971, Vol III

4. DESCRIPTIVE NOTES (Type of report and inclusive dates)

Technical Operating Report

5. AUTHOR(S) (First name, middle initial, last name)

W. D. McCauley

6. REPORT DATE

20 Dec 71

7a. TOTAL NO. OF PAGES

7b. NO. OF REFS

8a. CONTRACT OR GRANT NO.

F04701-71-C-0172

b. PROJECT NO.

9a. ORIGINATOR'S REPORT NUMBER(S)

TOR 0172(S2816-16)-5

9b. OTHER REPORT NO(S) (Any other numbers that may be assigned this report)

SAMSO TR 73-155, Vol III

10. DISTRIBUTION STATEMENT

**Distribution limited to U.S. Government Agencies Only. (Test & Evaluation) (20 Dec 71)
Other requests for this document must be referred to SAMSO/RSSE.**

11. SUPPLEMENTARY NOTES

12. SPONSORING MILITARY ACTIVITY

**Space & Missile Systems Organization
P.O. Box 92960, Worldway Postal Center
Los Angeles, CA 90009**

13. ABSTRACT

The third session presented recent data obtained from government laboratories. The workshop consisted of introductory remarks, a keynote address, four reporting investigation sessions and a session involving all participants on four committees. The objective of the meeting was to make transition specialists aware of the most recent data and techniques for transition prediction and to focus on the solution of design problems associated with boundary layer transition. The first session showed how transition affects reentry vehicle design in terms of nose tip thermostress and ablation, transpiration cooled nosetips, frustum ablation, reentry observables, plasma attenuation, vehicle dynamics and space shuttle design. The second session presented ABRES reentry vehicle transition data and prediction techniques obtained since the previous meeting four years ago. The third session presented recent data obtained from government laboratories. The fourth session presented recent applications of stability theory, a additional confirmation of the theory and work toward transition modeling. In the last session the meeting participants worked on four committees to arrive at recommendations for future efforts on boundary layer transition.

DD FORM 1473
1 NOV 65**UNCLASSIFIED**

Security Classification